ANALYSIS OF THE OPERATIONAL CHARACTERISTICS AND STABILITY OF MULTITUBULAR REACTORS

A thesis submitted for the degree of

Doctor of Philosophy

in

The University of Leeds

by

Brian Roy Dunbobbin, B.Sc. (Leeds)

under the direction of

C. McGreavy, B.Sc. (Leeds), M.Eng., D.Eng. (Yale), C.Eng.,

M.I.Ch.E., F.B.C.S.

Department of Chemical Engineering,

Houldsworth School of Applied Science,

The University of Leeds,

Leeds, LS2 9JT.

September, 1976.

Text cut off in original

ABSTRACT

Consideration has been given to various aspects of the behaviour of multitubular fixed bed catalytic reactors supporting highly exothermic reactions. In particular, the problem of adequately representing the detailed characteristics of such reactors has been investigated, and mathematical models describing the steady state and dynamic behaviour of both co- and counter-currently cooled systems have been introduced as a basis for design and control studies.

Valuable insight into the operational characteristics of large multitubular reactors has been obtained by investigating the phenomena related to the interactive heat transfer within the system, and such results provide a very useful assessment of how flexible the final unit might be in its ability to accomodate new operating conditions. The role of the coolant, and the manner in which it is presented to the tubes, has been shown to be especially important. Not only is the routing of the coolant through the bundle significant, but also the flowrate. Relatively small variations in the rate can cause very large changes in the temperature profiles within the tubes. This is not primarily a result of the heat transfer coefficient being modified, but because of the change in the residence time of the cooling fluid and the consequent effect on the coolant temperature rise.

The results of an investigation into the configuration and coolant flow direction have shown that there can be considerable economic advantages in using co-currently cooled reactors with more than two shell-side passes. Such an arrangement is significantly more stable than a counter-current configuration for a wide range of coolant flow conditions. Furthermore, the effective feedforward of the heat in the coolant gives more even temperature profiles inside the reactor tubes which can result in a greater overall conversion.

A steady state method has been developed which is capable of representing the ranges of coolant and reactant conditions under which the reactor is stable. It is shown how this may be extended to enable the local stability of the tubeside to be related to the overall stability of the unit. Thus, the stability of the system is related to easily obtainable variables, namely the coolant and reactant inlet temperatures and coolant flowrate.

Dynamic models of the reactor have been formulated and used to demonstrate that the initial transient response of the system can lead to temperature runaway even though both the initial and final stationary states are stable. This behaviour, which would not be predicted by normal frequency response techniques, clearly has significant effects on the design of the system and its control strategy.

ACKNOWLEDGEMENT

The following presentation is the product of three years work and I am particularly indebted to my supervisor, Professor C. McGreavy, for giving me the freedom to pursue this topic and the support to allow it to come to full fruition.

I would also like to thank Professor G.G. Haselden for permitting me to carry out this work in the Department of Chemical Engineering, and to the Science Research Council for financial support. I am also grateful to my friends and colleagues in the department for their interest and continual encouragement. Special thanks are due to Mr. L. Bailey for his assistance with many of the computational problems.

Last, but by no means least, I wish to thank my wife, Jane, for her patience and understanding throughout this research. In particular, I would like to congratulate her on so ably typing this thesis from my sometimes unintelligible hieroglyphics.

C O N T E N T S

		Page
ABSTRACT		i
ACKNOWLEDGEMENT		iii
CONTENTS		iv
LIST OF FIGURES		viii
LIST OF TABLES		xv
CHAPTER 1	Introduction and Reasearch Objectives	1
CHAPTER 2	Previous Work	7
2.1	Background	
2.2	The Catalyst Pellet	
2.3	The Tubular Reactor	
2.4	Coolant Effects	
2.5	Stability	
2.6	Final Comments	
CHAPTER 3	Model Development	24
3.1	Introduction	
3.2	Model Assessment	
3.3	Formulation of Alternative Representations	
3.4	Discussion	
3.5	Concluding Remarks	
CHAPTER 4	Steady State Models for the Multitubular Bundle	41
4.1	Introduction	
4.2	The Assumptions used for the Shell-Side Models	
4.3	The Co-Current Crossflowing Coolant Reactor Model	
4.4	The Counter-Current Crossflowing Coolant Reactor Model	
4.4.1	Counter-Current Continuum Model.	

4.5 Representation of the Tubeside in the Steady State Multitubular Reactor

4.5.1 Introduction

4.5.2 The Two Dimensional Tubeside Model

4.6 Conclusions

CHAPTER 5 The Steady State Behaviour of Multitubular Reactors. 67

1. Co-Current Cooling

5.1 Introduction

5.2 A Two Coolant Pass System

5.3 The Effect of the Number of Coolant Passes on the System

5.4 Effect of Configuration on the Position of the Tubeside Hotspot

5.5 Variation of the Overall Heat Transfer Coefficient

5.6 The Maldistribution of Reactant Feed to the Tubes

5.7 Heat Generation and Removal in the Co-Current Reactor

5.8 Conclusions

CHAPTER 6 The Steady State Behaviour of Multitubular Reactors. 106

2. Counter-Current Cooling

6.1 Introduction

6.2 The Effects of Coolant Flowrate and Reactor Configuration on the System Performance

6.2.1 Variation of the Coolant Flowrate

6.2.2 Influence of the Number of Coolant Passes

6.3 The Effect of the Configuration on the Position of the Tubeside Temperature Hotspot

6.4 The Variation of the Overall Heat Transfer Coefficient

6.5 The Maldistribution of Reactant Feed to the Tubes

6.6 Multiple Steady States

6.7 Heat Generation and Removal in the Counter-Current Reactor

6.8 Conclusions

CHAPTER 7	The Steady State Behaviour of Multitubular Reactors. 3. Some Factors Affecting Stability	158
7.1	Introduction	
7.2	Mechanisms of Heat Transfer in the Reactor Bundles	
7.3	Stability of Multitubular Reactors	
7.3.1	Counter-Currently Cooled Reactors	
7.3.2	Co-Currently Cooled Reactors	
7.3.3	Use of the $T_{c_{in}}$ Versus GG Phase Plots	
7.4	Alternative Flow Configurations	
7.5	Conclusions	
CHAPTER 8	The Dynamic Behaviour of Multitubular Reactors	188
8.1	Introduction	
8.2	Co-Current Cooling	
8.2.1	Formulation of the Equations	
8.2.2	The Transient Response of the Reactor	
8.2.3	The Frequency Response of the Reactor	
8.3	Counter-Current Cooling	
8.3.1	Formulation of the Equations	
8.3.2	The Transient Response of the Reactor	
8.4	Concluding Remarks	
CHAPTER 9	Final Comments	233
9.1	General Findings of the Present Work	
9.2	Assessment of the Present Work	
9.3	Suggestions for Further Work	
APPENDIX A	The Catalyst Pellet Models	243
A.1	The Fully Distributed Catalyst Pellet Model	
A.1.1	The Steady State	
A.1.2	The Unsteady State	
A.2	The Lumped Thermal Resistance Model of the Catalyst Pellet	

A.2.1 The Steady State

A.2.2 The Unsteady State

APPENDIX B The One Dimensional Reactor Model 250

B.1 The Steady State Model

B.2 The Unsteady State Model

APPENDIX C Single Tube, Flowing Coolant Model. (Model B of Chapter 3) 253

APPENDIX D The Continuum Coolant Heat Balance 254

APPENDIX E The Co-Current Mixing Cell Model 260

APPENDIX F The Counter-Current Mixing Cell Model 263

APPENDIX G The Two Dimensional Tubeside Reactor Model 266

APPENDIX H The Solution of the Co-Currently Cooled Transient Reactor Model 271

APPENDIX I The Solution of the Counter-Currently Cooled Transient Reactor Model 273

NOMENCLATURE 275

BIBLIOGRAPHY 280

LIST OF FIGURES

3.1 Schematic diagram of a parallel flow multitubular reactor.

3.2 Schematic diagram of a cross-flow multitubular reactor.

3.3 Schematic diagram of a radial flow multitubular reactor.

3.4 General representation of the reactor indicating the notation used in describing it.

3.5 Phase plots and temperature profiles for two shell-side coolant passes.

4.1 Schematic diagram of the shell-side coolant flow.

4.2 General representation of the reactor indicating the notation used in describing it.

4.3 Comparison of the tubeside temperature profiles produced by the various co-current shell-side models.

4.4 Comparison of the tubeside temperature profiles produced by the various counter-current shell-side models.

4.5 Schematic diagram showing the solution method used in the counter-current continuum model.

4.6 Comparison of the one- and two- dimensional tubeside models for a co-current reactor.

4.7 Comparison of the radial temperature profiles of the one- and two-dimensional tubeside models.

4.8 Comparison of the one- and two-dimensional tubeside models for a counter-current reactor.

5.1 Tubeside temperature profiles for differing coolant flowrates in a two coolant pass co-current reactor.

5.2 Tubeside temperature profiles for differing inlet coolant temperatures in a two coolant pass co-current reactor.

5.3 Tubeside temperature profiles for differing inlet reactant temperatures in a two coolant pass co-current reactor.

5.4 Effect of the number of coolant passes on the tubeside temperature profiles of a co-currently cooled system. Constant mass flowrate.

5.5 Effect of the number of coolant passes on the tubeside temperature profiles of a co-currently cooled system. Constant coolant velocity.

5.6 Tubeside temperature profiles of a three coolant pass co-current reactor under various conditions.

5.7 Tubeside temperature profiles of a four coolant pass co-current reactor under various conditions.

5.8 Tubeside temperature profiles for a six coolant pass co-current reactor under various conditions.

5.9 Tubeside hotspot positions in a two coolant pass co-current reactor.

5.10 Tubeside hotspot positions in a three coolant pass co-current reactor.

5.11 Tubeside hotspot positions in a four coolant pass co-current reactor.

5.12 Schematic diagrams used in the prediction of the tube containing the maximum tubeside temperature in co-current reactors.

5.13 The effect of variations in the wall Nusselt number on the tubeside temperature profiles in a four coolant pass co-current reactor.

5.14 Four coolant pass, co-current reactor subject to maldistribution of feed amongst the tubes. High coolant velocity case.

5.15 Four coolant pass, co-current reactor subject to maldistribution of feed amongst the tubes. Low coolant velocity case.

5.16 The tubeside temperature profiles for a four coolant pass reactor, used as a reference in the work on maldistribution of feed. High coolant velocity.

5.17 The tubeside temperature profiles for a four coolant pass co-current reactor, used as a reference in the work on the maldistribution of feed. Low coolant velocity.

5.18 The effect of varying the reactant flowrate in a single tube, constant coolant temperature reactor model.

5.19 Overall heat generation and removal curves for tube 1 in a four coolant pass co-current reactor.

5.20 Heat generation and removal curves for tube 1 in various coolant passes of the four coolant pass co-current reactor of figure 5.19.

6.1 Variation of the coolant flowrate in a four coolant pass counter-current reactor.

6.2 The effect of the number of coolant passes on the tubeside temperature profiles of a counter-currently cooled reactor.

6.3 The effect of the number of coolant passes on the tubeside temperature profiles of a counter-currently cooled reactor. Constant coolant velocity, $u_c = 0.25$ m/sec.

6.4 Tubeside temperature profiles for a two coolant pass counter-current reactor under various conditions.

6.5 Tubeside temperature profiles for a three coolant pass counter-current reactor under various conditions.

6.6 Tubeside temperature profiles for a four coolant pass counter-current reactor under various conditions.

6.7 Tubeside hotspot positions in a two coolant pass counter-current reactor.

6.8 Tubeside hotspot positions in a three coolant pass counter-current reactor.

6.9 Tubeside hotspot positions in a four coolant pass counter-current reactor.

6.10 Schematic diagram used in the prediction of the tube containing the maximum tubeside temperature in counter-current reactors.

6.11 The effect of variations in the wall Nusselt number on the tubeside temperature profiles for a four coolant pass counter-current reactor.

6.12 A four coolant pass counter-current reactor subject to maldistribution of feed amongst the tubes. Coolant velocity, u_c = 0.25 m/sec.

6.13 The tubeside temperature profiles for a four coolant pass, counter-current reactor, used as a reference in the work on feed maldistribution. Coolant velocity, u_c = 0.25 m/sec.

6.14 Inlet versus outlet coolant temperatures for a two coolant pass counter-current reactor.

6.15 Inlet versus outlet coolant temperatures for a four coolant pass counter-current reactor.

6.16 Inlet versus outlet coolant temperatures for a six coolant pass counter-current reactor.

6.17 Schematic plot of inlet versus outlet coolant temperature under conditions that give multiple steady states in the coolant temperature.

6.18 A plot of coolant inlet temperature versus GG showing the region of non-unique solutions for various numbers of coolant passes.

6.19 A plot of coolant inlet temperature versus GG for a two coolant pass counter-current reactor showing the non-unique region at various reactant inlet temperatures.

6.20 A plot of inlet coolant temperature versus GG for a four coolant pass counter-current reactor showing the non-unique region at various reactant inlet temperatures.

6.21 A plot of inlet coolant temperature versus GG for a four coolant pass counter-current reactor showing the non-unique region for various tube lengths.

6.22 A plot of inlet coolant temperature and overall coolant temperature rise versus coolant outlet temperature for a four coolant pass counter-current reactor. GG = 2.0

6.23 A plot of inlet coolant temperature and overall coolant temperature rise versus coolant outlet temperature for a four coolant pass counter-current reactor. GG = 5.0

6.24 Coolant temperature rise versus inlet coolant temperature for a two coolant pass counter-current reactor at various values of coolant flowrate.

6.25 Coolant temperature rise versus inlet coolant temperature for a four coolant pass counter-current reactor at various values of coolant flowrate.

6.26 Coolant temperature rise versus inlet coolant temperature for a six coolant pass counter-current reactor at various values of coolant flowrate.

6.27 Maximum tubeside temperature versus the coolant inlet temperature for a four coolant pass counter-current reactor at various coolant flowrates.

6.28 Fraction of reactant remaining versus inlet coolant temperature for a four coolant pass counter-current reactor at various coolant flowrates.

6.29 Overall heat generation and removal curves for tube 1 in a four coolant pass counter-current reactor. GG = 5.0

6.30 Overall heat generation and removal curves for tube 1 in a four coolant pass counter-current reactor. GG = 1.0

6.31 Heat generation and removal for tube 1 in different coolant passes of the four coolant pass counter-current reactor of figure 6.29.

7.1 Schematic diagram for the heat distribution around a three coolant pass co-current reactor.

7.2 Schematic diagram for the heat distribution around a three coolant pass counter-current reactor.

7.3 T versus B stability plot of a four coolant pass counter-current reactor under different coolant inlet temperatures. GG = 3.0

7.4 A plot of $T_{c_{in}}$ versus GG showing the safe operating region for a four coolant pass counter-current reactor.

7.5 Coolant temperature rise versus inlet coolant temperature for a four coolant pass counter-current reactor at various values of coolant flowrate.

7.6 The effect of decreasing the inlet reactant temperature on the stability and conversion lines of figure 7.4.

7.7 A plot of inlet coolant temperature versus GG showing the safe operating region of a four coolant pass co-current reactor.

7.8 Inlet versus outlet coolant temperatures for a four coolant pass co-current reactor at various values of the coolant flowrate.

7.9 Coolant temperature rise versus inlet coolant temperature for a four coolant pass co-current reactor at various values of the coolant flowrate.

7.10 The effect of decreasing the inlet reactant temperature on the stability and conversion lines of figure 7.7.

7.11 Schematic diagram of the mixed flow reactor.

7.12 The co-current, counter-current and mixed flow tubeside temperature profiles for tube 1 in a four coolant pass reactor. GG = 4.0

7.13 T versus B stability plot comparing the co-current, counter-current and mixed flow four coolant pass reactors. GG = 4.0

8.1 Tubeside temperature profiles of tube 1 for a co-current four coolant pass reactor following a step decrease of 10 K in the coolant inlet temperature. No account is taken of the heat capacitance of the reactor fittings. GG = 5.0

8.2 Tubeside temperature profiles of tube 50 for the case shown in figure 8.1.

8.3 Tubeside temperature profiles of tube 1 for a co-current four coolant pass reactor following a step decrease of 10 K in the coolant inlet temperature. The lumping of tubes assumption has been used with N = 6. No account has been taken of the heat capacitance of the reactor fittings. GG = 5.0

8.4 Tubeside temperature profiles of tube 1 for a four coolant pass co-current reactor following a step decrease of 10 K in the coolant inlet temperature. No account is taken of either the transient term in the coolant heat balance or the heat capacity of the reactor fittings. GG = 5.0

8.5 Tubeside temperature profiles of tube 1 for a co-current four coolant pass reactor following a step decrease of 10 K in the coolant inlet temperature. GG = 5.0

8.6 Tubeside temperature profiles of tube 50 for the case shown in figure 8.5.

8.7 Tubeside temperature profiles of tube 1 for a co-current three coolant pass reactor following a step decrease of 10 K in the inlet coolant temperature. GG = 5.0

8.8 Tubeside temperature profiles of tube 50 for the case shown in figure 8.7.

8.9 The transient response of a single tube, constant coolant temperature reactor following a step decrease of 10 K in the inlet reactant temperature.

8.10 Tubeside temperature profiles of tube 1 for a four coolant pass co-current reactor following a step decrease of 10 K in the reactant inlet temperature. GG = 5.0

8.11 Tubeside temperature profiles of tube 50 for the case shown in figure 8.10.

8.12 Tubeside temperature profiles of tube 1 for a four coolant pass co-current reactor following a step decrease of 10 K in the inlet reactant temperature. GG = 2.0

8.13 Tubeside temperature profiles of tube 50 for the case shown in figure 8.12.

8.14 Tubeside temperature profiles of tube 1 for a four coolant pass co-current reactor following a step decrease of 25% in the coolant flowrate. Initial value of GG = 2.0

8.15 Tubeside temperature profiles of tube 50 for the case shown in figure 8.14.

8.16 Tubeside temperature profiles of tube 1 for a four coolant pass co-current reactor following a step increase of 50% in the coolant flowrate. Initial value of GG = 2.0.

8.17 Tubeside temperature profiles of tube 50 for the case shown in figure 8.16.

8.18 Tubeside temperature variations, at various axial positions in tube 1, during the frequency response to a sinusoidal disturbance, of amplitude 10 K and frequency 0.01 Hz, in the inlet coolant temperature to a four coolant pass reactor. GG = 5.0

8.19 Plots showing the variation in the outlet concentratior of reactant, together with the inlet and outlet coolant temperatures for the case shown in figure 8.18.

8.20 Variations in tubeside temperature and outlet concentration of reactant at various axial positions in tube 1 during the frequency response to a sinusoidal disturbance of amplitude 10 K and frequency 0.02 Hz in the inlet coolant temperature to a four coolant pass reactor. GG = 5.0

8.21 Schematic diagram used to demonstrate the method of solution of the counter-current transient reactor model.

8.22 Tubeside temperature profiles of tube 1 for a two coolant pass counter-current reactor following a step decrease of 10 K in the coolant inlet temperature. The lumping of tubes assumption has been used with N = 6. GG = 5.0

8.23 Tubeside temperature profiles of tube 50 for the case shown in figure 8.22.

8.24 Tubeside temperature profiles of tube 1 for a two coolant pass counter-current reactor following a step decrease of 10 K in the coolant inlet temperature. GG = 5.0

8.25 Tubeside temperature profiles of tube 50 for the case shown in figure 8.24.

8.26 Tubeside temperature profiles of tube 1 for a three coolant pass counter-current reactor following a step decrease of 10 K in the coolant inlet temperature. GG = 5.0

8.27 Tubeside temperature profiles of tube 1 for a three coolant pass counter-current reactor following a step decrease of 10 K in the reactant inlet temperature. GG = 5.0

8.28 Tubeside temperature profiles of tube 50 for the case shown in figure 8.27.

8.29 Tubeside temperature profiles of tube 1 for a three coolant pass counter-current reactor following a step decrease in coolant flowrate from GG = 5.0 to GG = 4.0.

8.30 Tubeside temperature profiles of tube 50 for the case shown in figure 8.29.

E.1 Schematic diagram of the tube bundle, showing the arrangement of the mixing cells in the co-current cross-flow model.

F.1 Schematic diagram of the tube bundle, showing the arrangement of the mixing cells in the counter-current cross-flow model.

LIST OF TABLES

3.1 Typical data set used in the thesis.

5.1 The effect of the number of coolant passes on the performance of a co-current reactor at constant coolant mass flowrate.

5.2 The effect of the number of coolant passes on the performance of a co-current reactor at constant coolant velocity.

5.3 The effect of the number of coolant passes on the performance of a co-current reactor at constant coolant mass flowrate. Tube length, L = 4 m.

5.4 The effect of the number of coolant passes on the performance of a co-current reactor at constant coolant mass flowrate. Tube length, L = 6 m.

5.5 Fractional conversion for co-current reactor system.

5.6 The tube containing the maximum tubeside temperature peak, for various reactor configurations.

5.7 The conversions and coolant temperature rises in reactors subject to maldistribution of the feed to the tubes.

6.1 Effect of the number of coolant passes on the performance of a counter-current reactor at constant coolant mass flowrate.

6.2 Effect of the number of coolant passes on the performance of a counter-current reactor at constant coolant velocity.

6.3 Effect of the number of coolant passes on the performance of a counter-current reactor at constant coolant mass flowrate. Tube length, L = 4 m.

6.4 Effect of the number of coolant passes on the performance of a counter-current reactor at constant coolant mass flowrate. Tube length, L = 6 m.

6.5 Fractional conversions for counter-current reactor systems.

6.6 The position of the maximum tubeside temperature peak in counter-current reactors.

6.7 Variation of reactant flowrate to 10 tubes either end of the tube bundle.

7.1 Comparison of co-current, counter-current and mixed flow systems.

G.1 Collocation constants for cylindrical symmetry using the squares of Legendre zeros.

CHAPTER 1

Introduction and Research Objectives

The use of multitubular fixed bed chemical reactors to contact gaseous reaction mixtures with solid catalysts has long been an industrially important unit operation. Such reactors have been used on a wide range of commercially important reactions e.g. styrene manufacture, the synthesis of ammonia and the partial oxidation of hydrocarbons, such as the conversion of benzene to maleic anhydride. The basic reactor unit is the same in most cases, being a cylindrical tube packed with catalyst, the reactants are passed through and conversion to products takes place.

This mechanical arrangement, which can comprise of several thousand tubes operating in parallel to handle the heat load, is particularly effective in coping with either exothermic or endothermic catalytic reactions because of the ease with which a cooling or heating medium can be contacted with the external surface of the tube. Conventionally, this is achieved by building the reactor in the form of a shell and tube heat exchanger, the catalyst being placed inside the small diameter tubes with the cooling or heating medium flowing on the shell side. In the case of an endothermic reaction, as with styrene production, the heat is necessary to maintain the reaction at a reasonable rate in order to minimize the size of reactor needed for a given production rate. When the reaction is exothermic, however, the temperature and hence reaction rate can increase very rapidly along the length of the bed, which from the point of view of reducing the reactor size is desirable, but for other reasons, such as the promotion of competitive reactions is undesirable and so cooling is necessary. Moreover, excessively high temperatures can cause damage to the catalyst or tubes or both and result in the development of hazardous conditions.

This study is concerned with analyzing the behaviour of highly

exothermic reaction systems, typified by the partial oxidation of benzene to maleic anhydride, which by reference to this specific case study demonstrates the main characteristics of a whole range of hydrocarbon oxidation processes. This type of system can sometimes go unstable, and it is useful at this point to consider just what is meant by the term instability when referring to such systems. Although in a classical control sense stability (not instability) is rigorously defined, it is nevertheless convenient to adopt heuristic concepts related to the operability of systems which do not necessarily have such a precisely structured framework. Thus, a system is said to be unstable if it exhibits unacceptable behaviour during operation, such as temperature runaway. Temperature runaway in reactors can be caused by various factors, though mainly it is in situations where there is parametric sensitivity or multiple steady states. The former, where small changes in the state variables can lead to large changes in the operating state is easily reversible by restoring the original operating conditions. Multiple steady states on the other hand, which may result in large changes in the state of the system for small changes in the state variables, requires certain conditions to be fulfilled before the initial state is retrieved. This is due to the existence of hysteresis[15].

In the sense used here the definition of instability is necessarily subjective and somewhat arbitrary. Although it is clear that unacceptably large changes are a manifestation of instability, it is still convenient to include cases where sustained uncontrolled oscillations occur, whether or not they result in, for example, deactivation of the catalyst. Indeed, any mode of operation where an adequate control, or limitation of the value of the state variables, cannot be excercised, can reasonably be included in this classification since the emphasis is on operational characteristics.

Despite the fact that an operational level instability is essentially

a dynamic problem, steady state information can nevertheless be used to indicate regions of potentially unacceptable behaviour. However, it is not simply the specification of 'hard' boundaries which is of importance, but the broader view that can be expressed in terms of the intrinsic characteristics of the system in relation to the patterns of behaviour as undesirable operating regions are approached.

Obviously, current industrial practice requires that reactors be run well away from these undesirable regions of operation, which may represent a severe constraint when searching for optimum performance. An insight into the circumstances which can cause such effects and knowledge of how to prevent them are important aspects of reaction engineering which are generally not considered explicitly. Using this information, together with reliable design methods backed up by the use of optimization and good tight control, would enable the safe operation of packed bed reactors under the most economic conditions, often conditions that are close to the regions exhibiting temperature runaway.

It has commonly been the practice in developing large scale reactors to carry out preliminary studies using a pilot plant. This enables tests to be made to determine the region most suitable for safe operation. The commercial reactor can then be built and operated in that region. This technique, although satisfactory in many respects, has the disadvantage of being both time consuming and expensive and therefore cannot be used to identify the whole of the possible domain. Moreover, scale-up can also be a major problem and, because of the large margins of error often needed, the most appropriate tightness of design is not always permitted. An alternative approach is to use a mathematical model to explore the operational domain and identify where the limiting conditions might be encountered, and how the system might be expected to behave as these limits are approached. The model which should incorporate all the relevant kinetic, thermodynamic and transport data,

could even be used to explore alternative designs for the reactor, and could therefore complement pilot plant scale models. In practice however this is not usually possible for a variety of reasons, not least of which is the lack of accurate data for use in the model.

An approach based on this strategy involves the following stages:

1. A mathematical model is formulated containing what are thought to be all the most important mechanisms necessary for an adequate description of the reactor, this being characterized by physically and chemically identifiable parameters. Some of these parameters will be available to the required accuracy from existing correlations e.g. heat capacities, densities etc.

2. Experiments are designed to measure the unknown parameters, the accuracy to which these are required and the best experimental program to follow can be obtained by use of the above model.

3. Using the mathematical model, predictions of the reactor performance can be made and compared with appropriate test runs on the pilot plant. From this the reliability of the model is then tested. At this stage, the model may have to be updated and the procedure repeated until satisfactory agreement with the experiments is achieved for as wide a range of operating conditions as possible.

The resulting model, which should be as simple as possible whilst retaining all the features necessary to represent the system, can then be used to give a much better insight into the system than could be obtained by experimentation alone. Although computer time is expensive, the ease with which many simulations can be carried out in a relatively short time, often means that the development time necessary for a given reactor design can be less than that needed had only pilot plant experimentation been used. Moreover, because it was necessary to examine

some of the underlying effects in the process, not only has a greater understanding of the system been developed, but the best strategy of operation for the reactor should some disastrous condition arise, can be explored, which would not be feasible experimentally.

The reactor group at Leeds has been looking into the problems of the design, optimization and control of heterogeneous reactors for several years, with both theoretical and experimental work running in parallel. Early work on the formulation of the design model has been done by Cresswell[12] and Thornton[15], they attempted to isolate the major effects needed to describe the packed bed reactor. One of the main difficulties in the modelling approach is that a mechanistic model of the system is necessarily complex and can be unsatisfactory for use in optimization and control, often requiring too much computation even for routine design. With this in mind Turner[42] applied model reduction techniques to the problem and developed a steady state representation of a single reactor tube. While design problems usually involve only the steady state models, the increasing importance of optimization and control emphasises the need for a dynamic representation of the system. Dynamic studies have been carried out by Adderley[41] and Naim[35], and although the models they used are still unsuitable for on-line control owing to their complexity, the insight that they have given into the system performance can be very helpful in deciding the best control strategy for given conditions.

The normal design methods applied to large industrial systems assume that it is possible to represent the whole multitubular bundle by a single tube, considered to be typical of every tube in the reactor. This approach which does not take into account the influence of heat distribution within the coolant in specific terms, means that it is not possible to say how the pattern of heat release due to reaction affects the performance. The need to take this into account can be appreciated if it is recognized that in effect significant interaction between tubes can occur, depending on the relative magnitudes of the heat generation

and exchange terms. Consequently, failure to incorporate this interaction into the design of such systems, but basing it solely on a single tube analogy can result in significant discrepancies. This work is intended to identify how, and under what circumstances, such considerations must be taken into account, together with what approximations might be appropriate in formulating practical models for both design and control studies. Perhaps even more important, it shows what experimental data is critical in specifying the design. However, much of the value of the modelling is derived from the qualitative picture of the overall behaviour and the insight to the overall characteristics of the system that such a picture reveals. In much the same way as one views the terrain on a map without actually making the journey, a quantitative model can be used to give qualitative behaviour of the whole range of operation without having to run the plant under conditions which may lead to instability. Since the boundaries of these regions of instability can only be adequately defined once they have been crossed, and it is not feasible to operate pilot scale equipment under potentially dangerous conditions, mathematical simulation of the system can be very effectively used to provide useful guidelines to operational regions. Although, at the present time, conventional reactors do not operate close to these unstable regions, these areas are of some importance from a commercial point of view. Thus, if reliable design methods and control strategies can be developed, it is conceivable that reactors could be safely operated in regions close to conditions that might otherwise lead to temperature runaway. Economically this can be very attractive because of the much higher yields obtainable for a lower energy consumption and capital cost.

CHAPTER 2

Previous Work

2.1 Background

The detailed analysis of catalytic reaction systems has only really become feasible with the availability of high speed digital computers, although in certain idealized cases, analytical solutions had been available[1]. There is a wealth of literature on the subject and a general coverage of the relevant background can be had from textbooks such as: Thomas and Thomas[2], Satterfield[3], Aris[4, 75], Petersen[5], Denbigh and Turner[6] and Perlmutter[7]. Several state of the art reviews, relevant to the type of fixed bed reactor dealt with in this thesis, have also been published, some of the most recent being Froment[8, 9], Hlavecek[10] and Ray[11].

Since much of the published literature deals either with specific areas of reaction analysis, not relevant here, or with very simple models of little practical importance, an overall review of the subject is not intended. Instead, only areas of direct relevance to this thesis will be concentrated upon, in order to set the work presented into perspective. The main themes to be considered relate initially to the tubeside behaviour, namely the local effects produced by the catalyst particles and the overall global conditions within the tube, so this will involve drawing comparisons between previous work. This latter consideration is particularly important because of the necessity of demonstrating how many of the detailed analyses on single tubes previously reported, fail to identify a number of important features of multitubular assemblies. The cooling medium and its interaction with the tubes will then be considered, and finally the relationships of such models to reactor stability studies will be examined.

2.2 The Catalyst Pellet

As indicated earlier, highly exothermic catalytic reactions often take place in a reactor tube packed with solid catalyst particles. The catalyst, usually a transition metal oxide (e.g. vanadium pentoxide) in the class of reactions considered here, is supported on a porous ceramic support such as silica or alumina spheres. It is necessary to consider the catalyst pellet in detail for two important reasons. First, the presence of the pellets in the tube influences the flow distribution of the reacting fluid and hence the dissipation of both heat and mass within the reactor. Secondly, the pellets provide the sites on which the reaction takes place. Since porous supports are used to increase the number of sites available, the reactants have to diffuse into the catalyst, react and then the products diffuse away. This resistance to the transport of heat and mass has the effect of causing conditions within the pellet to differ from those of the fluid and thereby influence the rate of reaction. For design purposes a detailed description of the pellet conditions is not really required, a measure of the difference between the actual rate of reaction on the pellet and the rate predicted by the fluid conditions would be perfectly satisfactory. This can be achieved by the introduction of an effectiveness factor which can be obtained either empirically or theoretically. Thiele[76] and Zeldowitsch[77] were the first to recognize the significance of this, and introduced calculation formulae for the effectiveness factor, η , to relate the actual reaction rate in the pellet with that predicted by the fluid conditions. Appendix A outlines the main resistances for heat and mass transfer to the catalyst and demonstrates how the effectiveness factor can be evaluated by considering them.

A useful procedure has been developed by Petersen[5, 13, 14] using an asymptotic method to estimate the effectiveness factor. This, in fact, assumes that the reaction takes place in a thin layer of the

catalyst under conditions of strong intraparticle mass transport resistance and negligible interphase resistance. Paterson and Cresswell[16] extended this work by including the interphase processes and were able to simplify the effectiveness factor calculation to the solution of an algebraic equation. In particular it was demonstrated that failure to include the interphase resistance led to incorrect results, while inclusion of these effects gave quite a good approximation for highly exothermic reactions where the reactants are rapidly consumed.

Cresswell[12] showed by numerical computation that for most gaseous reaction systems, the pellets may be regarded as essentially isothermal over the entire range of practical operating conditions. On the basis of these results, he developed an isothermal pellet model, the temperature rise between fluid and pellet centre being lumped in the interphase region (i.e. the intraparticle heat resistance is neglected). For a first order reaction this is very convenient since it allows an analytical solution of the concentration equation to be obtained and hence the pellet temperature can be represented by a single non-linear algebraic equation in fluid temperature and concentration. Thornton[15] extended the isothermal pellet assumption to include a complex reaction scheme, as well as introducing the use of a pseudo-first order rate expression for the case of non-first order reactions. He also showed that the model gives an accurate estimate of the steady state conditions over a wide range of parameter values. This conclusion has been confirmed by Hlavacek and Kubicek[17, 18].

The experimental work confirming the results of the theoretical models has tended to be rather contradictory, and, although a great deal of work has been done, little conclusive evidence has been produced. This is not really surprising however, as the experimental difficulties are formidable, especially the measurement of intraparticle effects. Cunningham et al[19] demonstrated that large temperature differences

between fluid and pellet centre are possible, finding experimental values of the effectiveness factor as high as 25 in the hydrogenation of ethylene. Miller and Deans[20] obtained similar results, with η values greater than unity in the platinum catalysed hydrogen-oxygen reaction. Very large temperature gradients across the boundary layer, with only small differences in the pellet itself, were obtained by Irving and Butt[21], who carried out measurements on various pellets using extremely fine thermocouples 0.025 mm in diameter. Similar conclusions were obtained by Fulton and Crosser[66] and Hughes and Koh[23], where the importance of the film resistance was demonstrated in catalyst pellets of various sizes and shapes in the hydrogenation of ethylene. The former authors also reported work by Ramaswami[22], who suggest that interphase temperature differences of up to 420°C can occur. While this seems an excessive temperature rise it does indicate that the pellet temperature can be considerably higher than that of the fluid.

The dynamic behaviour of catalyst pellets was investigated theoretically by Thornton[15]. He demonstrated that the pellet can be regarded as being essentially isothermal at any instant, even in the transient state, and although an intraparticle temperature gradient does form initially, it rapidly disappears and does not seem to affect the isothermality assumption to any great extent. Thornton[15] also showed that, since the mass capacitance of the pellet is smaller than the heat capacitance, the rate of change of concentration within the pellet is faster than that of temperature. This result, which he confirmed computationally, means that the changing temperature drives the concentration profile, so that it can be assumed to be at a pseudo-steady state.

Experimental studies on the dynamics of single catalyst pellets have been performed by Hughes and Koh[23] who demonstrated that a small

intraparticle temperature rise during transient operation is possible. However, they also found that the interphase temperature gradient was far more important and was the dominating effect on the effectiveness factor. In the light of such results the approximations used by Thornton[15] seem acceptable, verifying that the assumption of isothermality applies equally well in the dynamic case as in the steady state.

2.3 The Tubular Reactor

The work reported here is primarily concerned with small diameter tubes packed with porous catalyst pellets, the gaseous reactants passing through the bed and reacting either on or within the pellets. In modelling such a system two broad types of model might be considered. The first, and simplest, is the quasi-homogeneous representation, essentially equivalent to the "empty-tube" reactor. This considers the pellet conditions (i.e. the temperature and reactant concentration) to be the same as those of the fluid, and so the packing only modifies the fluid dynamics, although it can have a much greater effect on the heat distribution of the system, especially under transient conditions. In such representations, it is only necessary to consider the fluid phase equations without explicit reference to the role of the catalyst, in the manner indicated in the previous section. However, many chemical reactions occurring in packed beds are associated with large heats of reaction, and it is often necessary to include the complications arising from the presence of the catalyst phase, owing to the differences between the solid and fluid conditions[8, 14, 15, 24]. In these circumstances, a more detailed reactor representation must be considered, which accounts for the heterogeneity of the system. In particular the differences between solid and fluid conditions are allowed for together with the fluid dynamic and heat effects, so that the overall rate of reaction is obtained by the use of an effectiveness factor which lumps together all

the rate limiting transport and kinetic effects.

Furthermore, because of the need for external cooling with these highly exothermic reactions, radial temperature (and hence concentration) gradients are induced in the tubes perpendicular to the flow of reactants. The resulting model should therefore describe temperature and concentration variations in at least two space dimensions i.e. axially and radially in the tubeside fluid phase. Axial diffusion of heat and mass parallel to the bulk gas flow can, in principle, also occur under certain circumstances, and although it has received a considerable amount of attention, several investigations[28, 29, 30] have shown that for the flow velocities used industrially the effect is negligible in beds larger than approximately one hundred pellet diameters. Since this is normally the case, it is not often necessary to include a description of axial heat and mass dispersion when representing an industrial scale unit.

The particular nature of the reactor bed means that a detailed microscopic model is required, taking into account the distributions of individual catalyst pellets. Such an analysis is not feasible at this time, and in any case, is not really needed. Many workers[15, 35, 38, 39, 41, 44] in this area have tackled the problem by space averaging the properties of the bed, forming a continuum which can be represented by differential equations in mass and heat transport. Although the bed properties have been averaged over the radius of the bed, the equations describing the heat and mass transfer within the pellet are solved for the actual size of pellet used[15]. This enables the rate of reaction and heat production per unit volume to be calculated at any point in the reactor, as though the pellet and its associated voidage were acting at that point.

An alternative to the continuum model has been proposed by Deans

and Lapidus[31]. This assumes that the reactor can be represented by an interconnected network of stirred tanks, where each tank has the dimensions of the catalyst pellet together with its associated voidage. Such mixing cell models have been used by several workers[32, 33] and although they have certain mathematical advantages the method corresponds to a modified finite difference representation of the continuum model[34]. Since the continuum model gives an adequate representation of the system and can be solved by much more efficient techniques, such as orthogonal collocation[28, 35, 36, 37, 73], there is general acceptance of this interpretation.

The earliest models used for the design or simulation of tubular reactors were concerned with either simple systems or approximations to more complex problems, so that homogeneous or pseudo-homogeneous models were adequate[25, 26]. Beek[27] gives an excellent review of such reactors including a useful discussion on the transport effects that can occur. McGreavy and Cresswell[38] and Thornton[15] proposed a two dimensional heterogeneous model, which took into account both axial and radial temperature and concentration gradients. Since the bed properties had been space averaged the equations were in a pseudo-homogeneous form, though the heterogeneity of the system was included by modifying the rate terms at each point to account for the resistance to heat and mass transfer in and around the catalyst pellets. The model predictions were significantly different from the pseudo-homogeneous models which only accounted for kinetic rate limitations, and in many cases the later predicted temperature runaway while the heterogeneous model gave stable profiles. These results indicated that for the highly exothermic reactions being studied, diffusion and mass transfer limitations can seriously affect the reaction rate on the catalyst and that for a detailed examination heterogeneous models are essential.

The heat and mass distribution within these heterogeneous reactor models normally consists of a set of simultaneous, non-linear partial differential equations, coupled with the catalyst pellet equations described in section 2.2. Because of the highly non-linear nature of the system analytical solutions are not possible and hence numerical techniques have been employed, the most general method being a finite difference approximation (such as the Crank Nicholson method). Although this approximation is reliable it is not computationally efficient, often requiring very small step sizes for convergence, and when solving equations as complex as those of the heterogeneous reactor models computation times can become very large, even for the steady state. Feick and Quon[39] looked at the problem of finding an accurate and efficient method of solving the transient reactor system and showed that the very large computation necessary using a finite difference method made it impractical for the design or control of reactors, and even for detailed studies related to specific problems. Two main approaches have been used. The first is to use a more efficient method of solution, such as the alternating direction explicit method[39] or one of the collocation methods[35, 36, 37, 40], so that the computation time necessary to solve the equations can be reduced, sometimes drastically. The second approach is to simplify the original equations by, for example, reducing the dimensionality. Since, the axial temperature and concentration profiles are the most important, it is possible to employ a simple model which accounts only for these, ignoring the radial transport. However, the radial gradients can be quite severe, so that this approximation cannot always be applied, and it has been shown[15] that it may be inappropriate in many cases. Thornton[15] developed a one dimensional heterogeneous model which uses a modified Nusselt number for heat transfer at the wall of the tube. This can be interpreted as being the result of a parabolic radial temperature profile and thus eliminates the need to calculate the profiles in this direction.

It was shown that this formulation gave satisfactory agreement for the steady state predictions of the two dimensional model and, because of the relatively small amount of computation necessary, it proved suitable as a basis for extensive studies of reactor performance. Adderley[41] used this approach and showed that even in the unsteady state, the predictions, when compared with a two dimensional model, were good enough for preliminary design and simulation studies. A more detailed attempt to reduce the dimensionality of the two dimensional heterogeneous model was tried by Turner[42]. Using a semi-empirical technique he introduced the concept of a distribution factor, analagous to the effectiveness factor for the pellet, defined by the relationship:

$$D = \frac{\text{The Mean Rate of Reaction}}{\text{The Rate of Reaction at the Mean Conditions}}$$

When combined with a modified Nusselt number, it can be used to approximate the radial profiles in the reactor. This method appears to be adequate for the steady state, and Naim[35] extended the work and showed that the predictions remained good even for dynamic studies. Although much more rapid to compute than the finite difference form of the two dimensional model, it still requires about three times as much computation time as the one dimensional model presented by Thornton[15].

It is convenient at this point to examine some of the assumptions commonly made in modelling studies. In all models axial symmetry of the bed properties and state variable profiles is assumed. This is certainly a valid assumption in single tube models where coolant conditions do not vary around the circumference. But in large industrial units with coolant flow across a tube bundle, large temperature gradients can, in certain circumstances, occur in the direction of coolant flow. There will also be coolant velocity variation around the tubes. Any attempt to account for these variations would clearly, be impracticable, since the detailed information on heat transfer coefficients

at each point of the circumference of every tube in the bundle is not available and is unlikely to be so in the forseeable future. Indeed, even if such data existed any estimates of the variations would be very system dependent, and the results would not be reproducable in other systems, or even the same one.

The flow conditions inside the tubes have to be treated in a similar manner, so that every point of the catalyst surface is assumed to be in contact with fluid of uniform concentration and temperature. Thus the rates of reaction and heat generation at each point in the bed may be calculated as though the catalyst particle is acting at that point. Catalyst pellets have been studied in non-uniform concentration and temperature environments[43, 44, 45]. Such studies however have been entirely theoretical and as experimental verification is virtually impossible, their use at present in realistic reactor models is therefore out of the question, and uniform conditions around the pellets must be assumed.

Most studies assume the catalyst pellets to be spherical and of uniform size and activity. This, however, is not a real limitation since it can be shown that it is possible to define a characteristic length equivalent to the diameter of a sphere for any shape of particle[5]. In the same way pellets of non-uniform size also present no difficulties provided an appropriate characteristic dimension is defined. This enables the problem of variable pellet sizes in different sections of the bed to be examined. In fact, this has been suggested as a convenient method of controlling the development of hotspots, large pellets being used in areas where reaction runaway may occur. Such effects have been studies by Brusset et al[46]. Calderbank[48] and Stewart and Sørenson[49] have modelled reactors containing inert spheres to dilute the packing, while Shadman-Yazdi and Petersen[47] considered the effect of varying activity within individual catalyst pellets, the object being to obtain

better yields in reactors where the product can be consumed. Very little is known about catalyst deactivation, but most catalysts are subject to it and apart from ageing, rapid increases in temperature can usually enhance it.

In most studies of the dynamic behaviour of reactors the perturbations have a relatively short life compared to the time necessary to cause significant deactivation by the ageing process. When long periods are considered however, the effects of deactivation may have to be included and a number of studies of long term performance in which it plays a major role have been carried out[50, 51]. When temperature runaway occurs, deactivation takes place very rapidly making the reactor model no longer representative of the system. From a practical design or control point of view, the purpose of modelling is to avoid such regions so the inclusion of an accurate representation of catalyst deactivation is not really necessary. All that is required is detailed knowledge of when such effects occur, the precise temperature profile of a reactor exhibiting temperature runaway would be of academic interest only.

A basic assumption, often applied in reactor modelling is that the physical and chemical parameters in a system are independant of concentration, temperature and position. Although this is obviously not true in practice, the increased computational effect needed to solve a model including such variations (even when known) cannot usually be justified by the increased accuracy obtained[15]. In the case of the heat transfer coefficients, for example, they can only be estimated to within about 10% accuracy, so that any variation along the length of the bed could not really be warranted.

The most doubtful assumption used is that of plug flow of the reacting fluid through the reactor, an assumption related to uniform

bed voidage. The bed voidage will not be uniform, being greatest near the wall[6], and as the gas takes the path of least resistance through the packing the velocity profile becomes distorted. This in turn will cause the mass and heat transfer parameters to vary across the bed. Valstar[52] compared two reactor models, one being an assumed velocity profile expression, the other using the plug flow assumption. Significant differences were observed. More recently, Stanek and Szekely[53] have suggested that significant flow maldistribution occurs, not only because of local variations in voidage, but also because of variations caused by the large radial temperature gradients that can arise. Hoiberg et al[54] however concluded that, in their system at least, the radial heat and mass transfer occurred rapidly enough to counteract the effects of any velocity profile present in the bed. Clearly, the problem needs further clarification, with special emphasis on the accurate formulation of the velocity variation across packed beds. As Valstar[52] and Hoiberg et al[54] have shown, the velocity profile is easily included in the model. The difficulty arises in predicting it, for the distribution of voidage and hence the form of the velocity profile are both very system dependant. Clearly then, until much more is known about the fluid dynamics of packed beds the plug flow assumption will have to be used in the representations.

2.4 Coolant Effects

While heat transfer between the coolant and reactor tube has received a great deal of attention, this has concentrated on the tubeside effects, and little work has been published on the effects of coolant heating or the method of heat transport through the system by the cooling medium. The extensive studies on reactor performance and stability have been largely confined to either adiabatic operation or the case of a constant coolant temperature surrounding the reactor tube[15]. In virtually all cases, a single tube is taken to be typical of all the

tubes in the multitubular bundle. Although it is possible to operate in this mode, the mechanical construction of the reactor, especially with the larger units, means that the behaviour of the coolant must be explicitly accounted for[41, 59, 67]. The effective interactions between the tubes, arising from the heat release, must also be taken into consideration. Also, since thermal instabilities can often be a problem in such systems, it is important to make allowance for them, especially when suitable design conditions are being sought[67].

One of the first attempts to include coolant effects was by Van Heerden[56], who examined the behaviour of an autothermal ammonia converter, where the feed gases are preheated by flowing counter-currently along the outside of the reaction tubes. Luss and Medellin[57] investigated the steady state multiplicity in an unpacked liquid reactor with a counter-current coolant flow. Both the above systems used simple non-heterogeneous, single tube representations, the first being a quasi-homogeneous model while the latter was adequately represented by a homogeneous system. Banchero and Smith[58] attempted to optimise the product yield of a shell and tube reactor containing a liquid homogeneous reaction, by manipulating the coolant flowrate and inlet temperature. Although they accounted for the fact that the reactor was multitubular they treated it as being a single tube with additional coolant heating. A similar approach to the problem was attempted by Drott[74], who modelled a phthalic anhydride reactor by assuming the coolant to be perfectly mixed but heated by the tubes in the multitubular bundle. His study was mainly concerned with tubeside effects, and the development of a tubewall reactor, and so not of any direct relevance to shell-side considerations. An interesting paper by Paris and Stevens[55] describes how, by appropriate cooling jacket design, the hotspot of a single tube reactor can be controlled.

None of the studies so far reported have examined either the steady

state performance or dynamics of gaseous fixed bed heterogeneous reactors in which the effects of coolant flow or temperature have been specifically considered. Adderley[41] looked at the problem of coolant heating in both single tube and multitube reactor systems containing a highly exothermic reaction. He found that in certain cases the behaviour of the coolant had an important effect on the reaction taking place and identified some of the areas which needed attention. Although Adderley's[41] work appears to be the first real attempt to investigate the effect of a coolant flowing over a bundle of tubes, Wanka and Güilhuber[59] have given an excellent account of the design factors used for such reactors. They report that the number of reaction tubes contained in a bundle can be as many as 30,000 though this is large even by todays standards, the average size being between 2,000 and 5,000 tubes. The limiting factor on the size of the reactor is the maximum shell diameter that can be transported from workshop to industrial site[59].

The inclusion of the coolant effects in the model is done simply by coupling the equations governing the reaction inside the tube with a heat balance over the coolant. Adderley[41] showed that the major problem with such a formulation was the very long computation time necessary, especially if the reactor bundle contains a large number of tubes. However, the fact that rapid computation of the model equations is not possible should not preclude the use of such representations should they be necessary.

2.5 Stability

It is well known that packed bed reactors supporting highly exothermic catalytic reactions can exhibit unstable conditions. These are said to occur when a small change in the reactor inlet conditions brings about large changes either within the bed or at the exit. Such

instability may be due solely to parametric sensitivity[41], and if this is the case removal of the disturbance restores the system to its original state. However, under certain circumstances the cause of the instability is due, not to parametric sensitivity, but to the existence of multiple steady states, whereby the original state is not returned to once the disturbance is removed, unless special conditions are fulfilled[15]. The potential existance of multiple steady states within the catalyst pellets can obviously pose difficulties in reactor design, since the history of each pellet must be known before the reactor performance can be predicted. This applies equally well to the transient case, since the pellets can exhibit hysteresis with respect to the permissible steady states. Thornton[15] investigated this phenomena and showed that great care must be taken when operating the reactor close to the region of multiplicity. He developed a method in which the region of multiple steady states in the catalyst may be plotted as a phase diagram. The reactor trajectories, when plotted on the same diagram indicating whether or not multiplicity of solutions is likely. Adderley[41] extended the work and went on to develop criteria whereby parametric sensitivity could be predicted near regions of multiplicity. The primary motive for identifying such regions is to keep the reactor operating conditions away from potential instabilities, thus avoiding the undesirable effects that would otherwise occur. These tend to be caused by the fact that the reaction rate at one steady state may be several orders of magnitude greater than at another. Hence, bad selectivity, catalyst deactivation or even tube blowout may result if the pellets change states in a region of non-uniqueness.

A vast amount of literature has been written on the stability problems associated with catalyst pellets. Unfortunately, as discussed in section 2.2 the complexity of the pellet equations means that consideration has mainly been given to special cases only. When an adequate

representation of the pellet is used three possible steady states can be obtained under certain fluid conditions[12, 15], the middle one being metastable. For conditions outside the practical operating range even more steady states have been reported, as an example, Hatfield and Aris[61, 62] obtained five steady states when working with low Sh /Nu ratios.

The catalyst pellet is not the only cause of multiplicity in reactors. Even with unpacked reactors, when axial heat and mass transport are important, three steady state profiles are possible for identical feed conditions. Multiplicity with relation to this type of system stability has been discussed by several workers, notably Perlmutter[7], with a review being given by Ray[11]. The cause of this phenomena is usually attributed to the backmixing of the fluid in the reactor. Froment[9] has pointed out however, that the degree of backmixing needed to produce such multiple steady states is unlikely to be found industrially. Several other mechanisms can cause multiple solutions, such as the use of recycle loops in the system. This effect has been studied both theoretically and experimentally for a number of cases[68, 64, 65]. Counter-current coolant flow can also produce non-uniqueness, and this has been demonstrated experimentally by Luss and Madellin[57] using an unpacked, liquid phase single tube reactor. Adderley[41] also reported the phenomena for a gas phase heterogeneous reactor.

2.6 Final Comments

The widespread use of computers has meant that increasingly complex models of chemical reactors have been produced, enabling the relaxation and testing of many of the normal assumptions used in them. Hence, it is possible to determine the degree of sophistication necessary in describing all the quantitative characteristics of a system while still using well defined physical parameters to represent it. One other

major consideration must be borne in mind when comparing different system representations, namely, that if a model is to be of practical interest, then it must also be mathematically tractable i.e. solutions must be obtainable either analytically or numerically at an acceptable cost and in a reasonable time.

Although empirical models of the system would be admirably suited for simulation studies with respect to ease of solution. They cannot be substituted for mechanistic system representations when regions of potential instability are being studied. The reason for this is that for an empirical model to give accurate results it must operate within the region for which the experiments, upon which the model is based, have been performed. Thus, close to regions of instability, where no experimentation is feasible, the empirical models are of limited value.

CHAPTER 3

Model Development

3.1 Introduction

Multitubular reactors are generally used for catalytic reactions which require temperature control along the reaction path. In the exothermic reactions under study here the main purpose of the heat transfer medium, frequently a molton salt, is to remove the reaction heat. Under certain conditions however, the reactor can be arranged so as to use this heat in the coolant to promote reaction in regions of depleted reactant. As pointed out in the last chapter, despite the coolant being recognized as having a significant effect on the behaviour of the system as a result of the importance of the heat removal terms in the equations, very little work has been done on the interaction between the tubes and the coolant.

This chapter extends previous analyses to consider a multitubular representation of the system, and compares this overall, macroscopic view of the reactor with the commonly adopted single tube models.

Although the basic mechanical features of the reactor are the same in most cases, essentially consisting of a shell and tube heat exchanger with a catalyst packing on the tubeside, there are several methods of contacting the coolant with the tubes. It is convenient to classify three main types of construction, identified by the flow direction of the coolant around the tube bundle, namely parallel, cross and radial flow reactors. Considering these separately an appreciation as to their various merits can be obtained.

a. Parallel Flow Reactor

Figure 3.1 shows the mechanical arrangement. The coolant is pumped

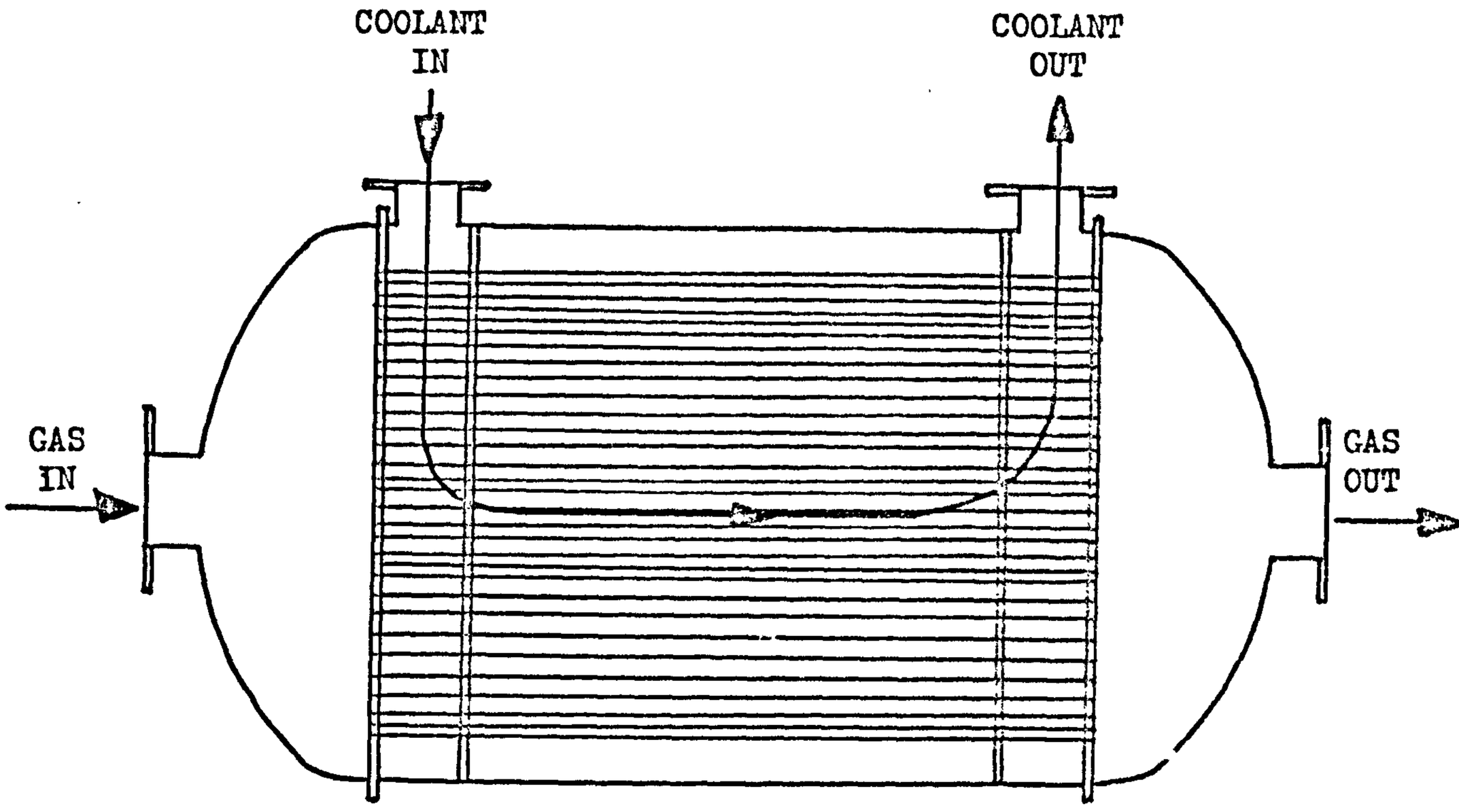

Figure 3.1 Schematic diagram of a parallel flow multitubular reactor.

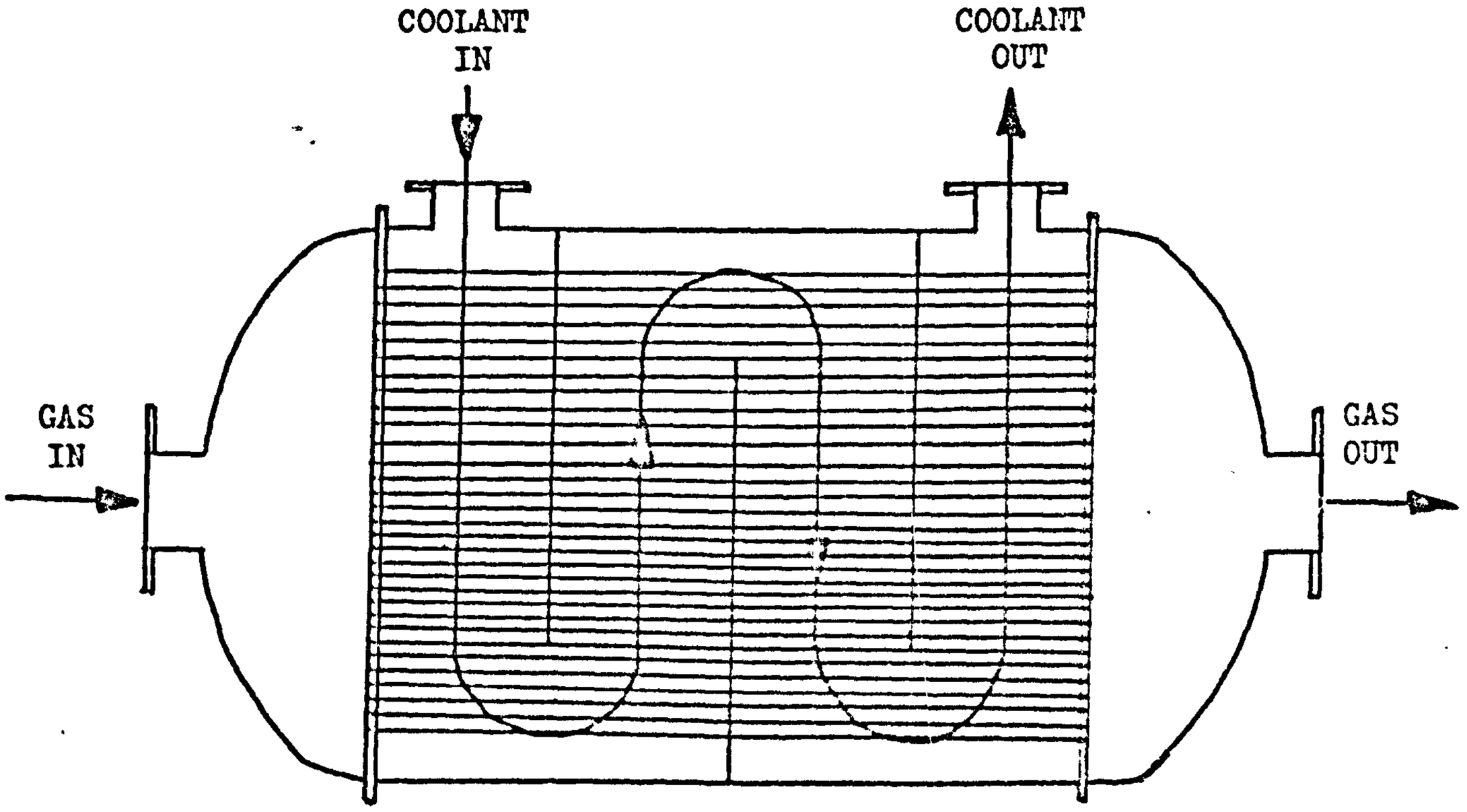

Figure 3.2 Schematic diagram of a cross-flow multitubular reactor.

across the tube bundle and diverted by a distribution plate so that it flows parallel to the tubes, either co- or counter-currently to the direction of the reacting gases. The advantage of this construction is that a uniform temperature distribution can be obtained perpendicular to the coolant flow making it very useful where temperature sensitive catalyst are used. The difficulties are that no reaction occurs before the coolant distribution plate, crossflow conditions exist in this region and as temperature gradients are present in the direction of coolant flow, tubes at opposite ends of the bundle experience different environments. An additional advantage stems from the broad cross-section available for coolant flow, since pumping costs are reduced because of the low pressure drop. Unfortunately, the resulting low coolant velocities produce tube to coolant heat transfer coefficients much lower than for other configurations, even when high circulating volumes are used.

b. Cross-Flow Reactor

This type of reactor, shown in figure 3.2, is arranged in several sections by means of baffle plates so that the coolant is always flowing perpendicular to the tube bundle. An element of coolant will therefore make several passes over the bundle before completing its journey through the reactor. The overall directions of flow can again be either co- or counter-current to the reacting fluid.

The main advantage of this reactor is the very high heat transfer coefficient possible with crossflow. However, there are several disadvantages. First, because of the high pressure drop, a large pump capacity is necessary, even for low circulation rates. Secondly, the long path through the reactor causes heating up of the coolant, and tubes on opposite sides of the bundle can exhibit very different behaviour owing to the changing conditions across the reactor diameter. Also,

because of the need to leave expansion gaps between the tubes and baffle plates significant coolant leakage can occur, so that unless care is taken, a distorted flow pattern can result which may lead to 'dead spots' in the coolant circuit and the possibility of overheating of the tubes. Despite these difficulties the crossflow reactor is very popular industrially and most of this study will be devoted to this type of configuration.

c. Radial Flow Reactor (Figure 3.3)

The coolant is guided by a ring pipe around the circumference of the reactor and enters the tube bundle through openings in the shell. Disc and doughnut baffle plates are placed in the system so that the coolant effectively traverses the bundle several times before leaving via another ring pipe at the extreme end of the shell from its entry.

This type, like the crossflow, has the advantage of a high heat transfer coefficient, but because of the large cross sections available for flow two main disadvantages are apparent. First unless very high coolant throughputs are used the coolant velocities are such that the heat transfer coefficients, though larger than for parallel flow, are still lower than the crossflow arrangement. Second, because of the low pressure drop uneven coolant distributions can occur, the resulting coolant temperature variations leading to large conversion differences from tubes around the bundle and even tube burnout. The main advantage of this configuration however is that, since the coolant only travels half the distance compared to the crossflow arrangement the temperature rise throughout can be considerably less, which, under certain circumstances can be an advantage.

As this reactor arrangement is essentially crossflow in its heat transfer characteristics, it can be treated as an equivalent crossflow reactor and so will not be given any further special configuration in the

Figure 3.3 Schematic diagram of a radial flow multitubular reactor.

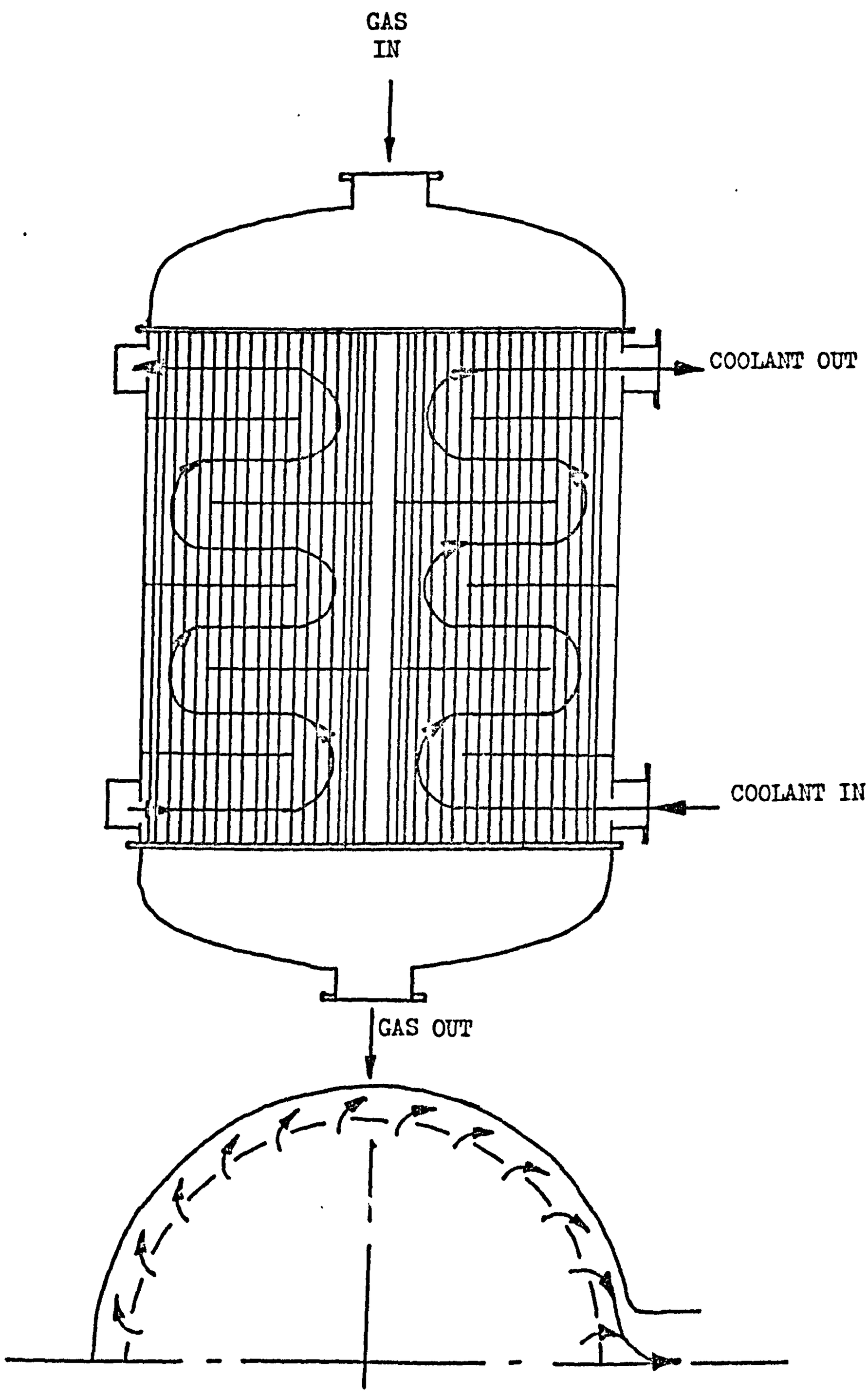

present study.

Industrial size units based on the above types of configuration may, using techniques recently evolved, consist of up to 30,000 tubes. The shell, may therefore be several metres in diameter, requiring it to be fabricated in several parts and expertly welded. The highly corrosive nature of the high temperature salts used as coolant, requiring every joint to be severly checked, usually means that fabrication cannot take place on site, hence the overall limit on the reactor size comes from the need to transport the unit from factory to site.

3.2 Model Assessment

Preliminary design calculations for the above types of reactors are usually based upon the assumption that it is possible to represent the system by a single typical tube in the bundle. In fact, when the reactant state variables at all the tube inlets are equal and the coolant enters the system at a uniform temperature, this assumption is valid for parallel flow reactors[41]. This is because there are no radial temperature gradients in the coolant and although coolant heating does occur this is restricted almost solely to the axial direction. Unfortunately, this approach does not allow a description of the influence of the coolant to be accounted for in the crossflow type of reactor configuration. Consequently, without such information, it is not possible to say how the distribution of the heat of reaction affects the performance, since in certain circumstances significant interaction between tubes can occur, depending on the relative magnitudes of the heat generation and exchange terms. In these circumstances therefore, it is important to know what considerations must be taken into account and, if possible, what approximations might be appropriate in formulating practical models for design and control studies.

Formulating a suitable model is not necessarily straight-forward

since certain incompatabilities in the alternative representations are possible. Overall, the heat balance for each representation must agree, but this can be achieved by a number of different flow distributions, each of which will result in characteristic internal heat exchange patterns. These, in turn, produce different temperature distributions, and consequently varying inter-tubular heat exchanges.

At present there appears to be no definitive answer to this problem, and it is more constructive to examine the consequences of using the various feasible alternative representations to try and draw some conclusions as to the most significant factors and the influence they have on predicted performance. Because of the highly interactive nature of the problem, it will not always be apparent which factors will be crucial, and so such a heuristic approach is particularly useful.

For a preliminary study it is realistic to confine attention to the simple reaction scheme, A→B, carried out in a multitubular co-current crossflow reactor. This is typical of a great many reactions where limiting conditions, such as temperature runaway, apply. As typical of a class of commercially important reactions it will be useful to adopt data for one particular system as the basis for a case study since this will ensure that a realistic balance between the various parameters is maintained. In what follows the system involving the partial oxidation of benzene with air will be considered. Although an essentially complex reaction, it nevertheless meets the proposed criteria for approximating a simple scheme, particularly in respect of the heat effects and sensitivity to temperature runaway under certain conditions. The major kinetic and heat transfer data for the above reactions are given in table 3.1, together with the basic reactor hardware information.

T A B L E 3.1

Typical Data Set Used in the Thesis

A_o	$8.29 * 10^{10}$	sec^{-1}
E	$1.114 * 10^{5}$	J $kgmol^{-1}$
$(-\Delta H)$	$1.256 * 10^{6}$	J $kgmol^{-1}$
D_{P_A}	$3.66 * 10^{-7}$	m^2 sec^{-1}
k_{g_A}	0.0436	m sec^{-1}
h	50.2	W m^{-2} $^oC^{-1}$
b	2.1	mm
L	5.0	m
u	2.62	m sec^{-1}
R	21.0	mm
R_2	25.0	mm
U	196.8	W m^{-2} $^oC^{-1}$
e	0.4	
c_p	1.05	kJ kg^{-1} $^oC^{-1}$
$\rho^* c_p^*$	0.074	MJ m^{-3}
K_p	0.211	W m^{-1} $^oC^{-1}$
T_o'	520.0	K
T_c'	520.0	K
C_o	$2.84 * 10^{-4}$	kgmol m^{-3}
e_c	0.43	
ϵ_c	0.2	
K_c'	$6.3 * 10^{-1}$	W m^{-1} ^oC
$\ddot{u}_c$	0.05	m sec^{-1}
m_c	0.281	kg sec^{-1}
ρ_c	$1.72 * 10^{3}$	kg m^{-3}
c_{p_c}	1.56	kJ kg^{-1} $^oC^{-1}$
P_D	0.0525	m
L_c	3.125	m

N_T	50	
Number of Coolant Passes	= 2	
Total Number of Tubes	= 2,500	
θ	$1.0 * 10^{6}$	
B_o	$4.602 * 10^{-5}$	
Sh_A	500.0	
Nu	1.0	
G_1	0.84	
G_2	0.0949	
G_3	0.84	
G_4	76.85	
Nu_w	14.6	
K_T	1.55	sec
T_o	0.03884	
T_c	0.03884	
C_{A_o}	1.0	
A_1	200.0	
A_2	26.25	
G_c	98.25	
G_{cc}	15.7	

3.3 Formulation of Alternative Representations

It is not realistic in the present state of knowledge to speculate on how the various interactions in the system will affect the behaviour in general terms. Rather, it will be more instructive to examine and compare alternative approximations of the same problem. There would appear to be three main approaches to the problem which merit further investigation:

(i) A constant coolant temperature around a single reactor tube, which will be referred to as model A.

(ii) A single tube with the coolant flowing parallel to the axis of the reactor tube, identified as model B.

(iii) A multitubular assembly, taking into account the heat distribution effects of the coolant as it flows across the tubes in the bundle; essentially it makes the problem analogous to a shell and tube heat exchanger with internal heat generation. This will be referred to as model C.

In each of the above cases it will be adequate to use the one-dimensional heterogeneous reaction model developed by Thornton[15] to represent the tubeside behaviour. This model, which uses a parabolic radial temperature profile assumption, is presented in Appendix B.

Model A:

This is obviously the simplest description of the reactor, no account being taken of the interactive heat transfer between the tubes, and so any feedback of heat through the coolant is ignored. It has been the model most commonly used when detailed calculations are carried out. For the reaction inside the tube, the dimensionless mass and energy balances, which are described in Appendix B, become:

Fluid Field

$$\frac{dC_A}{dz} + G_2 \theta^2 \eta \exp\left\{-\frac{1}{T}\right\} C_A = 0 \qquad (3.1)$$

$$\frac{dT}{dz} - G_4(t - T) + \frac{2Nu_w^*}{G_3}(T - T_c) = 0 \qquad (3.2)$$

with initial conditions $T = T|_{z=0}$

$$C_A = C_A|_{z=0} \qquad (3.3)$$

where T_c is the constant dimensionless temperature of the coolant and the effectiveness factor, η , is given by:

$$\eta = \frac{1.5\, Sh_A (r - g)}{\phi^2 (sg + r)} \qquad (3.4)$$

Reaction on the Solid:

The equations can be combined using the isothermal pellet assumption of Cresswell[12], as shown in Appendix A, to give:

$$t = T + \frac{B\, Sh_A (r - g)}{(sg + r)} \qquad (3.5)$$

which must be solved iteratively to find the solid temperature and hence the reaction rate.

Model B:

The working assumption here is that a single tube is representative of the entire assembly in the reactor, and although it takes into account coolant heating as it flows along the tube, it is not suitable for representing the effective heat transfer interaction between tubes. Nevertheless there is more scope than in the case of model A for approximating the description to that of a multitubular assembly by using a modified wall Nusselt number and by adjusting the mass flowrate

of the coolant so that the fraction associated with one tube is the same as in the multitubular case.

Together with the reactor tube equations of model A, it is necessary to consider the following heat balance for the coolant:

$$\frac{dT_c}{dz} = \frac{2Nu_w^*}{G_{cc}} (T - T_c) \qquad (3.6)$$

where $G_{cc} = \frac{M_c C_{p_c}}{\pi K_f e L}$ with an initial condition $T_c = T_c\big|_{z=0}$.

This model and its method of solution are detailed in Appendix C.

Model C:

This model is designed to give specific consideration to the flow of the coolant over the array of tubes and take account of the inter-active effects of heat transfer throughout the bundle. It formally allows for coolant temperature gradients not only parallel to the axis of the tubes, but also across the bank, i.e. it is essentially a two-dimensional field with respect to the coolant temperature distribution. The heat balance for the coolant, outlined in Appendix D, may then be described by the following equation:

$$\frac{\partial^2 T_c}{\partial z_c^2} - A_1 \frac{\partial T_c}{\partial x} + A_2 Nu_w^* (T - T_c) = 0 \qquad (3.7)$$

$$\text{with the inlet condition } T_c = T_c\big|_{x=0} \qquad 0 \leqslant z_c \leqslant 1 \qquad (3.8)$$

$$\text{boundary condition } \frac{\partial T_c}{\partial z_c} = 0 \quad @ \begin{cases} z = 0 \\ z = 1 \end{cases} \qquad 0 \leqslant x \leqslant 1$$

The nomenclature used in describing this representation is shown in figure 3.4.

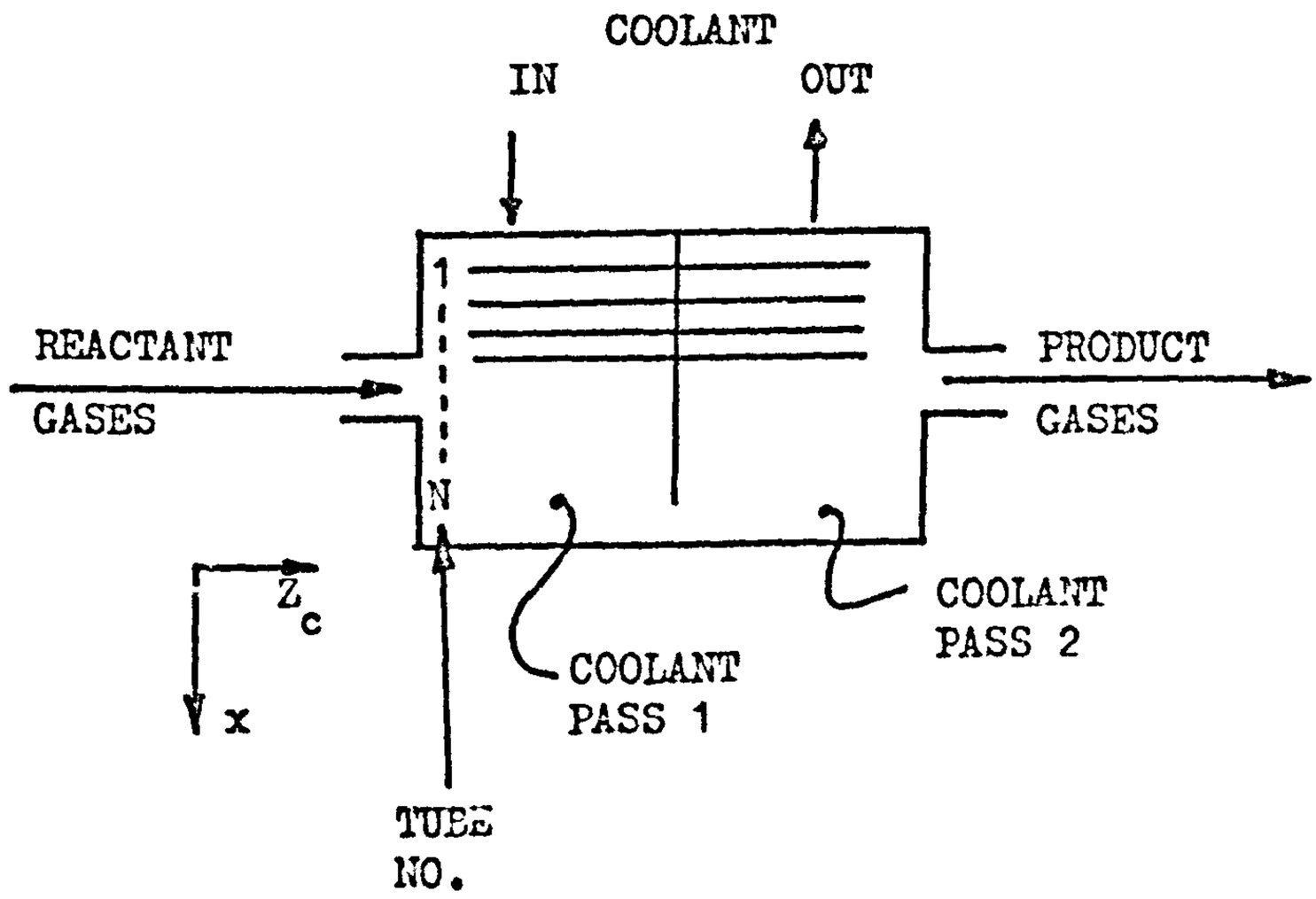

Figure 3.4 General representation of the reactor indicating the notation used in describing it.

Clearly, it is to be expected that there will be considerable differences in the computational requirements for each of these models, so that they are not all equally suitable for routine use. An important consideration, therefore, is to ascertain which will be suitable for surveys of operating conditions for control and optimization.

3.4 Discussion

A comparison of the operational stability of the reactor using the above models is conveniently done using the dimensionless T vs. B phase plots proposed by McGreavy and Adderley[68]. These essentially allow the reactor trajectory to be plotted along with regions of potential instability or multiplicity. Referring to figure 3.5, regions of parametric sensitivity (above line X-Y) and also regions of non-unique solutions of the catalyst pellet equations can be easily represented. The results obtained for each of the above models, for the data of table 3.1 and with model C used as a two coolant pass co-current reactor assembly, are then easily depicted on this diagram. Inspection of these trajectories shows that neither of the single tube approximations exhibit temperature runaway, but the multitubular model does for some of its tubes, i.e. those furthest away from the coolant inlet (tubes 30 to 50, as shown in figure 3.4).

A plot of T versus Z for the tubeside temperature profiles of the above cases is also included in figure 3.5, together with the coolant temperature profile of tube 1, model C. The increase in coolant temperature between inlet and outlet is approximately 22 K, with a 16 K increase across the first coolant pass. Although this would possibly be high for normal operation, it could arise under unfavourable conditions and causes a shift in the tubeside hotspot towards the reactor inlet. Such a shift can become important, especially during transient operation and will be considered in a later section. Under certain

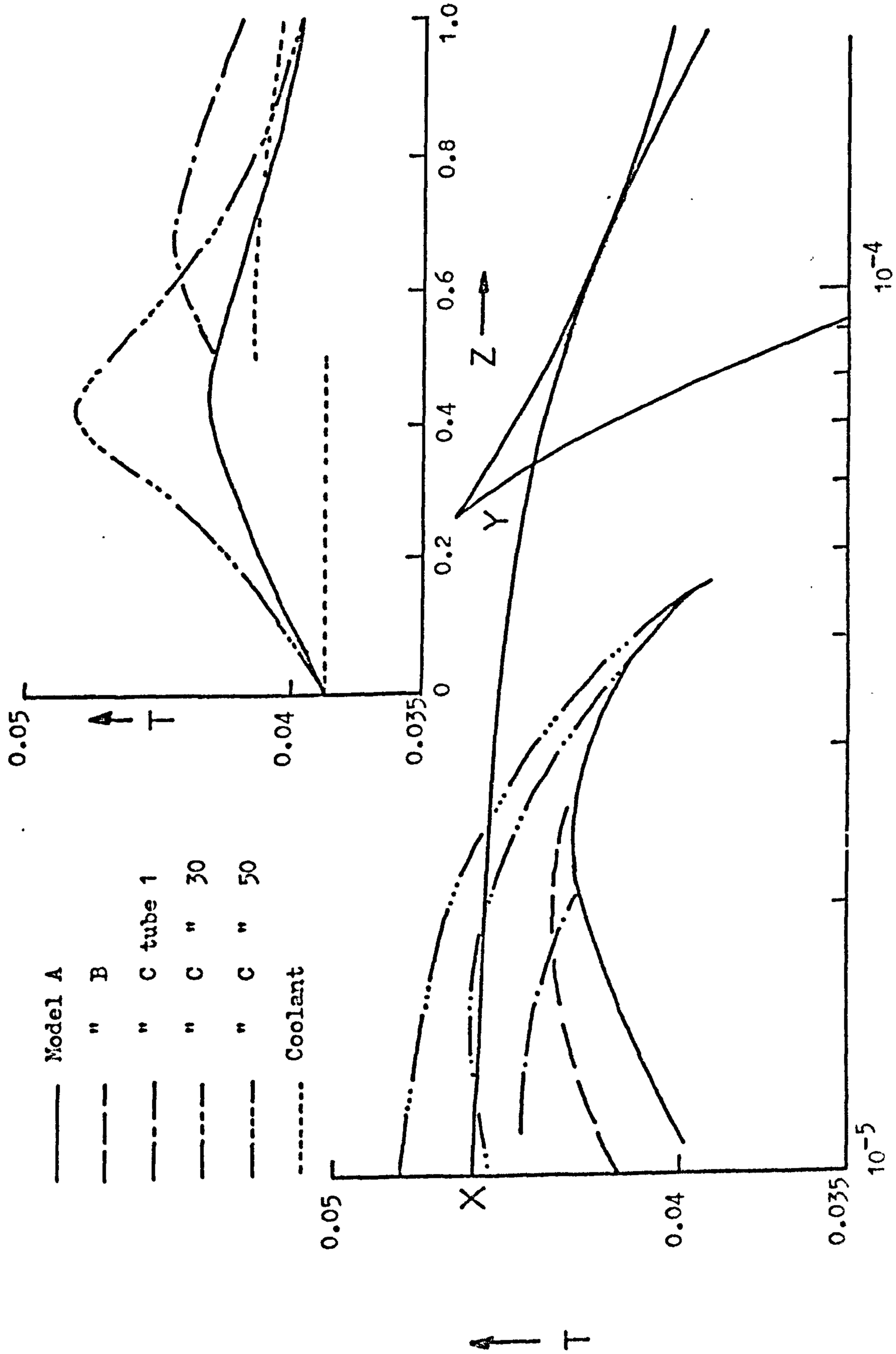

Figure 3.5 Phase plots and temperature profiles for two shell side coolant passes.

circumstances temperature rises of over 30 K are allowed in the coolant, this enables the heat of reaction to promote reaction in regions of depleted reactant, an important consideration in large units.

Inspection of the coolant temperature profile throughout the assembly shows that in fact nearly all of the temperature increase occurs in the direction of coolant flow, with very little occurring parallel to the axis of the tubes. This observation was used by Adderley[41], who developed a second representation of the tube bundle, which he called the cell model. This ignores the coolant temperature gradients parallel to the tubes and, because there is little loss of accuracy with a large reduction in computational requirements, it provides a very attractive representation. This will be used extensively throughout this work and is considered further in the next chapter.

For single tubes, stability studies have normally been carried out using an inlet coolant temperature equal to the inlet fluid temperature, on the assumption that this is the least favourable case for these reactors. An important problem when using multitubular representations is to select a suitable inlet coolant temperature for such studies. In the practical case, it is only possible to arrange for the inlet reactant and coolant temperatures to be equal for the first row of tubes, since, because of the heat exchange, the coolant will increase in temperature before meeting the others, and this can quickly lead to temperature runaway. Alternatively, the coolant temperature in the first coolant pass could be arranged such that it is never higher than that of the inlet fluid temperature, but this is difficult because of the non-linear nature of the temperature distribution across the section. To further complicate matters, although single tube studies would imply that the case of a lower inlet coolant temperature than fluid temperature is the most stable, it can in fact be unstable in the multitubular case. This is because, in tubes close to the coolant inlet, temperatures

are low enough to inhibit the reaction in the first coolant pass, enabling a high concentration of reactant to enter subsequent passes, where they are then subjected to coolant at a higher temperature. This high reactant concentration, coupled with a coolant containing heat accumulated from previous passes, can cause temperature runaway to develop. Stability studies on such reactors should therefore allow for the fact that single tube models cannot describe the coolant temperature distribution satisfactorily and hence, in such circumstances a more complex model is essential.

3.5 Concluding Remarks

A comparison between three alternative representations of a co-current, two coolant pass, crossflow multitubular reactor has shown that, in many important characteristics relevant to the design and stability studies of systems supporting highly exothermic reactions, more complex reactor models representing the overall configuration are necessary. The single tube approximations to the system commonly employed can give significantly different predictions, owing to their failure to account for the interaction between the tubes in the multitubular bundle. Furthermore, there are additional problems relating to reactor configuration to be taken into account, for which the single tube models make no provision. These problems, such as the number of passes to employ, or the best mass flowrate of coolant, are an intrinsic feature of the more complex multitubular model. In studies relating to the limits of safe operation, it is essential that these models be used, since it is just under such conditions that the discrepancies between the models are greatest, and the consequences of not meeting the basic assumptions of the simpler models of most significance.

CHAPTER 4

Steady State Models for the Multitubular Bundle

4.1 Introduction

Whilst digital simulation has provided a powerful tool in the study of chemical reactors, the considerable computational effort needed to adequately describe the behaviour of the tubeside of multitubular reactors has meant that, almost without exception, the interactive effects between tubes caused by the coolant have been ignored. As indicated in chapter three, unless the coolant is accounted for in the system heat balance, then the results of the simulation are limited to either specific systems where there is no coolant temperature rise (such as boiling or condensation), or to cases where the quantities of coolant available give rise to essentially constant coolant temperatures.

Adderley[41] made the first real attempt to tackle this problem, and his models will be introduced and used throughout this chapter. The essential requirements of any system model are that it should provide an adequate description of the system with the minimum of computational effort. This is especially true for a multitubular reactor model, where the tubeside equations have to be solved many times to give a complete description of the bundle. It is imperative therefore that such a representation contains a description of only the most important physical and chemical processes within the system.

4.2 The Assumptions Used for the Shell-Side Models

The hydrodynamics of the shell-side of large reactor assemblies is very complex. When tubes are placed into the shell a small clearance is necessary between the tube and the baffle plates to allow for thermal expansion. This annular region allows coolant to flow parallel to the tubes and through the baffle, by-passing the main coolant flow direction.

In practice the estimation of the resulting fluid by passing is one of the most difficult problems associated with heat exchanger design. The reasons for this can be visualized from figure 4.1. The quantity of coolant flowing through the tube-baffle plate clearance is determined by the pressure drop from one side of the baffle to the other. Since the pressure decreases as the fluid flows through the tube bundle, the pressure drop near the first tube row, e.g. $P_{c_1} - P_{c_5}$, will be larger than that near the last tube row, e.g. $P_{c_2} - P_{c_4}$. Clearly, the amount of fluid by-passing varies across the tube bundle. In addition, a portion of the coolant flows between the tube bundle and the reactor shell and through the annular region between baffle plate and reactor shell. However, because reactor tube bundles are not subject to the same degree of fouling as normal heat exchangers using steam, they can be built to quite small tolerances, so that these latter by-passing effects are often very small.

In the model to be derived, this by-passing of the coolant will be considered negligible. Hence, all coolant flowrates will be flowrates through the tube bundle itself. The basis for this assumption is the experimental work reported by Fricke et al.[69], which demonstrates that heat exchanger dynamics were adequately modelled when by-passing was neglected.

For a complete, accurate description of the bundle a momentum balance, as well as a heat balance, is necessary on the coolant. This would then give the pressure drop, and hence velocity, of the coolant at each point in the bundle. However, without the detailed hydrodynamic data necessary, an attempt to produce such a model would be pointless, and even when available would be very system dependant. Instead a simple model is considered, embodying specific assumptions about the coolant flow. Such models can then be used to identify which parameters were essential in more accurate surveys of specific systems.

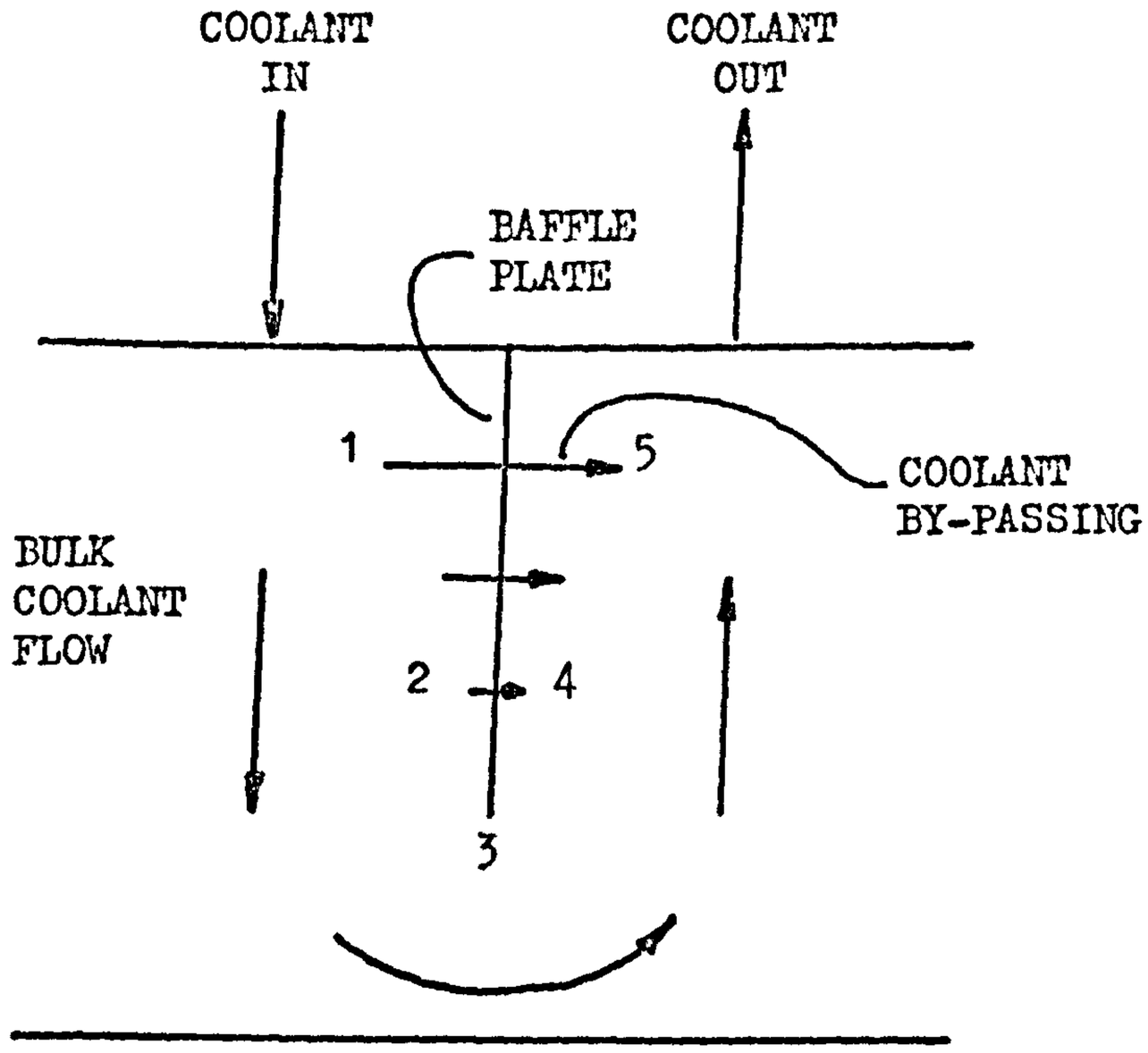

$$P_{c1} > P_{c2} > P_{c3} > P_{c4} > P_{c5}$$

Figure 4.1 Schematic diagram of the shell-side coolant flow.

One of the major assumptions made is that the coolant velocity is constant and unidirectional across the tube bundle. Clearly, this will not be the case in practice. The coolant will flow in one general direction, but it will also swirl around the tubes and vary in speed. However, as no data is available at present this assumption is necessary here. The errors introduced into the representation by this will affect the heat transfer coefficient between the tube and the coolant. Fortunately however, this outside, tube-coolant coefficient is ten to twenty times larger than the inside value[59], and so even larger variations in the external coefficient will tend to be damped out when the overall heat transfer coefficient is calculated. This can be illustrated by looking at a typical example. The internal coefficient for the system under study is typically 251.0 $W\,m^{-1}{}^{o}C^{-1}$, whilst Wanka and Guttlhuber[59] give a value for the external coefficient as 2510.0 $W\,m^{-1}{}^{o}C^{-1}$. Therefore neglecting the heat transfer resistance of the tube wall, the overall coefficient would be 228.2 $W\,m^{-1}{}^{o}C^{-1}$. On doubling the external value to 5020.0 $W\,m^{-1}{}^{o}C^{-1}$, the overall coefficient becomes 238.6 $W\,m^{-1}{}^{o}C^{-1}$. Thus, a 100% change in the value of the external coefficient has given only a 5% change in the value of the overall coefficient. Hence, it is the internal heat transfer that is limiting and so variations which arise from fluctuations in the external value of the coefficient can be neglected.

A second assumption is that although a temperature profile may develop in the coolant along the outside of the tube, there is no heat or mass transfer across the baffle plates, which are assumed to be of negligible thickness. The coolant leakage assumption has been covered earlier, and Adderley[41] has shown that the assumption of no heat transfer across the baffle causes large local gradients in the tubeside temperature profiles. While it is unlikely that such large gradients and the associated rapid changes in coolant temperature actually exist

in practice, he showed that they had little effect on the performance of the system.

While allowing for heat transfer between coolant passes would account for these effects, the extremely time consuming, nested-iterative calculations cannot be justified when compared to the accuracy of the model as a whole. Such effects will therefore not be included in this study.

Because of the tubeside model assumptions, it is satisfactory to assume a constant coolant temperature around the circumference of the tubes. Temperature variations will obviously occur around the tubes, but they would be small and could never be measured with the accuracy necessary for inclusion in a general model of the system.

A final assumption, related to that of constant coolant velocity, is that the row of tubes across the diameter of the tube bundle is characteristic of those in other parts of the bundle. The coolant velocity will, of course, be greatest at the bundle diameter and will decrease as the length of the coolant path decreases. However, such reactors are designed with an offcut in the baffle plates of approximately 20%, this portion being untubed, so that the actual cross-section of the bundle is almost rectangular. This design, in which the coolant can turn for the next pass without having to flow parallel to any of the tubes, means that no tubes have the lowered heat transfer coefficient (and hence potential hotspots) produced by parallel flowing coolant. Hence, only a small proportion of tubes close to the reactor shell will be affected by any errors introduced by this assumption, and as its relaxation would mean considering every row of tubes in the bundle, it is not considered necessary in view of the hydrodynamic data available at present.

4.3 The Co-Current Crossflowing Coolant Reactor Model

With the above assumptions, Adderley[41], using the nomenclature shown in figure 4.2, formulated two separate representations to this system. The first, a continuum model, described in Appendix D, has already been introduced in chapter three. This model assumes that the coolant can be described as a continuum containing heat sources to represent the tubes in the bundle. Temperature gradients in the coolant are accounted for both parallel and perpendicular to the coolant flow, but the large computational time needed (150 seconds on an ICL 1906A) and the very small temperature rise in the coolant perpendicular to the flow leads to the development of a second, simpler model.

This mixing cell representation of the system divides each coolant pass of the reactor into a set of cells. Each cell is assumed to contain perfectly mixed coolant so that the environmental temperature can be assumed constant along each tube section in each pass. A heat balance, using this assumption gives, as shown in Appendix E:

$$T_{c(i)} = T_{c(i-1)} + \frac{Nu_w^*}{G_c} \int_{z_1}^{z_2} (T - T_{c(i)}) \, dz \qquad (4.1)$$

where: Nu_w^* is a modified Nusselt number, used to account for the assumed parabolic radial temperature profile on the tubeside, $G_c = \dfrac{m_c \, C_{p_c}}{4 \pi K_f \, e \, L_B}$, i refers to the cell under consideration and T is the radial mean tubeside temperature, which is dependant upon $T_{c(i)}$.

Thus, for a bundle with N tubes across the diameter, for each coolant pass there are N equations of the form of equation (4.1) coupled with the tubeside equation, which produces the tubeside temperature at each point. The tubeside model used is presented in Appendix B. It is a one dimensional, heterogeneous model with an assumed parabolic radial temperature profile. The adequacy of this

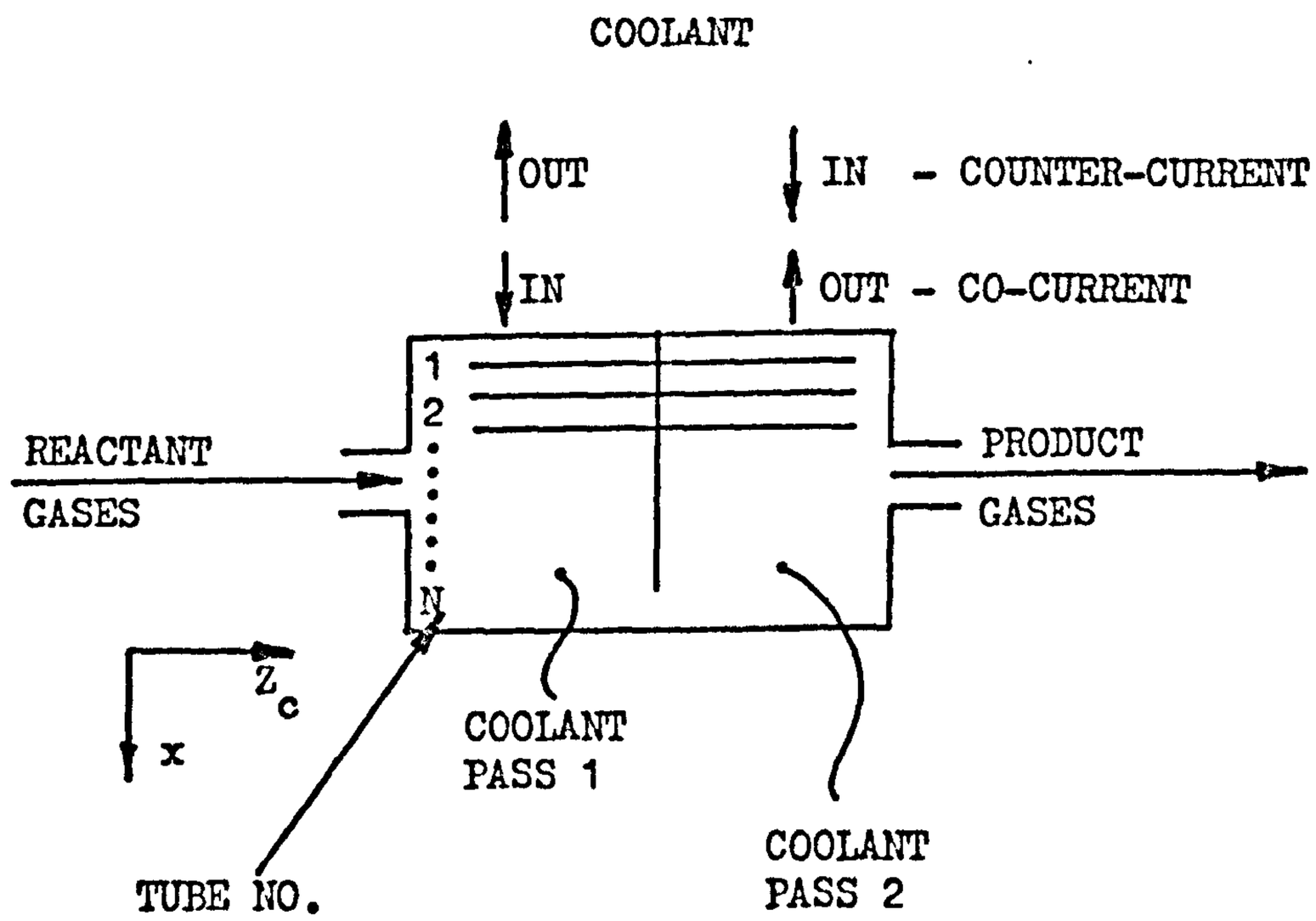

Figure 4.2 General representation of the reactor indicating the notation used in describing it.

representation will be discussed later in this chapter.

For a reactor of 50 tubes across the diameter (i.e. 49 cells) and four equal coolant passes, the computation time is approximately 60 seconds on an ICL 1906A when using the data presented in table 3.1. As can be seen from figure 4.3 the agreement between the two models is very good, the slight discrepancies occurring because of the temperature gradients perpendicular to the coolant flow predicted by the continuum model. As the flowrate of the coolant becomes very low, more and more heating of the coolant occurs and so the difference between the models becomes larger as the coolant temperature gradients become more pronounced. Nevertheless, agreement is still very good and so the cell model is evidently a perfectly satisfactory substitute for the continuum model.

Preliminary calculations have shown that, provided the coolant flowrate is not too low, a very effective simplifying assumption is possible in the case of the cell model, this being that the heat gained by the coolant in each cell is approximately constant over a certain number of cells. It is best illustrated in the following way:

From equation (4.1)

$$T_{c_{(i)}} = T_{c_{(i-1)}} + \frac{Nu_w^*}{G_c} F_{(i)} \qquad (4.2)$$

where $F_{(i)} = \int_{z_1}^{z_2} \left(T - T_{c_{(i)}} \right) dz$

similarly, for cell (i+1):

$$T_{c_{(i+1)}} = T_{c_{(i)}} + \frac{Nu_w^*}{G_c} F_{(i+1)} \qquad (4.3)$$

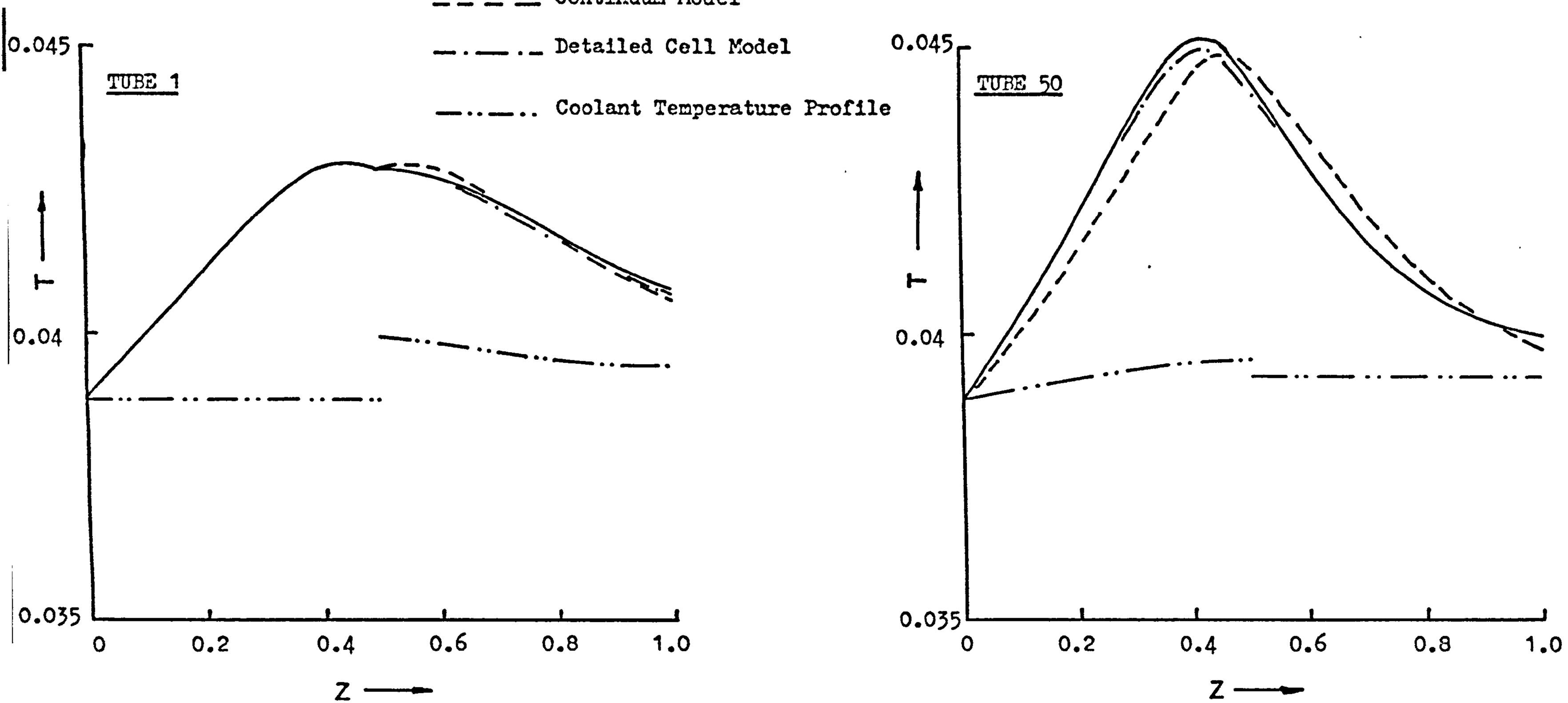

Figure 4.3 Comparison of the tubeside temperature profiles produced by the various co-current shell-side models. (Non-specified data as table 3.1)

Substituting for $T_{c_{(i)}}$ in equation (4.3) from equation (4.2) gives:

$$T_{c_{(i+1)}} = T_{c_{(i-1)}} + \frac{Nu_w^*}{G_c}\left(F_{(i)} + F_{(i+1)} \right)$$

Thus, for cell (i+n)

$$T_{c_{(i+n)}} = T_{c_{(i-1)}} + \frac{Nu_w^*}{G_c} \sum_{k=0}^{n} F_{(i+k)} \qquad (4.4)$$

Now, if $F_{(i)} \simeq F_{(i+1)} \simeq F_{(i+2)} \simeq \ldots \simeq F_{(i+n)}$, then equation (4.4) becomes:

$$T_{c_{(i+n)}} = T_{c_{(i-1)}} + \frac{Nu_w^*}{G_c} (n+1) F_{(i)} \qquad (4.5)$$

If an appropriate value of n is chosen, the approximation will be valid and equation (4.5) will hold.

Figure 4.3 shows the effect of this approximation with n = 24. The difference between the full and approximate cell models is not very large, and in fact although the saving in computer time is very great (the case shown took 9 seconds on the ICL 1906A), the loss of accuracy is quite small. If more accuracy is required then a smaller value of n can be chosen. It is interesting to note that normally the simplified model predicts higher temperatures than the detailed cell model, so that it may be treated as a safe approximation, since any operating conditions decided on the basis of the simplified model would tend to be conservative.

The simplified cell model is therefore a satisfactory representation of the co-current multitubular reactor, provided that care is taken in choosing the value of n.

4.4 The Counter-Current Crossflowing Coolant Reactor

The assumptions upon which these models are based are identical to those employed in the co-current crossflow models described in section 4.3. The only difference in the direction of flow of the coolant relative to the direction of flow of the reactant gases, this is shown schematically in figure 4.2 along with the nomenclature used in naming the tubes, passes etc.

Adderley[41] using the mixing cell arrangment as for the co-current system formulated the following model. A heat balance over cell i giving:

$$T_{c_{(i+1)}} = T_{c_{(i)}} - \frac{Nu_w^*}{G_c}\int_{z_1}^{z_2} \left(T - T_{c_{(i)}} \right) dz \qquad (4.6)$$

Again T is obtained from the one dimensional tubeside model presented in Appendix B.

For a tube bundle with N tubes across the diameter there are N equations of the form of equation (4.6) coupled with the tubeside equations, for each coolant pass. Because the coolant enters the tube bundle at the baffle section from which the reaction gases leave, an iterative approach has to be used in the solution of the equations owing to the fact that the tubeside equations must be solved from the gas inlet and, as only the coolant inlet temperature is specified, the coolant temperature at this point is not known. The coolant exit temperature is therefore assumed, and the equations solved by marching across the tube bundle in the opposite direction to the coolant flow, the coolant inlet temperature can then be computed. This can then be compared with the actual inlet temperature and if the two values do not agree, a new coolant exit temperature is assumed and the calculation repeated. Appendix F gives a full description of the procedure.

As with the co-current cell model, the assumption that the heat gained by the coolant in each cell is approximately constant over a number of cells can be used.

Putting $F_{(i)} = \int_{z_1}^{z_2} (T - T_{c_{(i)}}) \, dz$

Then from equation (4.6):

$$T_{c_{(i+1)}} = T_{c_{(i)}} - \frac{Nu_w^*}{G_c} F_{(i)} \qquad (4.7)$$

Similarly:

$$T_{c_{(i+2)}} = T_{c_{(i+1)}} - \frac{Nu_w^*}{G_c} F_{(i+1)}$$

Therefore, from (4.7)

$$T_{c_{(i+2)}} = T_{c_{(i)}} - \frac{Nu_w^*}{G_c} (F_{(i)} + F_{(i+1)})$$

Thus:

$$T_{c_{(i+n)}} = T_{c_{(i)}} - \frac{Nu_w^*}{G_c} \sum_{k=0}^{n-1} F_{(i+k)} \qquad (4.8)$$

Now, if $F_{(i)} \simeq F_{(i+1)} \simeq F_{(i+2)} \simeq \cdots \simeq F_{(i+n-1)}$

Then equation (4.8) becomes:

$$T_{c_{(i+n)}} = T_{c_{(i)}} - \frac{Nu_w^*}{G_c} n F_{(i)} \qquad (4.9)$$

Figure 4.4 shows the comparison between the detailed and approximate models for n = 6. The agreement is very good at normal coolant flow-rates, but when very low flowrates are investigated, the discrepancies between the representations become larger. In these cases a smaller value of n can be employed to obtain greater accuracy. It is interesting to note that a smaller value of n is needed in this case than was used for the co-current model of section 4.3. This arises from the much greater sensitivity to the coolant temperature caused by high outlet

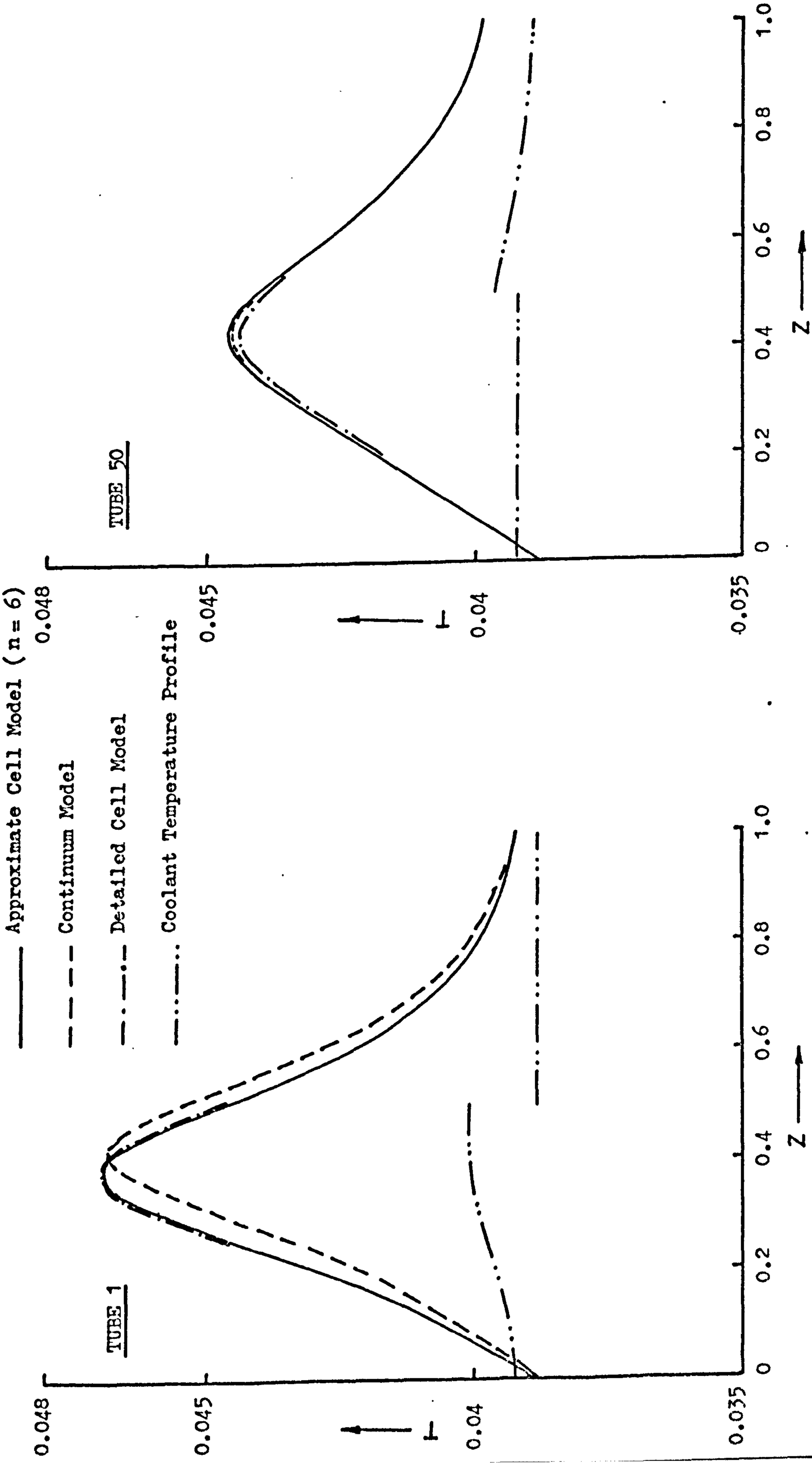

Figure 4.4 Comparison of the tubeside temperature profiles produced by the various counter-current shell-side models.
(Non-specified data as table 3.1)

coolant temperatures affecting the rich concentration of reactants entering the system. The results of this higher sensitivity will be discussed in later chapters.

The computation times of the detailed and approximate models (with n = 6) are in the ratio 5 : 1, so that the latter becomes very attractive when an initial survey of the operating region is required. Should a more detailed analysis be needed, especially at low coolant flowrates, then a smaller value of n can be used.

This counter-current model presented here is based upon the assumption that the thermal gradients in the coolant perpendicular to flow are negligible. This assumption has not been verified and in view of the greater coolant sensitivity in this case the results of the co-current representation should not be extrapolated to influence the degree of sophistication of this model. With this in mind the following continuum representation of the counter-current reactor can be formulated.

4.4.1 Counter-Current Continuum Model

The main problem in the solution of the counter-current reactor problem is that the coolant temperatures around the inlets to the reactor tubes are not known. This can easily be accounted for in the case of the mixing cell model, introduced earlier, by assuming an outlet coolant temperature and marching through the system in the opposite direction to the coolant flow, if the calculated inlet coolant temperature is equal to the true value (within error bounds) then the solution is complete. If not, the calculation is repeated using a new guess outlet temperature. In the continuum model proposed here however, the fact that a temperature gradient is allowed for parallel to the reactor tubes means that a temperature profile would have to be assumed if the same method of solution were employed. This presents computational difficulties, and in fact even if the solution converges

on the inlet coolant temperature it is doubtful that the coolant temperature gradients along the tubes are correct.

Instead a new approach is needed, one in which the start of the calculation has a known temperature profile. Figure 4.5 will help to demonstrate how this is achieved. The tubeside reaction equations are conveniently solved from the inlet to the outlet, so, using the assumption that the coolant is perfectly mixed in the turnround region between passes, the flat temperature profile entering coolant pass 1, $T_{c_{gues}}$, is assumed, and the equations solved for coolant pass 1 giving the coolant outlet temperature $T_{c_{out}}$. Coolant pass 2 can then be solved using the known inlet coolant temperature and the stored values of the tubeside state variables. Thus, the outlet coolant temperature from pass 2, T_{c_1}, is calculated. If $T_{c_{gues}}$ and T_{c_1} are equal, within the required accuracy, then the calculation is complete. If not, a new $T_{c_{gues}}$ is taken and the procedure repeated.

Using this method of solution, the equations are solved by marching across the tube bundle in the direction of coolant flow and so the heat balance derived for the co-current continuum model of section 4.3 may be used for each coolant pass in sequence. Thus, the equation governing the thermal gradients both parallel and perpendicular to coolant flow can be written as:

$$\frac{\partial^2 T_c}{\partial z_c^2} - A_1 \frac{\partial T_c}{\partial x} + A_2 Nu_w^*(T - T_c) = 0 \qquad (4.10)$$

with the inlet condition: $T_c = T_c\big|_{x=0}$ $\qquad 0 \leqslant z_c \leqslant 1$

boundary condition: $\frac{\partial T_c}{\partial z_c} = 0 \quad @ \begin{cases} z_c = 0 \\ z_c = 1 \end{cases}$ $\qquad 0 \leqslant x \leqslant 1$

The radial mean tubeside temperature, T, which is also a function of T_c, can be obtained from the heterogeneous reactor model of Appendix B.

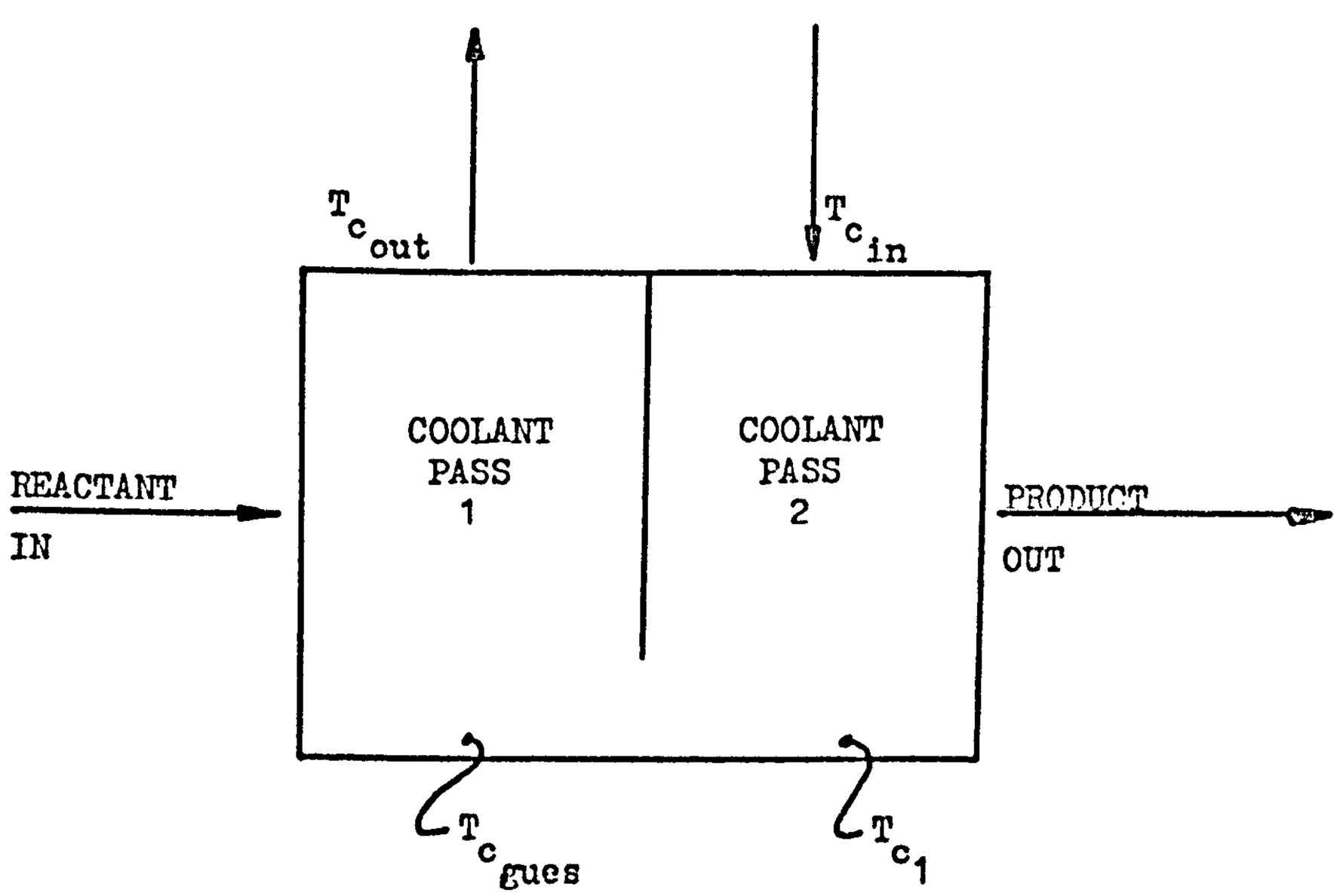

Figure 4.5 Schematic diagram showing the solution method used in the counter-current continuum model.

Equation (4.10) has been solved using the finite difference network as for the co-current reactor problem, the step lengths necessary for accurate convergence being the same. The complete solution method for a two coolant pass reactor, using the nomenclature of figure 4.5, is as follows:

1. Assume a coolant temperature profile, perpendicular to the direction of coolant flow, at the first (i.e. $T_{c_{gues}}$, the inlet temperature to coolant pass 1) or next position along the direction of coolant flow in coolant pass 1.

2. Using this temperature profile solve the tubeside model for the length of tube in this pass.

3. With the tubeside temperature profile from step (2) solve the coolant finite difference equations in the direction perpendicular to coolant flow to obtain a new coolant temperature profile in this direction.

4. Check whether the coolant temperature profile calculated at (3) agrees with that assumed at step (1). If not, using the profile of step (3), repeat the calculation from step (2). If convergence is obtained and $x < 1$ (i.e. the outlet of the coolant pass is not reached) go on to the next position in the direction of coolant flow and repeat from step (1). If $x = 1$ (i.e. the outlet from the first coolant pass is reached) continue to step (5).

5. Assume a coolant temperature profile perpendicular to the direction of coolant flow at the first (i.e. $T_{c_{in}}$, the coolant inlet to the reactor) or next position along the direction of coolant flow in coolant pass 2.

6. Solve the tubeside and coolant equations in this pass in the same way as for coolant pass 1. When $x = 1$ (i.e. the outlet from the

second coolant pass) is reached, the coolant temperature here, T_{c_1}, is compared to the value assumed in step (1). If adequate convergence is obtained the calculation is complete. If not the process is repeated from step (1) using a new value of $T_{c_{gues}}$.

The method of repeated substitution has been used for the assumed coolant temperature and is found to be adequate in most situations, giving three or four iterations. When very low coolant flowrates are used however, especially close to the region of multiple steady states in the coolant temperatures, then a more sophisticated method of approximation is recommended, such as a quadratic convergence technique, to keep the number of iterations required down to a minimum.

Reactors having more than two coolant passes can be represented in a similar manner. For example, a three coolant pass system requires two coolant temperatures to be assumed, these being the inlets to coolant pass one and two. A four coolant pass reactor requires three assumed temperatures. Obviously, the computational requirements increase dramatically as more passes are considered.

Figure 4.4 shows the comparison between the above continuum representation of a two coolant pass reactor and the detailed cell model introduced earlier. As can be seen the agreement between the models is very good, indicating that, as in the co-current reactor system, the coolant temperature gradients parallel to the tubes are small enough to be ignored when modelling the reactor. As the two coolant pass arrangement has the longest tube length per pass, as compared to three or four pass systems, it would be expected to have the most severe thermal gradients parallel to the tubes. Hence, if the gradients in the two pass system are small enough to be ignored, this is also true for systems containing more than two coolant passes.

If the approximate cell model is used with $n = 6$, again agreement

is very good (figure 4.4); in fact under the conditions used here, the approximate form of the cell model gives even closer agreement to the continuum model than the detailed form. As a result of this comparison it is concluded that the approximate cell model, with n = 6, can be used to adequately represent the counter-current reactor system, and as the computational requirements are much less than those of the continuum model for very little loss of accuracy, it will be used extensively throughout this thesis.

4.5 Representation of the Tubeside in the Steady State Multitubular Reactor

4.5.1 Introduction

The analysis of the multitubular assembly so far presented has used the one dimensional heterogeneous model of Appendix B to represent the tubeside behaviour. While this representation, using a modified Nusselt number based on a parabolic radial temperature profile, has been shown to give results suitable for an initial survey of operating conditions[15, 41], the differences between this and more accurate models accounting for tubeside radial heat and mass transport, can become significant, especially under severe operating conditions. The main problem with using such a one dimensional model is that the state variables are radial mean values. Since for non-linear functions the radial mean value is not the same as the value at the radial mean conditions, this is likely to raise problems in the evaluation of the reaction rate terms. Thornton[15] investigated this situation and concluded that, when using the one dimensional model with an assumed parabolic radial temperature profile, evaluation of the reaction rate at the radial mean conditions tended to underestimate the true values. Although the accuracy of the data used in the multitubular models is not, at present, good enough to warrant the use of a more complex

model during general studies of operating conditions, it is useful to produce such a model to see just how significant the errors introduced by the assumptions used in the one dimensional model are.

4.5.2 The Two Dimensional Tubeside Model

This model, proposed by Naim[35], is outlined fully in Appendix G. The dimensionless heat and mass balance equations, having had their radial differential operators reduced by the orthogonal collocation procedure, become:

$$\left.\frac{dT}{dz}\right|_J = \frac{1}{G_3}\sum_{i=1}^{N} W_{J,i}T_i + \frac{1}{G_3}\cdot V_J + G_4(t_J - T_J) \qquad (4.11)$$

$$\left.\frac{dC_A}{dz}\right|_J = \frac{1}{G_1}\sum_{i=1}^{N} Q_{J,i}C_{A_i} - G_2\ \eta_J\ \phi^2 C_{A_J} \qquad (4.12)$$

$$J = 1, 2, \ldots, N$$

with the initial conditions:

$$C_A(z) = C_{A_J}(0)$$

$$T(z) = T_J(0)$$

$$\text{at } z = 0,\ 0 < r < 1$$

where: $$\sum_{i=1}^{N} W_{J,i} = \sum_{i=1}^{N}\left\{B_{J,i} - \frac{B_{J,N+1}\cdot A_{N+1,i}}{Nu_w + A_{N+1,\,N+1}}\right\}$$

$$\sum_{i=1}^{N} Q_{J,i} = \sum_{i=1}^{N}\left\{B_{J,i} - \frac{B_{J,N+1}\cdot A_{N+1,i}}{A_{N+1,\,N+1}}\right\}$$

and $$V_J = \frac{B_{J,N+1}\cdot Nu_w\cdot T_c}{Nu_w + A_{N+1,\,N+1}}$$

The $A_{J,i}$ and $B_{J,i}$ are the collocation coefficients for the first and second order differential operators respectively, N being the number of interior zeros of the orthogonal polynomial used. Explicit forms for A and B may be found in Appendix G.

Equations (4.11) and (4.12) form an initial value problem and can be solved by any suitable method. Owing to the possibility of steep axial temperature gradients the fourth order Runge Kutta Merson routine, with a self adjusting step size, has been used in this study. The radial temperature profile, approximated by Legendre polynomials can give four significant figure accuracy when three interior collocation points are used. Increasing this value to N = 4 gave no significant increase in accuracy under the conditions used, though it is recommended that N = 4 be used when extremely steep radial gradients are encountered.

Coupling equations (4.11) and (4.12) with the mixing cell model the overall reactor performance can now be investigated. Since it is possible to find an accurate value of the tubeside temperature at the wall this can be used in the equations instead of the radial mean tube-side temperatures used in equations (4.1) and (4.6). Thus, the cell model equations become:

a) For the Co-Current Reactor Model

$$T_{c(i)} = T_{c(i-1)} + \frac{Nu_w}{G_c} \int_{z_1}^{z_2} \left(T|_{y=R} - T_{c(i)} \right) dz \qquad (4.13)$$

and b) The Counter-Current Model

$$T_{c(i)} = T_{c(i-1)} - \frac{Nu_w}{G_c} \int_{z_1}^{z_2} \left(T|_{y=R} - T_{c(i-1)} \right) dz \qquad (4.14)$$

where $T|_{y=R}$ = Tubeside temperature at the wall and from Appendix G,

$$T|_{y=R} = \frac{\left(Nu_w \, T_{c(i)} - \sum_{k=1}^{N} A_{k,N+1} \cdot T_{(k)} \right)}{\left(Nu_w + A_{N+1,\,N+1} \right)}$$

Figure 4.6 shows the axial centre-line temperature profiles for both the one and two dimensional tubeside models, when using the data of table 3.1 in a co-current, four coolant pass reactor with a low coolant

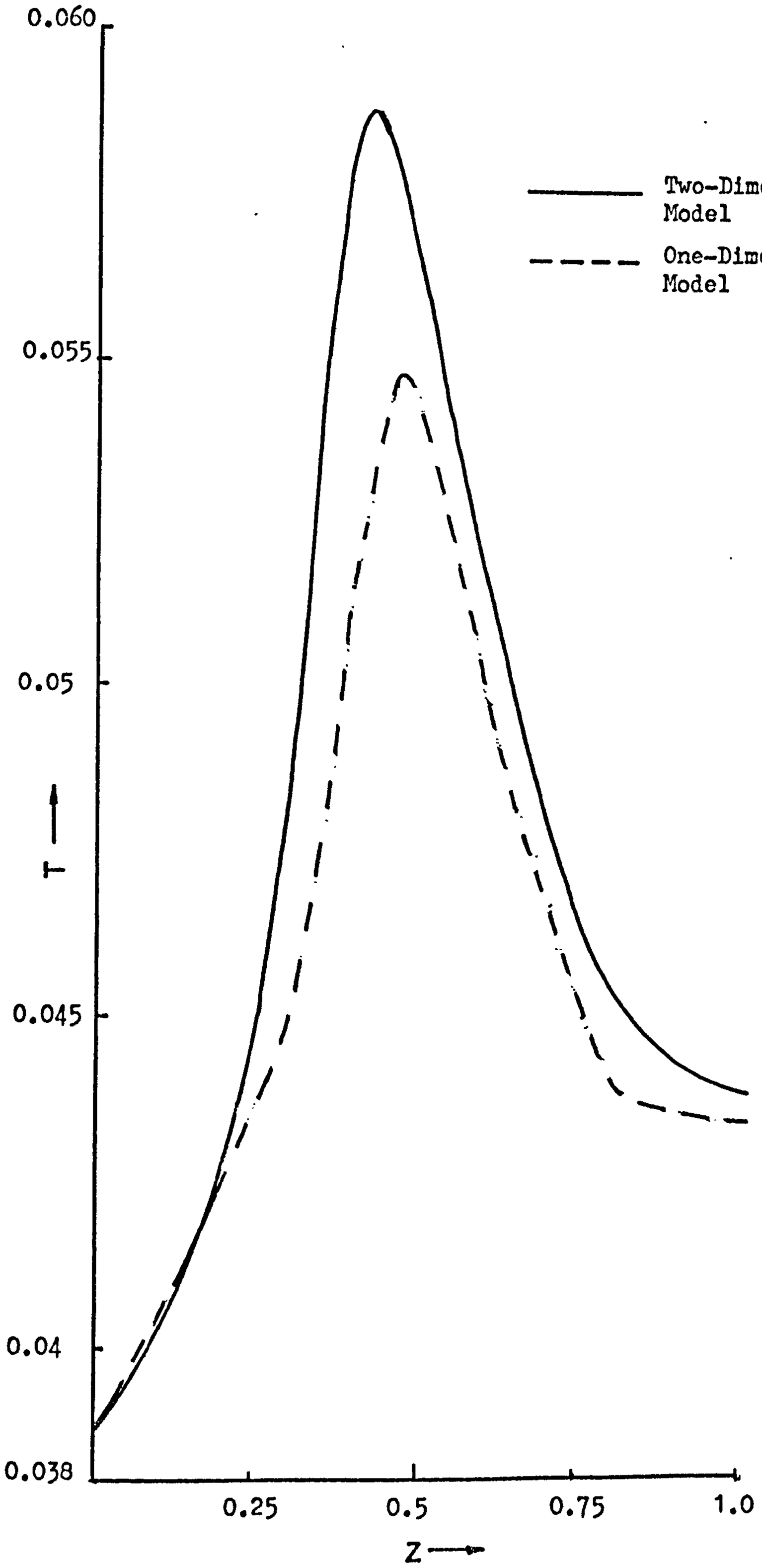

Figure 4.6 Comparison of the one- and two-dimensional tubeside models for a co-current reactor. (Non-specified data as table 3.1)

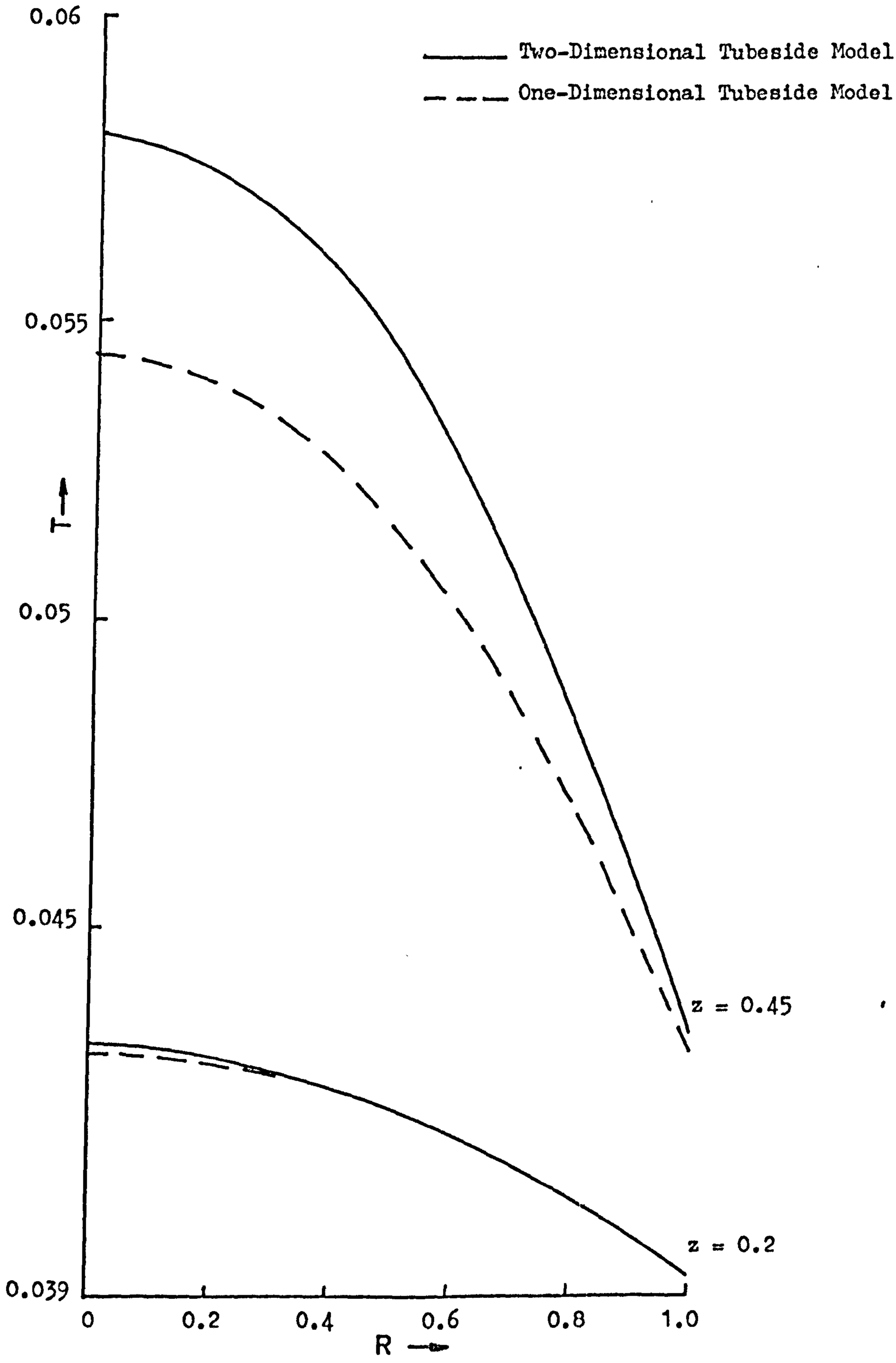

Figure 4.7 Comparison of the radial temperature profiles of the one- and two-dimensional tubeside models. (Non-specified data as table 3.1)

velocity (G_c = 98.25). The one dimensional model, which tends to overestimate the modified Nusselt number at the wall, Nu_w^*, underestimates the centre line temperature in the reactor. The radial temperature profiles produced in the two dimensional representation are given in figure 4.7, which shows how they depart from the parabolic profiles assumed in the simpler model.

Although the peak temperature is underestimated (the complex model gives a peak of 784K, and the one dimensional model 732K), the simpler model still shows all the qualitative features of the reactor and has the great advantage that its computation time is much less. Thus the profiles given here took approximately nine seconds on an ICL 1906A for the simple model, whereas the two dimensional representation, which used four collocation points because of the steep radial profiles, took approximately one minute on the same machine. Both representations used the simplified cell model given by equation (4.5) with n = 24, so that in the 49 cell per pass system used here the tubeside is evaluated three times per pass. Obviously, the complex tubeside model is unsuitable for use in the detailed cell model where the tubeside equations are evaluated 49 times per pass, and even when the simplified cell model is used, general surveys of reactor operating conditions would require an excessive amount of computation.

The corresponding reactor temperature profiles for counter-current coolant flow are shown in figure 4.8, the data being the same as for figure 4.6, except that the coolant flowrate is five times larger, i.e. G_c = 491.25. This higher flowrate is necessary because the counter-current reactor is much more sensitive to the coolant temperature and, as will be shown later, needs much higher coolant velocities than the co-current flow configuration.

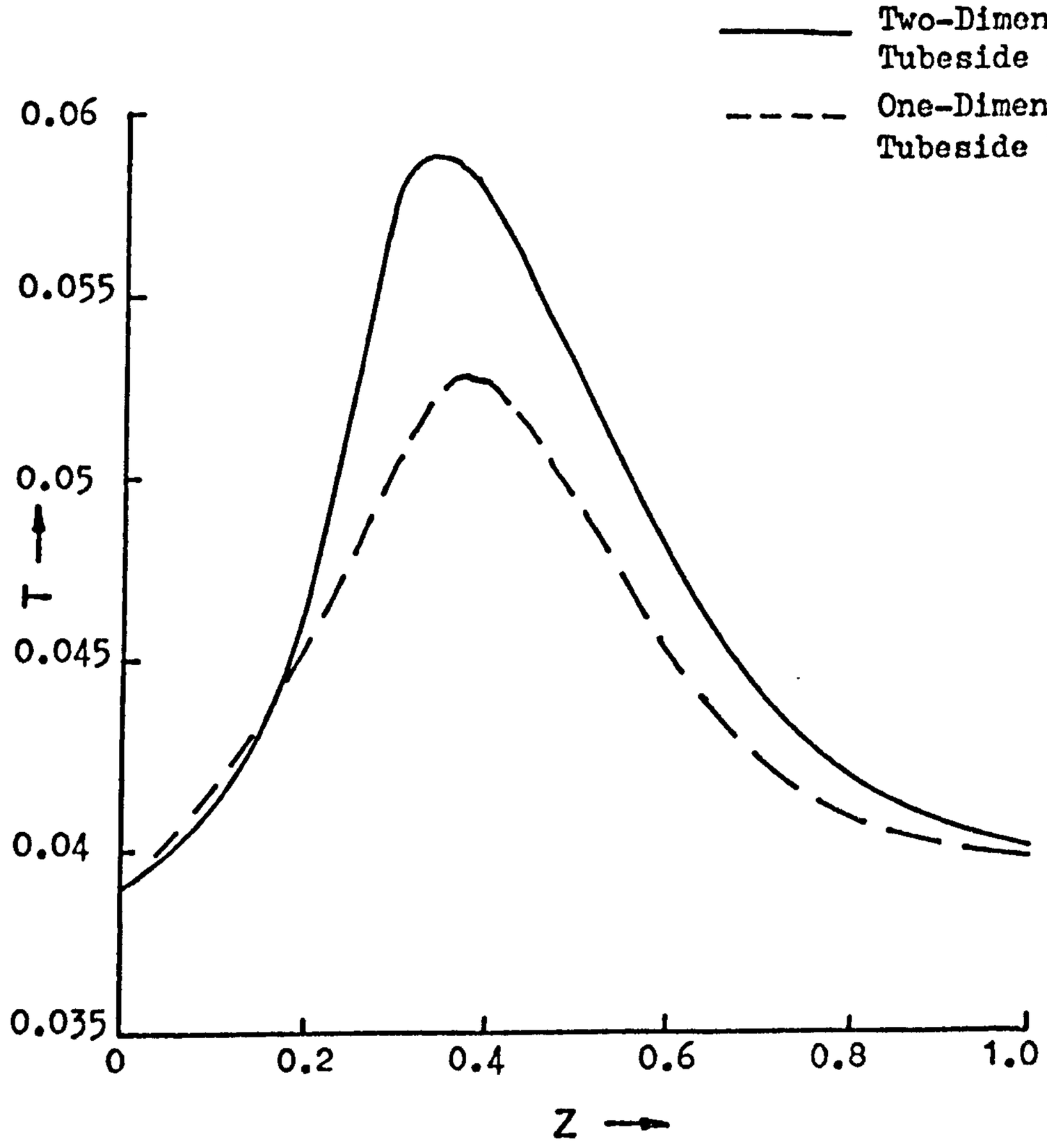

Figure 4.8 Comparison of the one- and two-dimensional tubeside models for a counter-current reactor. (Non-specified data as table 3.1)

Since the one dimensional tubeside model gives a good qualitative picture of reactor behaviour without the need for the excessive computation times of the more complex model, it will be used throughout this present study to give an insight into the interactions between the coolant and the tubes in large multitubular bundles.

4.6 Conclusions

Several different representations of multitubular reactor bundles have been introduced. On the shell-side it has been demonstrated that the temperature gradients in the coolant along the tubes could be ignored, so that the mixing cell model is suitable both in terms of accuracy and computation time. This model, with the added attraction of the ease with which it can be simplified, reducing its computation time still further, will therefore be used to represent both co- and counter-current reactor configurations throughout this study.

The representation of the tubeside has also been considered and, although the one dimensional model with its assumed parabolic radial temperature profile tended to underestimate the more complex two dimensional model, it gave very good agreement in its qualitative predictions. As this is primarily an initial study of the effects produced in large multitubular assemblies, a qualitative picture of reactor performance is adequate in formulating generalized criteria for the behaviour of such systems. Indeed, at the present time the accuracy of the data does not warrant the use of an unduly complex tubeside model, so that even if the two dimensional model were used the absolute value of the results would hardly be significantly improved. In view of this, the simple one dimensional model described earlier will be used throughout the remainder of this study.

CHAPTER 5

The Steady State Behaviour of Multitubular Reactors.

1. Co-Current Cooling

5.1 Introduction

Present reactor design methods, based on the assumption that the tube bundle can be represented by a single, typical tube are perfectly adequate when dealing with operating conditions that do not enter regions close to those of potential instability, or involve any abnormal behaviour such as maldistribution of feed stock among tubes. However, when seeking high performance from a given unit it is possible that the preferred operating state is close to these regions and, if such designs are to be considered it is essential to have reliable information on the behaviour of the system under these circumstances so that potential hazards can be evaluated.

The following chapters consider the effects of allowing for the multitubular characteristics by using the models developed in chapter four. This can result in significant effects, not only on the stability of the systems but also on the economic viability of using alternative reactor configurations. Because of the inherent differences between the co- and counter-current coolant flow reactors, these will be considered in separate chapters, a comparison and summary of their behaviour being given in chapter seven. This chapter deals with the co-current cooling configuration and shows the significance of the distribution of the reaction heat around the system. It is shown how single tube models cannot take into account the basic structure of the tube bundle and emphasizes the point that many designs fail to use the heats of reaction evolved in an effective way.

5.2 A Two Coolant Pass System

The overall configuration of multitubular reactors has already been dealt with in chapters three and four, and figure 3.4 shows the arrangement of this, the simplest form of crossflow reactor to be considered. During this study, unless otherwise stated, the data of table 3.1 will be used to ensure consistancy throughout; and in describing the tube bundle, tubes 1 and 50 will be shown, these representing the extreme conditions in the reactor. Other tubes have conditions intermediate between these two.

The tubeside profiles of tubes 1 and 50 for various coolant velocities are shown in figure 5.1. The most striking feature of these are the large differences between tubes at extreme ends of the bundle. The peak temperature is larger for tube 50 and always occurs in coolant pass 1, whereas that for tube 1 occurs in coolant pass 2. Increasing the coolant velocity (and hence decreasing the residence time of the coolant in the reactor) has a considerable effect on the shape of the temperature profiles, tending to make them more uniform across the bundle, reducing the peak temperature and moving the peak towards the reactant outlet. The coolant temperature rises for the cases shown in figure 5.1 are 56 K, 28 K and 13 K for the coolant velocities 0.05, 0.1 and 0.2 m/sec respectively. As a frame of reference, coolant temperatures of the order of 10-20 K can be considered normal operating conditions encountered industrially. However, higher temperature rises of over 30 K can be used to promote increased reaction in the latter half of the bed where the reactants are becoming depleted. This type of operation will be considered more fully at a later stage. The very high temperature rise of 56 K, considered in figure 5.1, would be unacceptable during normal operation. Though these cases should be considered when designing or studying the operability of a plant because low coolant velocities may arise under abnormal conditions such as pump

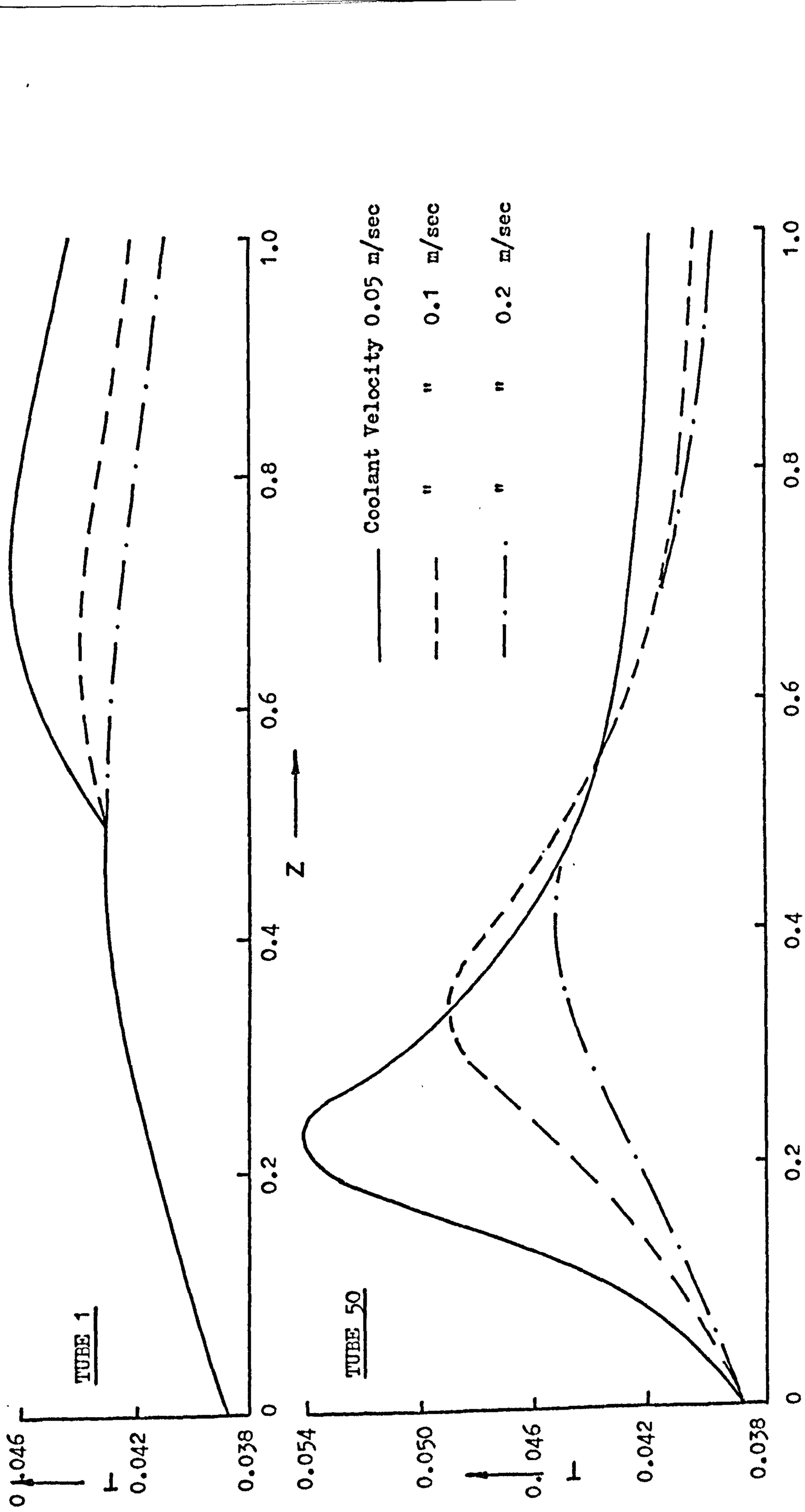

Figure 5.1 Tubeside temperature profiles for different coolant flowrates in a two coolant pass co-current reactor. (Non-specified data as table 3.1)

failure, pipe blockage or pressure leakage. It is under these conditions that safety measures must be quickly applied, and as these cannot be tested adequately on the plant, simulation methods can usefully be employed to plan appropriate emergency procedures. The main problems arising from very high coolant temperatures, apart from the large differences between tubes at either end of the bundle, are that the coolant might decompose or enhance corrosion of the shell and tubes. In the case of the molten salts considered here, charring and decomposition can occur, causing fouling of the coolant flowpaths and a lowering of the coolant-side wall heat transfer coefficient.

Figure 5.2 shows the effect of lowering the coolant inlet temperature below that of the inlet reactant temperature for the worst case in figure 5.1. The extent of conversion and maximum tubeside temperature are both reduced, and when the temperature is low enough (see the case with the coolant temperature of 500 K) the position of the maximum tubeside temperature moves across the tube bundle from tube 50 pass 1 to tube 1 pass 2. Movement of this type can present serious problems in monitoring the reactor performance, since it is preferable not to have to place thermocouples in every tube in the system.

Raising the reactant inlet temperature, figure 5.3, moves the tubeside temperature peaks towards the reactant inlet, increases the height and gives greater conversion. Once again it can be seen that the position of the maximum temperature on the tubeside of the bundle cannot be predicted <u>a priori</u>. Lowering the reactant temperature moves the position of this maximum from tube 50 pass 1 to tube 1 pass 2. The effects of hotspot movements will be considered more fully in section 5.4. It is significant that the highest tubeside temperature occurs in either tube 1 or tube 50, since these represent the two extremes within the bundle. The exact position depends upon the inlet parameters to the system and the configuration of the reactor.

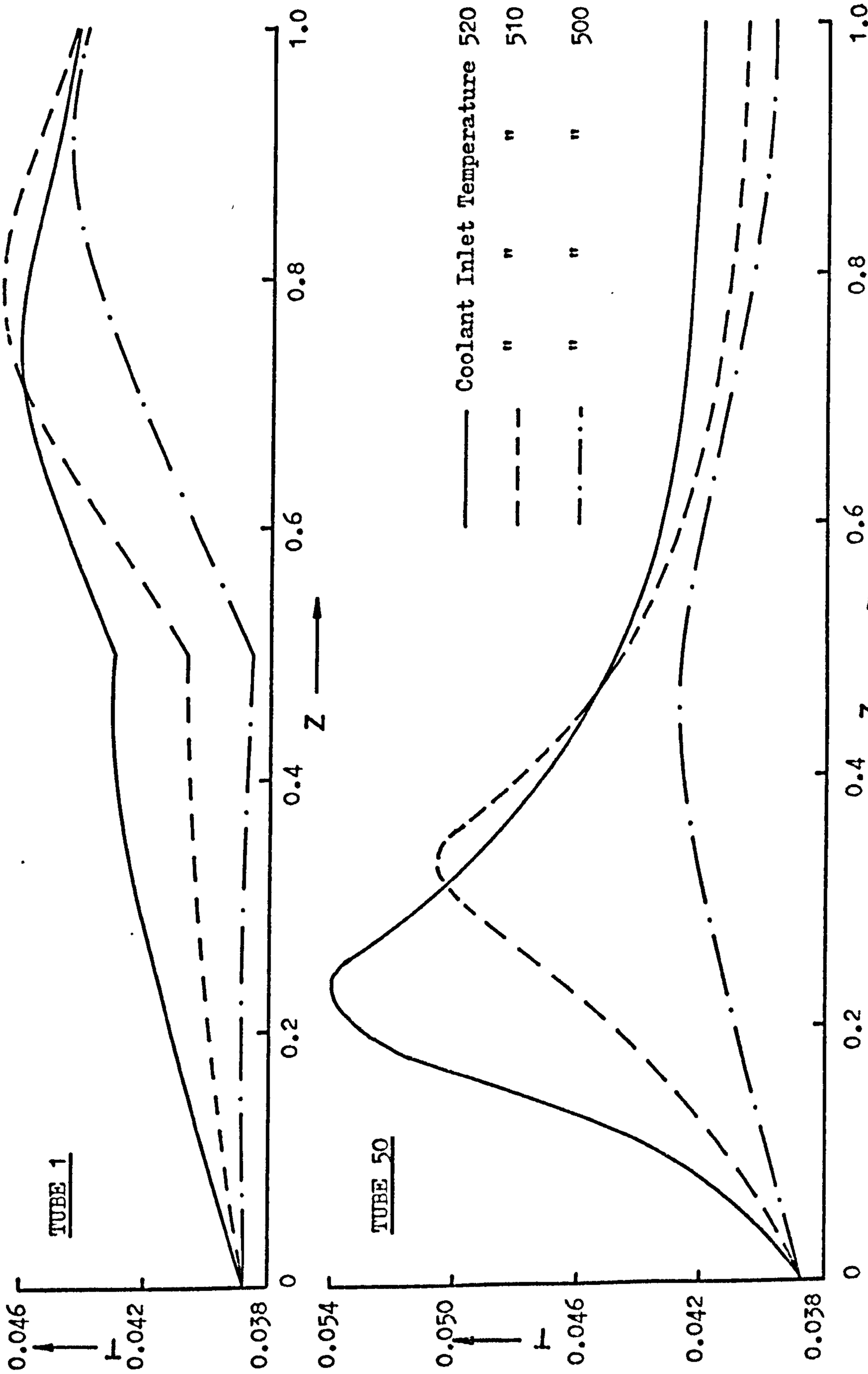

Figure 5.2 Tubeside temperature profiles for differing inlet coolant temperatures in a two coolant pass co-current reactor. (Non specified data as table 3.1)

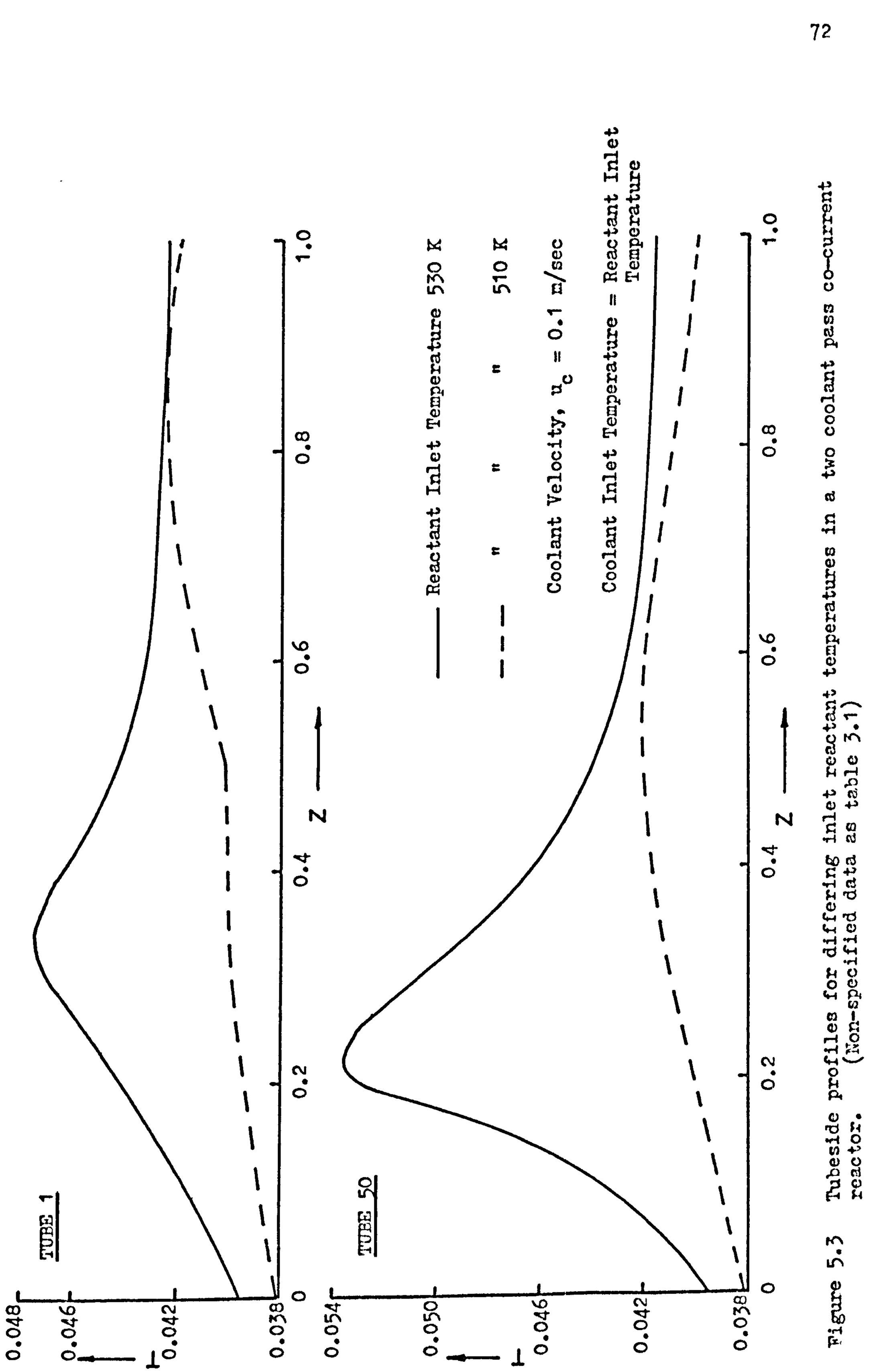

Figure 5.3 Tubeside profiles for differing inlet reactant temperatures in a two coolant pass co-current reactor. (Non-specified data as table 3.1)

5.3 The Effect of the Number of Coolant Passes on the System

It was explained in chapter three that baffle plates can be placed in the system to force the cooling medium into crossflow over the bundle and so achieve a high coolant to wall heat transfer coefficient. The number of coolant passes in multitubular reactors is a design variable and although no published work has been produced on the subject the number used can have significant effects both on the heat distribution in the system and the conversion obtained. Industrially, up to six coolant passes can be employed. Above this number the pressure drop in the coolant circuit tends to be so large that the additional pumping costs outweigh any advantage gained either in achievable heat transfer coefficient or in the distribution of reaction heat.

Basis For Comparison

When comparing different configurations, the immediate problem is the choice of a frame of reference. Since the size of reactor remains constant, having differing numbers of passes means that the comparison can be based either on a constant mass flowrate or a constant velocity coolant. Figures 5.4 and 5.5 show the tubeside temperature profiles that are produced when the number of coolant passes are increased from two to six, using the constant mass flowrate and constant coolant velocity bases respectively. The corresponding coolant temperature increases and conversions are given in tables 5.1 and 5.2

The most striking feature of figures 5.4 and 5.5 is that the profiles produced by systems with three or more coolant passes tend to be grouped together. The two pass system, however, tends to stand out both because of the large difference between profiles from extreme ends of the bundle and the fact that they tend to be different from the other configurations which are broadly grouped together. This is especially true in the constant mass flowrate case.

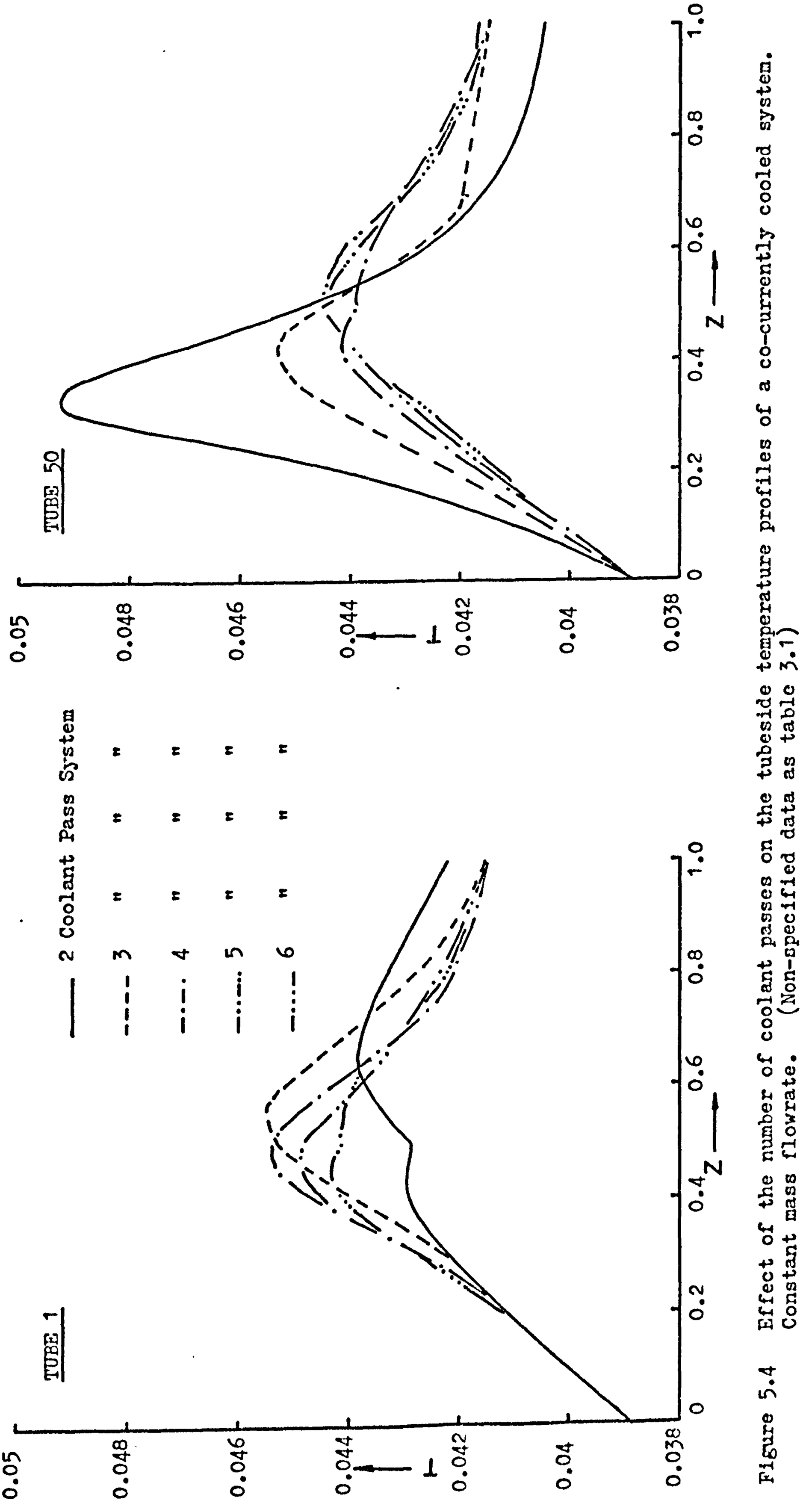

Figure 5.4 Effect of the number of coolant passes on the tube side temperature profiles of a co-currently cooled system. Constant mass flowrate. (Non-specified data as table 3.1)

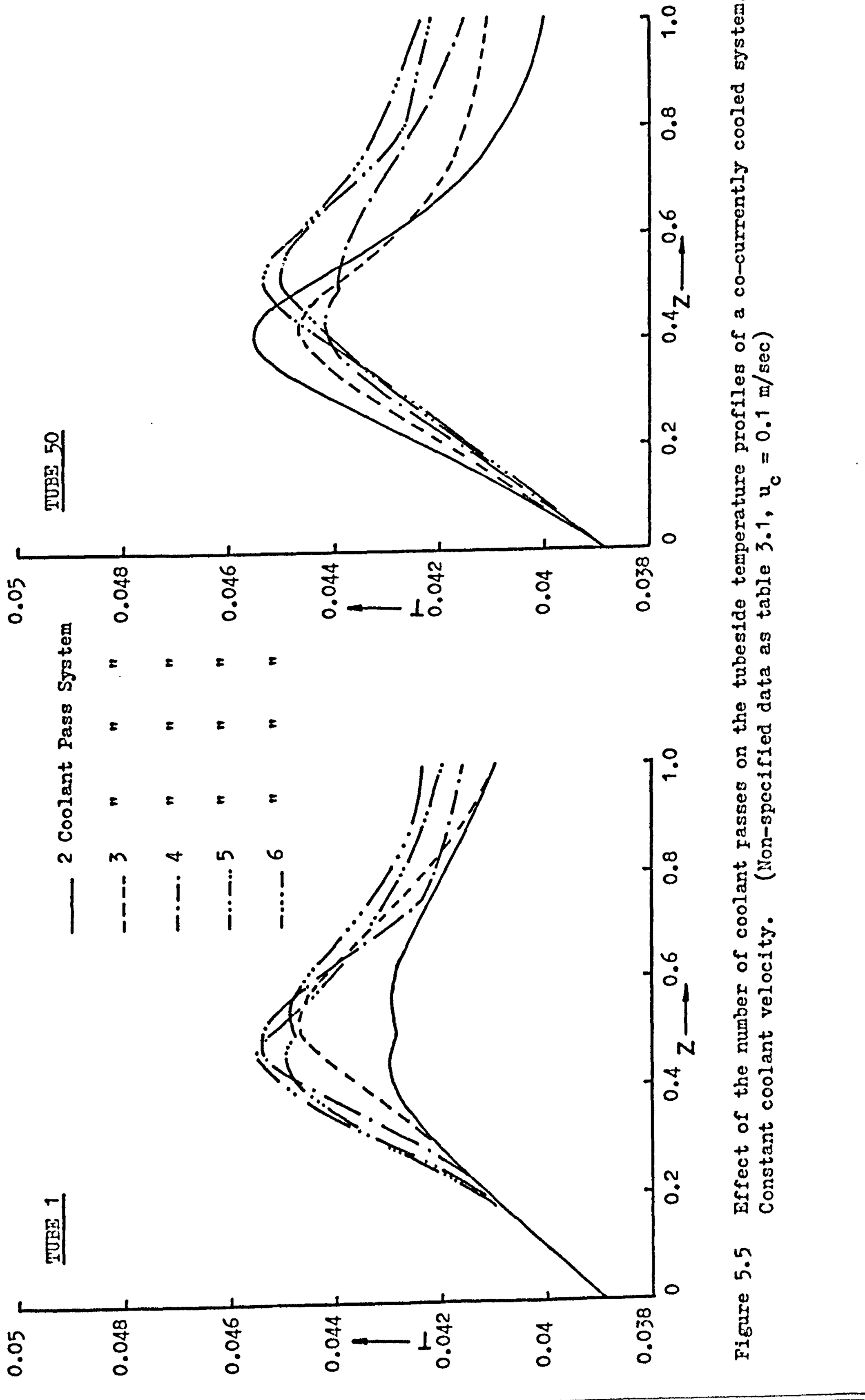

Figure 5.5 Effect of the number of coolant passes on the tube side temperature profiles of a co-currently cooled system. Constant coolant velocity. (Non-specified data as table 3.1, u_c = 0.1 m/sec)

T A B L E 5.1

The Effect of the No. of Coolant Passes on the Performance of a Co-Current Reactor at Constant Coolant Mass Flowrate.

No. of Passes	ΔT_c (°K)	% Conversion	
		TUBE 1	TUBE 50
2	28.5	87.2	96.3
3	27.6	90.7	89.5
4	27.2	90.0	88.3
5	27.0	88.98	88.5
6	24.9	87.69	87.6

T A B L E 5.2

The Effect of the No. of Coolant Passes on the Performance of a Co-Current Reactor at Constant Coolant Velocity

Coolant Velocity, U_c = 0.1 m/sec

No. of Passes	ΔT_c (°K)	% Conversion	
		TUBE 1	TUBE 50
2	13.6	81.7	88.6
3	20.4	87.6	86.8
4	27.2	90.0	88.3
5	34.0	91.2	90.7
6	37.6	91.7	91.7

Examination of table 5.1 shows that as the number of coolant passes increases, with the mass flowrate constant the difference between conversions in tubes at extreme ends of the bundle becomes less, with an accompanying decrease both in the overall conversion and the coolant temperature rise. The explanation can be appreciated by considering

a two and a four coolant pass reactor system. In the two pass case (refer to figure 5.4) the main reaction zone, around the tubeside temperature peak, would normally be in coolant pass 1, but, for tubes with a low tube number the cold inlet coolant decreases the amount of reaction occuring here. Because the coolant pass contains a large length of tube, the coolant heating in this first pass is quite large, so that when tubes with a high tube number are considered (e.g. tube 50) a high temperature coolant is in contact with a rich reactant concentration and vigorous reaction occurs. Although the coolant is even hotter when it reaches tube 1 pass 2 the temperature peak in this pass is still lower than that in tube 50, pass 1 because the reactant concentration in this part of the tube is much less. When the four pass system is considered, the tubeside temperature peak occurs in coolant pass 2 in all tubes in the bundle. The first coolant pass sees the cold coolant flowing over the tubes and in this pass little reaction occurs because the reactants temperature has not risen much above the inlet value. The coolant is therefore not heated very much in this pass (compared to pass 1 in the two pass system) both because little reaction occurs in this bed length and the length of tubes available for heat transfer is less. Therefore, in the region of high reactant concentration, the coolant is not as hot as around the high numbered tubes of the two pass case. Thus, although a temperature peak does develop, the excessive reaction region of the two pass system is not produced.

Table 5.2, which shows the constant coolant velocity case, indicates that, unlike the previous example, the conversion and coolant temperature rise both increase as the number of passes increases. This is to be expected, as the residence time of the coolant also increases with an increasing number of passes. (In the constant mass flowrate case, the residence time of the coolant is constant and it is the coolant velocity that changes with an increased number of baffle plates.) However, this

increased reaction is also due to another reason, caused by the method of heat generation and removal in the system. Consider, for example, the change from a five to a six coolant pass configuration. The increase in the number of passes results in a decrease in the length of each baffled section. In the first coolant pass the tubeside gases heat up as the reaction develops, leaving this pass at a higher temperature than when they entered. Thus, more heat is transferred from the tubes to the coolant near to exit of the tubes from this pass than near the reactor entrance. On shortening the length of the tubes in this pass by increasing the number of passes, the amount of heat which can be transferred to the coolant decreases and so the coolant does not heat up as much as it flows across the bundle. This occurs despite the decrease in mass flowrate of the coolant across this pass. Consequently, the tubeside gases do not become as hot in the first pass of a six pass system as in a five. In the second and subsequent passes more reaction takes place in the case of six passes since less reactant has been consumed in the first. This causes greater heat generation and, therefore, more heating of the coolant. The hotter coolant experienced by the tubes in turn causes more reaction to take place, causing even more heat generation. The process is enhanced by the lower mass flowrate caused by shortening the baffled sections at constant coolant velocity.

T A B L E 5.3

The Effect of the No. of Coolant Passes on the Performane of a Co-Current Reactor at Constant Coolant Mass Flowrate. Tube length, L = 4 m

No of Passes	ΔT_c (°K)	% Conversion	
		TUBE 1	TUBE 50
2	25.9	85.1	90.34
3	25.0	86.9	84.0
4	24.6	84.8	84.1
5	24.4	84.4	84.0
6	22.4	83.0	83.0

T A B L E 5.4

The Effect of the No. of Coolant Passes on the Performance of a Co-Current Reactor at Constant Coolant Mass Flowrate. Tube length, L = 6 m

No of Passes	ΔT_c (^oK)	% Conversion	
		TUBE 1	TUBE 50
2	29.5	88.8	98.2
3	28.8	92.3	94.0
4	28.5	92.9	91.4
5	28.4	92.2	91.2
6	26.2	90.8	90.5

Tables 5.3 and 5.4 show the effects of the number of coolant passes at constant mass flowrate on reactors of different tube lengths (4 m and 6 m rather than 5 m). As expected, the trends indicated earlier are still apparent. As the number of coolant passes increases, the coolant temperature rise and overall conversion decreases. The larger reactor shows both higher conversion and higher coolant temperature rise (for a given configuration) than the smaller reactor.

The tubeside temperature profiles for reactors having three, four and six coolant passes are shown in figures 5.6, 5.7 and 5.8 respectively, the conditions used being the same as those in the two pass examples of figures 5.1, 5.2 and 5.3. The main trend apparent in the configurations with more than three coolant passes is the increasing similarity between the profiles of tubes 1 and 50. Again, increasing the coolant velocity causes the tubeside hotspot to move towards the reactor exit, the coolant temperature rise to decrease and (table 5.5), the overall conversion to decrease. For the data used throughout this study the two coolant pass system shows large differences between conversions in tubes across the bundle. Three or four pass systems on the other hand

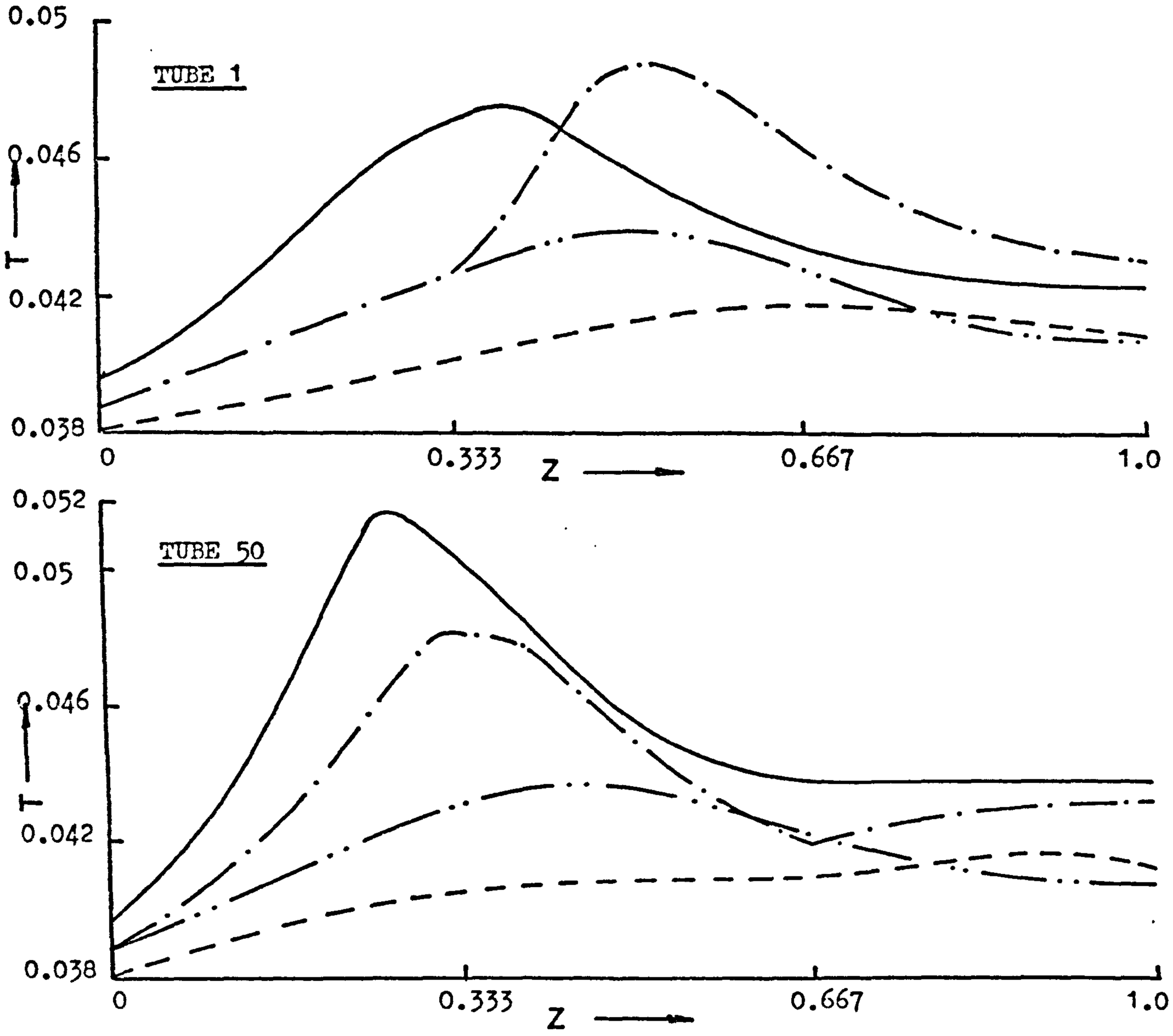

	Inlet Reactant Temperature	Coolant Velocity u_c
———	530 K	0.1 m/sec
– – – –	510 K	0.1 m/sec
– · – · –	520 K	0.05 m/sec
– ·· – ·· –	520 K	0.2 m/sec

Inlet Coolant Temperature = Inlet Reactant Temperature

Figure 5.6 Tubeside temperature profiles of a three coolant pass co-current reactor under various conditions. (Non-specified data as table 3.1)

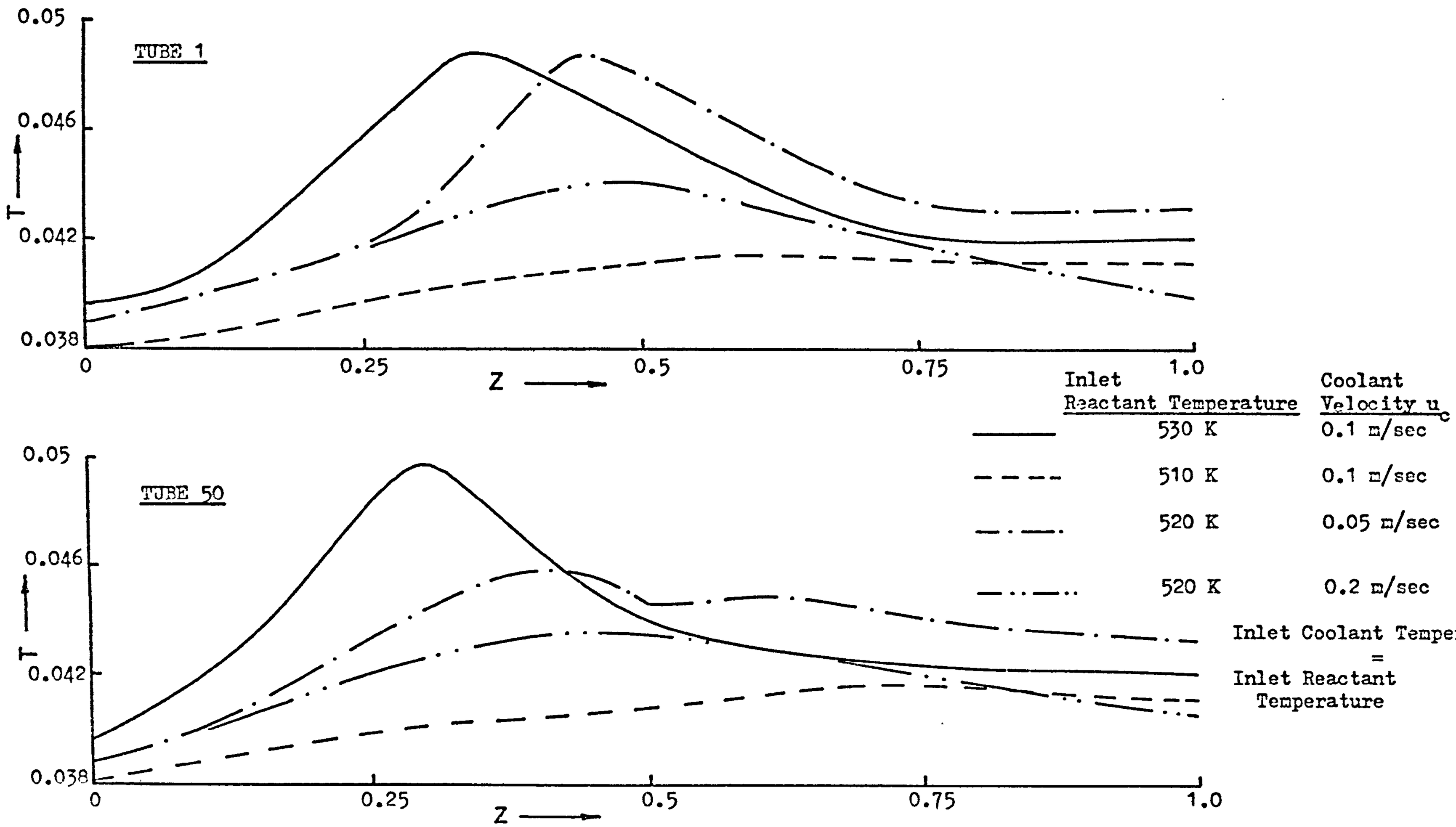

Figure 5.7 Tubeside temperature profiles for a four coolant pass co-current reactor under various conditions. (Non-specified data as table 3.1)

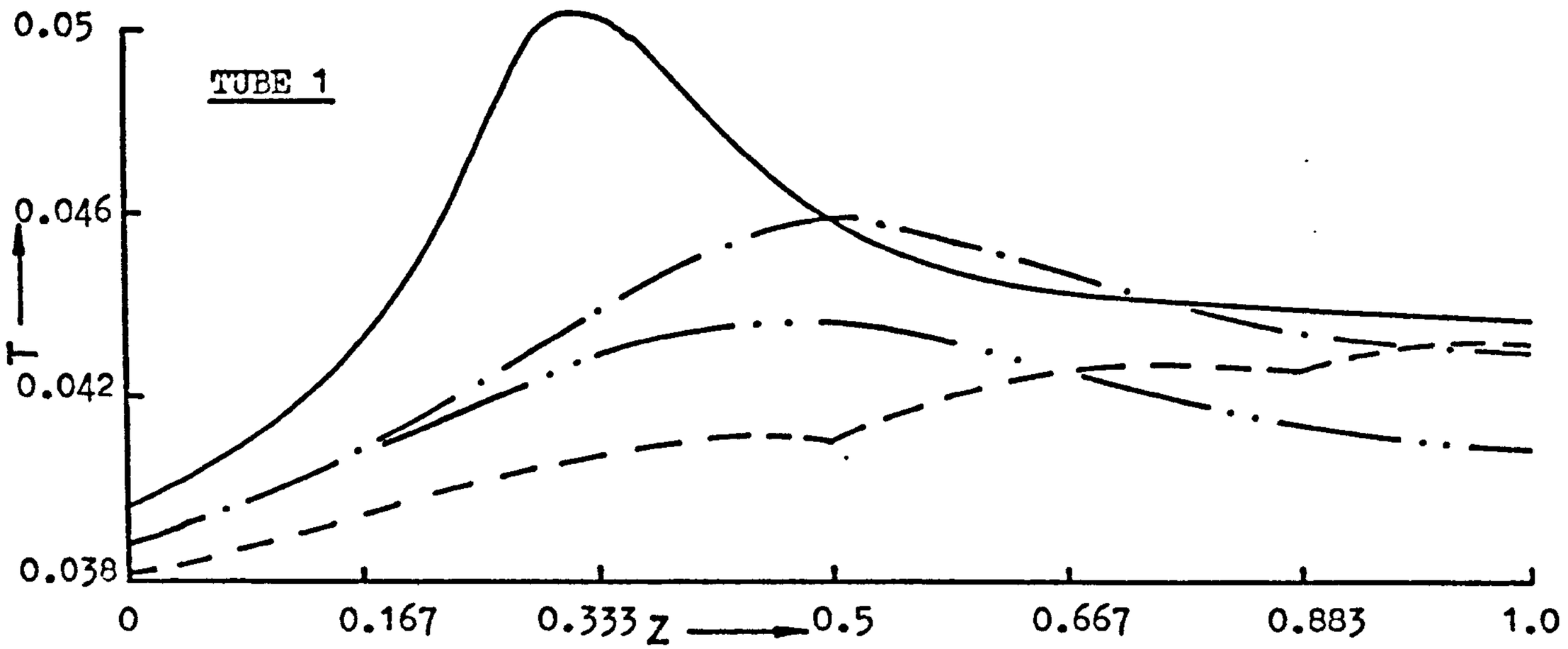

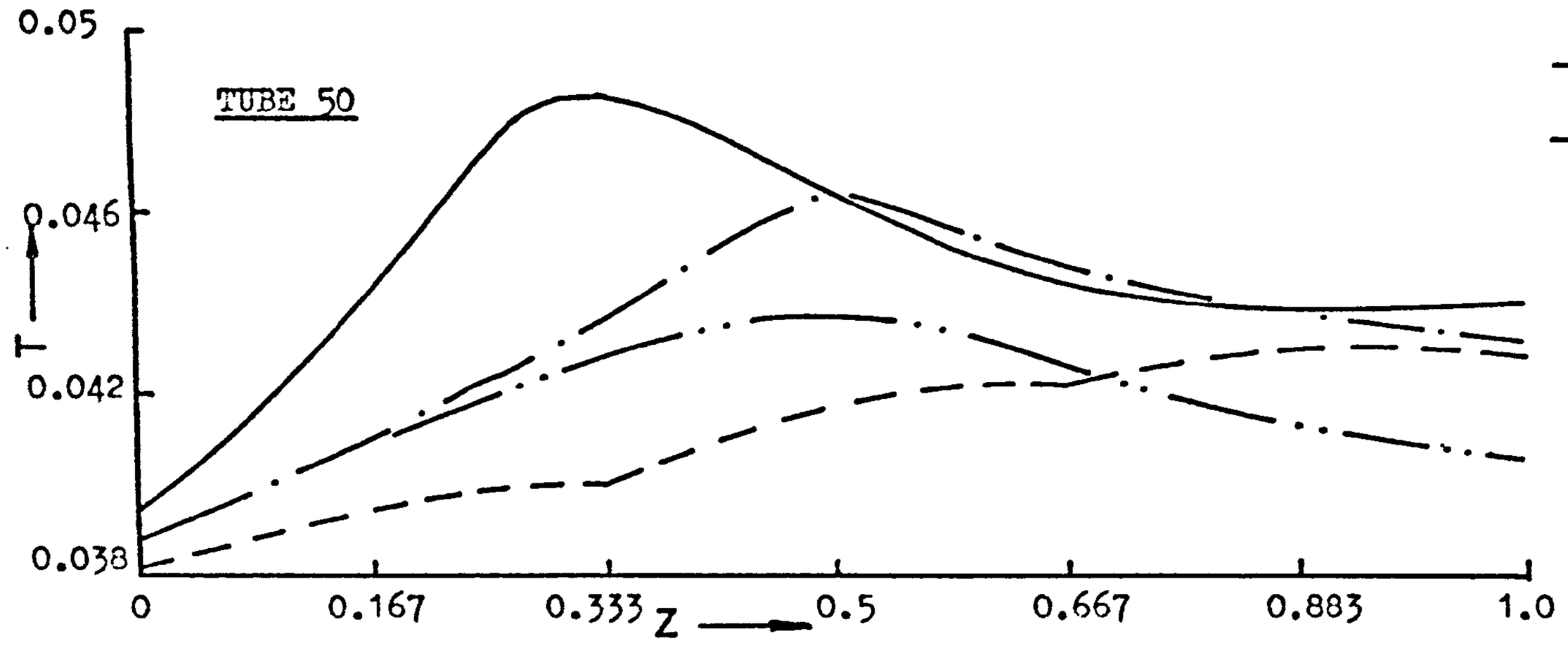

	Inlet Reactant Temperature	Coolant Velocity u_c
———	530 K	0.1 m/sec
- - - -	510 K	0.1 m/sec
— · —	520 K	0.05 m/sec
— ·· —	520 K	0.2 m/sec

Inlet Coolant Temperature = Inlet Reactant Temperature

Figure 5.8 Tubeside temperature profiles for a six coolant pass co-current reactor under various conditions. (Non-specified data as table 3.1)

T A B L E 5.5

Fractional Conversion for Co-Current Reactor Systems

INLET TEMP		510 K	520 K		530 K
COOLANT VELOCITY		0.1 m/sec	0.05 m/sec	0.2 m/sec	0.1 m/sec
2 PASS	TUBE 1	69.0 %	94.9 %	81.8 %	95.6 %
	TUBE 50	70.0 %	99.6 %	88.6 %	99.4 %
3 PASS	TUBE 1	67.0 %	97.8 %	84.0 %	97.0 %
	TUBE 50	65.0 %	96.6 %	83.7 %	98.6 %
4 PASS	TUBE 1	65.0 %	97.2 %	83.9 %	97.6 %
	TUBE 50	65.0 %	95.2 %	82.9 %	97.5 %

give reasonably high conversions with only slight differences between tubes at extreme ends of the bundle. The increased pressure drop that would be introduced by using more than four coolant passes can only be warranted when the spread of conversion across the bundle is very damaging to the quality of the product. Moreover, very high pressure drops in the coolant circuit may necessitate the use of a momentum balance on the shell-side equations, and so the results from the models used may not truly represent the system if it contains a large number of passes.

An important feature of the co-current multitubular reactor can be seen in several of the profiles so far presented, namely that of multiple tubeside temperature peaks. This effect is shown very well in figure 5.6, for the case of $T = 0.03884$ and $U_c = 0.05$ m/sec in a three pass reactor. Although the conditions used in this case are severe, giving a coolant temperature rise of approximately 40 K, the phenomena of enhancing the reaction in regions where the reactant has become depleted is clearly shown and can be used to advantage under milder operating conditions. The same effect is shown under possible industrial conditions by the four pass reactor in figure 5.4 where the coolant

temperature rise is 27 K (table 5.1). Ultimately, it should be possible to induce a controlled coolant temperature throughout the system, the heat of reaction produced in the early, high concentration parts of the reactor being used to produce a series of shallow peaks in the tubeside temperature. Then, the catalyst in the tube is not subjected to large temperature peaks in a single reaction zone, but rather to several smaller peaks spread along the length of the tube. Consequently, both catalyst deactivation and the risks involved in controlling large temperature hotspots can be reduced.

It should be pointed out that it is this effect of the heated coolant causing high reaction rates in the latter parts of the reactor which necessitates the use of these more complex multitubular models rather than the single tube models which do not account for the coolant behaviour.

5.4 Effect of Configuration on the Position of the Tubeside Hotspot

It has been shown in the previous section that the reactor configuration can significantly affect the performance of the system. Figures 5.9, 5.10 and 5.11 show how the tubeside temperature peaks are positioned in different tubes across the bundle. The same set of conditions have been plotted for two, three and four coolant pass systems so that the trends indicated earlier can be seen more clearly. It should be emphasized, however, that these plots do not give any indication of the level of the tubeside temperature or of the conversions achieved. For this information, the results given previously in this chapter will be used.

The diagrams show particularly well the effects of changing the coolant velocity or reactant inlet temperature, with the resulting movement of the steady state temperature peaks from one coolant pass to another. In practice the coolant velocity will vary and so it is

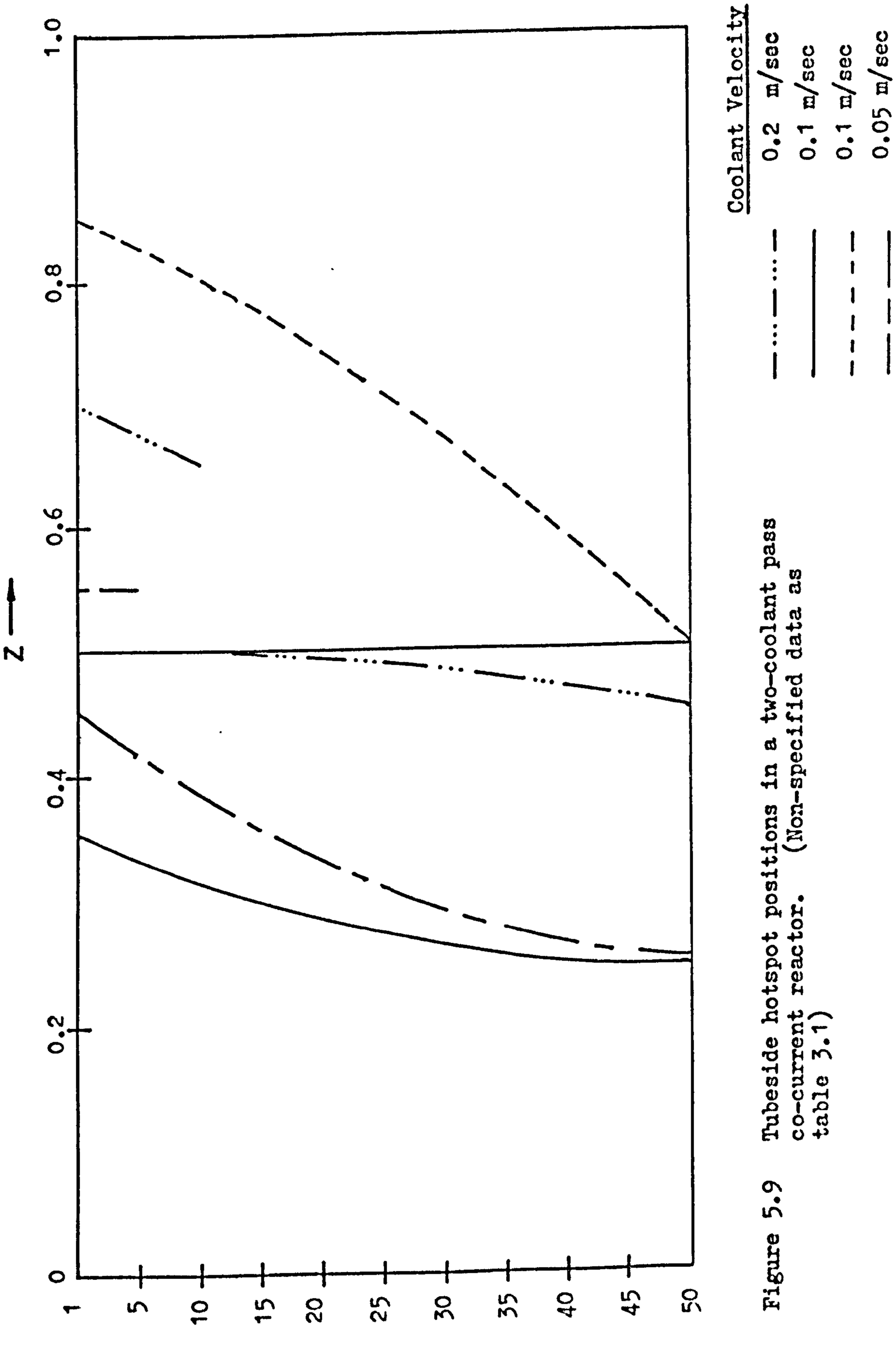

Figure 5.9 Tubeside hotspot positions in a two-coolant pass co-current reactor. (Non-specified data as in table 3.1)

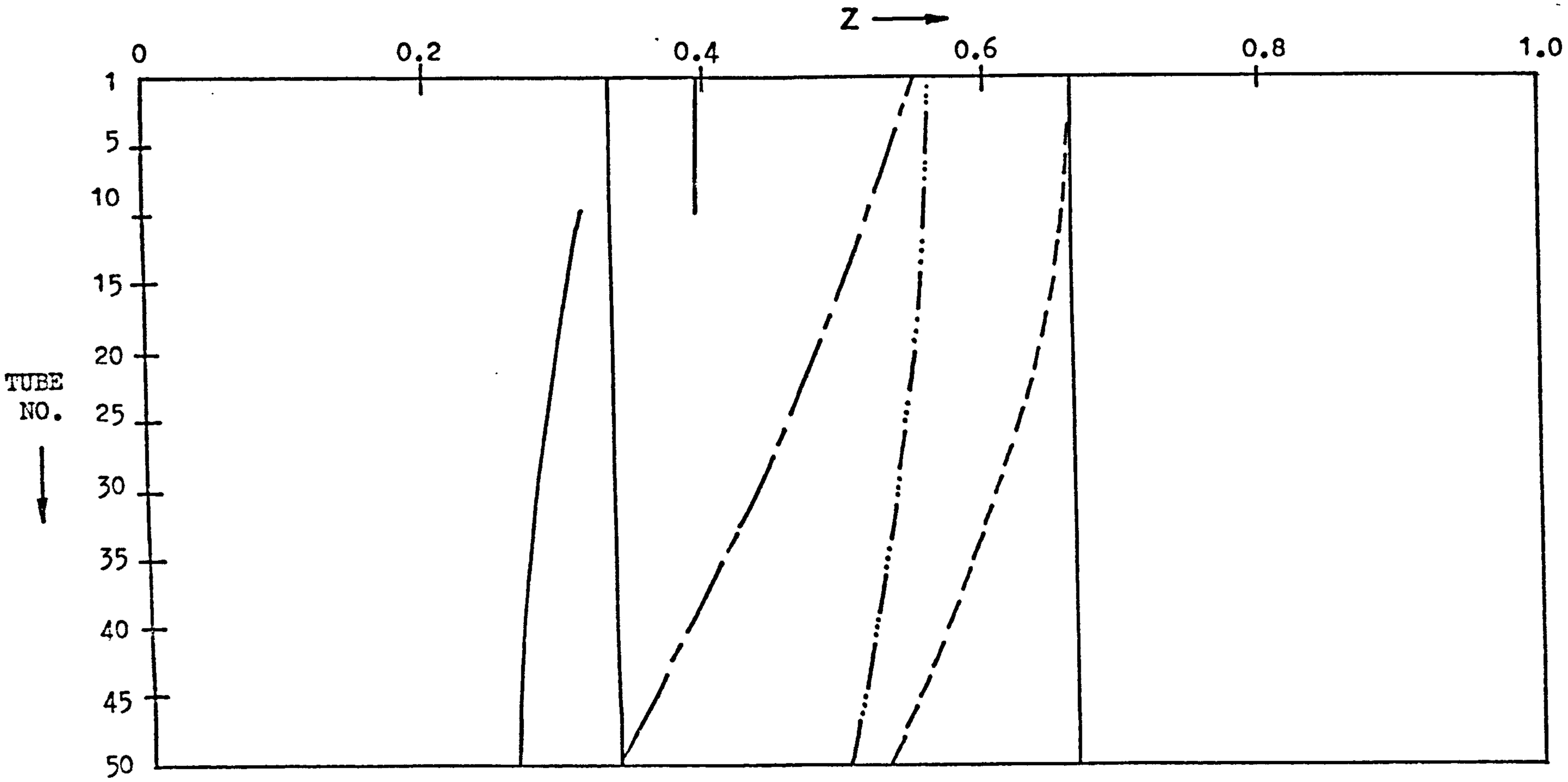

Figure 5.10 Tubeside hotspot positions in a three coolant pass co-current reactor. (Non-specified data as table 3.1)

	Coolant Velocity	$T'_{c_{in}} = T'_o$
— ... — ...	0.2 m/sec	520 K
————	0.1 m/sec	530 K
- - - - - - -	0.1 m/sec	510 K
—— - ——	0.05 m/sec	520 K

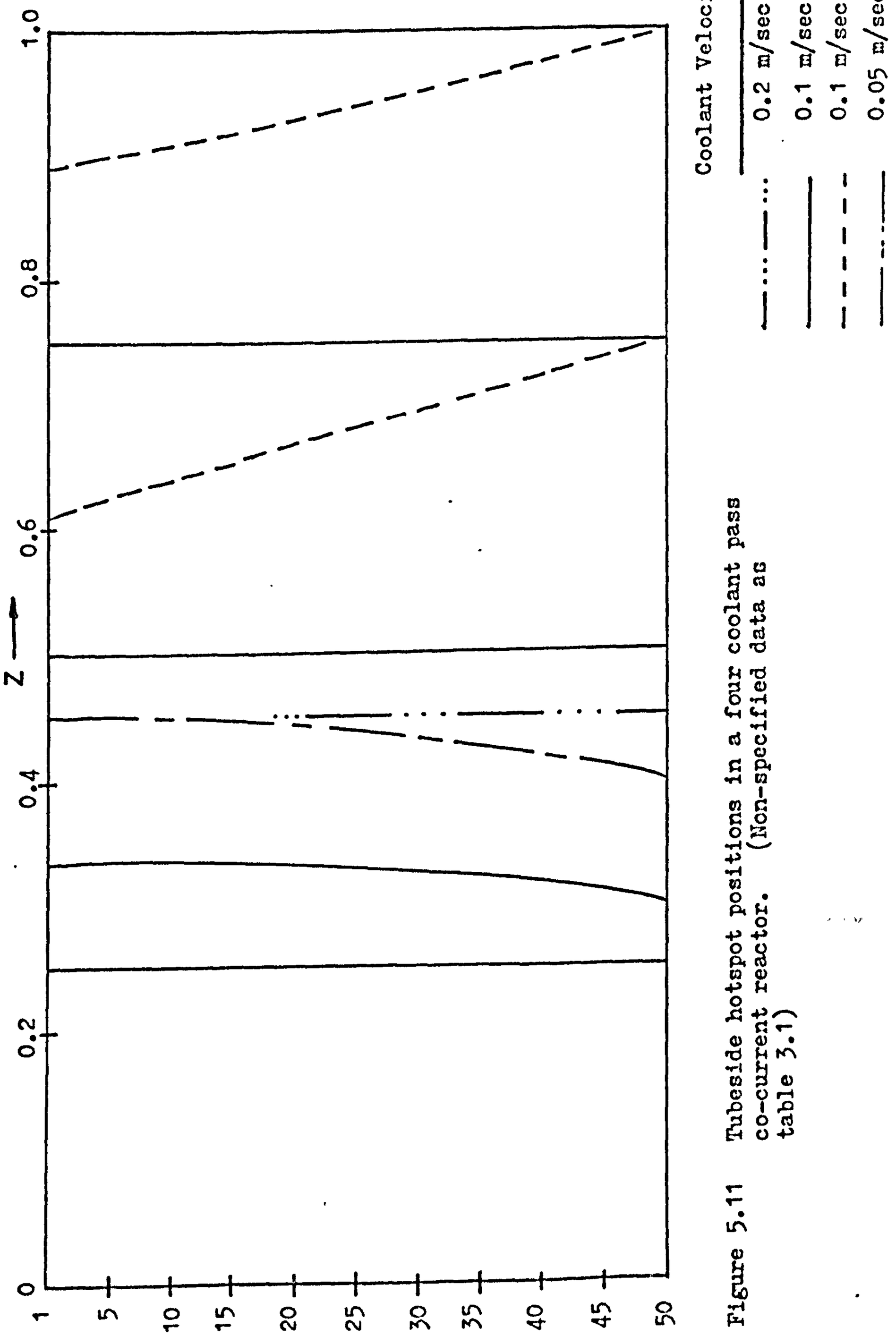

Figure 5.11 Tubes beside hotspot positions in a four coolant pass co-current reactor. (Non-specified data as table 3.1)

unlikely that the temperature peaks will remain in the same position for the entire life of the reactor. The results shown here could represent, for instance, the initial and final steady state positions of the tube-side hotspot had the coolant pump been allowed to deliver less coolant after say pump failure. The transient response of such action is considered later, in chapter eight.

As an example of the use of such a diagram, consider the two coolant pass system of figure 5.9. A decrease in the inlet reactant temperature of 20 K from 530 K results in the movement of the tubeside peak temperature of all the tubes in the bundle from coolant pass 1 to coolant pass 2. Referring to figure 5.3 and table 5.5 it can be seen that, in fact, the latter steady state has a very shallow peak with a very low conversion of approximately 70% of reactants being converted, as opposed to the 95% and above for the higher inlet reactant temperature.

In general it would be expected that, for any given coolant pass, the tubeside temperature peak would move towards the reactant inlet as the coolant temperature increases. However, this intuitive conclusion is not always true for reactors having multiple coolant passes. Referring again to the co-current, two coolant pass system shown in figure 5.9, for the conditions producing temperature peaks in pass 1, the position of the peak moves towards the reactant inlet as the tube number is increased i.e. tubes in pass 1 having a high tube number have a higher temperature coolant environment and hence the reaction accelc-rates, and a peak forms earlier in the bed. For coolant pass 2, however, the conditions of the dotted line ($T = 0.0381$ and $U_c = 0.1$ m/sec) produce unexpected temperature peak positions. As the coolant temperature increases from tube 50 to tube 1, the peak position in the tubes moves towards the reactor outlet, opposite to the expected direction. This behaviour is caused by the heating/cooling effect of the coolant in pass 1. Since the coolant around tube 1 pass 1 is cooler than that

around tube 50 pass 1 the reactant gases leave pass 1 hotter in tube 50 than in tube 1. Hence the temperature peak in tube 50 occurs closer to the bed inlet than that of tube 1 even though the coolant temperature around tube 1 pass 2 is higher than that of tube 50 pass 2. Although the peak occurs earlier in the bed, because the coolant temperature is lower than for tube 1, the height of the peak in tube 50 is less (see figure 5.3) and the conversions in tubes at extreme ends of the bundle are very close, being 69% for tube 1 and 70% for tube 50. An example of the multiple peak effect, produced by the heated coolant inducing reaction in the outlet regions of the bed, can be seen in figure 5.11.

Because of the coolant temperature gradient across the tube bundle, tubes at either end of the bundle diameter do not exhibit the same behaviour, and hence there will be one tube in the bundle with conditions more severe than in any of the others. From a control point of view, it would be very useful to be able to predict, a priori, which tube this will be so that it can be monitored. Then, as long as it is kept within the required operational safety limits, it would be known that all the tubes in the bundle are within these safety limits. Unfortunately, there does not appear to be any means available for identifying this tube. However, the above studies have demonstrated that the most extreme conditions are to be found in either tube 1 or tube 50, so the problem of selecting monitoring positions is now manageable. It should be obvious in these discussions that under no circumstances should the results obtained just from one tube be taken as representative. Indeed, this is emphasized by the well known fact that, in large tube bundles, maldistribution of feed among the tubes (see section 5.6) can occur so that a number of tubes from the positions experiencing extreme conditions should be monitored. The work described here offers the possibility of obtaining reliable information about critical areas in the bundle.

It is particularly instructive to consider the position of the tube with the maximum tubeside temperature peak (the monitoring tube) in more detail. The dependance of the position on reactor configuration can be investigated by using the cases studied in figures 5.4 and 5.5, the monitoring tube being shown for various reactor configurations at both constant coolant mass flowrate and constant coolant velocity. Table 5.6 summarizes the position of the monitoring tube for each configuration.

T A B L E 5.6

The Tube Containing the Maximum Tubeside Temperature Peak, for Various Reactor Configurations.

No. of Coolant Passes	Constant Coolant Flowrate Case	Constant Coolant Velocity Case
2	tube 50	tube 50
3	tube 1	tube 1
4	tube 1	tube 1
5	tube 1	tube 1
6	tube 50	tube 50

In some cases a simple pattern becomes apparent, as can be seen with the aid of figure 5.12, although this is not universal and only applies to certain cases the diagram shows the configuration being studied, the approximate positions of the tubeside temperature peaks and the direction of flow of the coolant. The monitoring tube is often the tube at the outlet of the coolant pass containing the tubeside temperature hotspots. For a two pass system, figure 5.12(a), the maximum tubeside temperature peak is in tube 50. Unfortunately, the method fails in two cases. The first, demonstrated in figure 5.12(e), occurs when the tubeside hotspots are in more than one coolant pass,

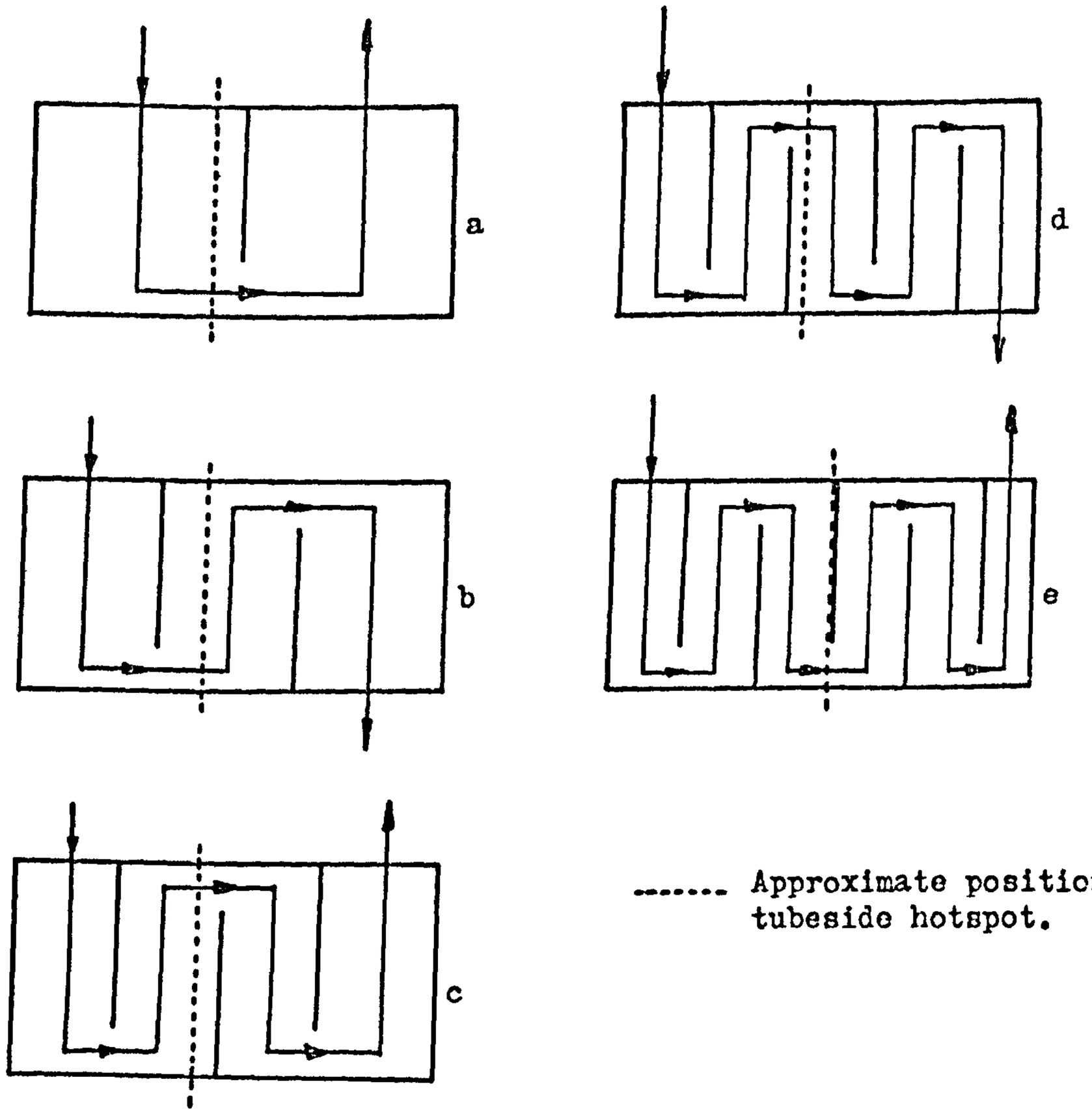

Figure 5.12 Schematic diagrams used in the prediction of the tube containing the maximum tubeside temperature in co-current reactors.

possibly even stradling the baffle plate. The second case has been demonstrated earlier in this section, when the tubeside temperature peaks move towards the reactor exit as the coolant temperature increases across the tube bundle. This behaviour is due to the heating/cooling effect of the previous coolant passes, the higher reactant temperature entering that pass in tubes close to the coolant inlet to that pass, more than compensating for the increasing coolant temperature as it flows across the tube bundle. Hence, even though a tube has a high coolant temperature around it, if the reactant temperature is lower than that of a tube with a lower coolant temperature, then the temperature peak in that tube may be lower.

5.5 Variation of the Overall Heat Transfer Coefficient

One of the most difficult parameters to obtain accurately in a reacting system is the heat transfer coefficient, values obtained from standard correlations varying by up to approximately 25%. Figure 5.13 shows how the variation of the wall Nusselt number affects the tubeside temperature profiles in a four coolant pass reactor with a coolant velocity of 0.1 m/sec. As the Nusselt number decreases the overall coolant temperature rise increases and the tubeside profiles produce much higher peak temperatures. This behaviour results from the initial decrease in the heat transfer to the coolant because of the lower heat transfer coefficient, so that the tubeside fluids are hotter in the low Nusselt number case and more reaction occurs making them even hotter. Ultimately, although the Nusselt number is low, implying low heat transfer, the driving force caused by the higher tubeside temperature produces higher coolant temperature rises in the low Nusselt number case than in the high.

5.6 The Maldistribution of Reactant Feed to the Tubes

The use of a model which considers the entire bundle of reactor

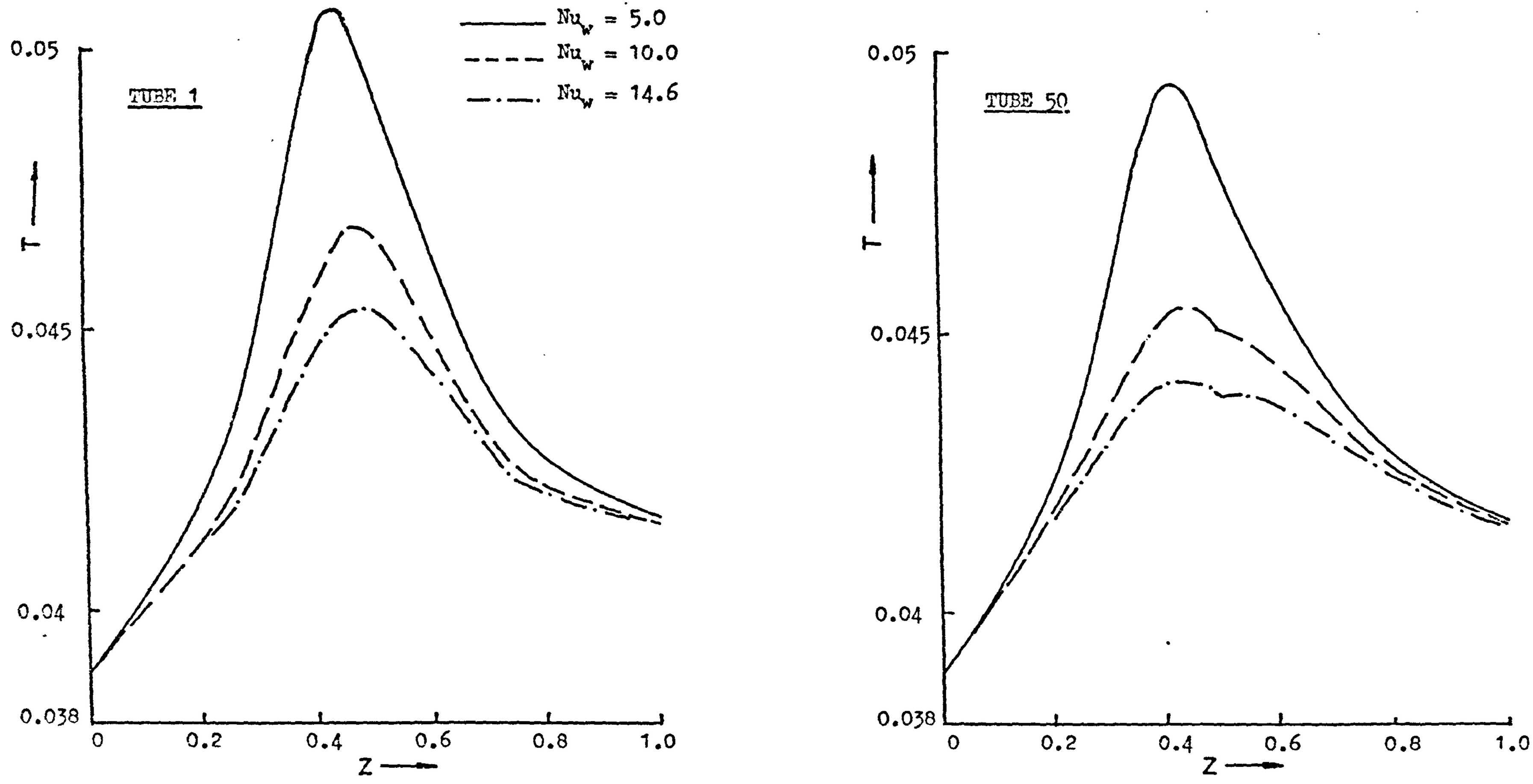

Figure 5.13 The effect of variations in the wall Nusselt number on the tubeside temperature profiles in a four coolant pass co-current reactor. (Non-specified data as table 3.1)

tubes enables an examination of the consequences of not meeting the basic assumptions used in the single tube models normally applied to studies of the operability of reactor units. Earlier sections of this chapter have considered the effects of the shell-side configuration and the results of changes in coolant variables, such as the mass flowrate. This section concentrates on a common problem encountered in all systems containing parallel reaction units, the maldistribution of the inlet reactants to the tubes. In the large reactors used industrially, the number of tubes used can be as high as 30,000, and the chances of the reactant flowrate being constant for all the tubes in the bundle is very small. The randomness of the packing will cause different pressure drops (and hence velocities) in the bundle even before the reactor has been commissioned, and, as demonstrated earlier, since all the tubes do not have the same performance, even with the same feed parameters, the degree of coking within the bed will vary significantly from tube to tube.

A four coolant pass reactor has been taken as a typical industrial unit and, using the data of table 3.1, the feed flowrate of reactant varied in some of the tubes. Flowrate changes in single tubes in the bundle have no effect on the overall performance of the system, the tube with the abnormal flowrate being the only one affected. However, when abnormal flowrates occur in groups of tubes the performance of every tube in the bundle can be affected. For example, figures 5.14 and 5.15 show the tubeside temperature profiles obtained when a reactant flowrate deviation of $\pm$10% or $\pm$20% is applied to groups of ten tubes at either end of the tube bundle. That is, of the fifty tubes across the bundle diameter, twenty (ten at each end) are subjected to reactant flowrates different from the rest of the bundle. Figure 5.14 covers the industrially acceptable coolant velocity of 0.25 m/sec, while figure 5.15 shows an extreme case with a coolant velocity of 0.05 m/sec and very

Figure 5.14 Four coolant pass, co-current reactor subject to maldistribution of feed amongst the tubes. High coolant velocity case, u_c = 0.25 m/sec. (Remaining data as table 3.1)

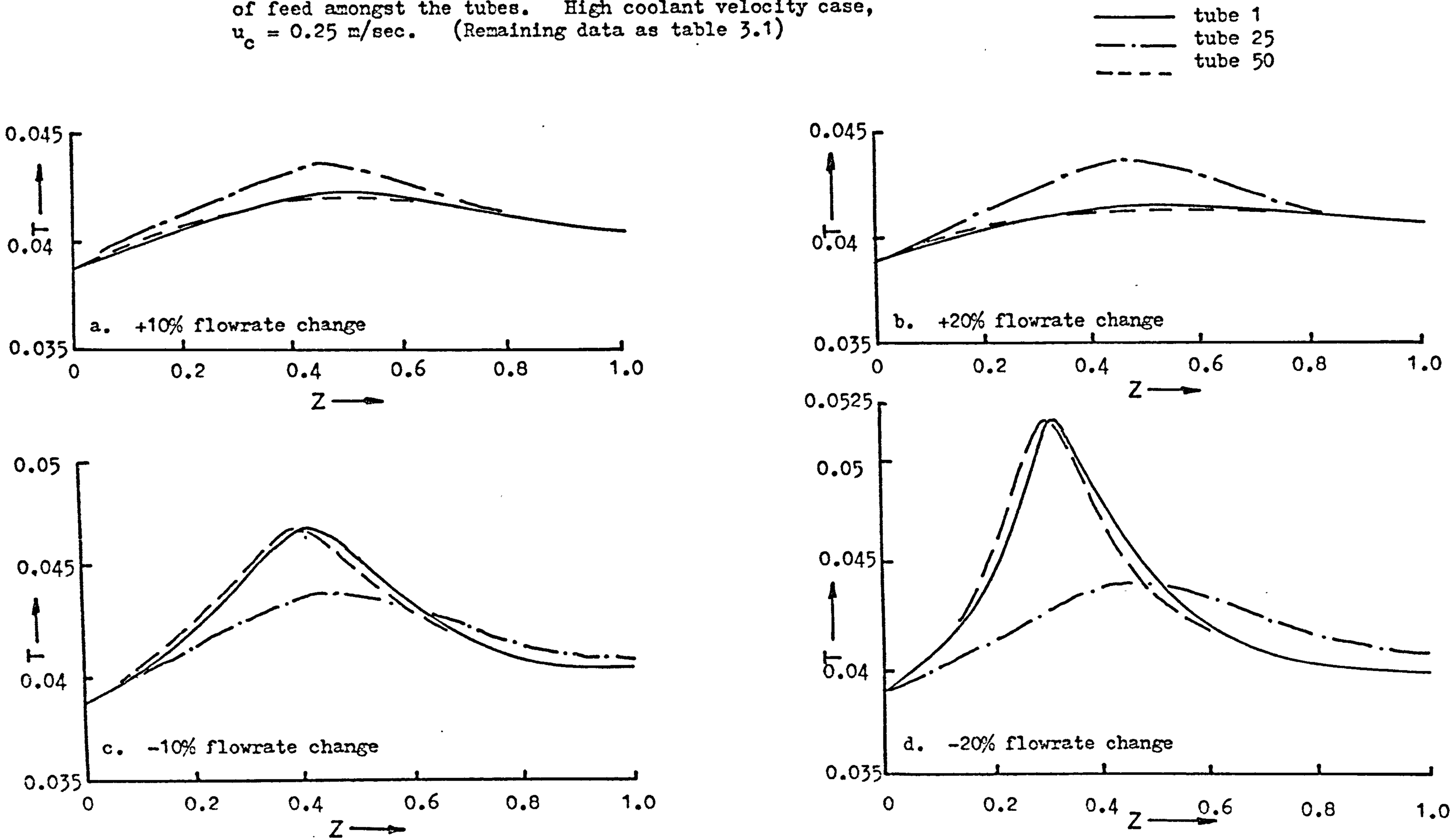

Figure 5.15 Four coolant pass, co-current reactor subject to maldistribution of feed amongst the tubes. Low coolant velocity case, u_c = 0.05 m/sec. (Remaining data as table 3.1)

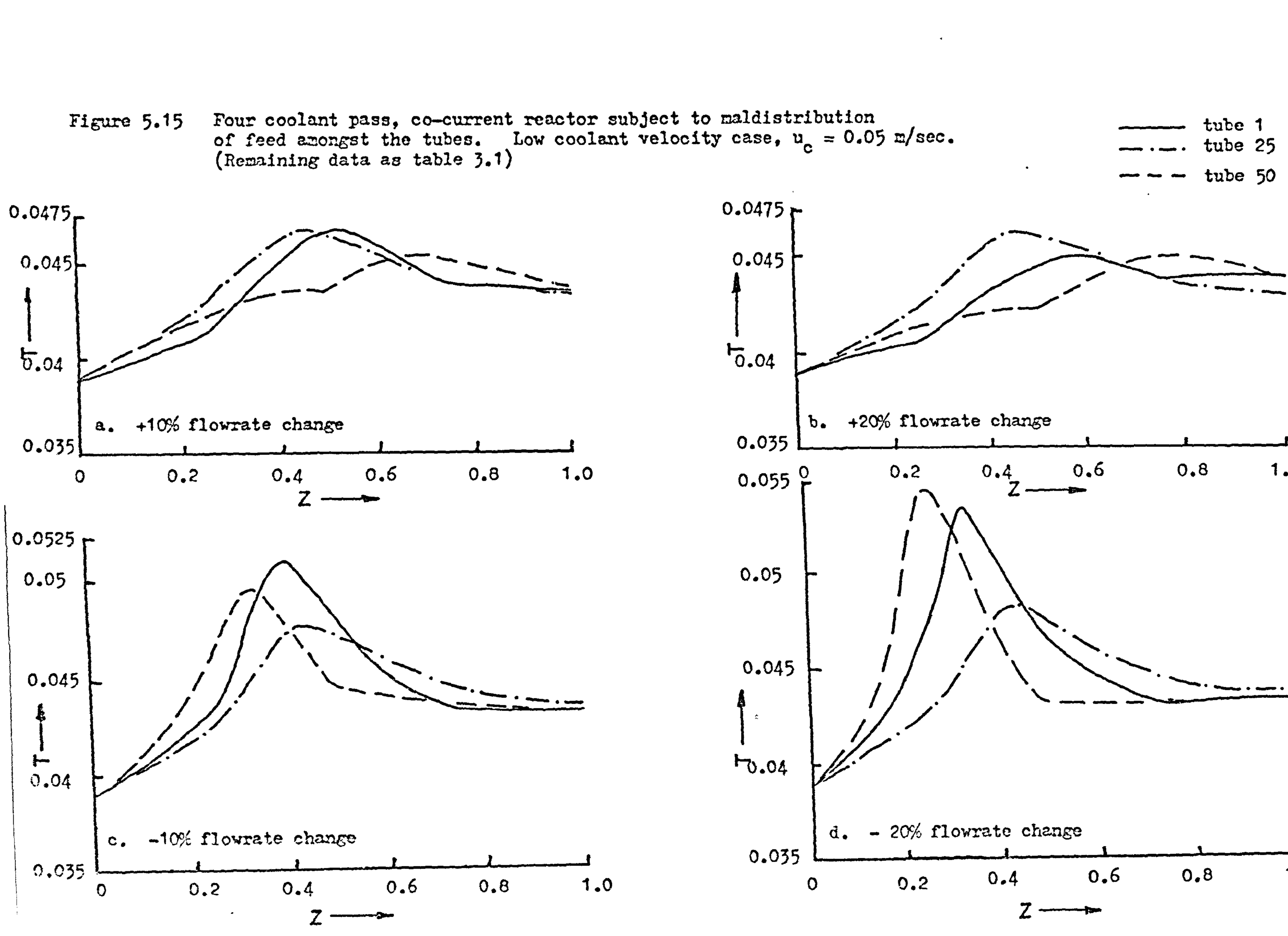

Figure 5.16 The tubeside temperature profile for a four coolant pass reactor used as a reference in the work on maldistribution of feed. High coolant velocity, u_c = 0.25 m/sec. (Non-specified data as table 3.1)

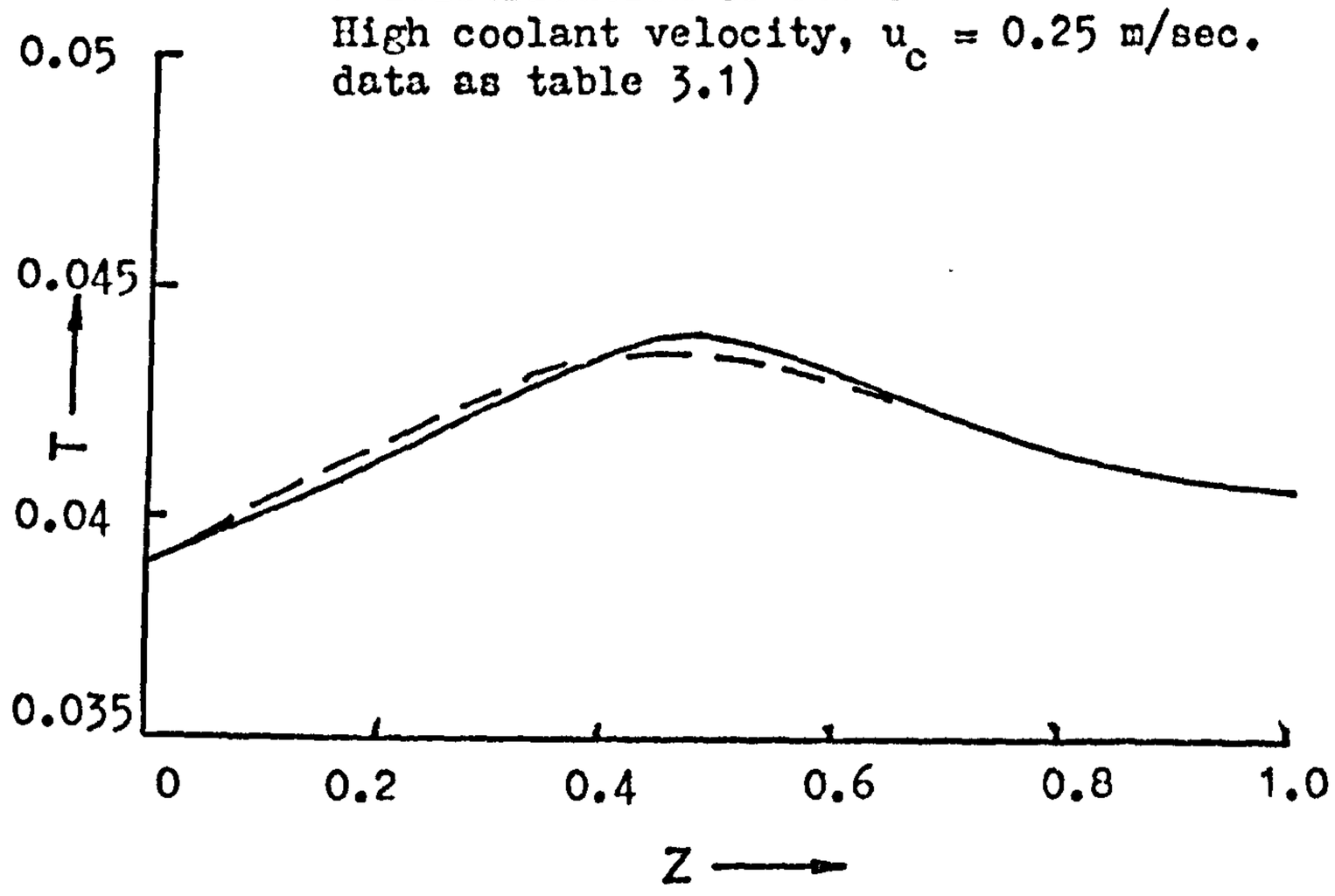

Figure 5.17 The tubeside temperature profiles for a four coolant pass co-current reactor, used as a reference in the work on the maldistribution of feed. Low coolant velocity, u_c = 0.05 m/sec. (Non-specified data as table 3.1)

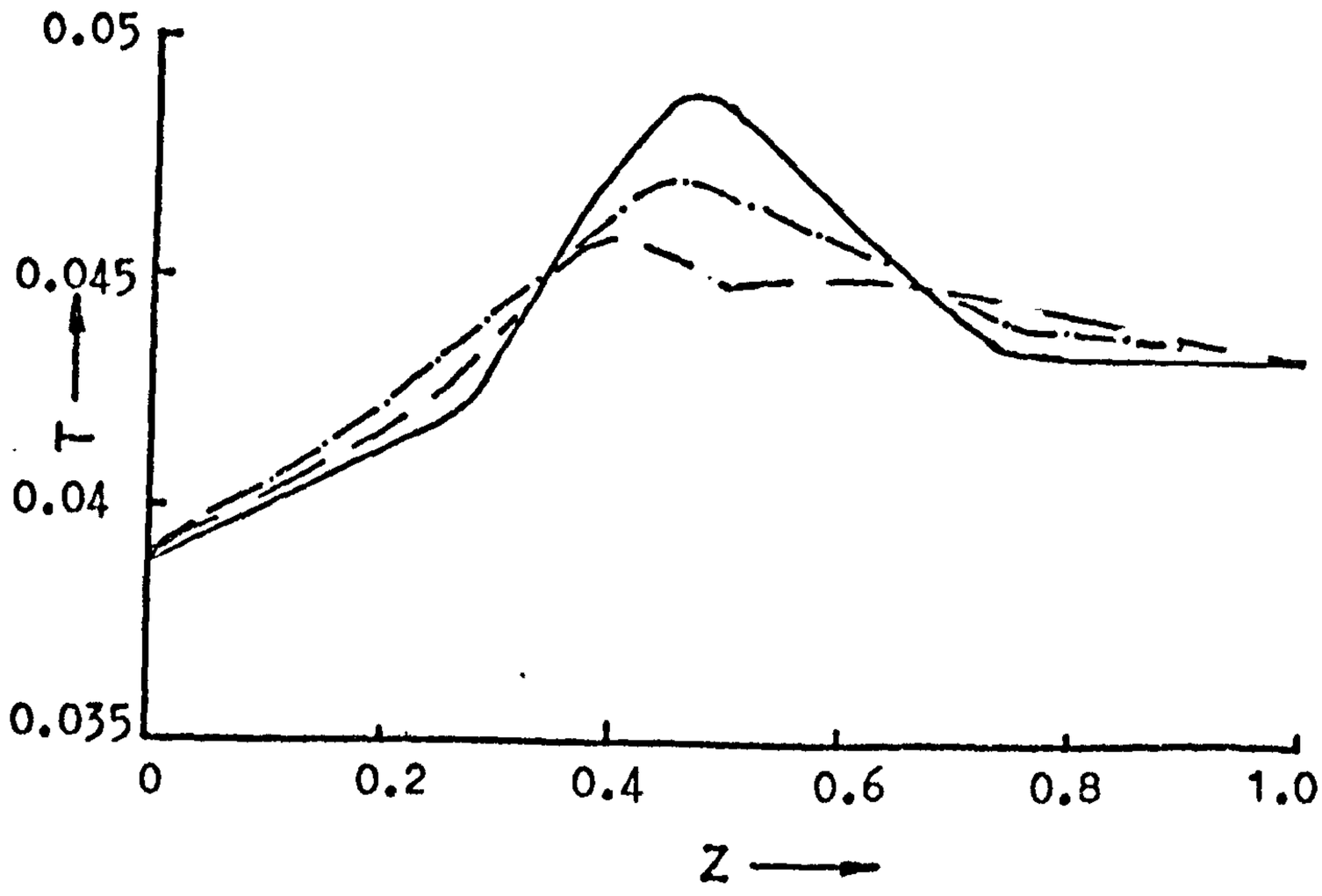

large coolant temperature rises. For comparison figures 5.16 and 5.17 respectively show the above cases without maldistribution of the feed.

Referring to the above figures, together with table 5.7, it can be seen that changes of up to 16% can be obtained in the overall coolant temperature rise when maldistribution occurs. The effects on the other tubes in the bundle can become significant. In the case of U_c = 0.25 m/sec the peak temperatures are raised by approximately 6 K in the most severe case, while with the lower coolant velocity the temperature peak is raised by 18 K when the flowrate in the abnormal tubes is decreased by 20%.

T A B L E 5.7

The Conversion and Coolant Temperature Rises in Reactors Subject to Maldistribution of the Feed to the Tubes. Coolant Velocity, U_c = 0.25 m/sec

% change in flow velocity in affected tubes	ΔT_c (^oK)	% change in coolant temp rise	% conversion tube 25
NONE	10.6	-	82.1 %
-10 %	11.5	8.5 %	83.0 %
+10 %	9.6	-9.4 %	81.6 %
-20 %	12.3	16.0 %	84.0 %
+20 %	9.0	-15.1 %	81.2 %

U_c = 0.05 m/sec

% change of flow velocity in affected tubes	ΔT_c (^oK)	% change in coolant temp rise	% conversion in tube 25
NONE	54.5	-	95.7 %
-10 %	57.0	4.6 %	97.2 %
+10 %	51.8	-5.0 %	95.3 %
-20 %	59.0	8.3 %	97.8 %
+20 %	49.0	-10.1 %	94.6 %

Obviously, such interactions between tubes cannot be accounted for in the single tube representations commonly employed in the design of large reactors. Although the effects of differing flowrates can be studied in these models (see figure 5.18 which shows a 20% decrease in flowrate), the information gained refers only to the tube in question, not to the tube bundle as a whole. Table 5.7 shows the overall conversions obtained in tube 25 of the tube bundle for varying degrees of flowrate maldistribution in tubes at extreme ends of the bundle. It should be noticed that although the values of the conversions change by up to 2%, the single tube model could never predict this as it is only concerned with the tube in which the flowrate is actually varying. Moreover, these predictions are invariably too low. Thus, for the case shown in figure 5.18, the conversions obtained by the single tube model are 76.4% for the reference conditions and 97.8% when the flow velocity is decreased by 20%. Tube 1 (one of the tubes subjected to a 20% decrease in flowrate), from the case shown in figure 5.14, gives conversions of 82.4% and 98.4% for the standard and maldistributed cases respectively.

It is clearly of some importance that maldistribution of feed to the tube bundle should be accounted for, and this is not possible in single tube models. Failure to do so can lead to significant errors in predicting system behaviour which can be particularly important in the case of the highly exothermic reactions being considered here.

5.7 Heat Generation and Removal in the Co-Current Reactor

An important step in attempting to understand the overall behaviour of multitubular reactors involves the interpretation of the relationship between the heat generation and removal. Figure 5.19 shows the overall heat generated and removed from tube 1 at various inlet coolant temperatures in a four coolant pass reactor operated at a coolant velocity of

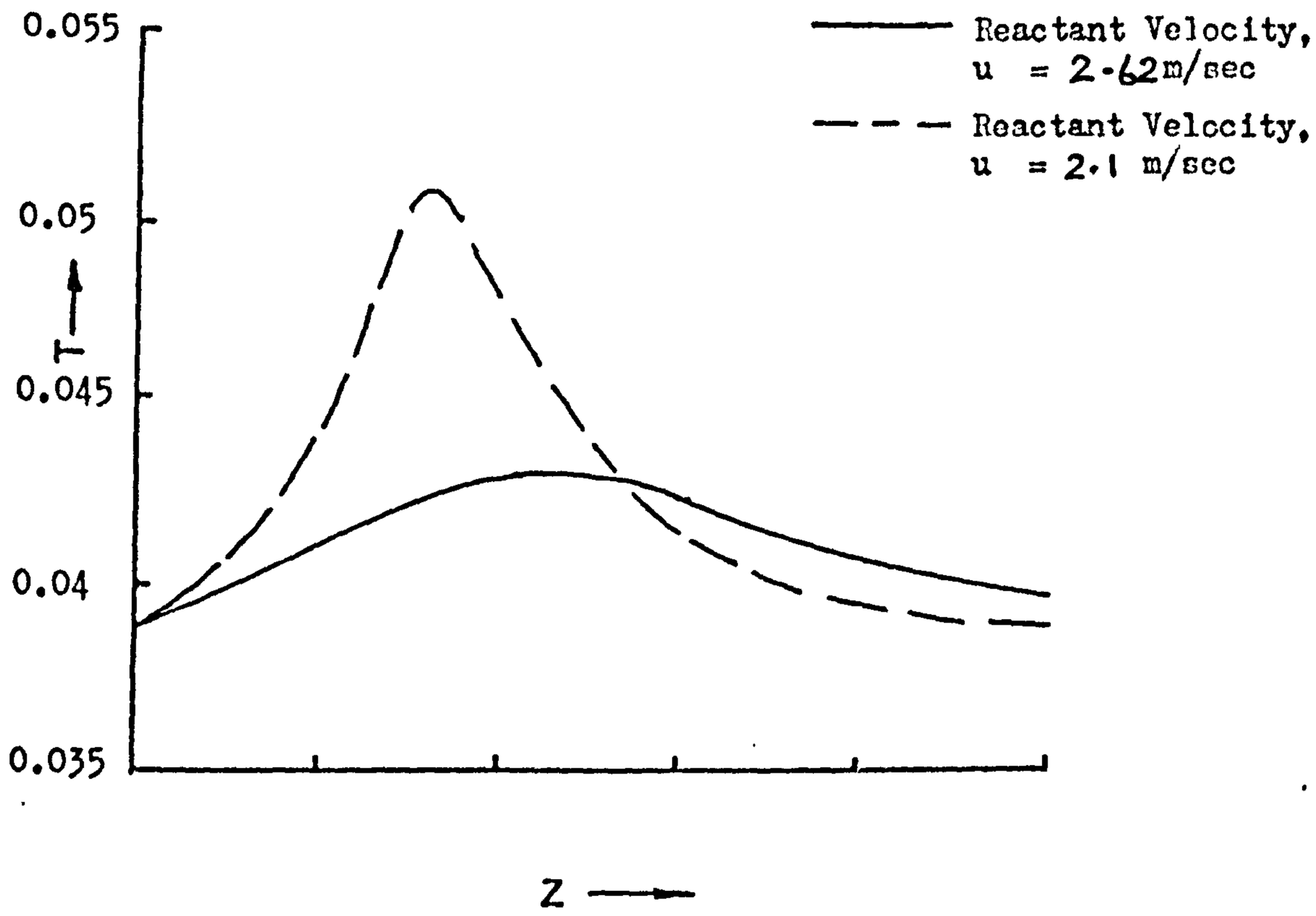

Figure 5.18 The effect of varying the reactant flowrate in a single tube, constant coolant temperature reactor model. (Non-specified data as table 3.1)

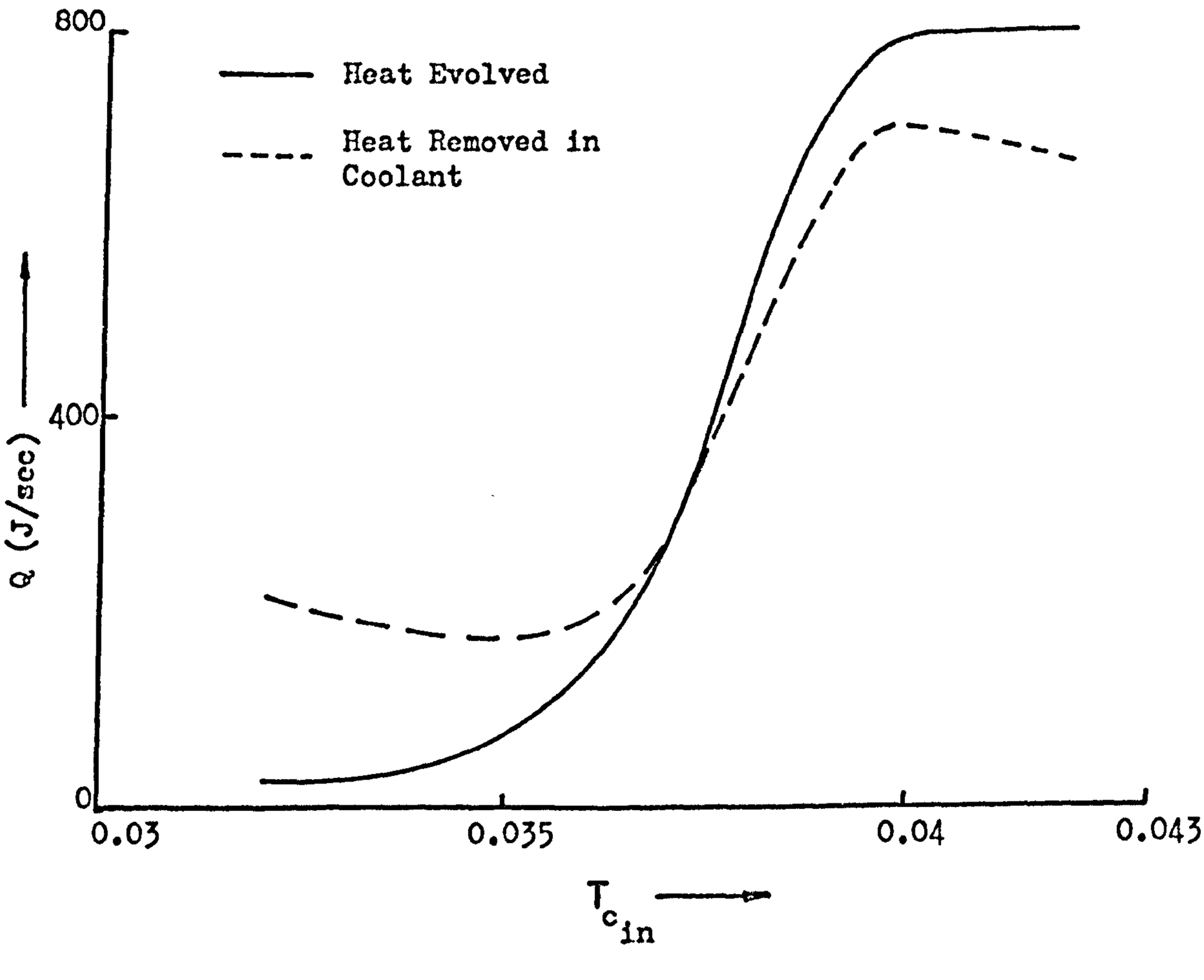

Figure 5.19 Overall heat generation and removal curves for tube 1 in a four coolant pass co-current reactor. Coolant velocity, u_c = 0.15 m/sec. (Remaining data as table 3.1)

U_c = 0.15 m/sec, the remaining data being given in table 3.1. The immediate impact of the curves is the highly non-linear nature. Referring to heat generation, increasing the inlet coolant temperature causes the reaction to accelerate, until, at high values total conversion of reactants occurs, and the generation of heat reaches its maximum value. Consideration of the heat removal indicates three regimes. The first, where the coolant quenches most of the reaction causing the system to behave as a heat exchanger. Increasing the inlet coolant temperature decreases the heat removal, since the driving force for heat transfer is decreased i.e. the tube to coolant temperature decreases. As the temperature is increased still further, the tubeside reaction generates more and more heat, the temperature driving force increases rapidly and in this, the second regime, the gradient of the heat removal line increases rapidly. Finally, as the coolant temperatures causing complete reaction are reached the curve levels off. Increasing the coolant temperature beyond this point once again causes the system to behave as a heat exchanger, since the maximum heat generation is occurring on the tubeside increasing the coolant temperature decreases the heat transfer driving force, and the heat removal therefore decreases. The point of intersection of the curves represents operating conditions such that all the heat evolved is removed by the coolant. When the heat removal curve lies above the heat generation curve the tubeside gases leave the system cooler than when they entered, when it lies below, they leave the system hotter.

It is now instructive to consider how the heat removal and generation are distributed amongst the coolant passes. Figures 5.20 (a), (b), (c) and (d) show the heat removal and generation curves for tube 1 in each pass of the system above. In coolant pass 1 the generation curve is always increasing with increasing coolant temperature, the heat removal going through a minima at $T_{c_{in}}$ = 0.0385. All other

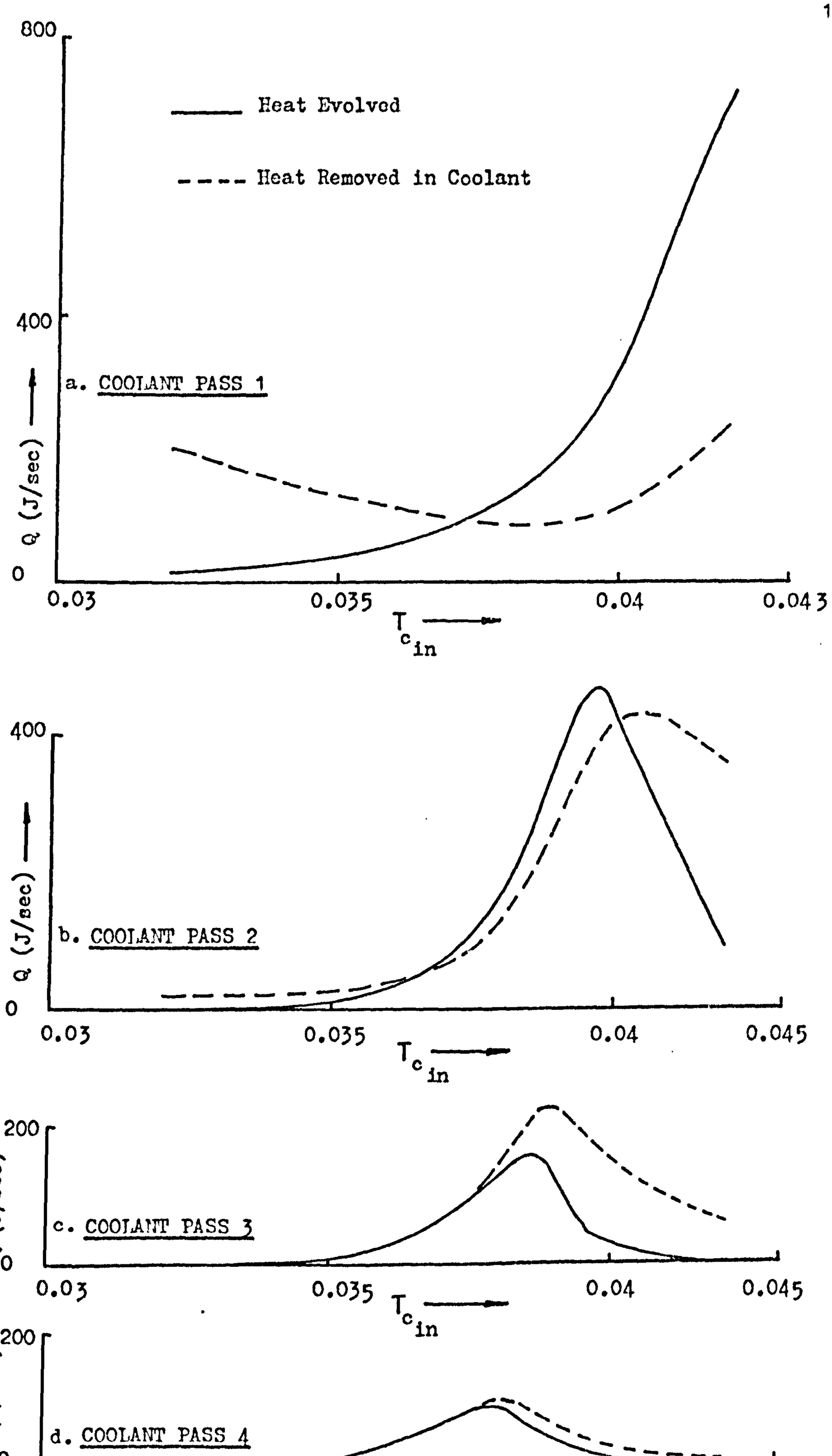

Figure 5.20 Heat generation and removal curves for tube 1 in various coolant passes of the four coolant pass co-current reactor of figure 5.19.

coolant passes show both heat curves passing through maxima. At low inlet coolant temperatures there is very little reaction (and therefore low heat loads) throughout the system, then as the coolant temperature increases more and more reaction occurs in all coolant passes. Thus, in all passes the heat loads increase. At high coolant temperatures however the amount of reaction in the early passes allows very little reactant to pass into subsequent regions of the bed, therefore, as the coolant temperature increases above a certain point, the heat loads on later coolant passes decrease. Ultimately, at very high coolant inlet temperatures, all the reaction will occur in coolant pass 1 and the heat generation in subsequent passes will fall to zero.

The information gained from studying such plots will be looked at in greater detail in chapter seven, where consideration will be given to the predictions of the most desirable operating conditions in both co- and counter-currently cooled reactor systems.

5.8 Conclusions

The reactor configuration has been shown to have significant effects both on the stability and achievable conversion of co-currently cooled reactors. As the number of coolant passes is increased, the overall conversion of the system decreases slightly, as do the differences between tubes at extreme ends of the bundle. Three or four coolant passes seem, for the data used here, to give the best performance for a wide range of operating conditions. Two coolant passes can have a large distribution of conversions across the tube bundle and therefore tend to exhibit undesirable operating characteristics.

The coolant, often ignored in the initial design stages, can be used to distribute the heat of reaction around the assembly, inducing further reaction in regions of depleted reactant. If adequate consideration is given to the effects of coolant flowrate and reactor

configuration the increased conversions and reduced pumping costs possible are economically very attractive, considering the small amount of effort required for such surveys when using the models developed in chapter four.

Although single tube models can be considered adequate for initial studies under relatively mild operating conditions, problems can arise when the basic assumptions of the models are not met. Hence, in very large multitubular bundles, where maldistribution of feed to the tubes can be a serious problem, the use of the simple models can result in misleading conclusions being reached, owing to the failure to account for the interactive nature of the heat transfer around the tube bundle.

CHAPTER 6

The Steady State Behaviour of Multitubular Reactors.

2. Counter-Current Cooling

6.1 Introduction

This chapter complements chapter five by considering the steady state behaviour of reactors operated counter-currently. Although there are many similarities between the two modes of operation, the major points of difference are the greater coolant flowrates necessary when operating counter-currently, and also the possibility of multiple steady states in the coolant. In particular, the former is due to the configuration of the reactor. The coolant, being heated as it travels through the system, is relatively hot when it reaches the coolant exit/reactant inlet, and consequently affects the high concentration feedstock at the inlet regions of the reactor. In the co-current mode, the cold inlet coolant affects the high concentrations of reactants. Hence, under critical operating conditions, if the co-current arrangement is at the limits of stability, the coolant exit temperature in the counter-current must be kept low for it to be stable, and this is most easily achieved by using a higher coolant flowrate than in the co-current system.

Multiple steady states are always a feature of systems containing a feedback loop. In the counter-currently cooled reactor the feedback consists of the reaction heat carried in the coolant. The phenomenon has been mentioned by Adderley[41], who modelled the counter-current multitubular reactor and Luss and Medellin[57] who observed three different steady states in a single tube homogeneous reactor with counter-current cooling.

Throughout this chapter the detailed cell model developed in chapter

four has been used. The lumping assumption is not applied so that the results at both high and low coolant flowrates can be consistantly compared.

6.2 The Effects of Coolant Flowrate and Reactor Configuration on the System Performance

6.2.1 Variation of the Coolant Flowrate

A major difference between the counter-currently cooled reactor and the co-current system considered earlier is the much greater sensitivity of the former to the coolant outlet temperature. This phenomenon, which is due to the outlet coolant temperature affecting the inlet, high concentration reactant gases necessitate greater coolant mass flowrates for the same degree of stability than would be needed for the identical system operated co-currently.

Figure 6.1 shows the effect of varying the coolant mass flowrate in a four coolant pass, counter-current reactor. The lower the coolant velocity, the higher the residence time and therefore the increased coolant temperatures cause higher rates of reaction. The overall coolant temperature rises are 68 K, 33 K and 15 K respectively for the coolant velocities U_c = 0.05 m/sec, 0.1 m/sec and 0.2 m/sec. Note that the corresponding temperature rises for a co-current system are 54 K, 27 K and 13 K.

6.2.2 Influence of the Number of Coolant Passes

The tubeside temperature profiles that are obtained under different shell-side configurations are shown in figures 6.2 and 6.3. As in the co-current case, both constant coolant flowrate and constant coolant velocity are considered, the resulting coolant temperature rises and conversions being given in tables 6.1 and 6.2. Referring to the constant flowrate case first, it can be seen that there is little

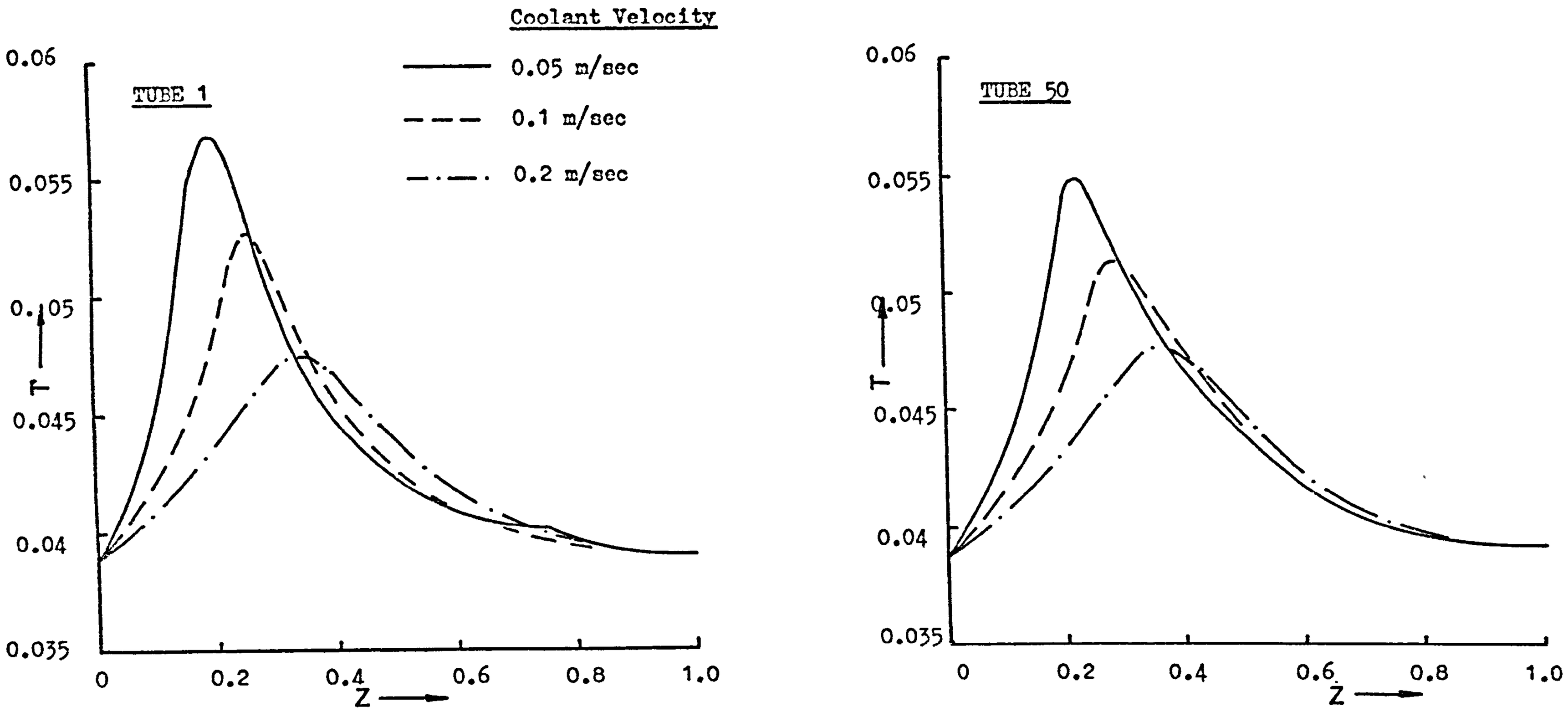

Figure 6.1 Variation of the coolant flowrate in a four coolant pass counter-current reactor. (Non-specified data as table 3.1)

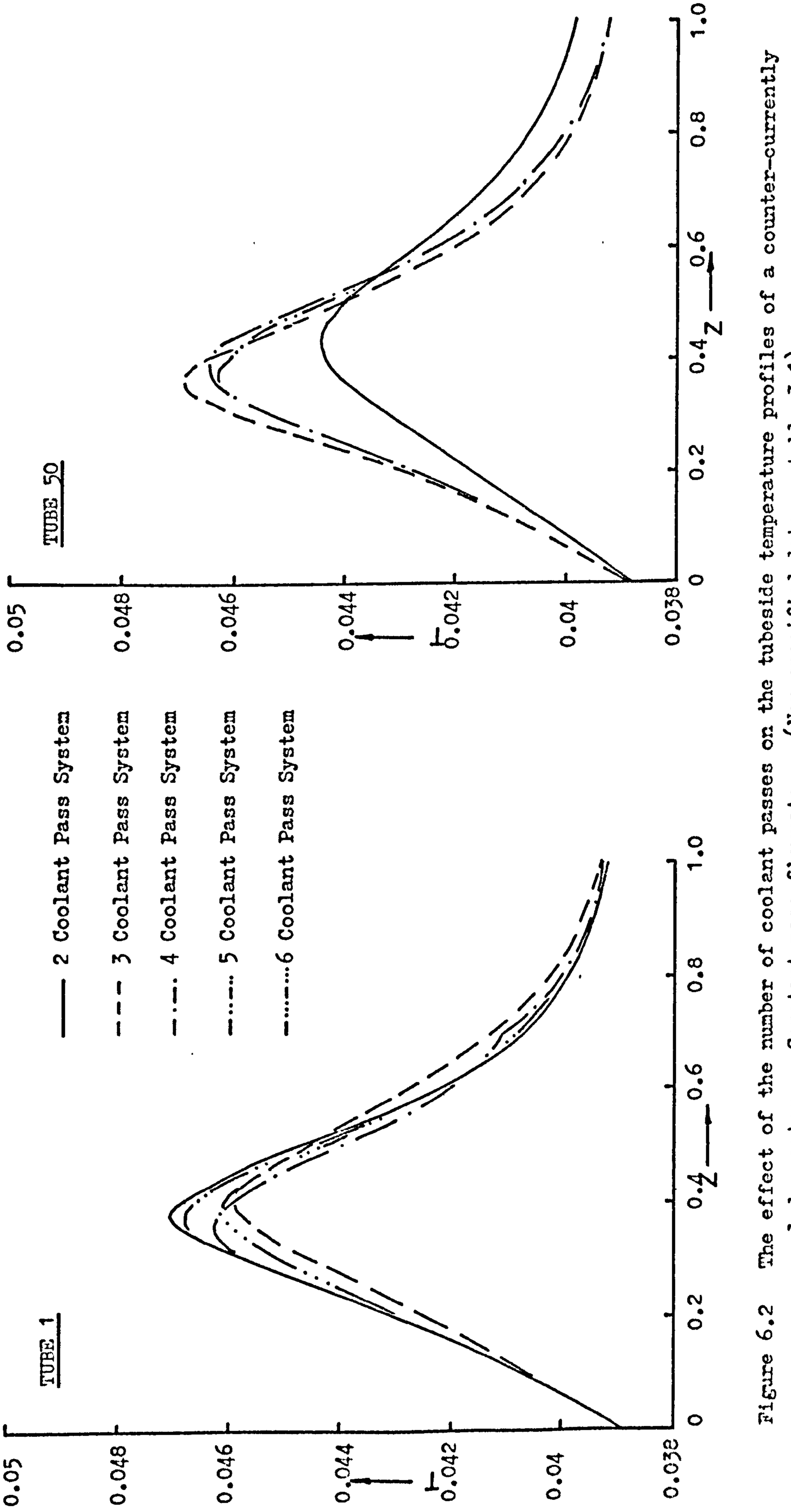

Figure 6.2 The effect of the number of coolant passes on the tubeside temperature profiles of a counter-currently cooled reactor. Constant mass flowrate. (Non-specified data as table 3.1)

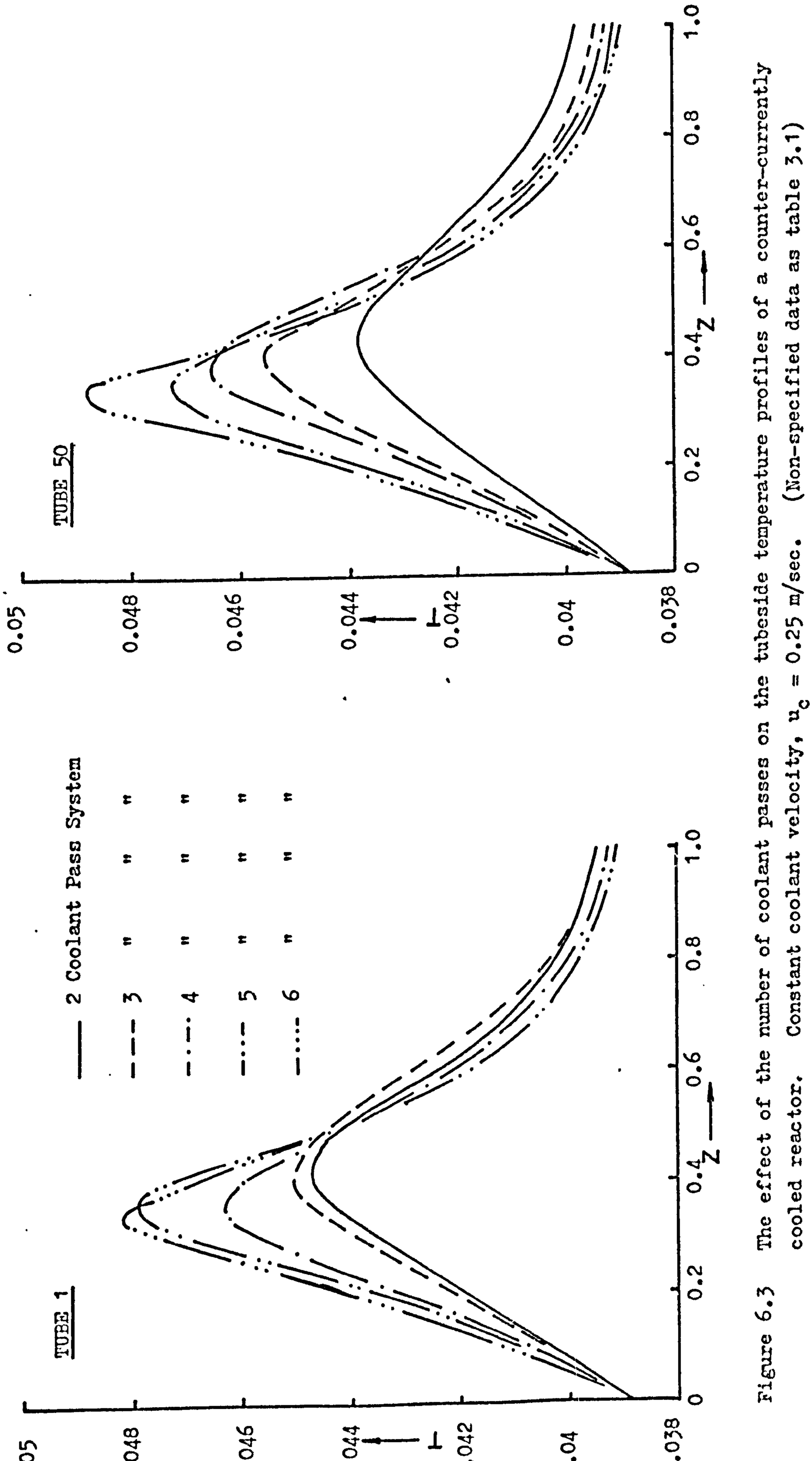

Figure 6.3 The effect of the number of coolant passes on the tubeside temperature profiles of a counter-currently cooled reactor. Constant coolant velocity, u_c = 0.25 m/sec. (Non-specified data as table 3.1)

T A B L E 6.1

Effect of the Number of Coolant Passes on the Performance of a Counter-Current Reactor at Constant Coolant Mass Flowrate

No. of Passes	ΔT_c (^oK)	% Conversion	
		TUBE 1	TUBE 50
2	11.7	91.3	84.2
3	12.0	89.0	90.3
4	12.2	89.5	90.3
5	12.3	90.7	89.8
6	11.4	89.3	89.7

T A B L E 6.2

Effect of the Number of Coolant Passes on the Performance of a Counter-Current Reactor at Constant Coolant Velocity, U_c = 0.25 m/sec

No. of Passes	ΔT_c (^oK)	% Conversion	
		TUBE 1	TUBE 50
2	5.5	84.6	81.3
3	8.8	86.6	87.3
4	12.3	89.8	90.5
5	15.8	93.1	92.2
6	18.1	93.7	94.4

difference between any of the configurations containing more than two passes. Once again, this two pass configuration differs from all the others, having a wider variation of conversions across the bundle diameter. Table 6.1 shows that, as in the co-current reactor, increasing the number of coolant passes causes the conversion to go through a maximum value. This maximum occurs at five coolant passes.

However, as the difference between the conversions obtained from three, four and five passes is very small, the use of more than four passes would not be justified owing to the increased pressure drop and hence pumping costs that would follow.

The reasons for the similarity between the reactors containing more than two coolant passes can be explained by considering the interaction between the coolant and the tubeside gases. Because the coolant temperatures are high in the first part of the tube bundle near the tube inlets, a large amount of reaction takes place here consuming most of reactant. Heat generation is therefore the dominant process, as will be shown later in section 6.7. In the second part of the reactor, near the coolant inlet, very little reaction occurs and heat transfer from the tubes to the coolant is the dominant process. This is caused by the low reactant concentration and the low coolant temperature environment. Consequently, the later stages of the system act essentially as a heat exchanger, and since the gases entering it are at approximately the same temperature regardless of the number of coolant passes, with the mass flowrate of coolant the same in each case, they are therefore cooled by similar amounts and hence the coolant is heated to the same extent. In the first half of the reactor, heat is being generated much faster than it can be removed and so the tubeside temperatures tend to be similar, whatever the number of coolant passes. Thus, there is a similar amount of heat available to the coolant in each configuration, so, although the amount of heating of the coolant in each pass varies with the length of the tubes in that pass, the overall effect in this part of the reactor is similar in each case. As a result the overall conversions and temperature rises are approximately the same.

Intuitively, it may be argued that cases in which the majority of the reaction, and therefore the tubeside hotspot, occur in the latter part of the reaction tubes, then the number of coolant passes would have

a greater effect on the system performance. However, for this to happen the outlet coolant temperature would have to be low enough to stop the reaction occurring in the early stages of the bed. Consequently, the coolant temperature must be low throughout the system. Hence, the rate of reaction and the rate of heat generation must also be low, resulting in the amount of heat removal necessary being so small that the number of coolant passes makes little difference.

Predictably, the constant coolant velocity case shows that the more coolant passes used, the greater the conversion obtained. This is because increasing the number of passes increases the coolant residence time and consequently higher coolant temperature rises are obtained. The larger coolant temperatures then result in greater conversions.

T A B L E 6.3

Effect of the Number of Passes on the Performance of a Counter-Current Reactor. Tube Length 4 m. Constant Coolant Mass Flowrate

No. of Passes	ΔT_c (^oK)	% Conversion	
		TUBE 1	TUBE 50
2	11.1	88.7	84.6
3	11.5	88.1	87.6
4	11.5	87.5	88.5
5	11.7	88.4	88.0
6	10.7	87.4	87.44

T A B L E 6.4

Effect of the Number of Coolant Passes on the Performance of a Counter-Current Reactor. Tube Length 6 m. Constant Coolant Mass Flowrate

No. of Passes	ΔT_c (°K)	% Conversion	
		TUBE 1	TUBE 50
2	11.9	92.7	85.3
3	12.3	89.4	92.21
4	12.6	91.5	91.3
5	12.6	91.1	91.8
6	11.7	90.6	91.3

Comparing different lengths of reactor tubes, at constant mass flowrate, gives the same results as in the co-current case. Tables 6.3 and 6.4 show the results obtained for tube lengths 4 m and 6 m respectively. The coolant temperature rise and conversions are higher the longer the tube. An important difference between the co- and counter-current modes of operation should be pointed out here. In the co-current case, the longer tubes have no effect on the performance of the up-stream sections of the reactor tubes. Hence, reactors with a stable temperature peak at one tube length will still be stable with a longer tube. (Unless instability is caused by the extra heating of the coolant forming a hotspot in the additional length of tube. For instance a 4 m tube might not contain a hotspot and be stable, whereas a 5 m tube could have an unstable temperature peak in the last metre of the bed. This should be unlikely in the systems under study here, as most of the reactants should have been used up in the earlier parts of the bed.) However, in a counter-current system, the extra heating of the coolant, when using a longer tube, is fed back into the upstream section of the tubeside making the hotspot for a long tube higher than that for a shorter tube. Thus, it is important to consider the feedback of heat

through the coolant when considering using longer tubes in a counter-current reactor.

T A B L E 6.5

Fraction Conversions for a Counter-Current Reactor System

INLET TEMPERATURE		510 K	520 K	530 K
COOLANT VELOCITY		0.1 m/sec	0.2 m/sec	0.1 m/sec
2 PASS	TUBE 1	94.3 %	93.7 %	99.5 %
	TUBE 50	80.0 %	85.6 %	96.2 %
3 PASS	TUBE 1	93.9 %	92.9 %	99.4 %
	TUBE 50	92.4 %	91.2 %	98.1 %
4 PASS	TUBE 1	92.4 %	92.1 %	92.24 %
	TUBE 50	94.8 %	92.8 %	98.9 %

Tubeside temperature profiles for two, three and four pass reactors under various operating conditions are shown in figures 6.4, 6.5 and 6.6. The conversions associated with these are given in table 6.5. In all cases, increasing the coolant velocity decreases and moves the tubeside hotspot towards the reactant outlet, though in general, they always remain in the first half of the tube. Reducing the reactant inlet temperature has a similar effect. The outstanding feature of these examples is once again the large spread of conversions from tubes across the bundle diameter in the two coolant pass configuration.

An interesting feature of the counter-currently cooled reactor is that unlike heat exchangers, the maximum coolant temperature is not always at the outlet of the system. This phenomenon occurs in three or more coolant pass reactors, when, under mild conditions, small temperature peaks occur in the second pass, very little reaction occurring in the first. Consequently, the temperature of the coolant decreases

through the coolant when considering using longer tubes in a counter-current reactor.

T A B L E 6.5

Fraction Conversions for a Counter-Current Reactor System

INLET TEMPERATURE		510 K	520 K	530 K
COOLANT VELOCITY		0.1 m/sec	0.2 m/sec	0.1 m/sec
2 PASS	TUBE 1	94.3 %	93.7 %	99.5 %
	TUBE 50	80.0 %	85.6 %	96.2 %
3 PASS	TUBE 1	93.9 %	92.9 %	99.4 %
	TUBE 50	92.4 %	91.2 %	98.1 %
4 PASS	TUBE 1	92.4 %	92.1 %	92.24 %
	TUBE 50	94.8 %	92.8 %	98.9 %

Tubeside temperature profiles for two, three and four pass reactors under various operating conditions are shown in figures 6.4, 6.5 and 6.6. The conversions associated with these are given in table 6.5. In all cases, increasing the coolant velocity decreases and moves the tubeside hotspot towards the reactant outlet, though in general, they always remain in the first half of the tube. Reducing the reactant inlet temperature has a similar effect. The outstanding feature of these examples is once again the large spread of conversions from tubes across the bundle diameter in the two coolant pass configuration.

An interesting feature of the counter-currently cooled reactor is that unlike heat exchangers, the maximum coolant temperature is not always at the outlet of the system. This phenomenon occurs in three or more coolant pass reactors, when, under mild conditions, small temperature peaks occur in the second pass, very little reaction occurring in the first. Consequently, the temperature of the coolant decreases

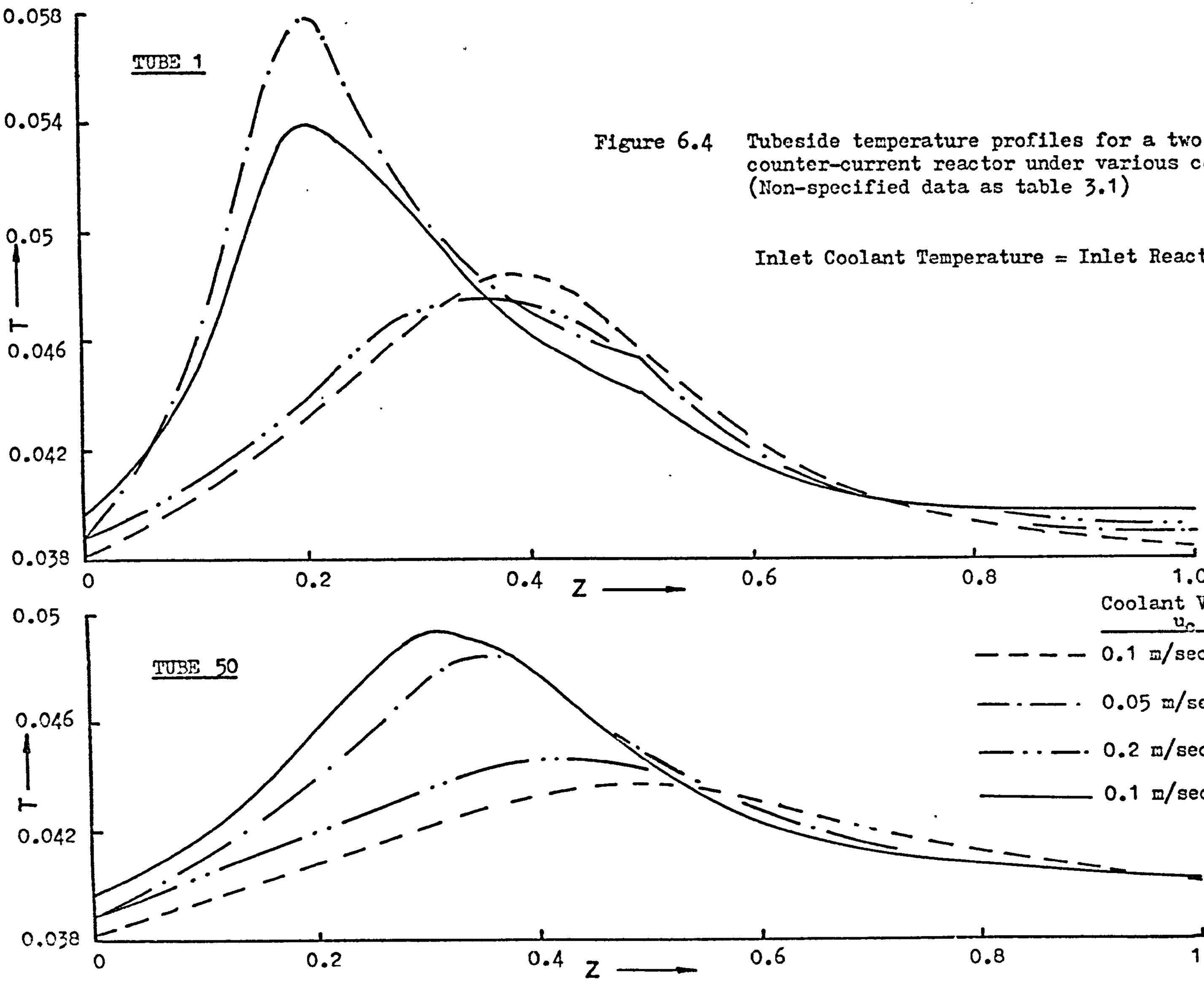

Figure 6.4 Tubeside temperature profiles for a two coolant pass counter-current reactor under various conditions. (Non-specified data as table 3.1)

Inlet Coolant Temperature = Inlet Reactant Temperature

Figure 6.5 Tubeside temperature profiles for a three coolant pass counter-current reactor under various conditions. (Non-specified data as table 3.1)

Coolant Velocity u_c	Inlet Reactant Temperature
0.1 m/sec	530 K
0.1 m/sec	510 K
0.05 m/sec	520 K
0.2 m/sec	520 K

Inlet Coolant Temperature = Inlet Reactant Temperature

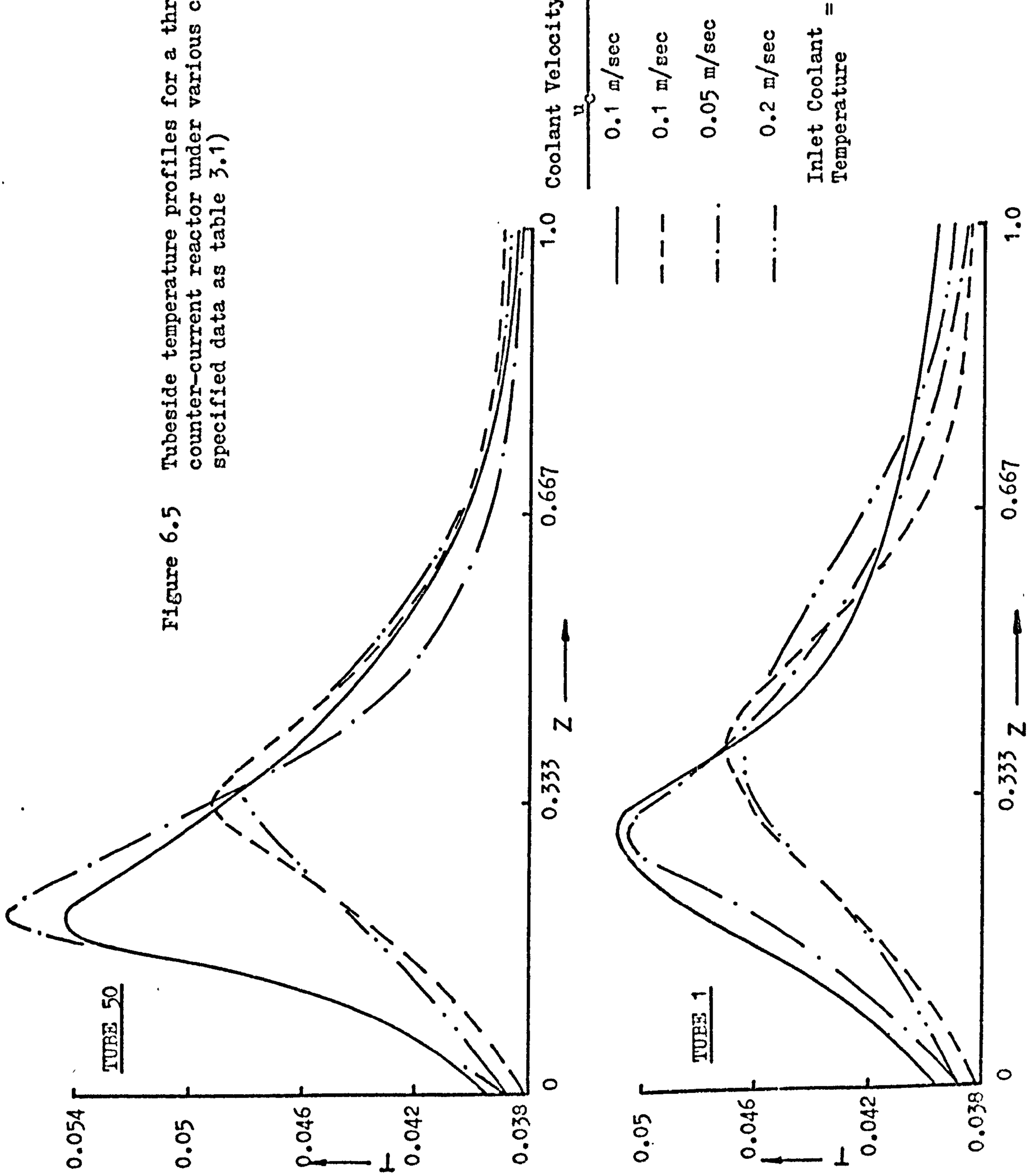

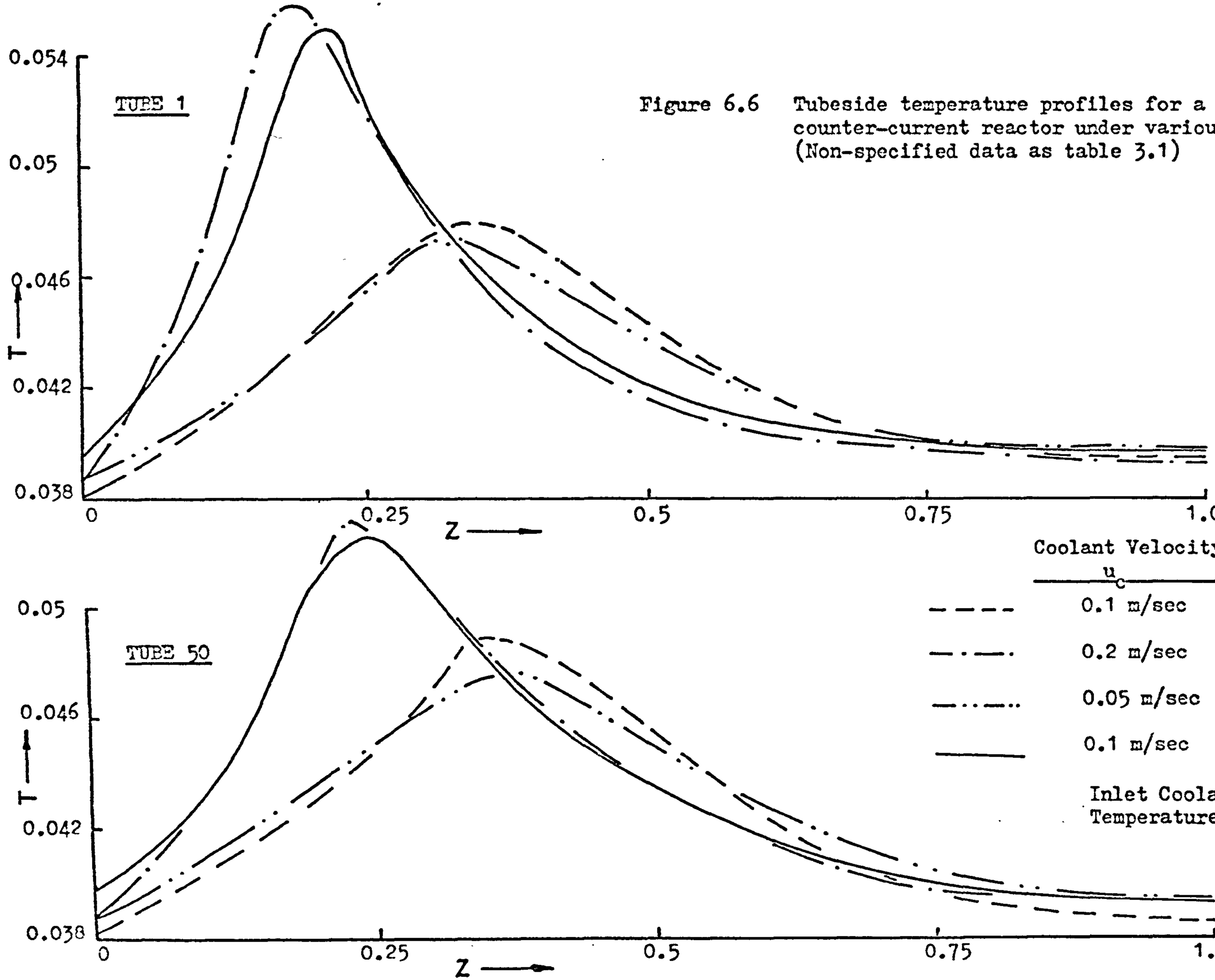

Figure 6.6 Tubeside temperature profiles for a four coolant pass counter-current reactor under various conditions. (Non-specified data as table 3.1)

	Coolant Velocity u_c	Inlet Reactant Temperature
- - - -	0.1 m/sec	510 K
— · — ·	0.2 m/sec	520 K
— · · — · ·	0.05 m/sec	520 K
———	0.1 m/sec	530 K

Inlet Coolant Temperature = Inlet Reactant Temperature

across the first pass due to heat loss to the reactants. The resulting maximum shell-side temperature is then at the exit of coolant pass 2 and not 1.

6.3 The Effect of the Configuration on the Position of the Tubeside Temperature Hotspot

The position of the tubeside temperature peaks for each tube are shown in figures 6.7, 6.8 and 6.9, for different configurations and operating conditions. The outstanding difference between these plots and those shown in chapter five for the co-current system is the absence of temperature peaks in the later sections of the reactor tubes. This situation arises because of the low coolant temperatures and low reactant concentrations in these regions. Overall, the conclusions of the co-current system apply here, increasing the coolant flowrate or decreasing the reactant inlet temperature moves the tubeside temperature peaks towards the reactant outlet. However, in this case the absence of the feed forward of heat in the coolant does not allow the production of the multiple tubeside temperature peaks evident in the co-currently cooled system. In all the configurations considered the variation in the position of the tubeside temperature peaks is much less than in the case of the co-current reactor. This is due to the increased coolant temperatures around the main reaction zone, and in the cases where the hotspot is in the same position across the entire tube bundle it is probable that temperature runaway has occurred. The variation in the coolant temperature across the bundle will then have little effect on the reaction inside the tube, mass transfer considerations will form the rate limiting step under these conditions. This indicates the need for higher coolant velocities when running a reactor counter-currently rather than co-currently.

The prediction of the tube containing the maximum temperature peak

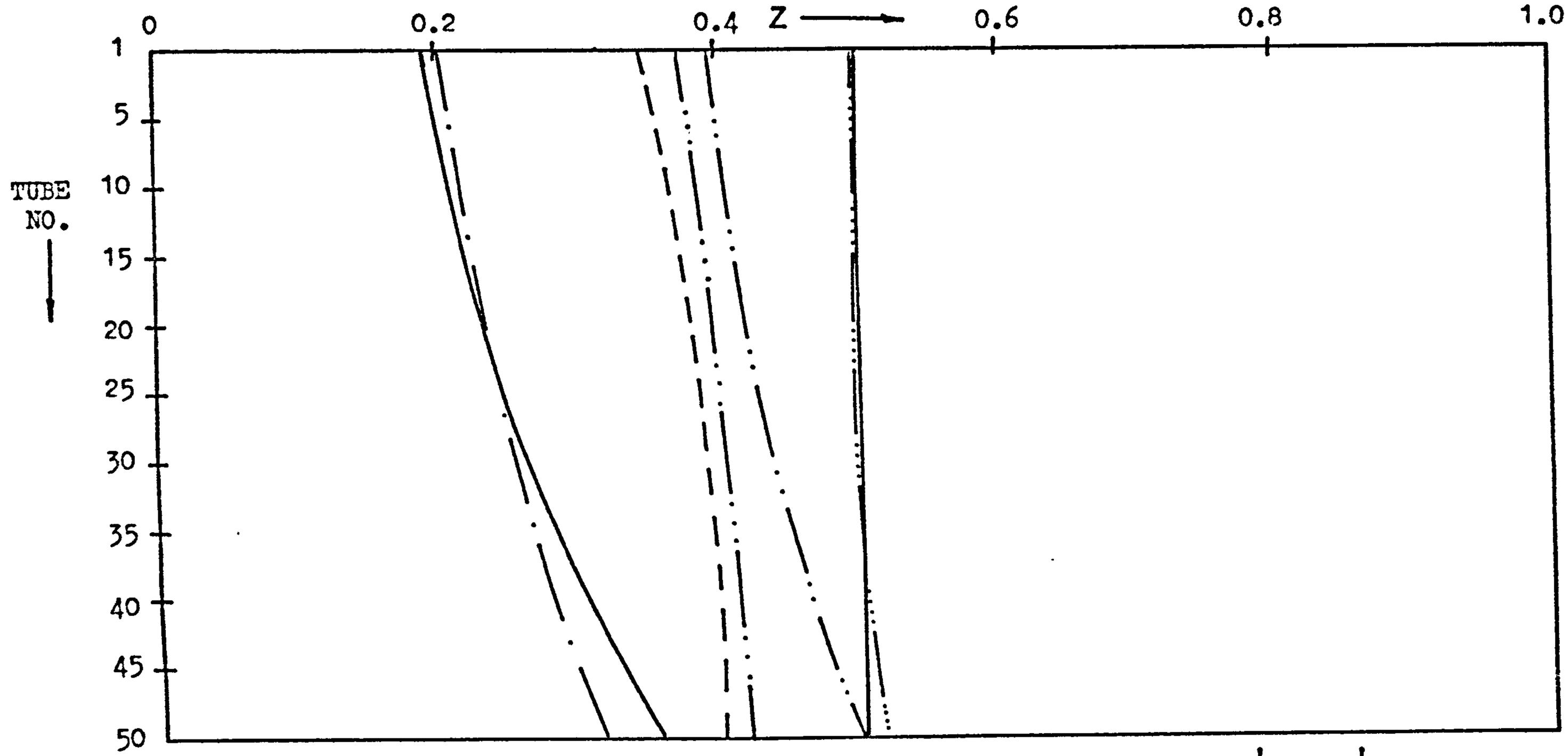

——— Coolant Velocity 0.05 m/sec $T'_{c_{in}} = T'_{o} = 520$ K

– – – – " " 0.20 m/sec " " = 520 K

—·—· " " 0.10 m/sec " " = 530 K

—··—·· " " 0.10 m/sec " " = 510 K

—···—··· " " 0.25 m/sec " " = 520 K

—····— " " 0.25 m/sec " " = 510 K

Figure 6.7 Tubeside hotspot positions in a two coolant pass counter-current reactor. (Non-specified data as table 3.1)

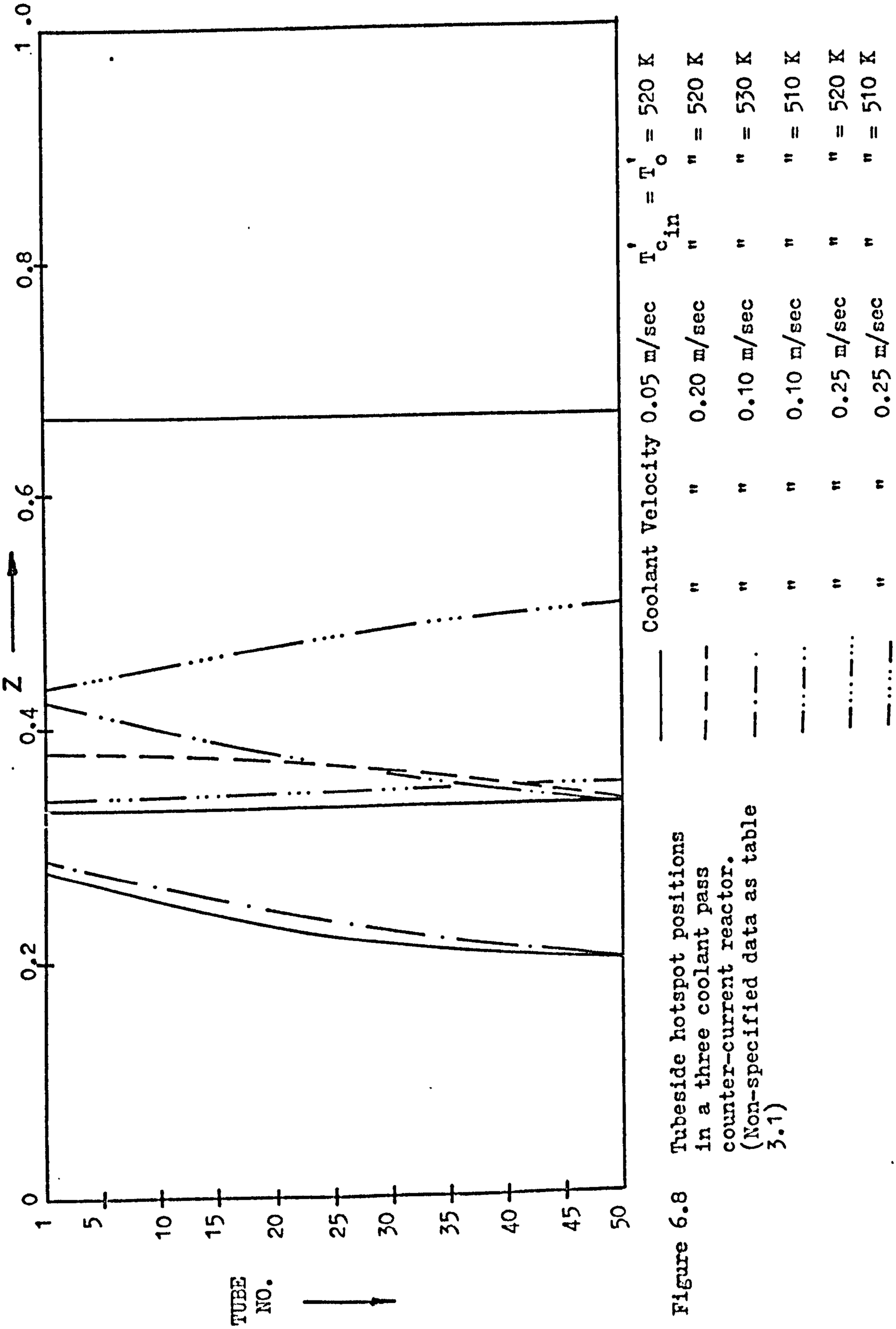
1.0
0.8
0.6
0.4
0.2
0
Z
1
5
10
15
20
25
30
35
40
45
50
TUBE NO.
Coolant Velocity 0.05 m/sec T'cin = To' = 520 K
" 0.20 m/sec " = " = 520 K
" 0.10 m/sec " = " = 530 K
" 0.10 m/sec " = " = 510 K
" 0.25 m/sec " = " = 520 K
" 0.25 m/sec " = " = 510 K
Tubeside hotspot positions
in a three coolant pass
counter-current reactor.
(Non-specified data as table
3.1)

Figure 6.8

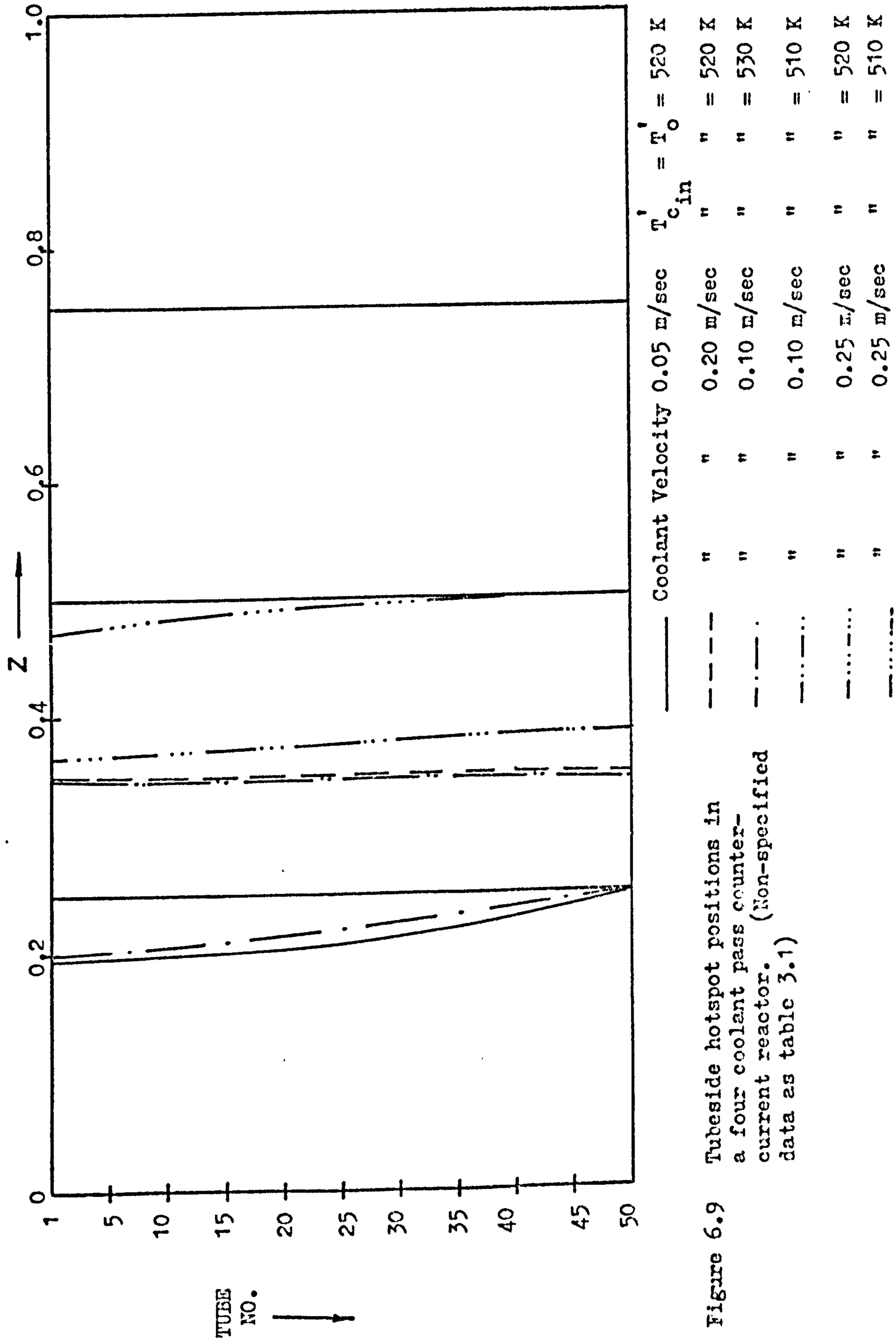

Figure 6.9 Tubeside hotspot positions in a four coolant pass counter-current reactor. (Non-specified data as table 3.1)

is, as in the case of the co-current system, not possible in the present state of knowledge. However, it is known that this tube will be either tube 1 or 50, and using the technique developed in chapter five it is possible to give an estimate of which tube it will be for a given configuration. Unfortunately, there is no guarantee that this estimate will be correct. Table 6.6 shows the position of the tube containing the maximum tubeside temperature peak for different numbers of coolant passes based on the operating parameters used in figures 6.2 and 6.3.

T A B L E 6.6

The Position of the Maximum Tubeside Temperature Peak in Counter-Current Reactors.

No. of Coolant Passes	TUBE IN WHICH MAXIMUM PEAK OCCURS	
	CONSTANT MASS FLOW CASE	CONSTANT VELOCITY CASE
2	1	1
3	50	50
4	50	50
5	1	1
6	50	50

In chapter five it was shown that for co-current reactors it is often true that the tube containing the maximum temperature peak is the tube at the outlet of the coolant pass containing the tubeside hotspots. The difficulty in using this information, a priori, is that there is no way of knowing accurately the position of the hotspot without solving the reactor heat and mass balances. Figure 6.10 uses the data of figure 6.2 to test the above procedure in the case of the counter-current reactor. Comparing the results with the true positions of the maximum tubeside temperature peak given in table 6.6, the procedure

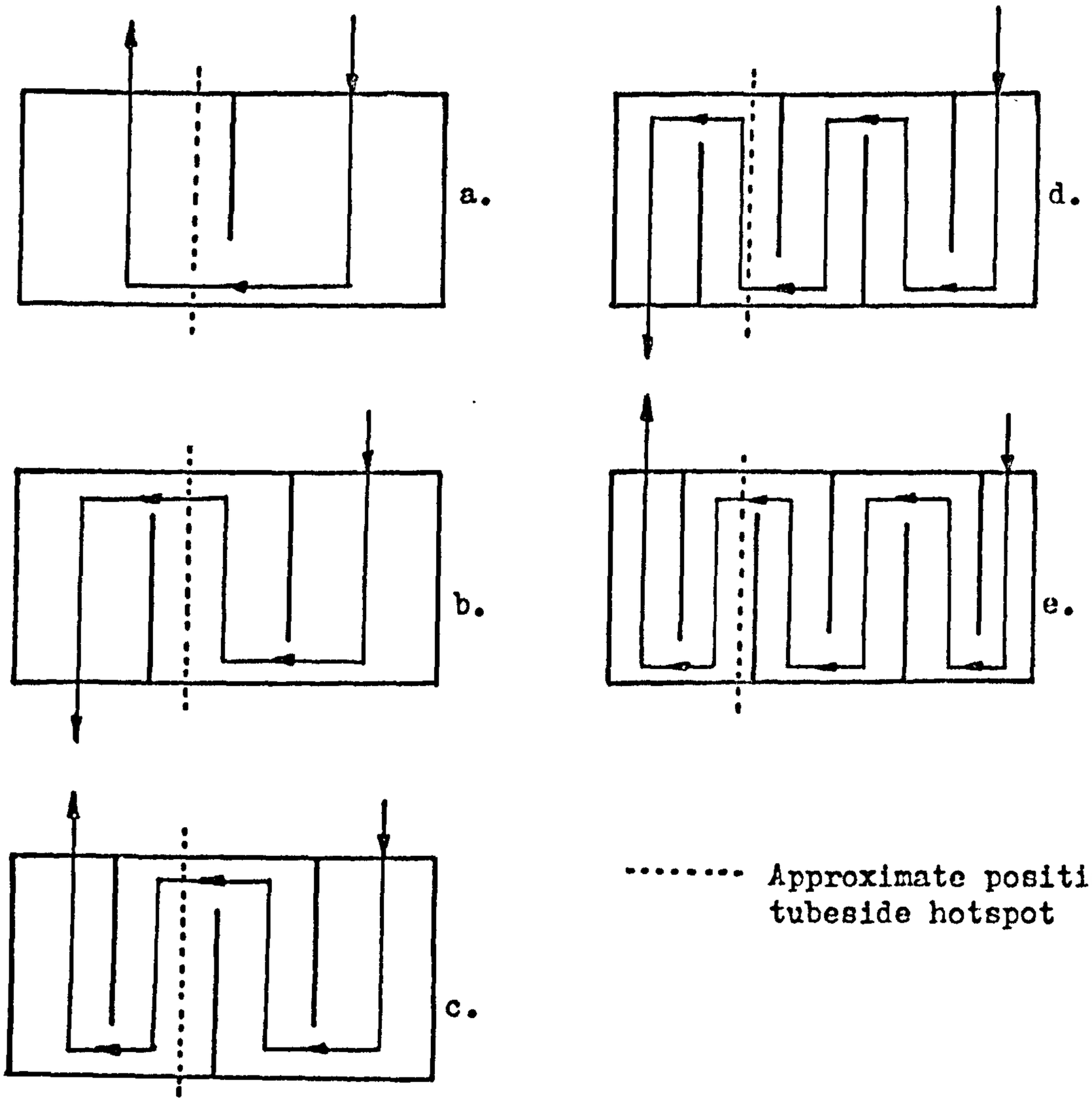

Figure 6.10 Schematic diagram used in the prediction of the tube containing the maximum tubeside temperature in counter-current reactors.

fails in the case of the three pass system, figure 6.10(b). It would be expected, using the above, that tube 1 would contain the maximum hotspot, but actually it is tube 50. This behaviour is caused by the heating/cooling effect of the coolant in the first coolant pass. The reactant gases leaving tube 1 pass 1 are cooler than those leaving tube 50 pass 1, and, even though the coolant temperature around tube 1 pass 2 is higher than that around tube 50 pass 2, the latter tube contains the higher temperature peak. Hence, as in the co-current system there is no general rule which gives the position of the tube containing the most severe reaction conditions. Clearly, in monitoring the performance of such systems measurements must be taken at both extremities of the bundle diameter.

6.4 The Variation of the Overall Heat Transfer Coefficient

The effect of varying the heat transfer coefficient is important because of the difficulty of accurately measuring the heat transfer coefficients in the system. Using the common correlations, errors of up to 25% can be introduced into the estimation of certain parameters, so it is therefore useful to examine how the predicted system performance is affected by such uncertainty. Figure 6.11 gives the tubeside temperature profiles for a four coolant pass reactor with different values of the wall Nusselt number.

As in the co-currently cooled configuration, decreasing the inside heat transfer coefficient increases the temperature of the tubeside fluids. Two mechanisms are important here; first, the lower heat transfer coefficient means that less heat is given to the coolant, and second, because the temperature of the reactants is higher, the reaction rate is increased, producing more heat. The coolant temperature rises for the three cases shown, Nu_w = 14.6, 10.0 and 5.0 are 12.3 K, 12.9 K and 13.4 K respectively. Thus, instead of decreasing the amount of heat

Figure 6.11 The effect of variations in the wall Nusselt number on the tubeside temperature profiles for a four coolant pass counter-current reactor. (Non-specified data as table 3.1)

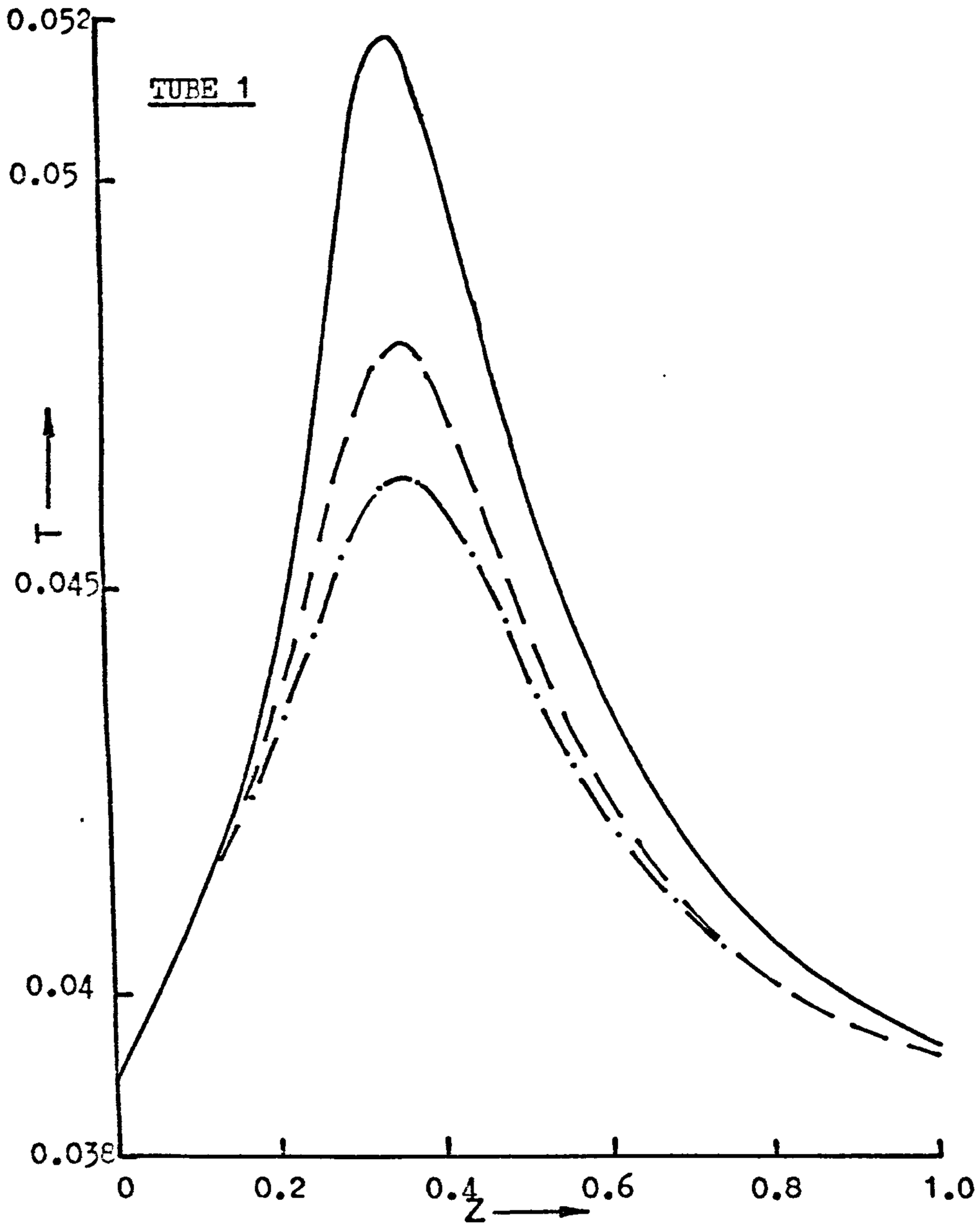

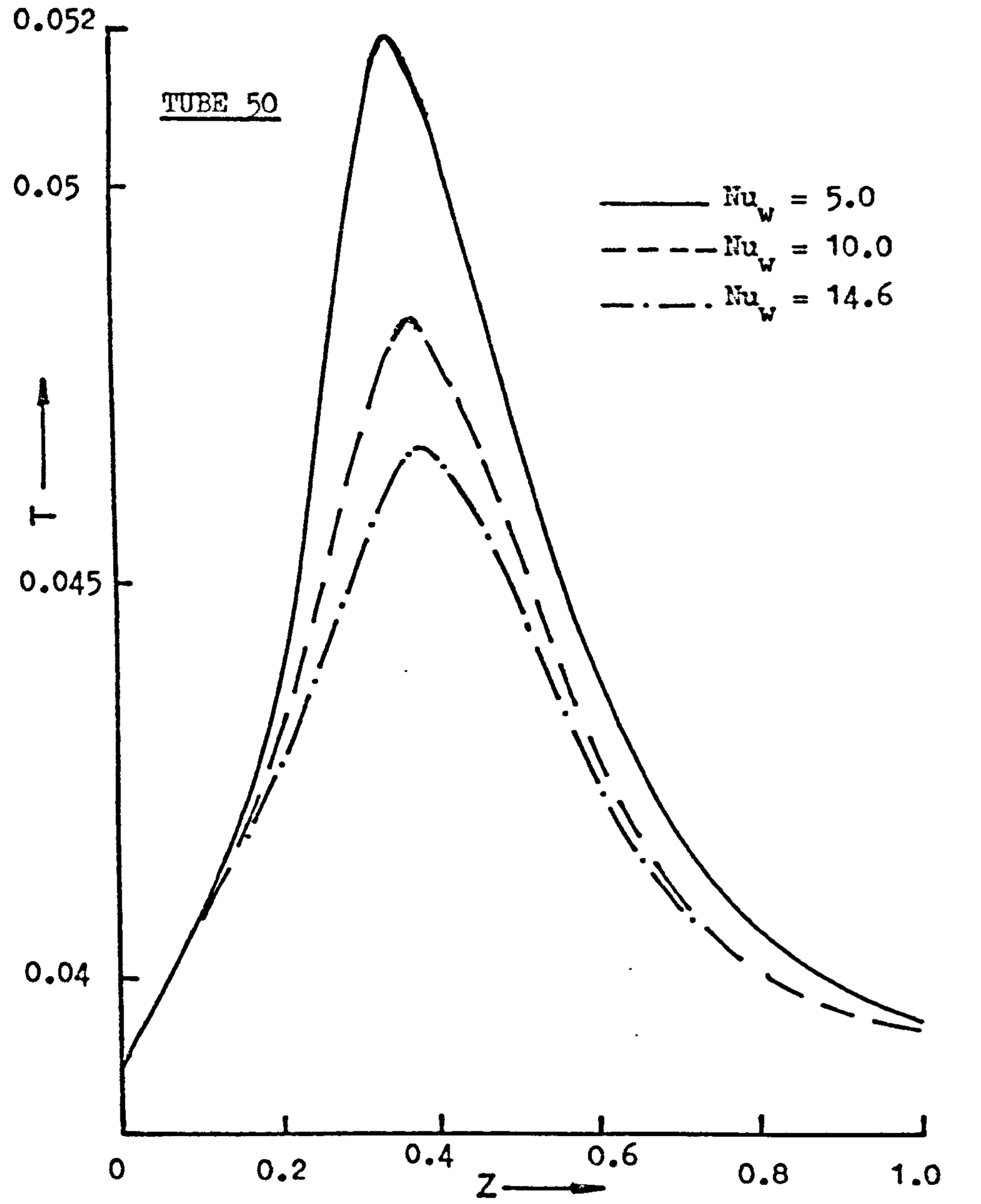

given to the coolant, a low heat transfer coefficient causes more reaction on the tubeside and consequently, more heat is evolved and given to the coolant than with a high coefficient.

6.5 The Maldistribution of Reactant Feed to the Tubes

As indicated in chapter five, the maldistribution of the feed amongst the tubes in a large tube bundle is a common problem and can have significant effects, not only on the affected tubes, but also, because of the interactive nature of the bundle to coolant heat transfer, on other tubes having the correct flowrate of reactants.

Investigation has shown that the effects of maldistribution affecting only one or two tubes in the bundle cannot be seen in the overall performance of the system. For instance, if the flowrate in one tube is 20% less than in all the other tubes, there will be no observable change in the coolant temperature rise even though the tube-side temperature in that particular tube is increased substantially. Thus, because there is no change in the coolant temperature the rest of the tubes in the bundle are not affected.

However, as with the co-current case, changes in the reactant flowrates to groups of tubes in the bundle can have significant effects on the overall performance. Figures 6.12(a), (b), (c) and (d) show the influence of flowrate changes of $\pm$10% and $\pm$20% in ten tubes at either end of the bundle diameter. That is, of the fifty tubes across the diameter, twenty (ten at either end) are subjected to a different flowrate from the rest. As a reference, figure 6.13 shows the same four coolant pass, counter-current reactor, with its reactant flowrates being equal in every tube. Table 6.7 shows the overall coolant temperature rises and the conversions obtained in tube 25 for all the above cases.

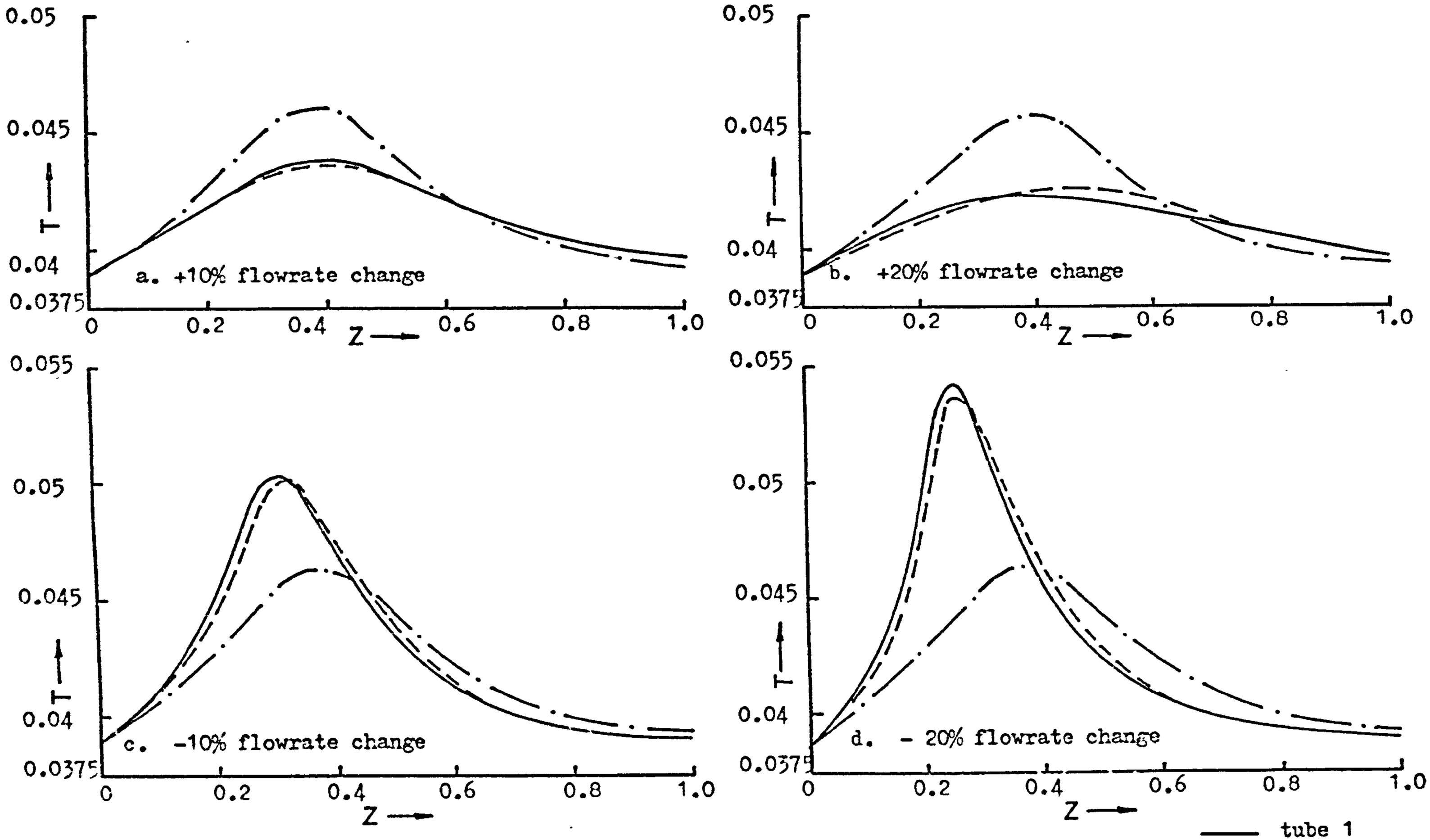

Figure 6.12 A four coolant pass counter-current reactor subject to maldistribution of feed amongst the tubes. Coolant velocity, u_c = 0.25 m/sec. (Non-specified data as table 3.1)

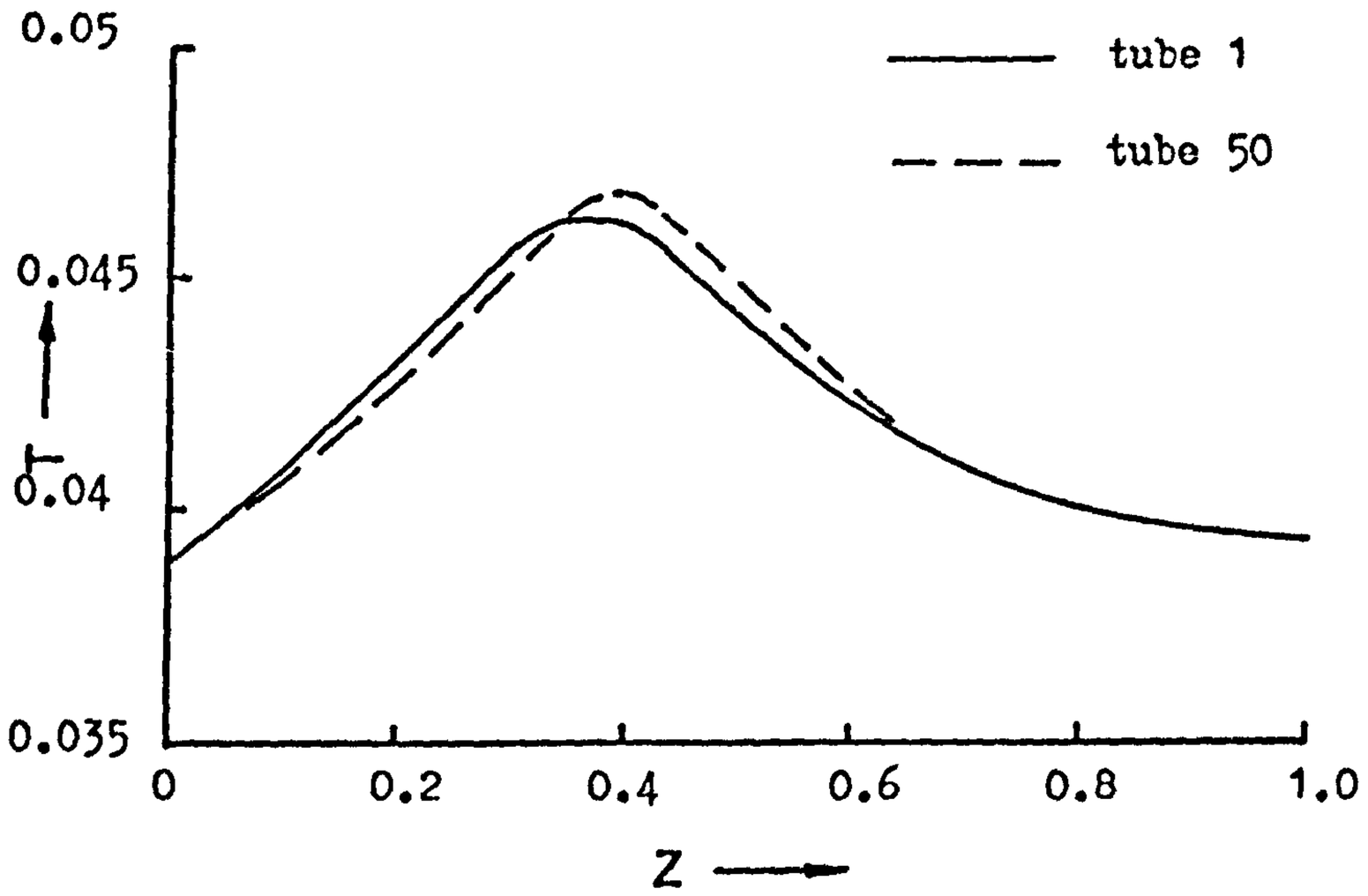

Figure 6.13 The tubeside temperature profiles for a four coolant pass, counter-current reactor, used as a reference in the work on feed maldistribution. Coolant velocity, u_c = 0.25 m/sec. (Non-specified data as table 3.1)

TABLE 6.7

Variation of Reactant Flowrate to 10 Tubes Either End of the Tube Bundle

Coolant Velocity U_c = 0.25 m/sec

% Change in flowrate	ΔT_c (°K)	% difference of ΔT_c compared to reference	Conversion in Tube 25
NONE	12.3	-	90.0 %
-10 %	13.0	5.7 %	90.25 %
-20 %	13.5	9.8 %	90.25 %
+10 %	11.4	-7.3 %	89.4 %
+20 %	10.4	-15.4 %	88.7 %

Referring both to the tubeside temperature profiles of figure 6.12 and table 6.7, it is apparent that increasing the flowrate in the outer tubes by 20% decreases the coolant temperature rise by approximately 2 K and decreases the conversion, not only in the tubes subject to a low flowrate (where, for example, tube 1 suffers a drop in conversion from 89.6 % to 78.3 %), but also in, say tube 25, where the conversion is down by over 1%. Hence, when studying the effects of maldistribution of the feed to the tubes it is essential that the interaction of the tubes in the bundle be taken into account, since the effects of flowrate changes in one tube are carried, via the heat transferred by the coolant, throughout the system, and can significantly affect the performance of others.

In the example shown here, an interesting result is obtained when the flowrate in the extreme tubes is decreased. Referring to table 6.7, it can be seen that although a greater coolant temperature rise is obtained for the case with the flowrate decreased by 20% than that decreased by 10%, the conversions at tube 25 are the same in both cases. This result can be explained by looking at the positions of the main

reaction zones. In the tubes containing lowered flowrates the temperature peak (and hence main reaction zone) occurs in the first coolant pass, while for normal tubes it occurs in the second pass. Hence, in normal tubes, e.g. tube 25, the coolant temperature around the main reaction zone is approximately the same as in the reference case. The increase in the coolant temperature is confined mainly to the first coolant pass and hence does not seriously affect the reaction in the other tubes in the bundle.

Thus, the overall performance of counter-current reactors is not significantly affected by decreases in the reactant flowrates to the tubes, provided that the tubeside temperature hotspots are in the first coolant pass, and the hotspots of unaffected tubes are in the second or subsequent coolant passes.

In large tube bundles, it is therefore useful to know the effects of maldistribution and by using the above procedures it is possible to simulate how the production rate of a given unit will be affected by, say, coking of the hottest tubes. Strategies for the optimization of catalyst renewal can then be studied enabling the downtime of a given system to be reduced.

6.6 Multiple Steady States

The existence of multiple coolant steady states in the counter-current, heterogeneous reactors under study has been demonstrated by Adderley[41], who showed that multiple solutions occurred in a four coolant pass reactor when the coolant was allowed to heat up appreciably at low coolant flowrates. It should be noted that this multiplicity is due solely to the feedback of heat by the coolant and not to multiplicity of the catalyst pellet solutions. This is most easily demonstrated by referring to the analysis of the reactor considered in chapter three, where figure 3.5 shows the tubeside reactor trajectories

on a T vs. B phase plot for the same reactant inlet values used here. The trajectories lie well to the left of the non-unique region and so the reactor will never be subjected to multiple steady states in the catalyst pellet. Figures 6.14, 6.15 and 6.16 show coolant inlet temperature plotted against outlet temperature for various values of the parameter GG (where GG = $G_c/G_{c\ reference}$, $G_{c\ reference}$ = 98.25), under two, four and six coolant pass configurations. In all cases, as the value of GG is decreased a region develops where the coolant outlet temperature becomes very sensitive to the inlet value. A further decrease of GG leads to multiple steady states. For a given system, decreasing GG represents a decrease in the coolant mass flowrate or velocity across the tube bundle.

Figure 6.17 represents a schematic diagram of a plot of coolant inlet versus outlet temperature for a value of GG where multiple steady states are possible. The region of multiple steady states is bounded by an upper and a lower value of the coolant inlet temperature. Below coolant inlet temperature T_{c_1}, multiple steady states do not occur because here the coolant temperature is so low that no significant heating of the coolant occurs; the coolant temperature is so low that heat removal, by the coolant, dominates throughout the bed preventing any reaction taking place. Coolant temperatures above T_{c_2} give only one steady state, the temperature is high enough to cause high heat generation by reaction and so heat generation is at its naximum. If the coolant inlet temperature is slowly raised from a value below the multiple steady states region, at a constant value of GG, say point A in figure 6.17, then the coolant outlet temperature also increases and follows the curve AB. Raising the coolant inlet temperature above T_{c_2} will cause the outlet value to jump from T_{c_4} to T_{c_6}, further increases in the inlet temperature will cause the system to follow the curve D-E. Slowly lowering the inlet temperature from say, point E, will cause the

Figure 6.14 Inlet versus outlet coolant temperatures for a two coolant pass counter-current reactor. (Non-specified data as table 3.1)

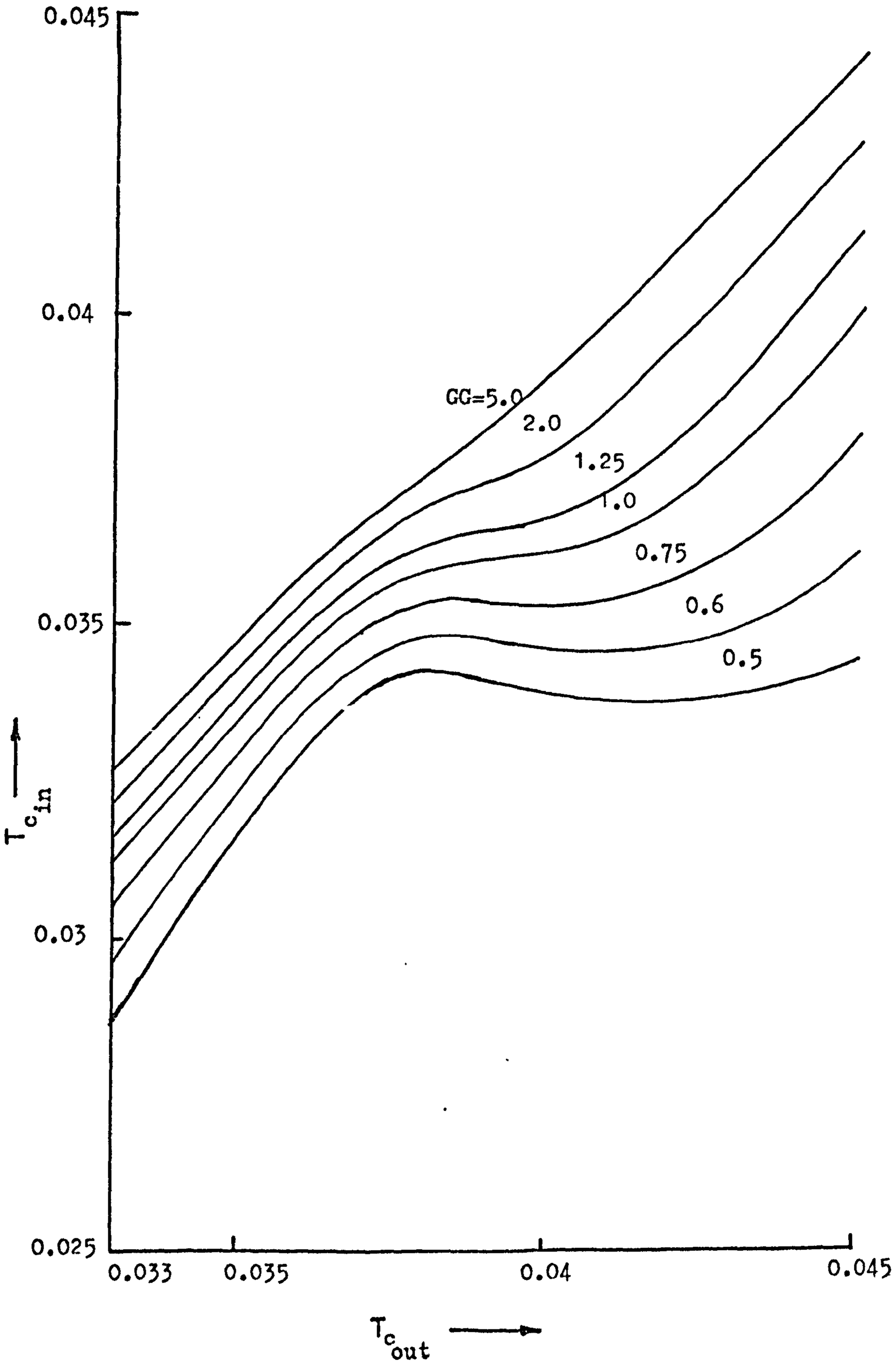

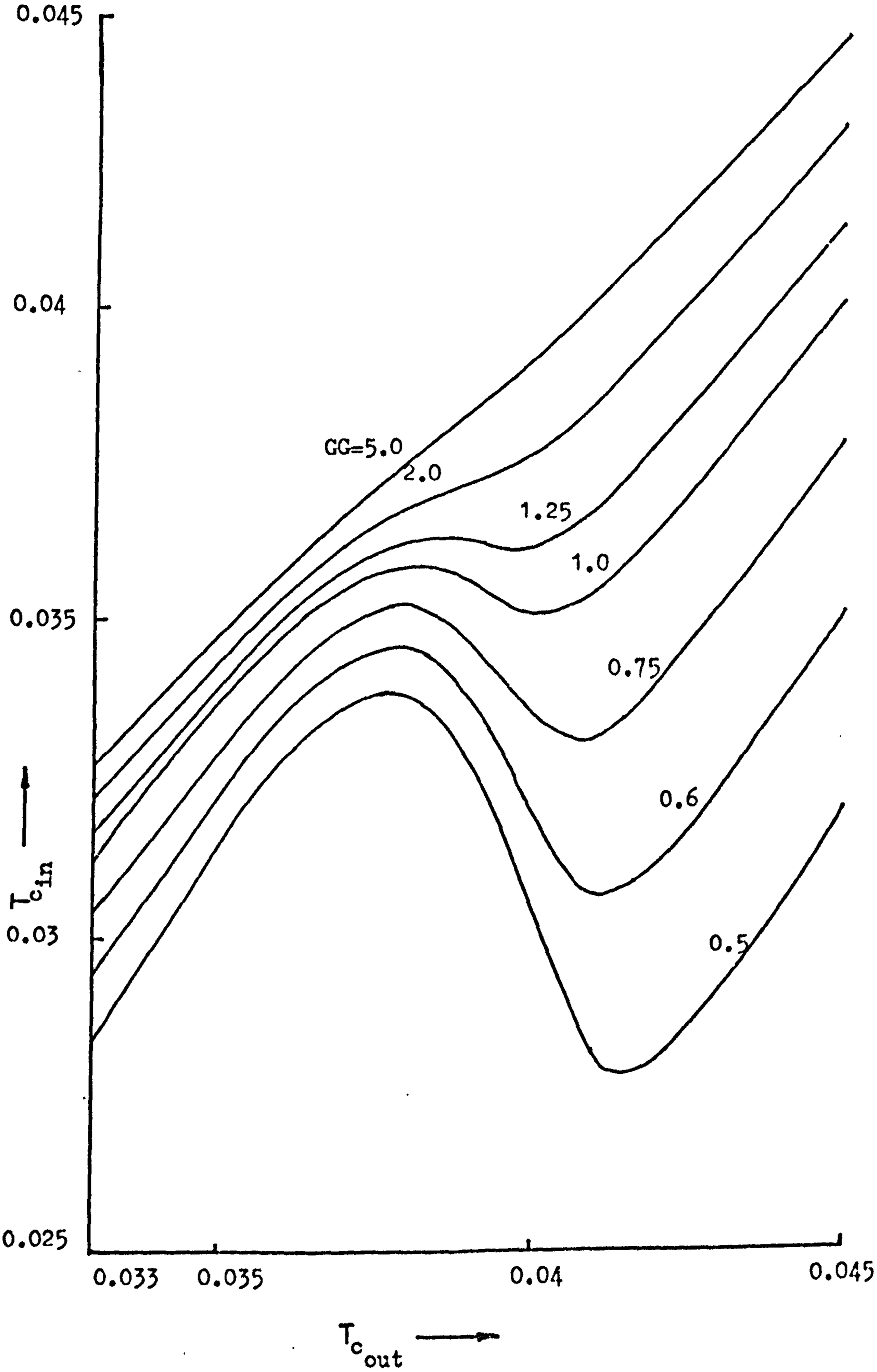

Figure 6.15 Inlet versus outlet coolant temperatures for a four coolant pass counter-current reactor. (Non-specified data as table 3.1)

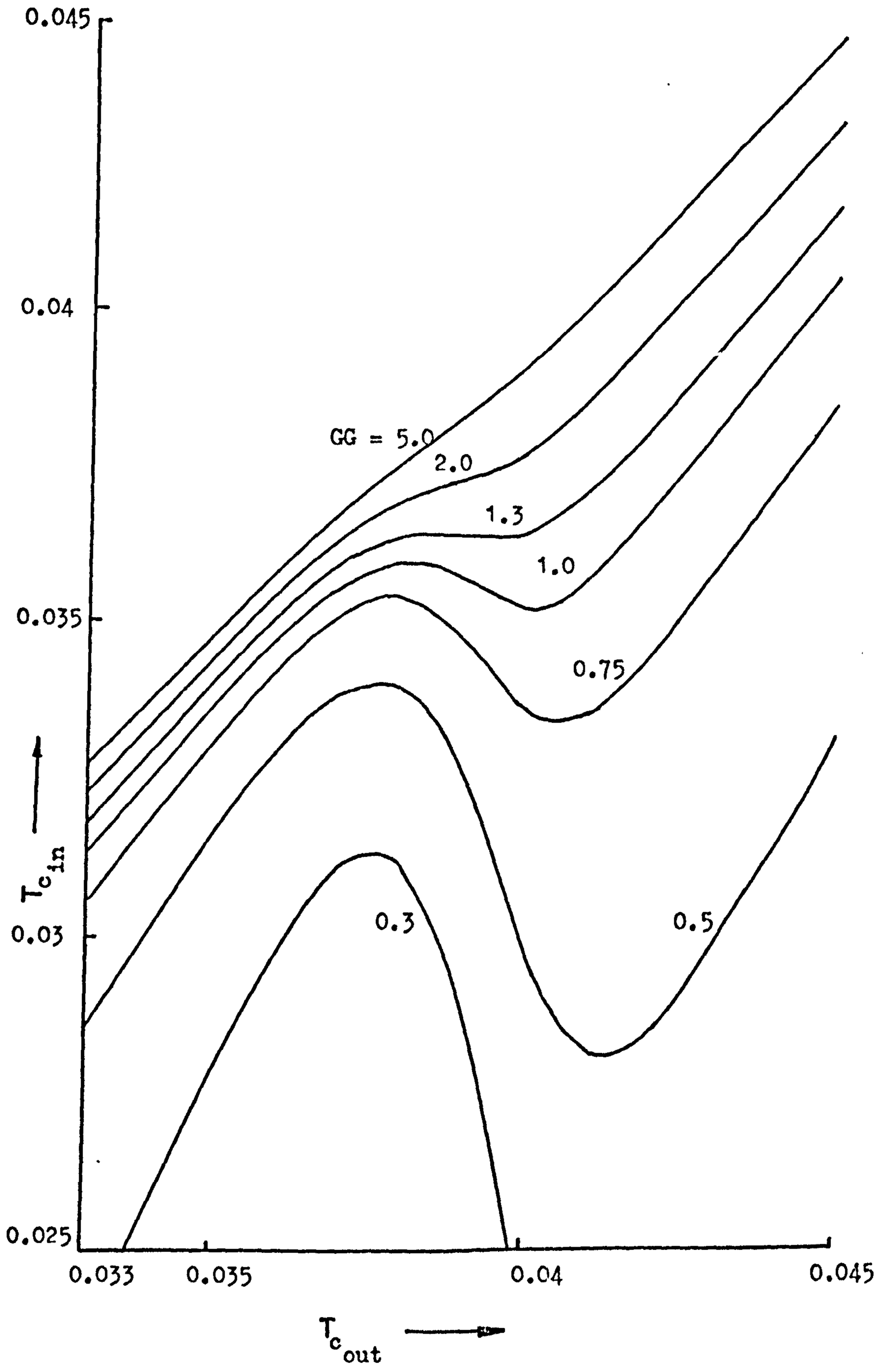

Figure 6.16 Inlet versus outlet coolant temperatures for a six coolant pass counter-current reactor. (Non-specified data as table 3.1)

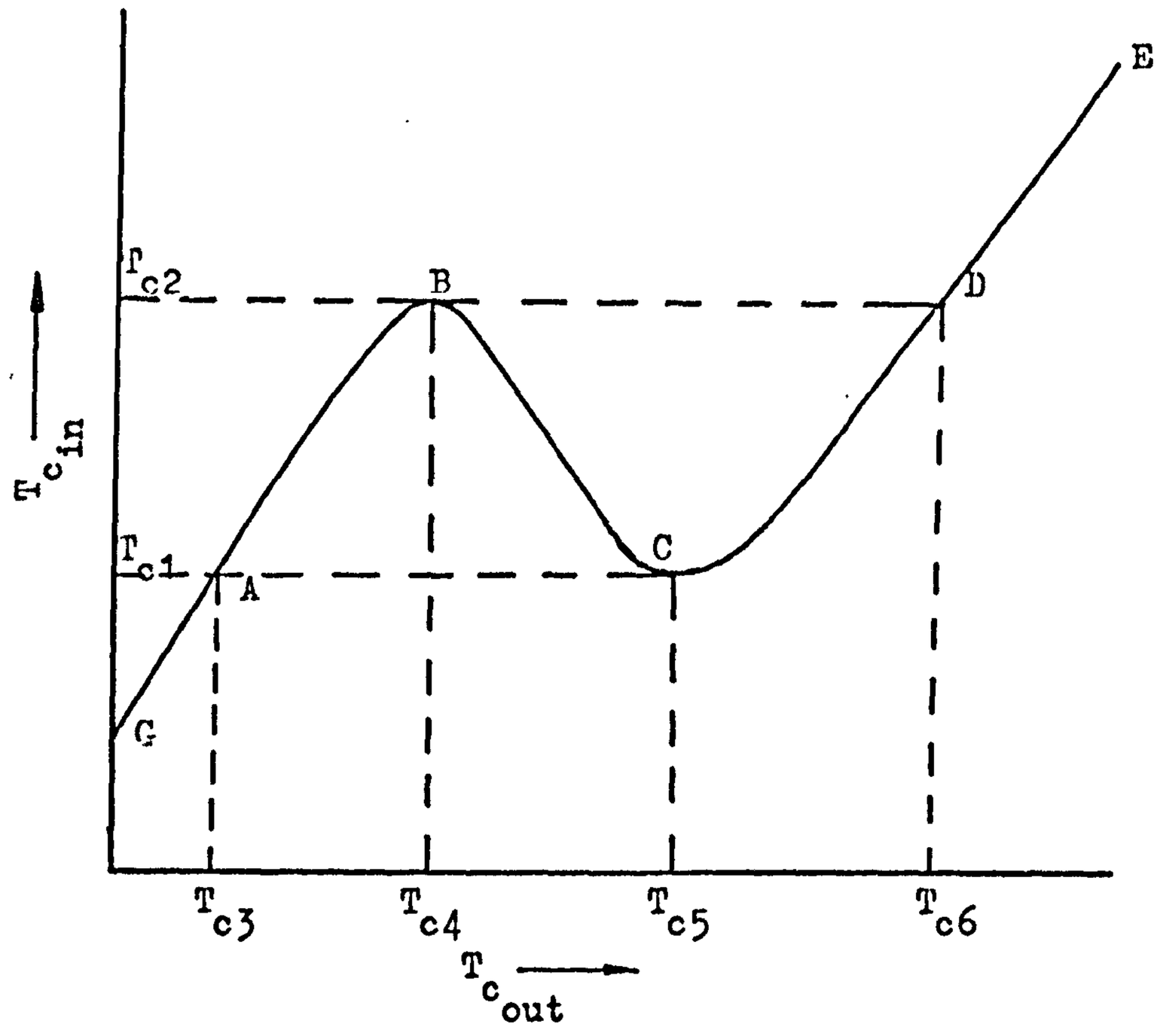

Figure 6.17 Schematic plot of inlet versus outlet coolant temperature under conditions that give multiple steady states in the coolant temperature.

outlet coolant temperature to fall following the curve E-C. Then at point C, a further reduction from T_{c_1} will cause the outlet temperature to jump from T_{c_5} to T_{c_3} and then follow the curve A-G. This hysteresis effect, caused by the multiple solutions, makes it very undesirable to operate in these regions as severe changes in the system performance can occur for some perturbations in the coolant inlet temperature.

Figure 6.18 shows a plot which should help in describing the non-unique region in the coolant heat balance. This semi-logarithmic plot of the coolant inlet temperature maxima and minima (T_{c_2} and T_{c_1} of figure 6.17) versus the parameter GG gives an immediate visual indication of the relationship between the coolant flowrate (which is proportional to GG) and the coolant inlet temperature. The three configurations of figures 6.14, 6.15 and 6.16 are compared in figure 6.18, the non-unique region of the two pass system being much smaller than that of the four or six pass configurations. This demonstrates that the feedback effect of the two pass reactor is less than those containing a greater number of coolant passes. For the four coolant pass system, coolant temperatures below $T_{c_{in}} = 0.0365$ (489 K), coupled with coolant flowrates below GG = 1.4 ($G_c = 141.5$), may result in multiple steady states in the coolant when the data of table 3.1 is used.

Variation of the inlet reactant temperature is shown for a two coolant pass system in figure 6.19 and four pass system in figure 6.20. In both cases, decreasing the reactant temperature increases the size of the non-unique region, moving it both to the right and upwards, encompassing both higher coolant flowrates and higher coolant inlet temperatures. This behaviour is due to the fact that higher coolant temperatures can be tolerated and indeed are necessary to cause reaction on the tubeside.

Increasing the length of the reactor tubes is demonstrated in figure 6.21, where tubes of 5 m, 8 m, and 12 m show that the non-unique

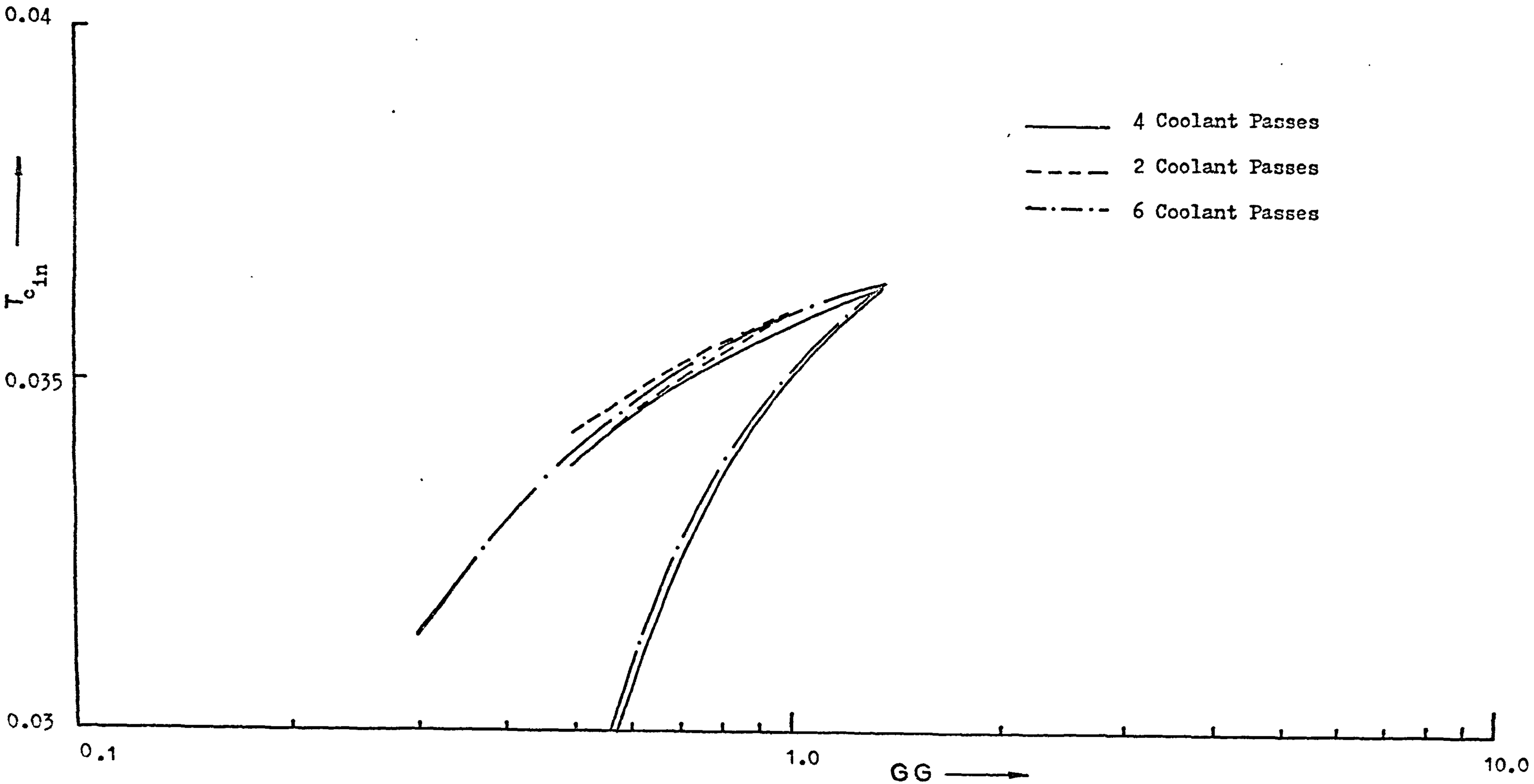

Figure 6.18 A plot of coolant inlet temperature versus GG showing the region of non-unique solutions for various numbers of coolant passes. (Non-specified data as table 3.1)

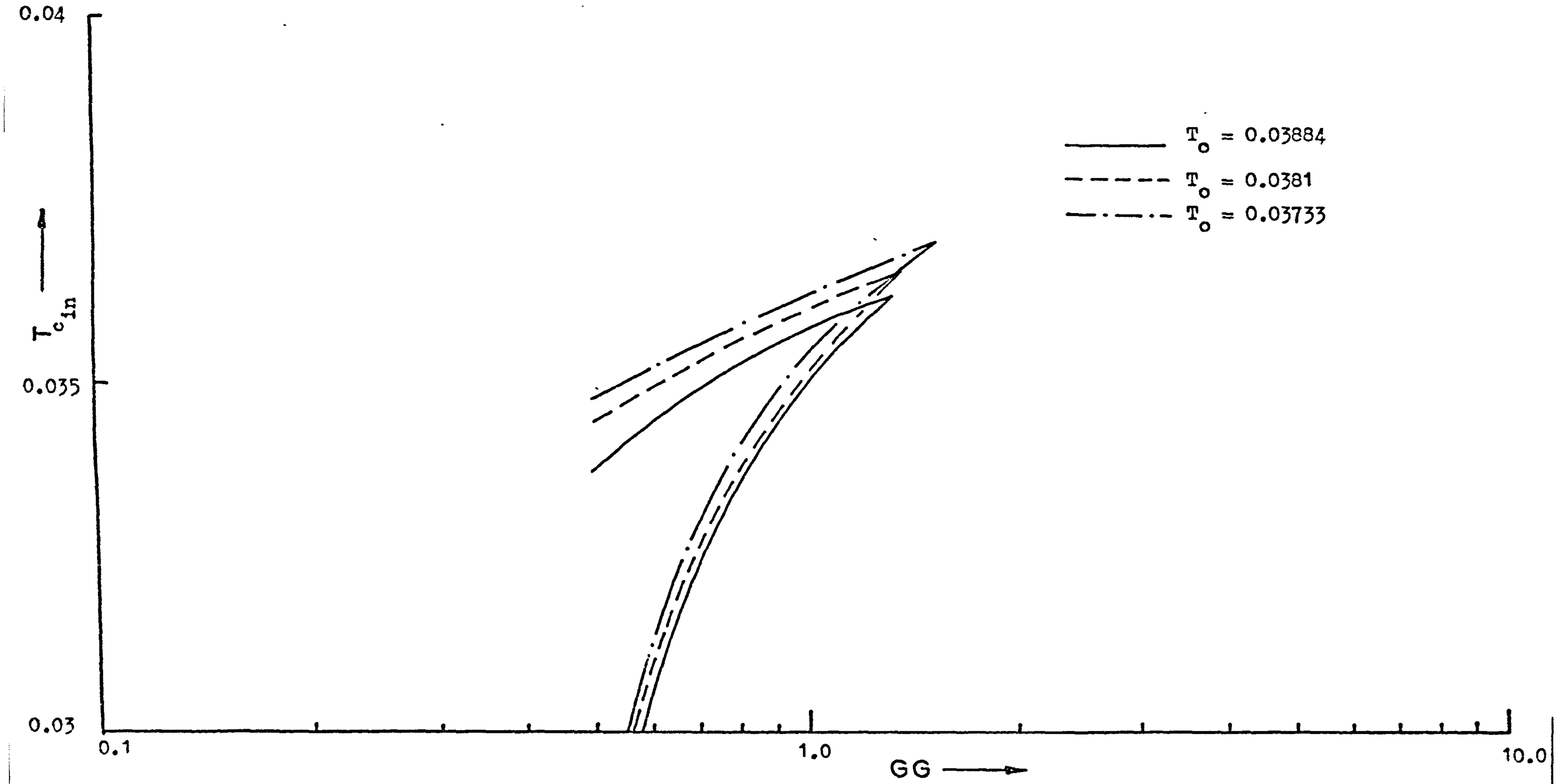

Figure 6.20 A plot of inlet coolant temperature versus GG for a four coolant pass counter-current reactor showing the non-unique region for various reactant inlet temperatures. (Non-specified data as table 3.1)

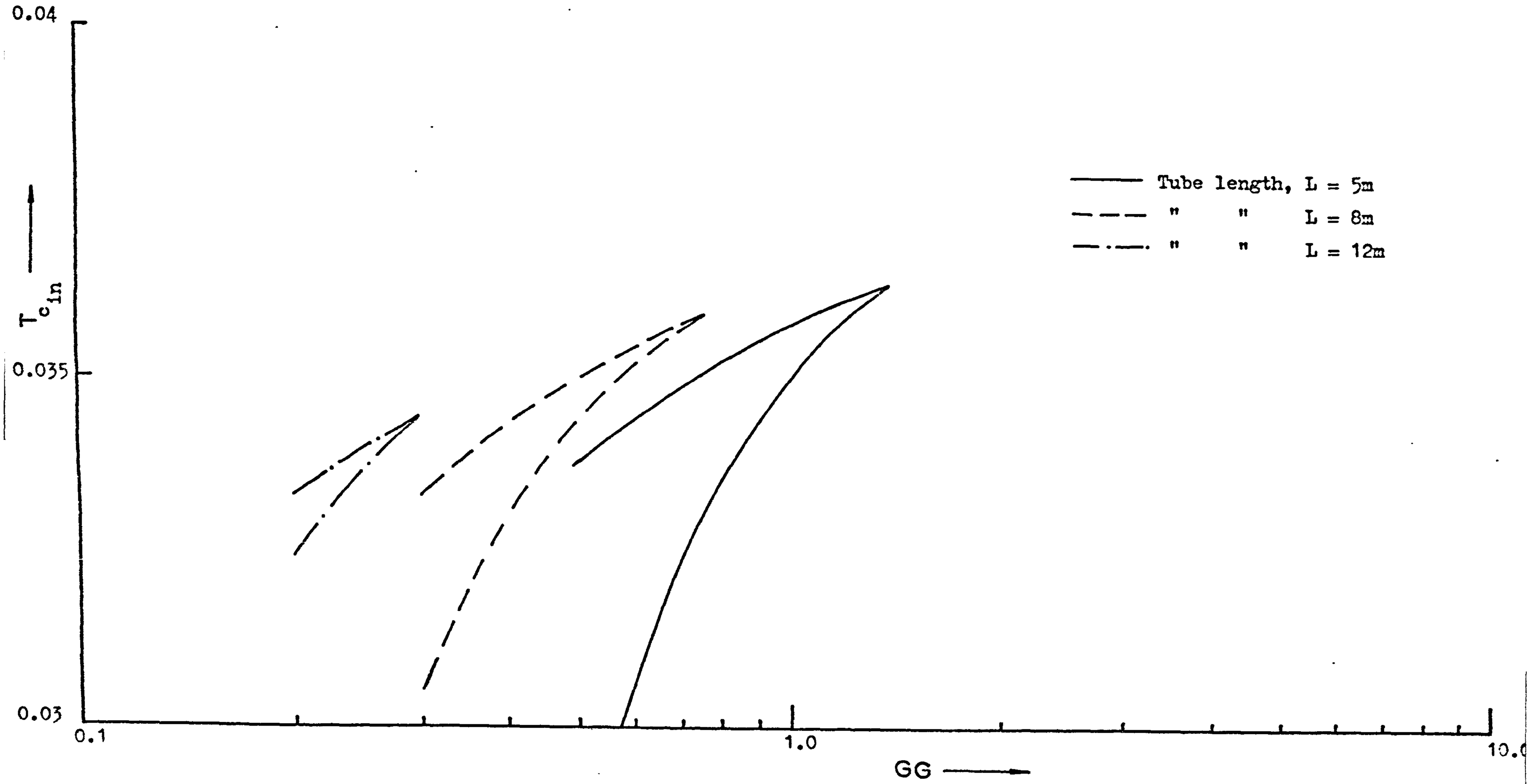

Figure 6.21 A plot of inlet coolant temperature versus GG for a four coolant pass counter-current reactor showing the non-unique region for various tube lengths. (Non-specified data as table 3.1)

region is moved to the left and slightly down on the phase plot as the tubes get longer. The interpretation of this result is difficult owing to the dependence of the coolant flowrate and GG on the tube length.

The $T_{c_{in}}$ versus GG plots, although showing the position of the non-unique region, give no real indication of the behaviour of the system or the temperature increases present therein. Figure 6.22 shows the plot of inlet versus outlet coolant temperature for GG = 2.0 from figure 6.15, together with a plot of the coolant temperature rise. In explaining the cause of the maxima and minima in the phase plot of ΔT_c vs $T_{c_{out}}$, refer to figure 6.22. Starting at point A, increasing the inlet coolant temperature decreases the overall coolant temperature rise, which follows the curve A-B. This behaviour is because the coolant temperature is low enough to quench the reaction, and so heat removal is the dominant process causing the system to act as a simple heat exchanger. As the inlet coolant temperature increases the driving force for heat transfer to the coolant from the fluid decreases. Hence, the temperature rise in the coolant decreases. When point B is reached the coolant temperature is high enough to cause the reaction to proceed faster, and the coolant begins to receive much larger amounts of reaction heat. The coolant inlet temperature increases still further causing the ΔT_c versus $T_{c_{out}}$ curve to follow B-C. This reactor exhibits parametric sensitivity in the coolant temperature, a small increase in the inlet coolant temperature giving large increases in the outlet value. Therefore, there is a large gradient on the ΔT_c vs $T_{c_{out}}$ curve between B and C.

When point C is reached, the coolant is at a temperature where complete reaction has occurred. That is, all of the reaction heat has been given to the coolant from the reactants. Increasing the inlet coolant temperature still further now merely means that the system is a heat exchanger. The coolant begins to give its heat to the reactant

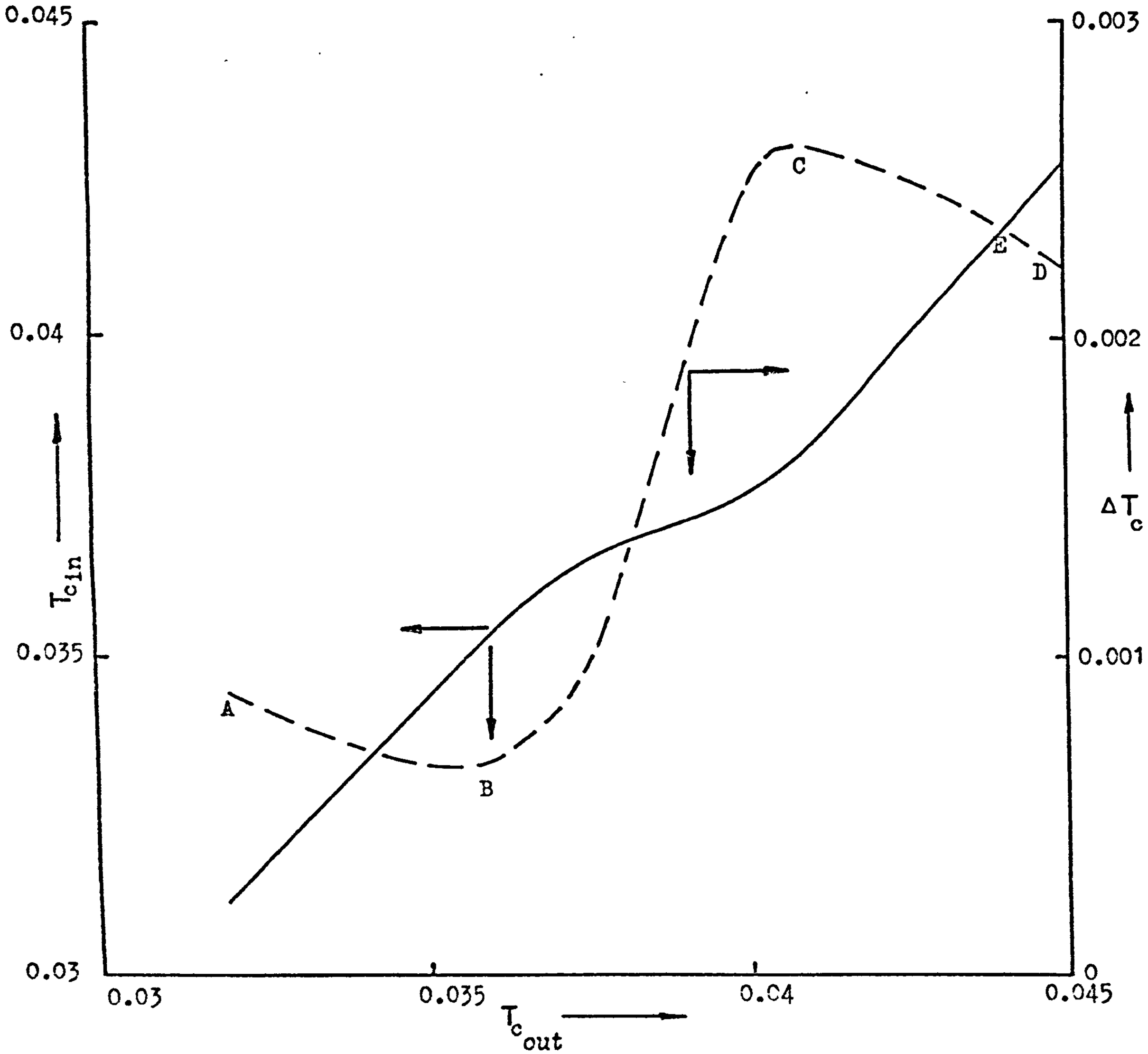

Figure 6.22 A plot of inlet coolant temperature and overall coolant temperature rise versus coolant outlet temperature for a four coolant pass counter-current reactor. GG = 2.0 (Non-specified data as table 3.1)

fluid stream and so as the inlet coolant temperature is increased the overall temperature rise of the coolant decreases. Although the conditions used above are outside the region of non-unique solutions (see figure 6.18), the reactor is still prone to parametric sensitivity in the coolant temperature, and hence is unsuitable for normal operation. Increasing the coolant flowrate decreases this sensitivity and the corresponding curves for a more practical set of operating conditions are shown in figure 6.23 where GG = 5.0 and the plot of inlet versus outlet coolant temperature does not exhibit parametric sensitivity. Figures 6.24, 6.25 and 6.26 show plots of the coolant temperature rise versus the inlet coolant temperature for various values of the mass flowrate for two, four and six coolant pass reactor configurations. The lower the value of GG (that is the lower the coolant flowrate) the greater is the parametric sensitivity of the system and hence the greater the slopes of the curves. Indeed, in regions of multiple solutions the curves double back on themselves.

So far, only the effects within the coolant have been considered, no account being taken of the parametric sensitivity possible on the tubeside of the reactor with respect to the reactant temperature. Figures 6.27 and 6.28 show respectively plots of the maximum tubeside temperature in the reactor versus the inlet coolant temperature and the outlet fraction of reactant remaining in the tube with the maximum temperature versus the inlet coolant temperature. Both are shown for various values of GG. The existence of multiple steady states in the coolant is demonstrated at values of GG = 1.0 and GG = 0.75, where the curves give multiple values at certain coolant temperatures. From the parametric sensitivity line on the T vs B phase plots proposed by McGreavy and Adderley[68], an example of which is shown in figure 3.5, parametric sensitivity occurs on the tubeside of the reactor when the tubeside temperature reaches approximately T = 0.046. From figure 6.27,

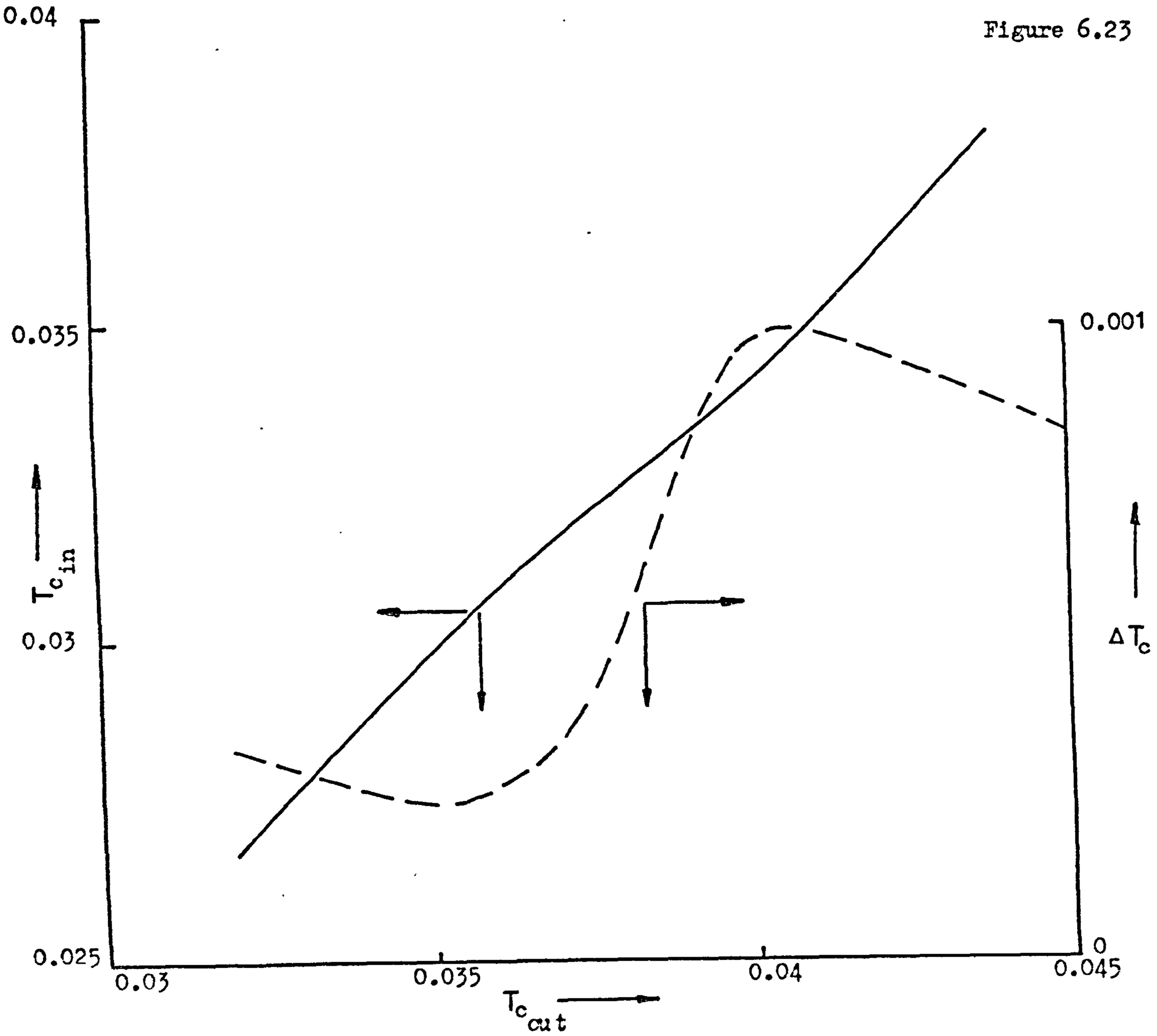

Figure 6.23 A plot of inlet coolant temperature and overall coolant temperature rise versus coolant outlet temperature for a four coolant pass counter-current reactor. GG = 5.0. (Non-specified data as table 3.1)

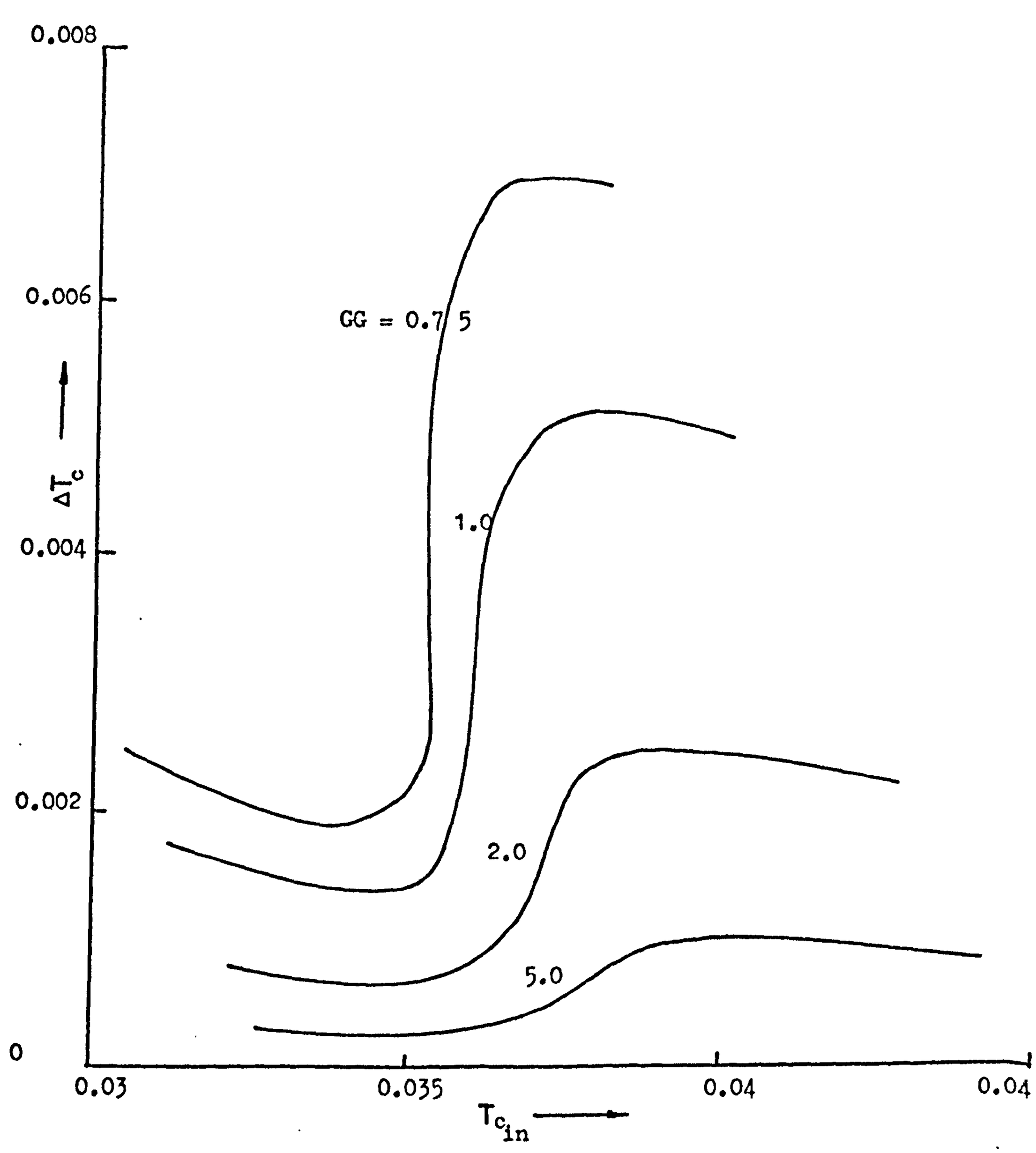

Figure 6.24 Coolant temperature rise versus inlet coolant temperature for a two coolant pass counter-current reactor at various values of coolant flowrate. (Non-specified data as table 3.1)

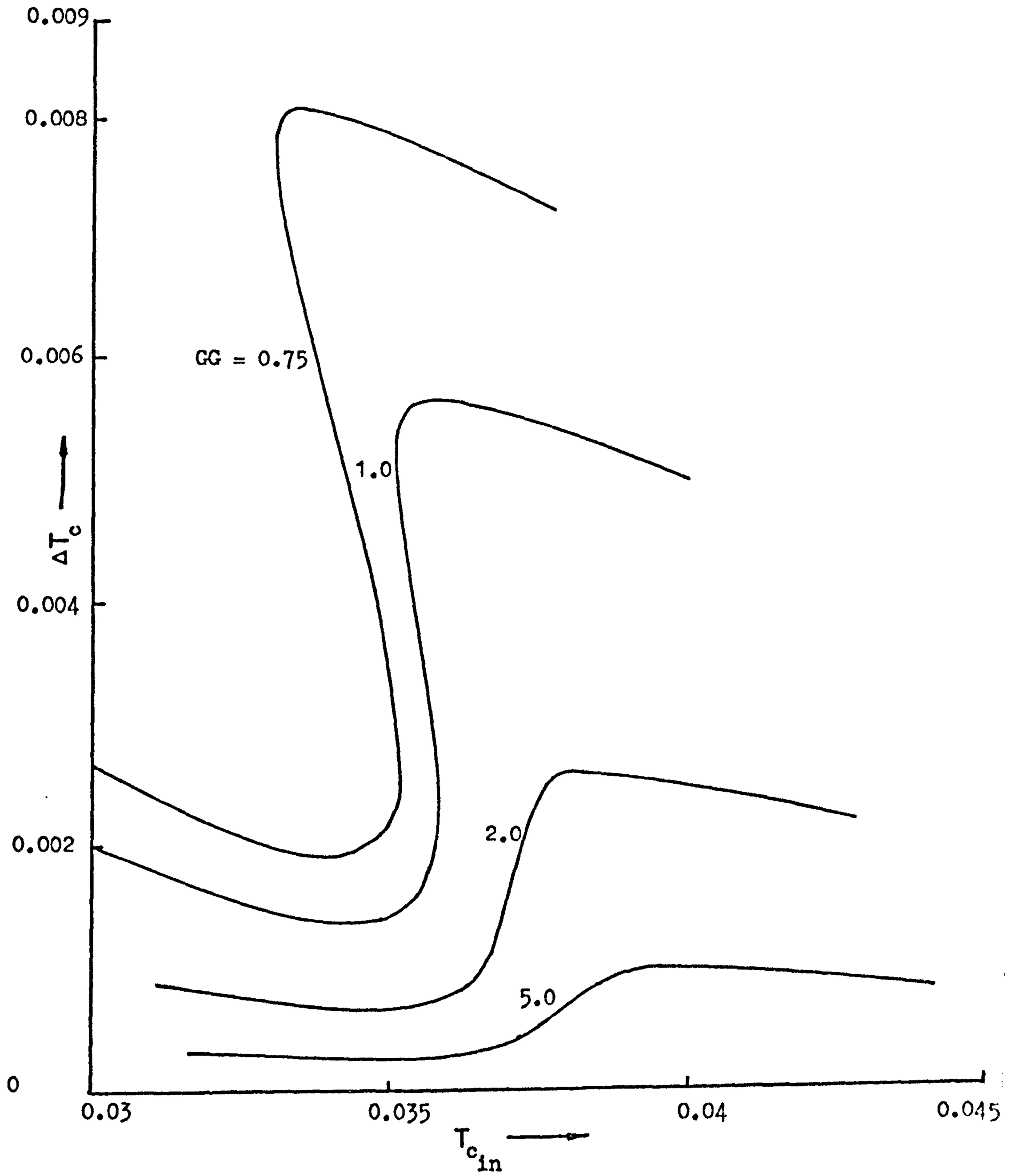

Figure 6.25 Coolant temperature rise versus inlet coolant temperature for a four coolant pass counter-current reactor at various values of coolant flowrate. (Non-specified data as table 3.1)

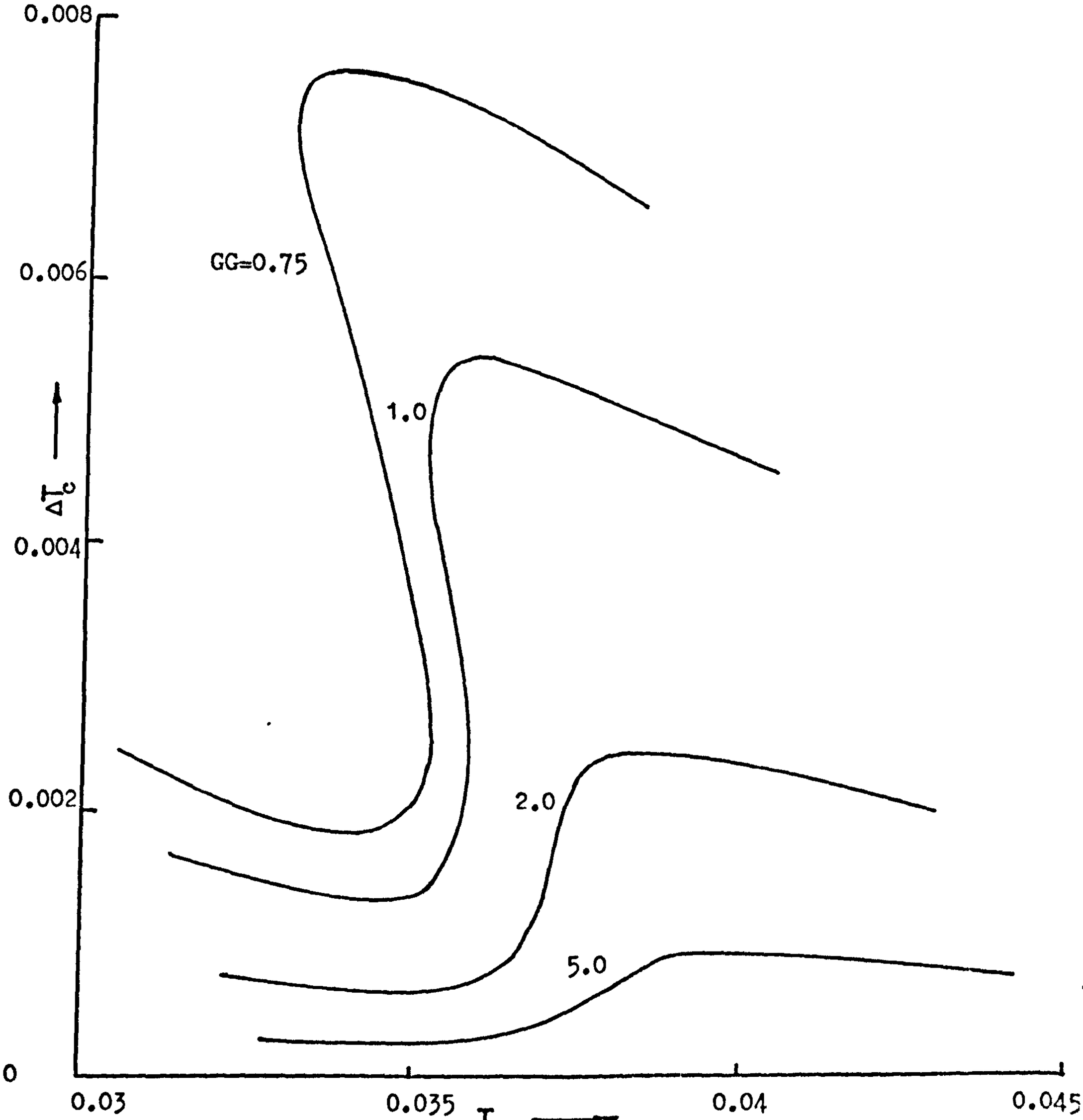

Figure 6.26 Coolant temperature rise versus inlet coolant temperature for a six coolant pass counter-current reactor at various values of coolant flowrate. (Non-specified data as table 3.1)

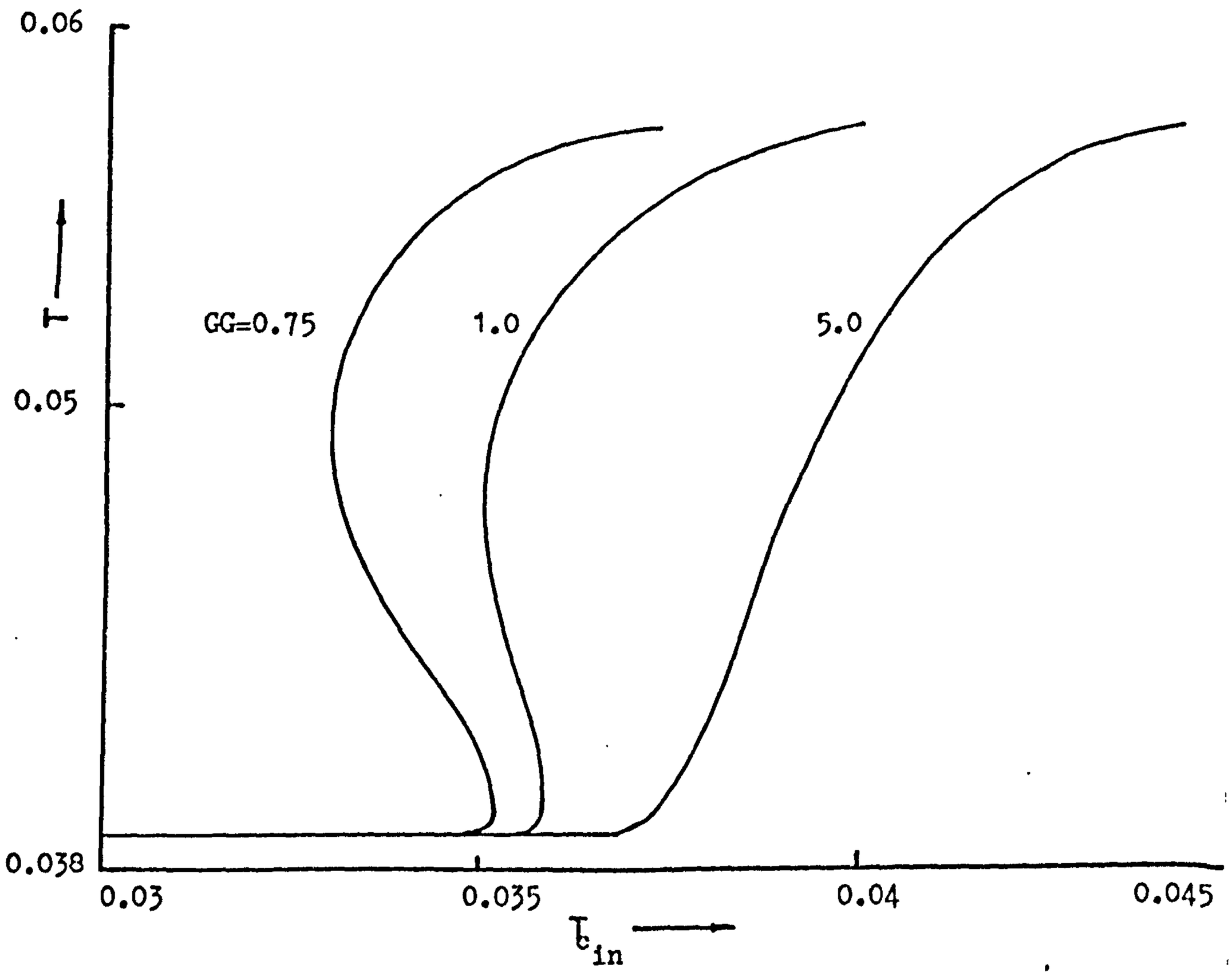

Figure 6.27 Maximum tubeside temperature versus the coolant inlet temperature for a four coolant pass counter-current reactor at various coolant flowrates. (Non-specified data as table 3.1)

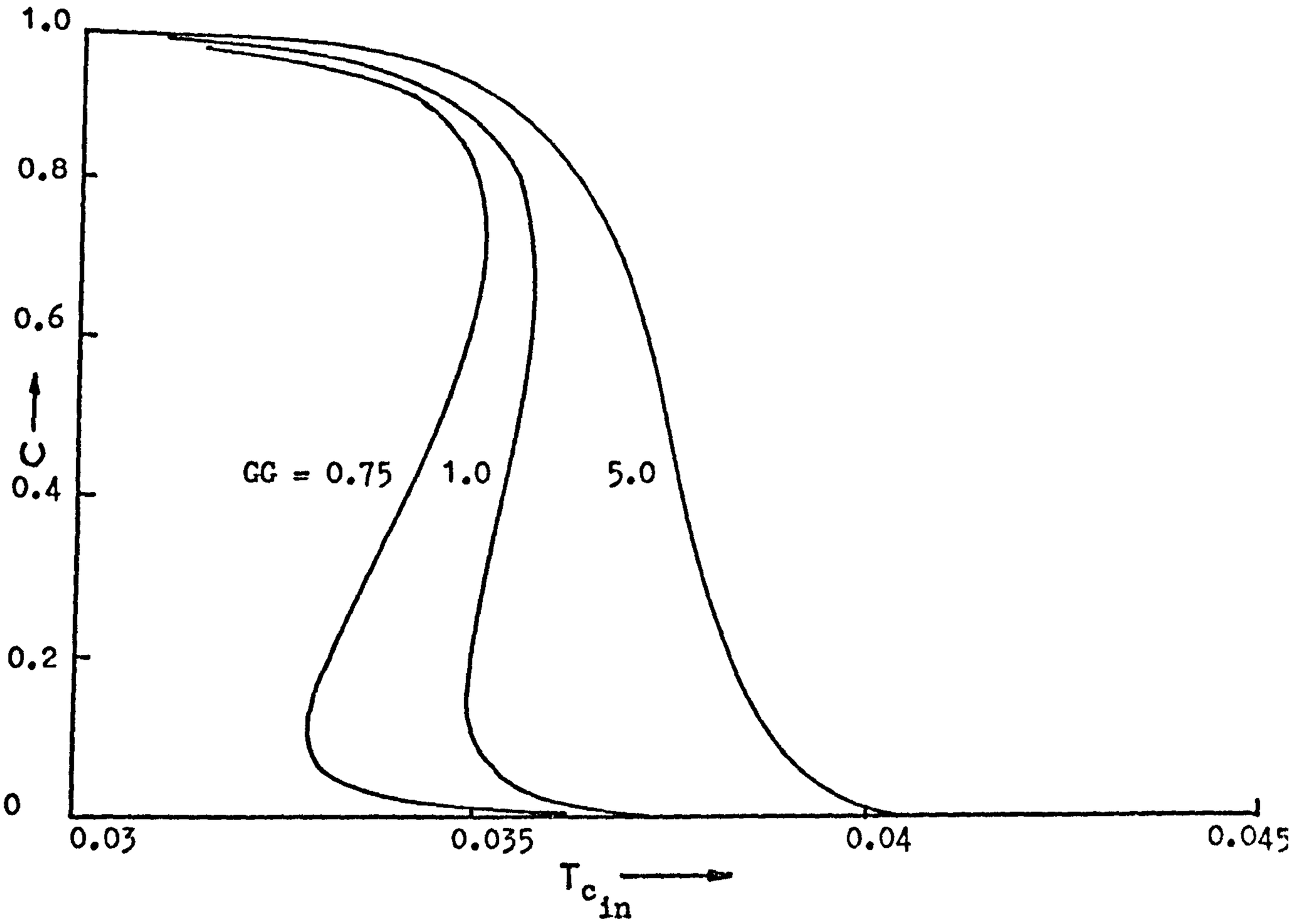

Figure 6.28 Fraction of reactant remaining versus inlet coolant temperature for a four coolant pass counter-current reactor at various coolant flowrates. (Non-specified data as table 3.1)

this corresponds to an inlet coolant temperature of approximately $T_{c_{in}} = 0.0388$ when a value of GG = 5.0 is considered. Lower values of GG therefore require lower values of the inlet coolant temperature to keep the tubeside of the reactor out of regions which may lead to instability. In the GG = 1.0 case for instance, for a stable condition on the tubeside, the reactor is in a region of multiple steady states. If the reactor were operated at the value of the inlet coolant temperature corresponding to a peak temperature of, say, T = 0.04 on the tubeside (i.e. $T_{c_{in}} = 0.035$), then a small perturbation in the inlet coolant temperature, say a reduction to $T_{c_{in}} = 0.0349$ (a change of approximately 1 K), the reaction on the tubeside is quenched if the system falls to the lower steady state, which it is likely to do since the intermediate states are meta-stable.

These factors are important, since consideration of the $T_{c_{in}}$ versus GG plots earlier could lead to the wrong conclusion that by operating outside of the non-unique region shown in, say, figure 6.18, it would be possible to avoid unstable conditions. However, when the stability of the tubeside is considered it is seen that operating above the upper arm of the non-unique region in figure 6.18 causes instability on the tubeside because of the high inlet coolant temperatures. Operating below the lower arm the reaction is quenched because the inlet coolant temperatures are too low. Furthermore, operation of the reactor close to the region of non-uniqueness, for example with GG = 2.0, can lead to parametric sensitivity in the coolant temperature which cannot be tolerated under normal operating conditions. A detailed study of the relationship between the tubeside stability and the coolant conditions will therefore be dealt with in chapter seven.

6.7 Heat Generation and Removal in the Counter-Current Reactor

Consideration of the overall heat evolution and removal in tube 1

of a counter-current reactor is shown in figures 6.29 and 6.30, both being four coolant pass reactors under values of GG = 5.0 and GG = 1.0 respectively. The high coolant flowrate reactor, with GG = 5.0, demonstrates that at low inlet coolant values the heat removed by the coolant is greater than that evolved by reaction. This means that the coolant temperature is too low for the reaction to be initiated and the system is effectively a heat exchanger. As the coolant temperature increases, so does the heat evolved and removed, the gradients of the curves becoming steeper. Finally, the heat evolved by reaction is greater than that removed, hence, the reaction has almost been completed and further increasesin the inlet coolant temperature have no effect on the heat generation, this has reached its maximum value. Since the reactor is now acting as a heat exchanger, increases in the coolant temperature decrease the amount of heat removal because of the decreasing driving force for heat transfer between the tube and the coolant.

With a low coolant flowrate, see figure 6.30, the existence of multiple steady states distorts the shape of the heat generation and removal curves, causing them to fold back on themselves. Even so the trends indicated above are still present. Heat evolution being very low at low coolant temperatures and increasing rapidly as the inlet coolant temperature is increased, only to flatten off at high inlet values when the reaction goes to completion. The heat removal curve crosses the generation curve three times, and unlike the high flowrate case, there are three regions in which heat removal is greater than generation. The points of intersection of the curves represent operating conditions such that all the heat generated is removed by the coolant. When the heat removal curve lies above the heat generation curve the tubeside gases leave the system cooler than when they entered, when it lies below, they leave the system hotter.

Figures 6.31(a), (b), (c) and (d) show the variations of heat

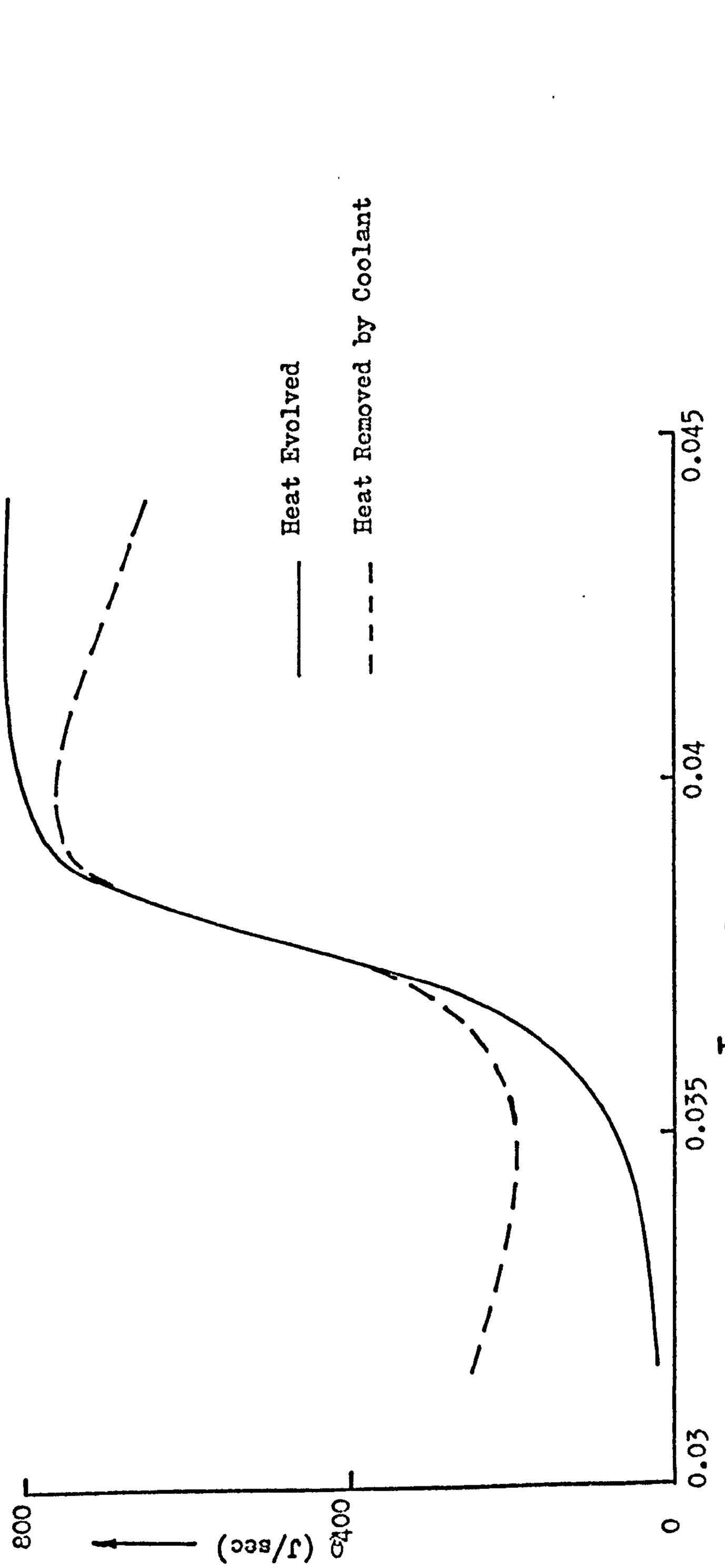

Figure 6.29 Overall heat generation and removal curves for tube 1 in a four coolant pass counter-current reactor. GG = 5.0. (Non-specified data as table 3.1)

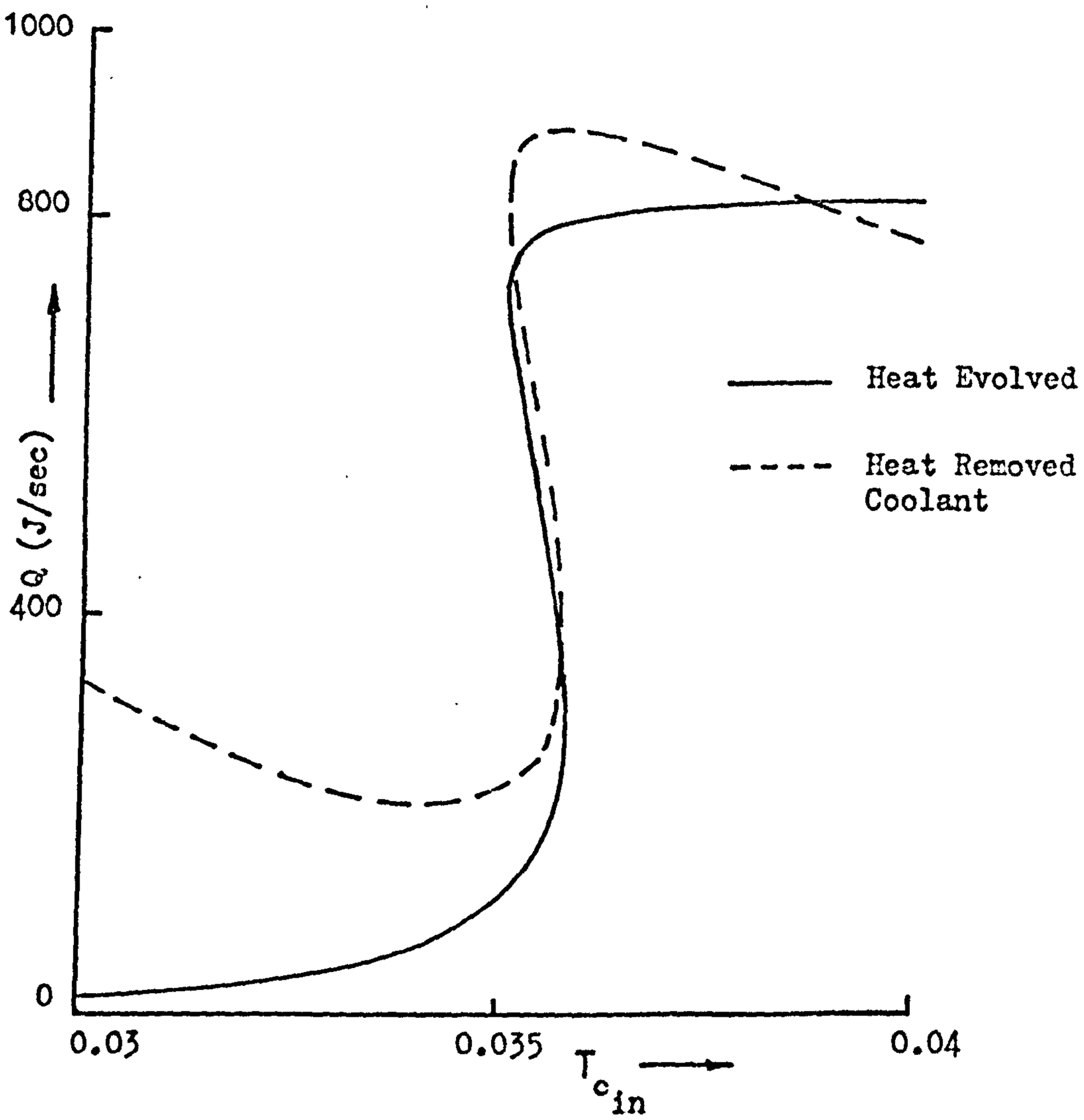

Figure 6.30 Overall heat generation and removal curves for tube 1 in a four coolant pass counter-current reactor. GG = 1.0. (Non-specified data as table 3.1)

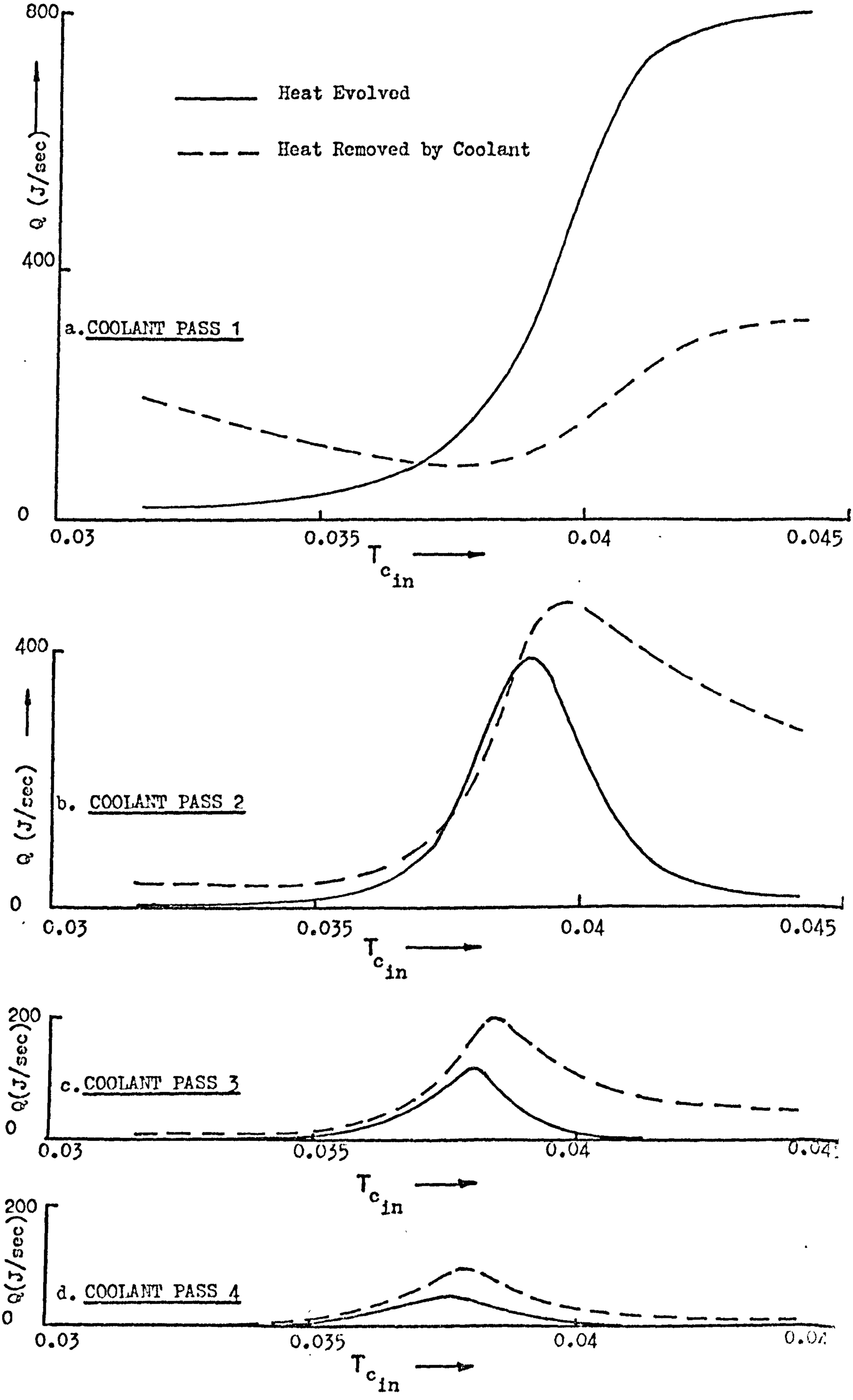

Figure 6.31 Heat generation and removal for tube 1 in different coolant passes of the four coolant pass counter-current reactor of figure 6.29.

generation and removal with inlet coolant temperature for tube 1 in the separate coolant passes of the case shown in figure 6.29, the high coolant flowrate example. At low coolant inlet temperatures there is little reaction in any of the passes, though heat removal by the coolant is high in the first pass because there is a large heat transfer driving force caused by the large temperature differences between the cold coolant and the inlet reactants. As the inlet coolant temperature is increased the heat generated in all passes increases, while heat removal decreases in coolant pass 1 and increases in subsequent passes. This decrease in the heat removal of coolant pass 1 is due to the increasing coolant temperature decreasing the driving force for heat transfer between the coolant and the tube. As the inlet coolant increases in temperature the heat generation is greatest in pass 1 until a point is reached where most reaction occurs in coolant pass 2, at this point the removal of heat from pass 2 is less than the generation of heat. Further increases in coolant temperature cause most of the reaction to occur in pass 1, until eventually virtually all the reaction occurs there. Finally, the heat generation and removal curves in all passes tend to flatten off as the system acts essentially as a heat exchanger.

These heat generation/removal curves demonstrate the way that the second half of the reactor acts as a coolant preheater, most of the reaction occurring in the early part of the bed. The results indicated here lead to the conclusion that the second half of the bed could be packed with an inert packing with little loss of conversion and a saving in the capital cost of the system. Thus, for a given conversion a smaller size unit is possible if counter-current cooling is used. This study, based on co- and counter-current reactors of equal size should therefore be treated with caution, and in comparing the systems, only general trends should be considered. This problem of comparison is considered further in chapter seven.

6.8 Conclusions

Counter-current reactors cannot tolerate large coolant temperature rises, hence high coolant flowrates have to be used to reduce the coolant temperature in the regions of high reactant concentration. As in the co-current system considered in chapter five, three or four coolant passes give the best overall performance under the conditions used. Two coolant pass reactors gave a large spread of conversions across the bundle diameter unless very high coolant flowrates were used.

Maldistribution of the reactants to the tubes has been shown to have significant effects, not only on the affected tubes, but also on the 'normal' tubes because of interactive heat transfer between the coolant and tube throughout the bundle. The use of multitubular models is therefore essential when investigating such effects.

The phenomenon of multiple steady states in the coolant has been shown to be caused by the feedback of reaction heat throughout the system. The dangers of operating in these regions have been indicated and a phase plot of inlet coolant temperature versus the parameter GG developed to enable such regions to be easily identified.

CHAPTER 7

The Steady State Behaviour of Multitubular Reactors.

3. Some Factors Affecting Stability

7.1 Introduction

The general operational characteristics of co- and counter-currently cooled multitubular reactors have been investigated in previous chapters. However, the mechanism of the interactive heat transfer in the tube bundle, and its relation to the stability of the various configurations has only been touched upon. This chapter brings together many of the concepts already introduced and attempts to look at the question of the best configuration. Clearly, such a question must be qualified by the operating conditions, type of reaction and many other specific factors, but any general indications that may lead to an answer would be of considerable value. There is no published literature on the subject and industry seems to have no general rule as to recommendations for good practice in deciding on the best flow direction for the coolant. Indeed, it would appear that most designs for multitubular reactors assume that the system behaves in essentially the same way as a shell and tube heat exchanger. Thus, it is often assumed that a counter-current unit is preferable on the basis that the heat transfer will be much more efficient. This fails to take into account the fact that there is heat generation inside the tubes and that this is non-linearly dependent upon the shell-side temperature. In fact, it is not unknown for large reactors to be designed and built to run with counter-current cooling, only to find that the same unit when operated co-currently gives much better performance. Although there is probably no definitive answer to the above question, this chapter compares the operability of both co- and counter-current units of identical size. This leads to the suggestion that an alternative flow configuration might be introduced

which contains the advantages of both modes of operation.

Although it is probably true that, from a heat transfer point of view, the counter-current reactor may be smaller than a co-current system for the same heat load, in this study it has been considered adequate to use the same tube bundle for both configurations, switching the inlet and outlet coolant ports where appropriate. Clearly this approach will not account for effects such as differing capital costs of various sizes of unit should one type of configuration require smaller heat transfer areas. However, it is hoped that by studying the operability of identically sized units, some light may be thrown on the question posed earlier.

The control of fixed bed catalytic reactors is a subject which, compared to the above problems, has received an enormous amount of attention. This reflects the importance of being able to operate not only safely but also economically. Making use of previously devised procedures, a method of representing the stability and achievable conversion of a multitubular reactor on phase plots of inlet temperature and the parameter GG (which is proportional to the coolant flowrate) can be developed. These plots may then be used for the evaluation of control policies for such systems in terms of easily obtainable external variables such as, coolant flowrate, inlet coolant temperature and inlet fluid temperature.

7.2 Mechanisms of Heat Transfer in the Reactor Bundles

Throughout chapters five and six, effects such as the existence of multiple tubeside temperature peaks have been observed, these being caused by the interaction between the tubeside heat generation and the shell-side heat transfer. It is particularly instructive at this point to consider the characteristics of this heat transfer through the bundle.

The first and obvious difference between the heat transfer mechanisms of the co- and counter-currently cooled reactors is that the former operates with a feedforward and tha latter a feedback of heat along the reactor tubes. Thus, co-current reactors have cold coolant affecting high reactant concentrations with pre-heated coolant causing reaction in the lean reactant regions towards the tubeside exit. Counter-current reactors on the other hand have pre-heated coolant affecting high reactant concentrations and cold coolant in the exit regions of the tubeside. Thus, the reaction is essentially restricted to the initial portions of the bed. Also, because of the higher coolant temperatures in the region of the tubeside hotspots, the counter-current reactor gives higher peak temperatures, and conversions, for any given conditions. However, because of the restricted region available for high reaction (since the reaction is very slow in regions of low concentration and coolant temperature) high conversion often results in temperature runaway, making the co-current system more attractive in many circumstances. This is discussed in detail in section 7.4 where a more formal comparison of the system is attempted.

Examination of the interactive heat transfer in the tube bundle requires the reduction of the systems into simplified approximations, as shown for the co- and counter-current reactors in figures 7.1 and 7.2 respectively. For illustration, a three coolant pass system is considered, the full lines representing extreme tubes in the bundle, while the coolant flow is shown as the dotted line. Consider first figure 7.1, the co-currently cooled reactor. The two main types of interaction are shown by the circled areas, A, representing feedforward of heat in one tube, and B, representing feedforward of heat from tube to tube. The first effect is responsible for the formation of multiple peaks in the tubeside temperature, cold coolant around tube 1 pass 1 causes low rates of reaction and hence a relatively high concentration of

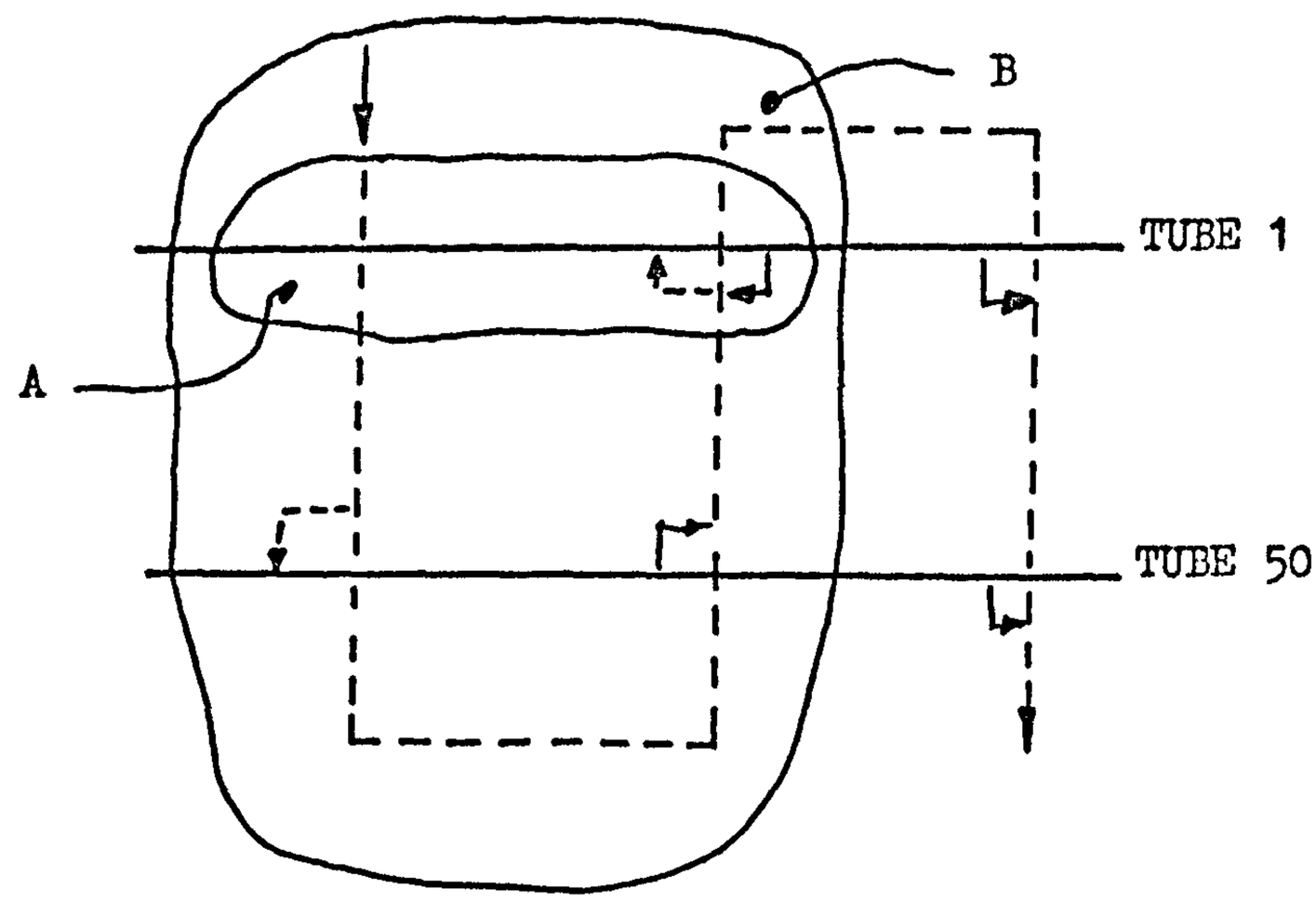

Figure 7.1 Schematic diagram for the heat distribution around a three coolant pass co-current reactor.

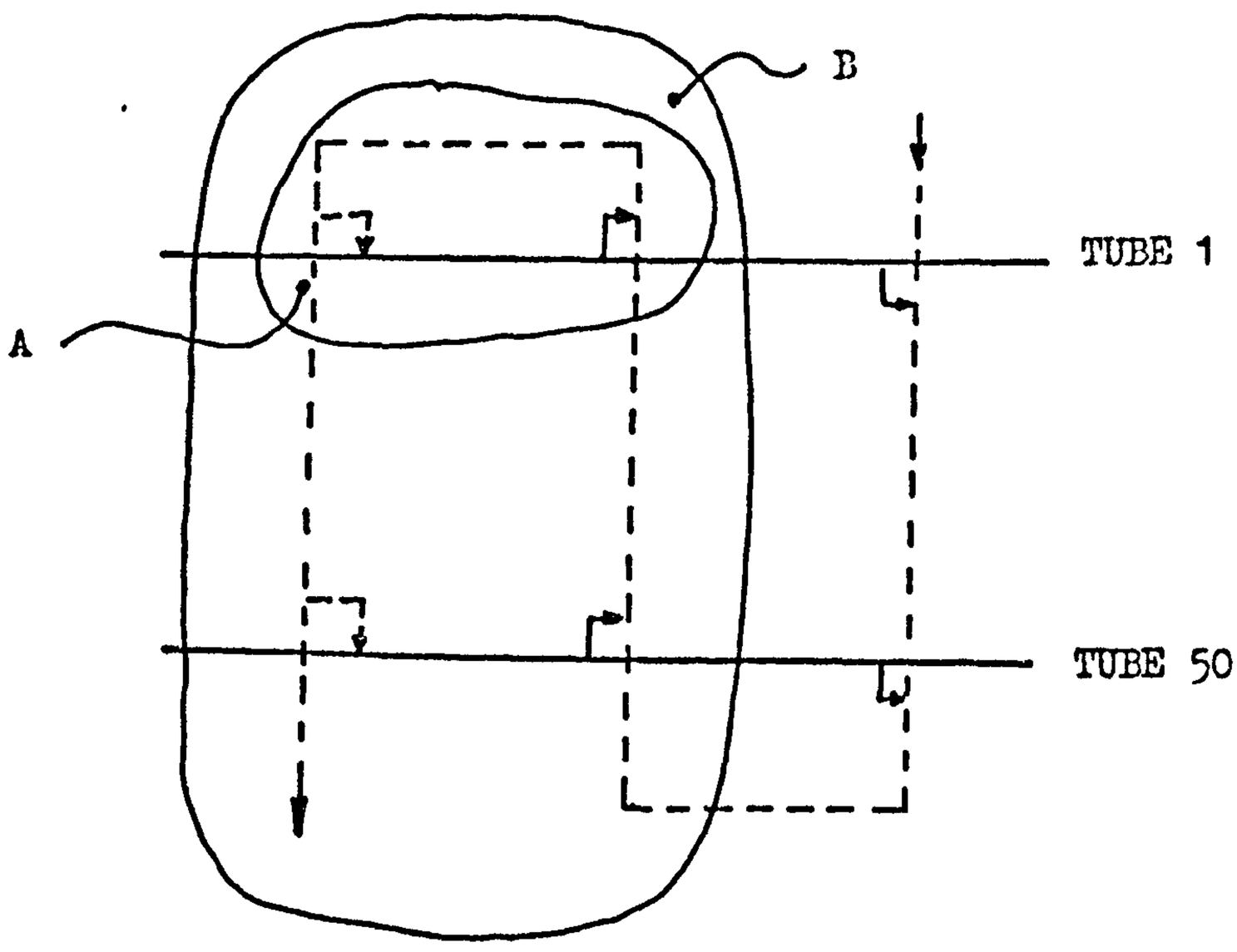

Figure 7.2 Schematic diagram for the heat distribution around a three coolant pass counter-current reactor.

reactant goes into the next coolant pass. The coolant is heated by the other tubes as it flows over the bundle and in pass 2, tube 1 has a high concentration and high coolánt temperature and so the reaction becomes extremely fast and a temperature peak forms. If a relatively high concentration of reactant then leaves this pass, the same effect can be observed in subsequent passes. The feedforward of heat labelled B, represents the increasing coolant environment of the tubes across the bundle diameter. This causes the tubeside temperature peaks to vary in position as the bundle is traversed. Hence, in most cases, the temperature peaks are closer to the reactant inlet at the hot coolant end of the pass containing the peaks, than the cool end.

An indication of the interaction between tubes is given by the schematic representation of the heat transfer shown in figure 7.1. The reactant to coolant heat transfer is shown by the full arrows, while the dotted arrows show coolant to reactant heat exchange. It can be seen that, in the first pass of the coolant, the inlet reactants are equal in temperature to the inlet coolant, but, as the coolant heats up across the bundle, it becomes hotter than the inlet reactants and so heat is given to them from the coolant. (Note that this is a simplified view. Only very close to the tube entrance would this happen, as the heat generation would quickly increase the tubeside temperature and limit or stop this transfer of heat. Indeed, normally towards the end of the tube in pass 1 the heat will be given from the tubeside to the coolant and the net flow of heat over the whole pass will be in this direction.)

The above technique has been applied to the counter-current system in figure 7.2. Circled area A represents feedback of heat in each tube and B the feedback of heat around the bundle. The phenomenon of feedback, shown by A, means that the early sections of the tube 'know' what has happened in the end sections. Thus, the tube length is a more important variable in the stability of such systems than for co-current

reactors, where, because of the feedforward effect, the early sections of the bed are independant of tube length. Feedback around the bundle, area B, indicates the effects caused by the accumulation of heat as the coolant flows across the bundle. The cold coolant enters the system in a region of low concentration and high tubeside temperature, it gains heat as it travels through the system, so that at the reactant inlet, hot coolant is in contact with high reactant concentrations. The coolant heats up the reactants in the early entry sections of the bed and so the reaction occurs much nearer the entrance than in the co-current reactor.

Although a gross simplification, the above view of the transfer of heat around the reactors does help to demonstrate how some of the complex interactions in the tube bundle occur. Moreover, such an approach, if used with care, giving due allowance to the simplifications made, can prove helpful not only in interpreting the results of reactor models but also in developing the most suitable approach to the problem of verifying the findings experimentally.

7.3 Stability of Multitubular Reactors

The stability of fixed bed catalytic reactors supporting highly exothermic reactions has received a considerable amount of attention in recent years. Unfortunately, most of the work has concentrated solely on the tubeside phenomena and hence the results obtained are only applicable to certain specific cases, usually where the coolant temperature is at a constant fixed value. In the large multitubular units used industrially, the coolant inlet temperature and coolant flowrate are important design variables, both having significant effects on the stability of the tubeside reaction. This section extends the use of the coolant inlet temperature versus GG phase plots introduced in chapter six and demonstrates how such diagrams, coupled with a suitable tubeside stability criterion, can be used to design or control

multitubular fixed bed reactors.

7.3.1 Counter-Currently Cooled Reactors

A simple and effective method of determining the stability of a fixed bed reactor[68] has been used to compare multitubular and single tube representations of the tube bundle in chapter three. Applying this technique to the effects of variation of inlet coolant temperature on the stability of the tubeside gives plots like figure 7.3, which shows the maximum tubeside centre line temperatures versus thermal load factor for a four coolant pass counter-current reactor under three different inlet coolant temperatures. The coolant mass flowrate is kept constant (GG = 3.0) and all other data is shown in table 3.1. These cases demonstrate that too high a coolant temperature causes temperature runaway on the tubeside (the reactor trajectory has crossed the runaway line), while too low a coolant temperature quenches the reaction. With all the other system parameters constant, the coolant temperature that causes the reactor trajectory to just touch the runaway line is the best in terms of conversion while keeping the reactor stable. Varying the coolant mass flowrate, a set of these optimum coolant inlet temperatures can be obtained and figure 7.4 shows the locus of these stable coolant temperatures, plotted as the stability line, on the $T_{c_{in}}$ versus GG charts introduced in chapter six.

In defining an operating region attention must also be directed to the problem of too low a coolant inlet temperature. As before, varying the inlet coolant temperature and coolant mass flowrate for a given system, locii of coolant temperatures which give a specified conversion can be obtained, figure 7.4 shows such a locus for coolant temperatures giving 40% conversion (the 40% conversion line). Other conversion requirements could be plotted but these have not been included for the sake of clarity. Figure 7.4 now gives a region of operability for various coolant inlet temperatures and mass flowrates at given system

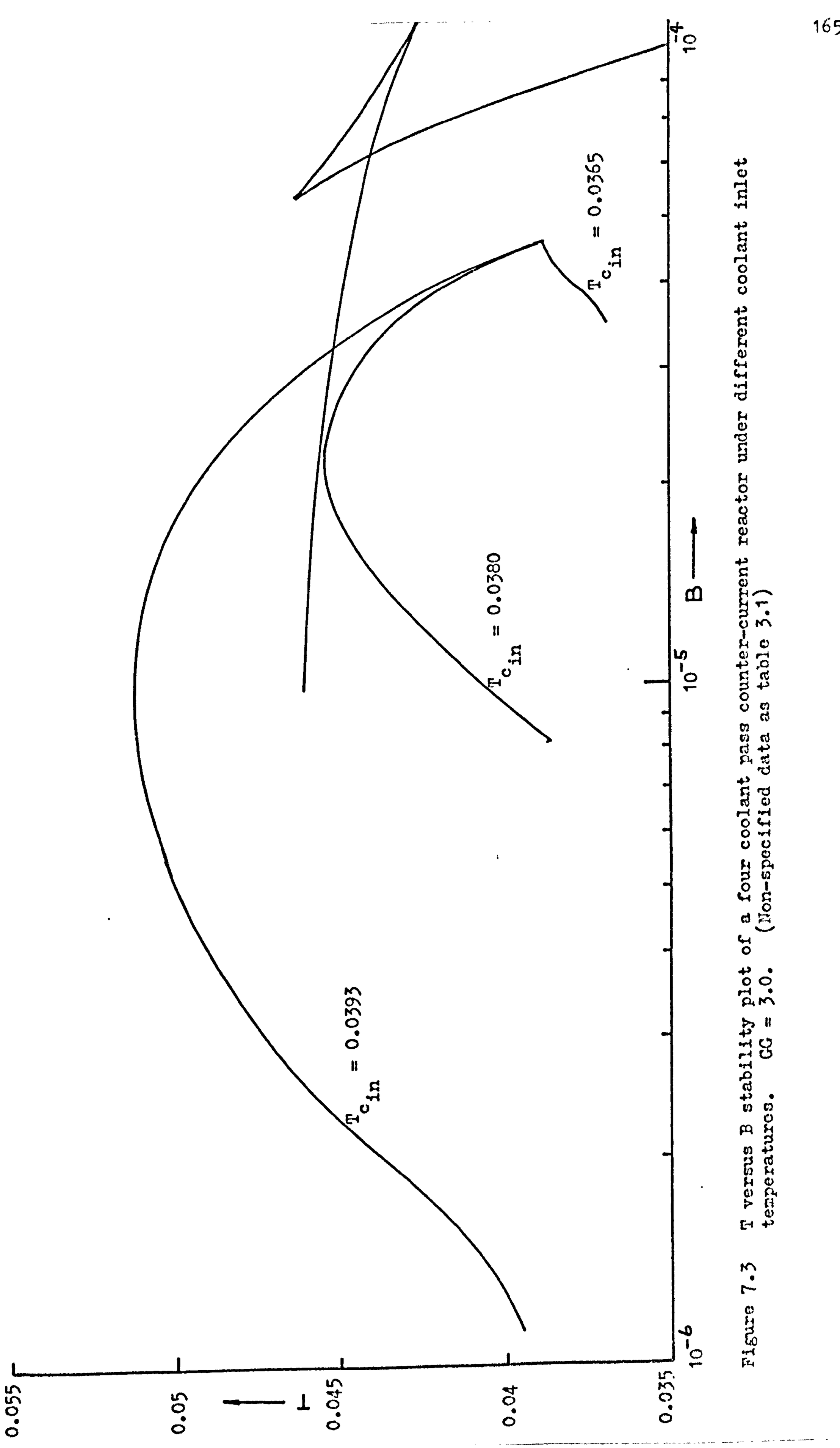

Figure 7.3 T versus B stability plot of a four coolant pass counter-current reactor under different coolant inlet temperatures. GG = 3.0. (Non-specified data as table 3.1)

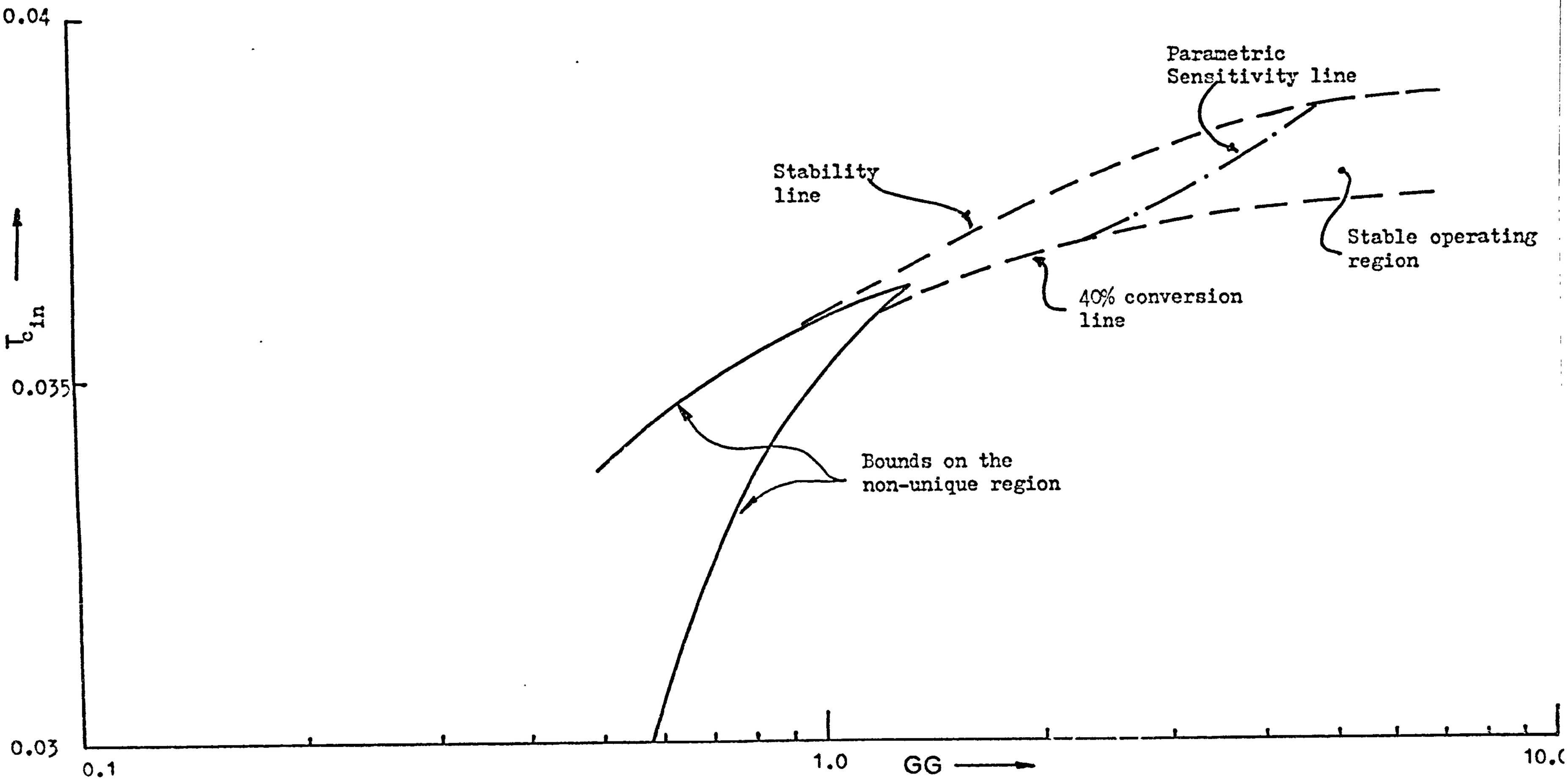

Figure 7.4 A plot of $T_{c_{in}}$ versus GG showing the safe operating region for a four coolant pass counter-current reactor.
(Non-specified data as table 3.1)

parameters. Inlet coolant temperatures above the stability line can cause tubeside runaway and operation below the 40% conversion line give conversions lower than this.

In addition to these criteria, there is also the phenomena of multiple steady states and parametric sensitivity of the coolant temperature to be considered before deciding upon operating conditions. The bounds on the non-unique region, defined in chapter six, are shown in figure 7.4. However, the parametric sensitivity region is more difficult to define. Figure 7.5 shows the coolant temperature rise versus the coolant inlet temperature for various GG values and the data used in figure 7.4. A simple, and effective method of excluding regions of parametric sensitivity is to limit the temperature rise allowed in the system, using figure 7.5 we therefore obtain a set of values of $T_{c_{in}}$ versus GG which can be plotted on figure 7.4. Limiting the temperature rise to $\Delta T_c = 0.001$ (approximately 13 K) gives the parametric sensitivity line shown in figure 7.4. The choice of temperature rise allowable is, at present, arbitrary, and will depend on various factors such as how tight a control or design is required, the type of coolant etc.

The operating region for the reactor is now defined fully in figure 7.4. For a given system the operational variables of coolant inlet temperature and coolant flowrate (present in the parameter GG) should lie with the region bounded by the stability line, the 40% conversion line (or any specified conversion line) and the parametric sensitivity line (defined by an arbitrary, given coolant temperature rise).

The effect of a decrease in the major design variable, the inlet reactant temperature is shown in figure 7.6, the operating region being moved upwards, allowing higher inlet coolant temperatures to be used for any given value of GG.

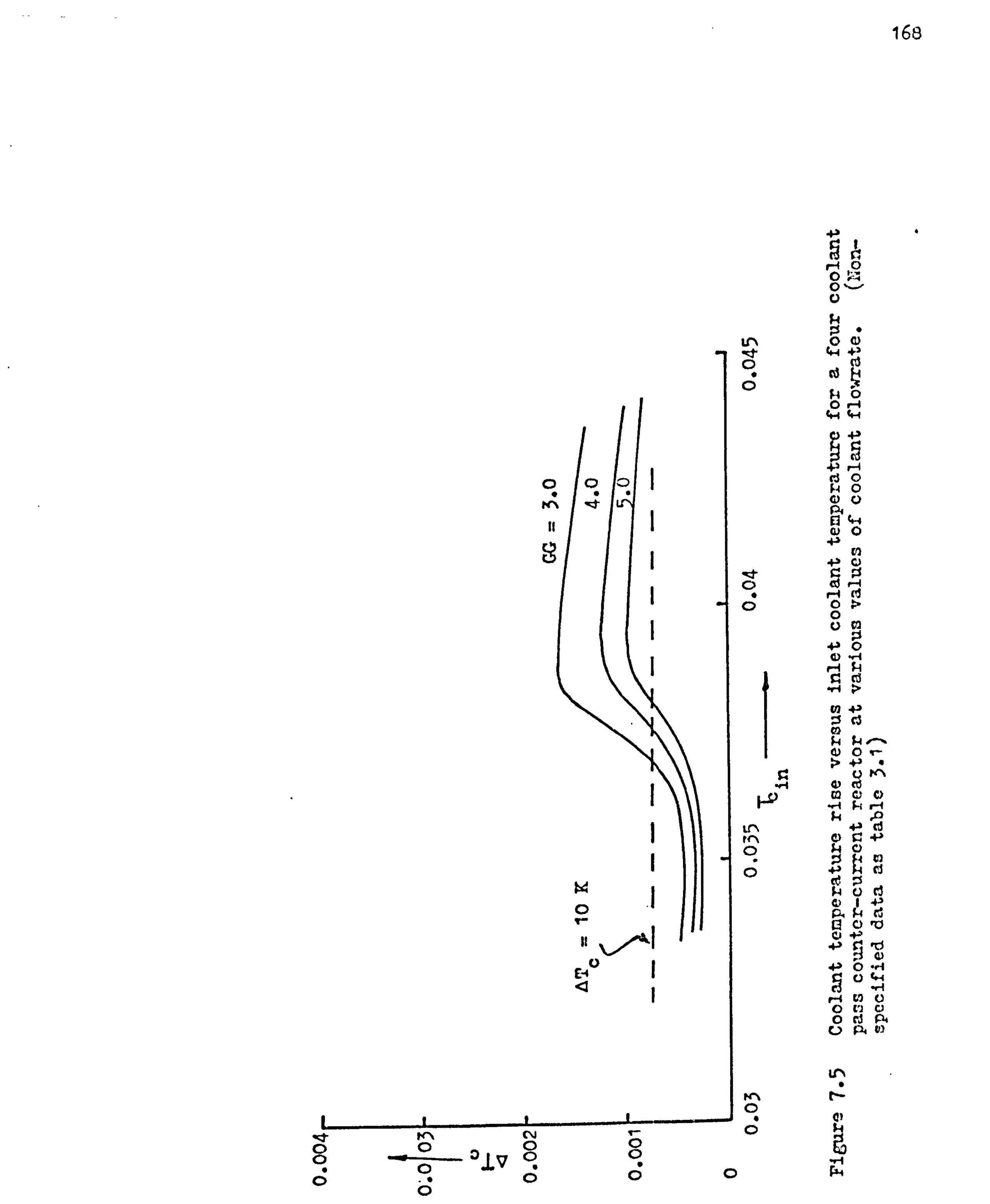

Figure 7.5 Coolant temperature rise versus inlet coolant temperature for a four pass counter-current reactor at various values of coolant flowrate. specified data as table 3.1)

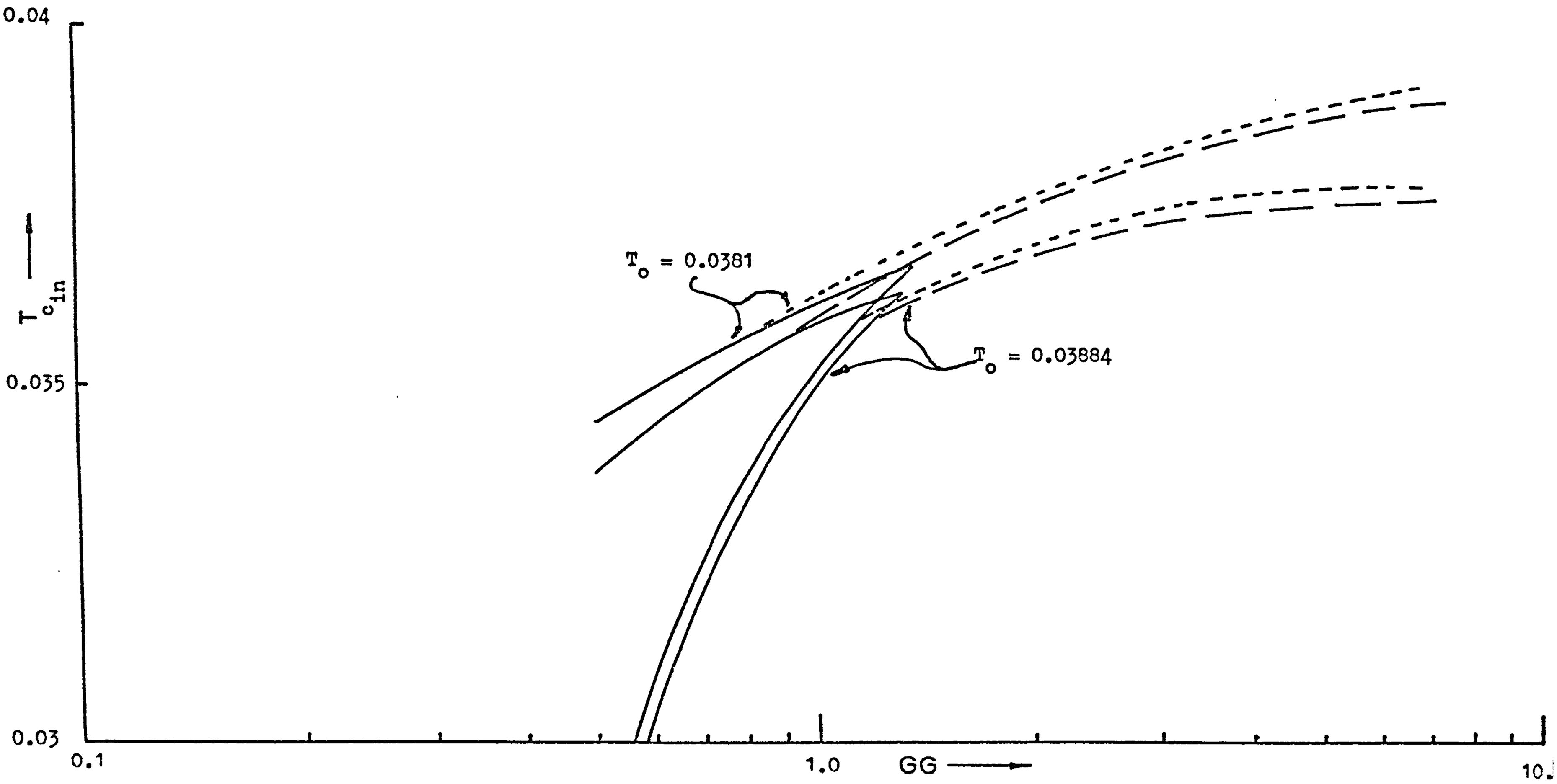

Figure 7.6 The effect of decreasing the inlet reactant temperature on the stability and conversion lines of figure 7.4.

7.3.2 Co-Currently Cooled Reactors

The stable operating regime of a co-currently cooled reactor can be obtained in an analogous manner to that of the counter-current reactor given earlier. Figure 7.7 shows a phase plot of inlet coolant temperature versus the parameter GG, containing the stability line, the 40% conversion line and the parametric sensitivity line. As for the counter-current system the stability line represents the locus of the conditions at the limit of temperature runaway as defined by the stability criteria of McGreavy and Adderley[68]. The 40% conversion line represents the locus of conditions giving 40% conversion in a co-current reactor. Other specified conversion lines could be plotted, but for the sake of clarity these are omitted.

Although co-current reactors do not exhibit multiple steady states in the coolant, they do show parametric sensitivity with respect to coolant temperature at low coolant flowrates. This is demonstrated in figure 7.8 where, as the value of GG is reduced, a region develops in which small variations in inlet coolant temperature lead to large variations in coolant outlet temperature i.e. a region of parametric sensitivity. As in the counter-current case, representing this region is difficult, and so the same technique will be used here, namely the arbitrary choice of a maximum allowable coolant temperature rise. Unlike the counter-current reactor, quite large coolant temperature rises can be tolerated (provided the coolant does not decompose or cause corrosion under these conditions) because the hot coolant only affects parts of the reactor containing low reactant concentrations. Figure 7.9 shows a plot of the overall coolant temperature rise versus the inlet coolant temperature under various values of GG, the remaining data being as used in figure 7.7. Allowing a coolant temperature rise of $\Delta T_c = 0.0025$ (approximately 30 K), values of inlet coolant temperature and parameter GG are obtained enabling the parametric sensitivity line of

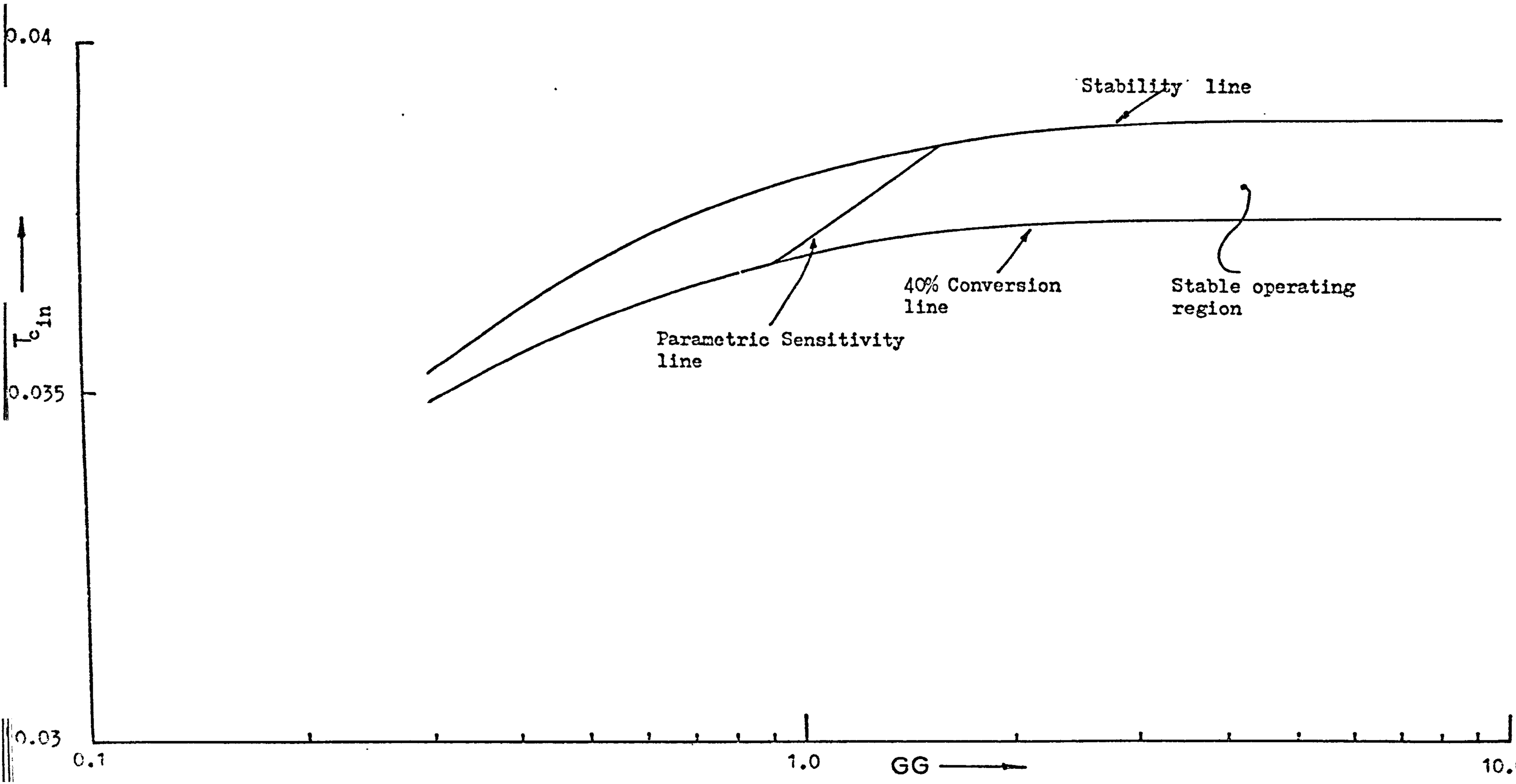

Figure 7.7 A plot of inlet coolant temperature versus GG showing the safe operating region for a four coolant pass co-current reactor. (Non-specified data as table 3.1)

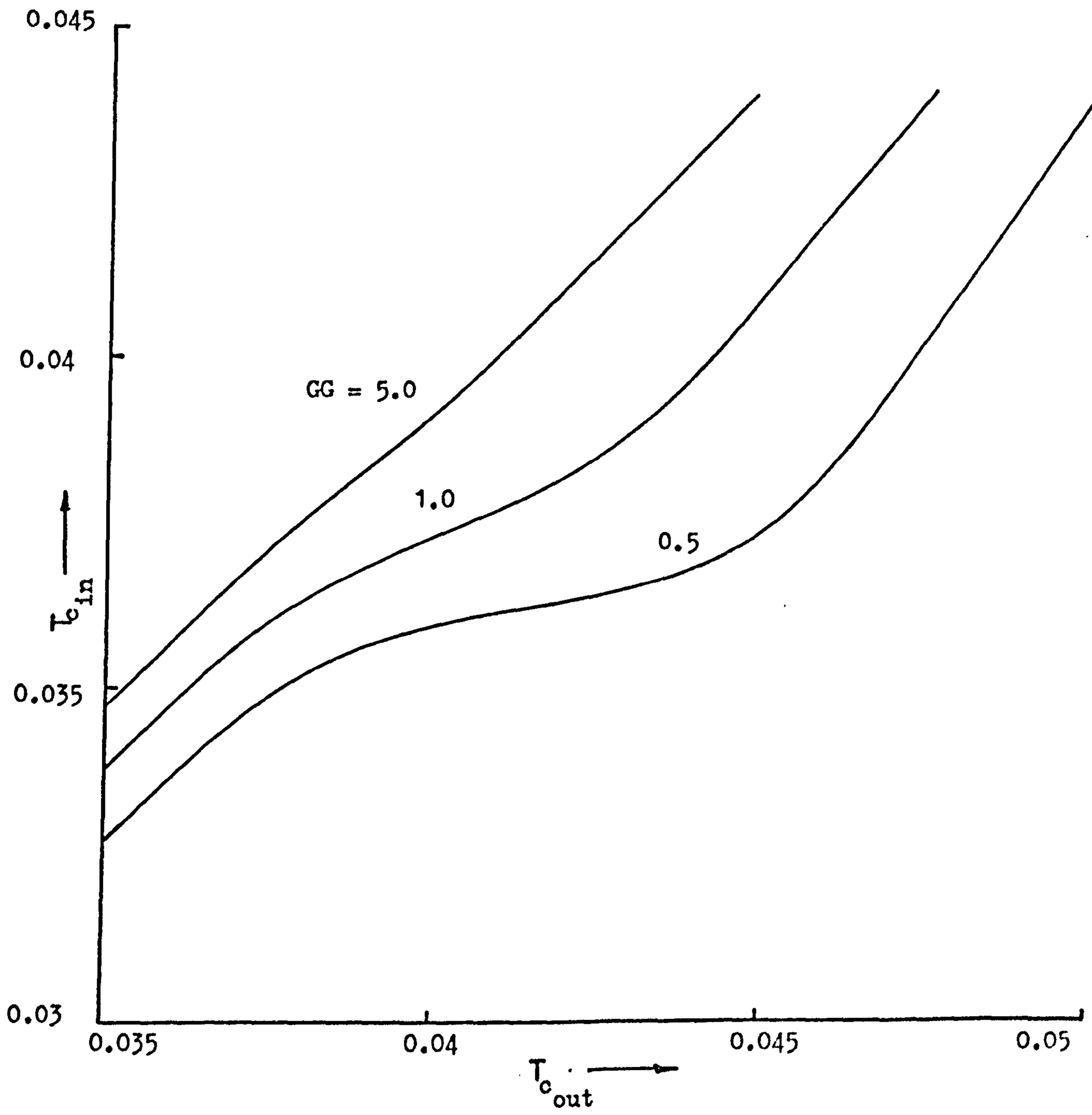

Figure 7.8 Inlet versus outlet coolant temperatures for a four coolant pass co-current reactor at various values of the coolant flowrate. (Non-specified data as table 3.1)

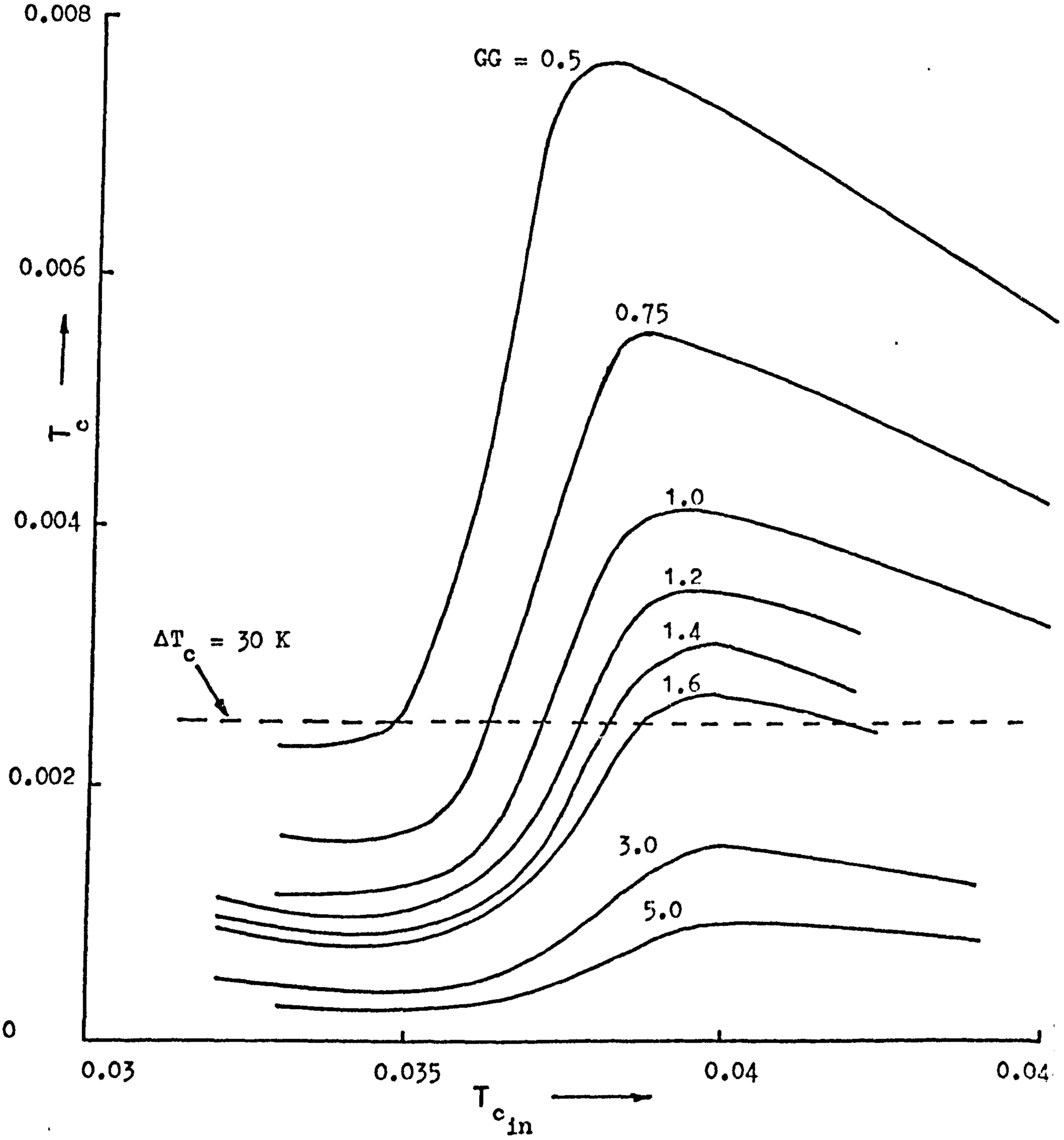

Figure 7.9 Coolant temperature rise versus inlet coolant temperature for a four coolant pass co-current reactor at various values of the coolant flowrate.

figure 7.7 to be drawn.

The operating region for the reactor is now fully defined in figure 7.7. For a given system, the operational variables of coolant inlet temperature and coolant flowrate (obtained from GG) should lie within the region bounded by, the stability line, the 40% conversion line (or any other specified conversion line) and the parametric sensitivity line (defined by an arbitrary, given overall coolant temperature rise).

The effect of a decrease in the inlet reactant temperature is shown in figure 7.10, the stable operating region is raised allowing higher inlet coolant temperatures to be used for any given value of GG.

7.3.3 Use of the $T_{c_{in}}$ versus GG Phase Plots

The phase plots showing regions of operability can be used both in the design and control of multitubular reactors. When designing systems of this complexity, there are several variables which need optimizing, the most important being the pumping costs, the conversion and the system energy input/loss. Fixing the inlet reactant temperature, the phase plots shown in figures 7.4 and 7.7 can then be used to minimise the coolant flowrate (and hence pumping costs), whilst keeping both the conversion and stability of the system within acceptable limits. Indeed, because modern chemical plants are highly interactive by nature, the coolant, possibly transferring heat with another unit, may have its inlet value fixed. Then the above plots can be used to obtain the value of GG necessary for a given conversion under a given inlet reactant feed condition.

Having designed the reactor a control scheme has to be implemented which enables the measurement and manipulation of externally available variables. Referring to the $T_{c_{in}}$ versus GG plots of figures 7.4 and 7.7, it can be seen that both the stability and conversion lines are

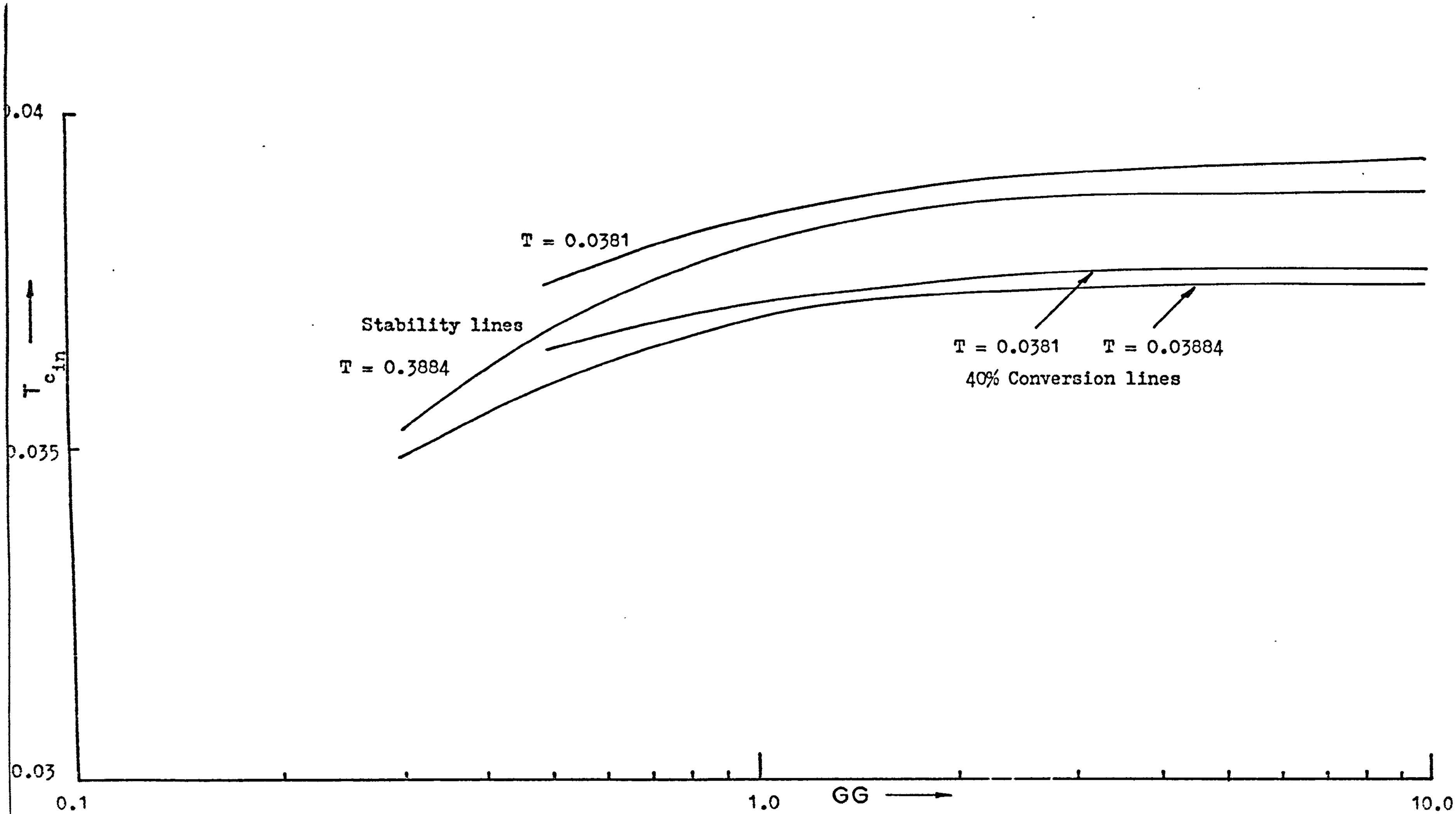

Figure 7.10 The effect of decreasing the inlet reactant temperature on the stability and conversion lines of figure 7.7.

essentially linear in the region of operability. Equations of the form:

$$T_{c_{in}} = a \cdot \text{Ln } GG + b \qquad (7.1)$$

can then be formulated for various values of reactant inlet temperature. Thus, by measurement of the inlet reactant and coolant temperatures, plus the coolant flowrate, the conversion and stability of the unit can be calculated from equation (7.1).

As an illustrative example, take for instance a co-current reactor which is designed for 80% conversion of reactants at given inlet reactant and coolant temperatures of, say $T_o = 0.03884$ and $T_{c_{in}} = 0.03854$ respectively, with a coolant flowrate giving a value $GG = 2.0$. The control system has the ability to measure the values of the three variables and for each possible value of inlet reactant temperature there are equations of the form of equation (7.1) representing the 80% conversion line and the stability line of the reactor in question. If, during operation, the value of the inlet reactant temperature changes from $T_o = 0.03884$ to a new value, say $T_o = 0.0381$, then the conversion of the reactor may no longer be 80%. Selecting the stability line for the new temperature, the stability of the system can be ascertained, as can the conversion, which is, from a conversion line equation found to be approximately 65%. By cross-plotting the conversion line for varying conversions against inlet coolant temperature and GG, equations for the conversion at differing inlet reactant temperatures can be obtained which depend on $T_{c_{in}}$ and GG. Thus, for any given system inlet parameters both the stability and conversion of the reactor can be quickly calculated using easily measured external variables.

The application of control action to bring the conversion of the system back to the desired value can be achieved in several ways, depending upon the choice of the manipulative control variable. This

variable can be the inlet reactant temperature, and bringing the temperature back to T_o = 0.03884 in the above example would return the conversion to the desired value of 80%. However, it is not really feasible to manipulate temperatures, because the large heat capacitance of the system means that instantaneous temperature response is very difficult to achieve. Anyway, care must be taken in using the temperatures to control fixed bed reactor systems, as there is the possibility that these can lead to temperature runaway under certain transient conditions. Several workers[15, 35, 41] have shown that reducing the inlet reactant temperature can cause increased temperature peaks on the tubeside of the reactor during the initial transient response, similar effects are shown in chapter eight, when the coolant inlet temperature is decreased in co-currently cooled reactors.

After consideration of the impracticality of using the temperatures as control variables it might be thought that the coolant flowrate (the parameter GG) could be used instead. Unfortunately, as shown in figures 7.4 and 7.7, under the conditions used, in the operating range the stability and conversion lines are not very sensitive to the parameter GG. Indeed, at high values of GG these lines become horizontal. Hence, although it would have resulted in a simple control scheme, the coolant flowrate cannot be used as the manipulative variable.

Clearly, in practical systems there are a large number of variables that should be considered in the control scheme. Many, such as variation of the tubeside flowrate, have not been included in the above discussion, not because they are not important, but because the number of permutations in a generalized survey is much too large. When developing a control scheme based on the above method, these other parameters are easily included in the system models. For instance, a set of stability lines corresponding to variations in tubeside flowrate could be built up and used in the same way as a set of lines

corresponding to variations in the inlet tubeside temperature.

Consideration of the tubeside flowrate as the manipulative control variable leads to some surprising conclusions. For example, if a reactor goes unstable, does the controller increase or decrease the reactant flowrate. If it is decreased then it might be argued that less reactant is being given to the system per unit time and hence the heat generation should decrease and the reactor become more stable. However, decreasing the flowrate, decreases the reactant fluid velocity and so not only does the residence time of the reactants increase causing greater reaction, but the heat transfer coefficients at the wall and pellet surface decrease resulting in less heat removal. Hence, it is possible that this control action actually causes the reactor to become more unstable. Of course, in the limit, a zero flowrate would result in no reaction, but as this would stop the production process it can only be used as an emergency procedure not for routine control. Moreover, even if the flowrate is reduced to zero, this cannot be achieved instantly and dangerous transient conditions may arise from using the flowrate in this way.

Increasing the reactant flowrate, although apparently giving more potential energy to the system in the form of more reactant per unit time, can result in more stable operation. This is because of the decreased residence time of the reactants and the improved heat removal produced by the increased wall and pellet heat transfer coefficients.

The above hypothetical arguments have to some extent been demonstrated in chapters five and six where reactant flowrate variations were applied to selected tubes. Clearly, the results of such variations are not intuitively obvious and, although they will not be considered in this study, deserve further investigation before being applied to any control mechanisms.

7.4 Alternative Flow Configurations

The comparison of alternative configurations of multitubular reactors is very difficult, mainly because of the variety of different bases available for it. This study confines attention to the comparison of the operability a given, fixed size reactor unit. The various configurations are realised by different positioning of the inlet and outlet ports, together with any associated movement of the baffle plates.

From what has been learned so far, it is useful to consider an alternative configuration, containing the merits of both the co- and counter-current systems. This reactor, shown in figure 7.11, requires no complex shell-side modifications and is achieved simply by rearranging the inlet and outlet ports as above, having the coolant entering at pass 2 and leaving at passes 1 and 4. Thus both co- and counter-current coolant flows are present simultaneously. The counter-current stream is heated by coolant pass 2 before entering pass 1 so that the incoming reactant is contacted by warm coolant, since the flowpath is not as long as in a conventional counter-current reactor, the coolant is not heated as much and so the very large temperature peaks of these reactors can be avoided. The co-current stream is also heated and causes reaction in the lower concentration regions of the bed. Clearly then, this system contains the advantages of both the co- and counter-current systems, namely that the incoming reactants are contacted by warm coolant so that the reaction takes place early in the bed, and any reactants left in the latter half of the reactor are also contacted with warm coolant causing reaction here too. Therefore, compared to the co-current system the reaction starts earlier in the bed and compared to the counter-current reactor the temperature hotspots are not so severe because the coolant is not heated to the same extent in the counter-current direction. In effect this mixed-flow configuration contacts the coldest coolant in the position it is most required, at the tubeside

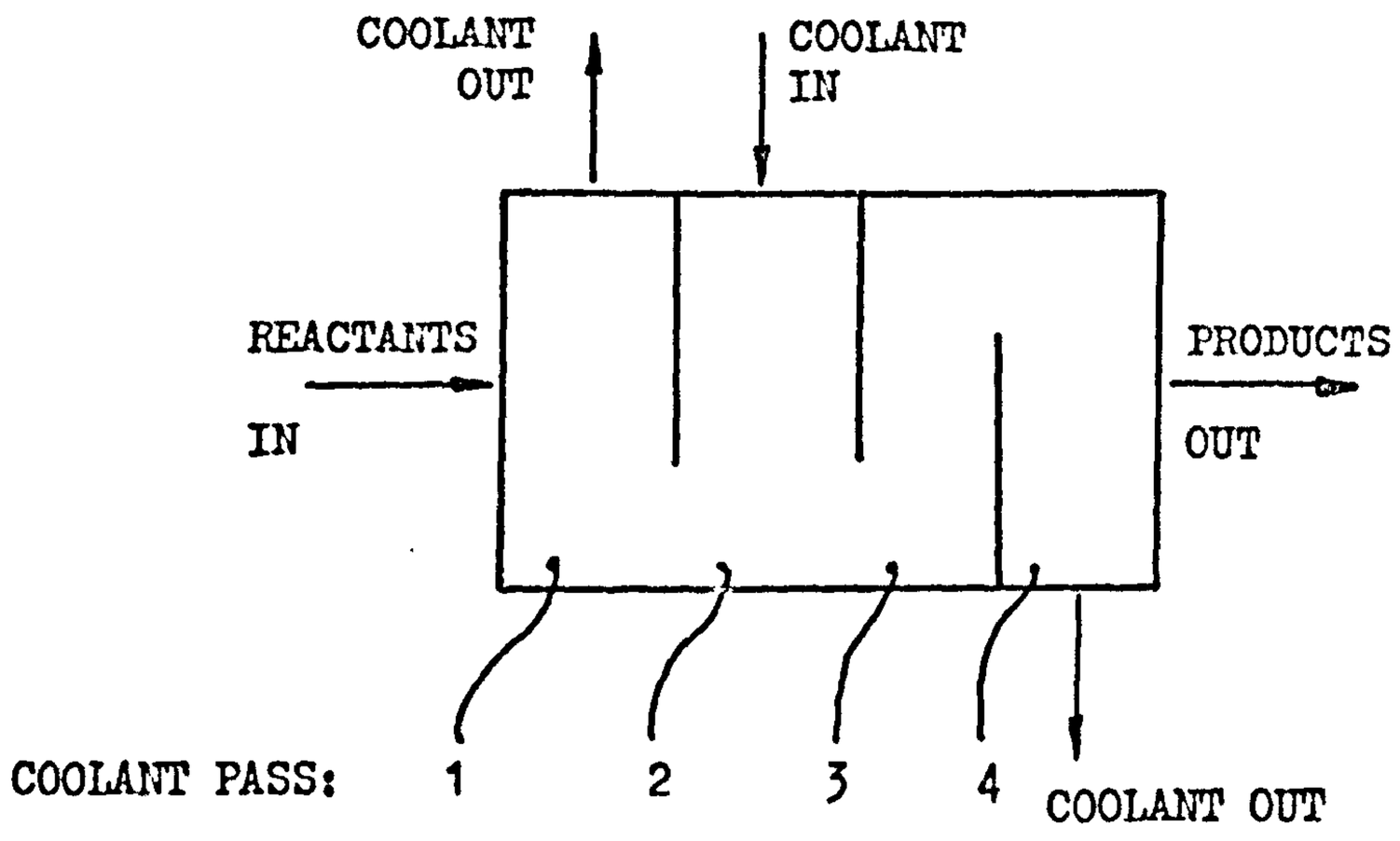

Figure 7.11 Schematic diagram of the mixed flow reactor.

hotspot. Other methods of increasing the heat transfer in the region of the hotspot have been tried. Paris and Stevens[55] devised a complex shell-side arrangement for a single tube reactor and several workers[46, 48, 49] have considered using various sized packings or inert spheres at different points in the tubes. These methods, while successful, are often difficult to apply industrially, the mixed-flow reactor, which can be used on existing tube bundles with very little structural change, overcomes this problem and has greater flexibility.

To see the inherent advantages of the proposed system, a comparison of three configurations will be made assuming that the same mass flow-rate of coolant enters each reactor. This is equivalent to connecting the units to the same constant flowrate pump. The units are all of the same size, the only difference being the direction of flow of the coolant. This means that although the residence time of the coolant is the same in the co- and counter-current reactors, it will be smaller in the mixed flow configuration. By suitably positioning valves in the coolant circuit several different flow variations can be visualized for the latter system. Thus, three different flow patterns will be used in the comparison:

type 1 - $\frac{1}{2}$ the coolant flow from pass 2 flows counter-currently into pass 1

type 2 - $\frac{2}{3}$ the coolant flow from pass 2 flows counter-currently into pass 1

type 3 - $\frac{3}{4}$ the coolant flow from pass 2 flows counter-currently into pass 1

The flowrate through coolant pass 2 is always the same as in the co- and counter-current cases.

The tubeside temperature profiles of tube 1 for the three types of mixed flow system, together with the profiles for the co- and counter-current reactors, are given in figure 7.12 for a value of GG = 4.0, the remaining data being from table 3.1. The lowest, and most stable, temperature profile is obtained from the co-current reactor, with the

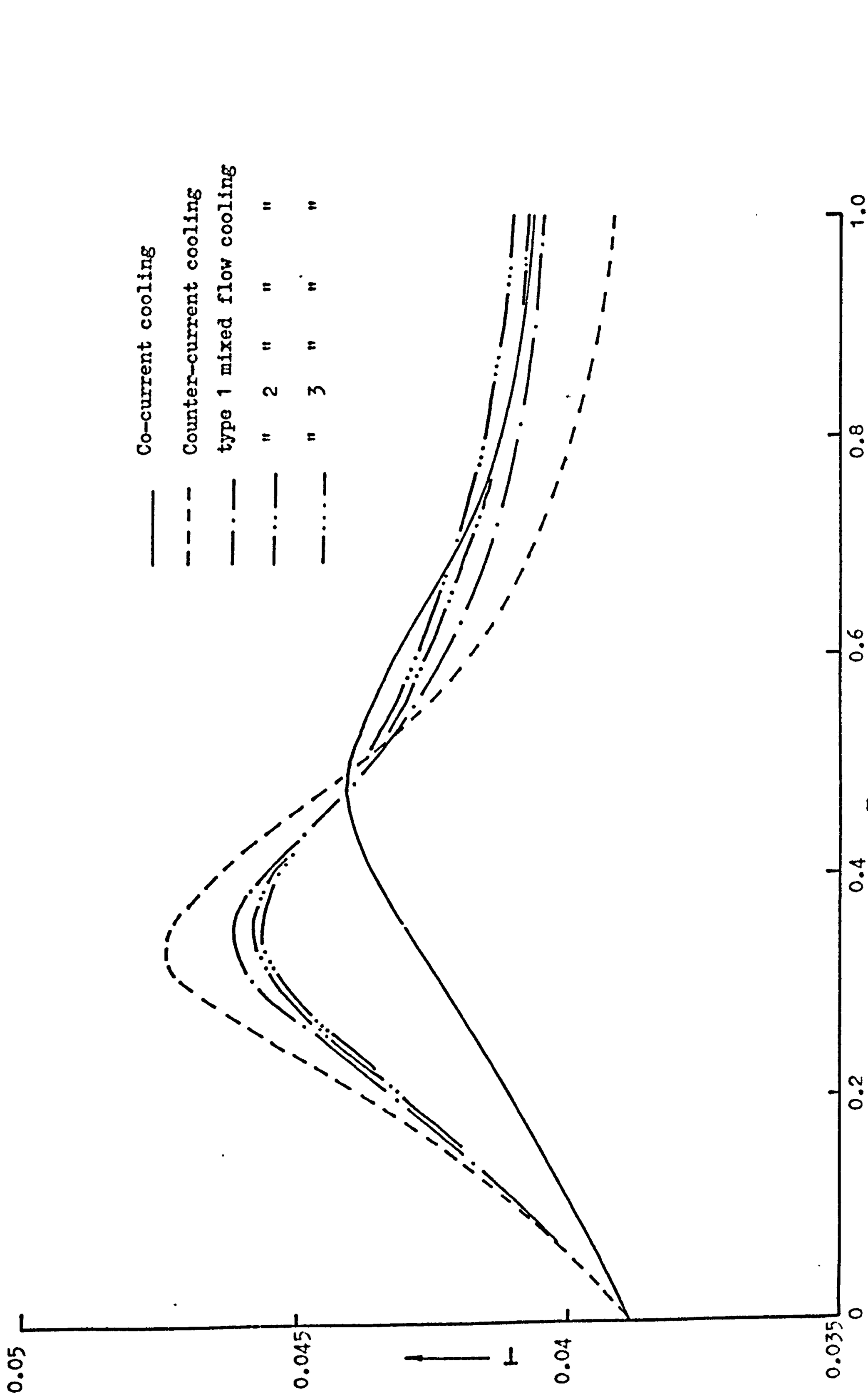

The co-current, counter-current and mixed flow tubeside temperature profiles for tube 1 in a four coolant pass reactor. GG = 4.0. (Non-specified data as table 3.1)

Figure 7.12

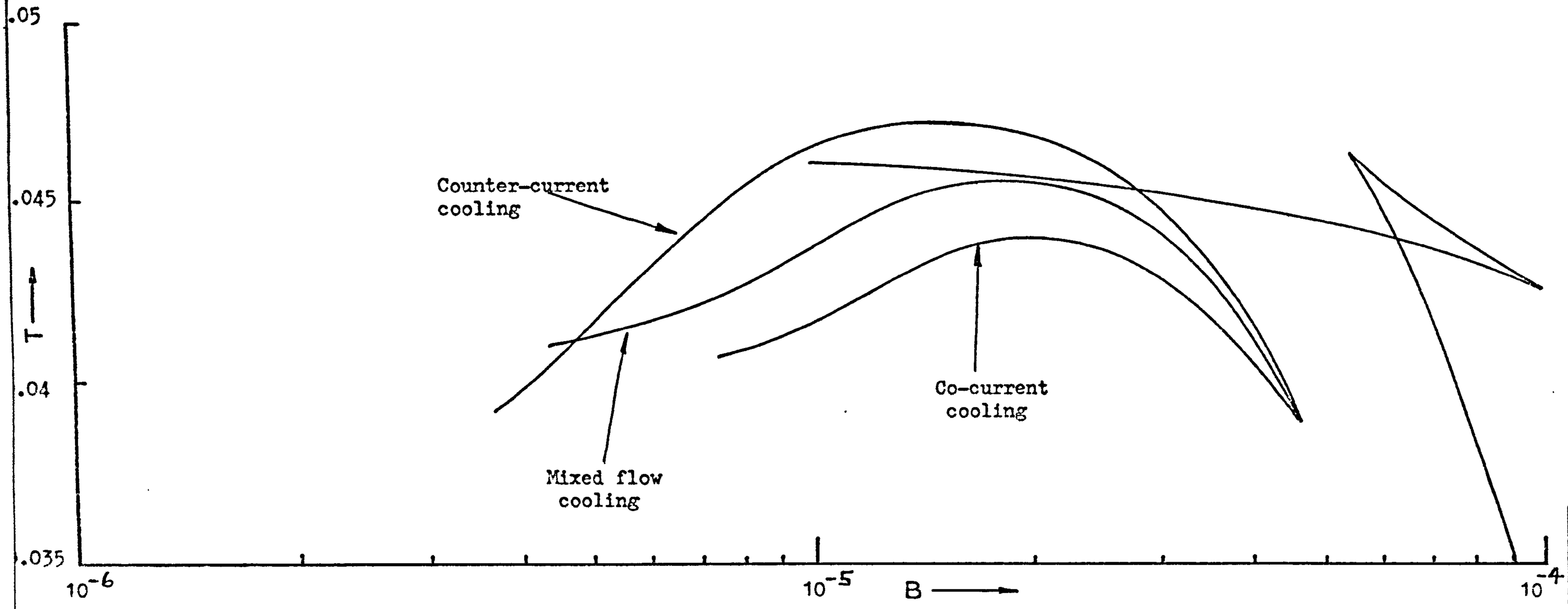

Figure 7.13 T versus B stability plot comparing the co-current, counter-current and mixed flow four coolant pass reactors. GG = 4.0. (Non-specified data as table 3.1)

largest temperature peak being given by the counter-current. The three mixed flow profiles are intermediate to these with the type 3 giving the lowest profile. Figure 7.13 gives the T versus B stability plots of the co-current, counter-current and type 3 mixed flow systems at GG = 4.0, this being the limit of stability of the latter. Table 7.1 shows the coolant temperature rises and conversions for the above configurations under varying values of GG. To compare performance it is sufficient to look at the conversions of each configuration at the limit of stability, so as to compare the best possible conversions. Using the stability plots of section 7.3, and noting that the inlet reactant and coolant temperatures are equal, the limit of stability of the counter-current is seen to be GG = 5.0 and the co-current GG = 2.0.

T A B L E 7.1

Comparison of Co-Current, Counter-Current and Mixed Flow Systems

CONFIGURATION		ΔT_{c_1} counter-current temp rise ^{o}K	ΔT_{c_2} co-current temp rise ^{o}K	FRACTIONAL CONVERSION	
				TUBE 1	TUBE 50
GG=5.0	Co-Current		10.7	83.2 %	82.5 %
	Counter-Current	12.2		89.5 %	90.3 %
	Mixed Flow type 1	9.4	13.7	87.3 %	86.8 %
	type 2	8.6	17.5	87.2 %	86.9 %
	type 3	8.2	21.2	87.6 %	87.0 %
GG=4.0	Co-Current		13.25	83.8 %	83.4 %
	Counter-Current	15.7		92.0 %	92.7 %
	Mixed Flow type 1	12.9	16.9	90.3 %	89.6 %
	type 2	11.9	21.2	90.1 %	89.8 %
	type 3	11.5	25.1	90.4 %	89.9 %

GG=3.0	Co-Current		17.8	86.1 %	84.9 %
	Counter-Current	21.7		95.1 %	95.5 %
	Mixed Flow				
	type 1	16.6	22.1	93.0 %	92.4 %
	type 2	14.9	26.9	92.5 %	92.4 %
	type 3	14.2	31.4	92.7 %	92.45 %
GG=2.0	Co-Current		27.2	90.0 %	89.2 %
	Counter-Current	33.6		97.9 %	97.8 %
	Mixed Flow				
	type 1	32.0	29.1	97.8 %	97.1 %
	type 2	28.1	33.2	97.5 %	97.1 %
	type 3	26.9	36.6	97.4 %	97.1 %

Thus, from table 7.1, at the limit of tubeside stability the conversions for all the systems are approximately the same. The coolant temperature rise is much higher in the co-current reactor, being over twice the value of the counter-current system. However, the coolant flowrate is much lower, and hence the pumping costs, to give the same conversion, are much higher in a counter- than a co-current system. The largest coolant temperature rise of the type 3 mixed flow reactor (see table 7.1) with GG = 4.0, is only slightly less than that of the co-current reactor, being 25.1 K as opposed to 27.2 K.

For the conditions used here, therefore, the co-current reactor, with its low coolant flowrate (low value of GG) exhibits the best characteristic behaviour of all the configurations considered. However, if the high coolant temperature rises (up to 30 K) cannot be tolerated in the coolant then the counter-current or mixed flow system could be used, the former giving the smallest coolant temperature rise. The main advantage of the mixed flow system is that, with coolant flowrates lower than those for the counter-current system, conversions of comparable magnitude can be obtained, which, though they result in higher coolant

temperature rises, these are still less than those in co-current systems.

Thus, the above configurations can be used in the following circumstances when giving conversions close to the limits of stability:

1. Co-current reactor: preferable when pumping costs are high and the coolant can withstand relatively high temperature rises (say up to 30 K).

2. Counter-current reactor: essential when the coolant is very temperature sensitive.

3. Mixed flow reactor: can be used when the conflicting requirements of low pumping costs and low coolant temperature rises (say up to 20 K) are needed.

A more qualitative advantage of the configurations with co-currently flowing coolant is that the reaction is spread along the reactor length. Counter-current systems tend to cause most of the reaction in the initial stages of the bed causing one large temperature hotspot in the tubes. The more shallow peak of co-current reactors means that the catalyst bed gets a more even thermal load and so should age much more slowly. A factor often ignored in the initial stages of reactor design.

7.5 Conclusions

A convenient and simple method of plotting regions of operability has been developed for both co- and counter-current reactor systems. The method, suitable for either design on control studies enables the conversion and stability of a multitubular reactor to be established from easily obtainable variables, namely the inlet reactant and coolant temperatures and the coolant flowrate (used as the parameter GG).

A comparison of co- and counter-currently cooled reactors leads to the conclusion that, for equally sized systems, the co-current

reactor is recommended provided large coolant temperature rises can be tolerated on the shell-side. If not then the counter-current system with its small coolant temperature rises and higher pumping costs can be used to produce the same reactant conversions. An alternative configuration, the mixed flow reactor, has been suggested which tends to result in conditions intermediate to the co- and counter-current reactors. The pumping costs and coolant temperature rises in this case make it useful when a compromise between the need for low energy costs conflict with the need for low coolant temperature rises.

CHAPTER 8

The Dynamic Behaviour of Multitubular Reactors

8.1 Introduction

The essential requirements of any model are that it should provide an adequate description of the system with the minimum of computational effort needed in its solution. This is especially true for a dynamic model of a fixed bed reactor where usually, the equivalent of a steady state solution must be generated many times in order to describe the reactor behaviour over a period of time. Several workers[15, 35, 39, 41, 49] have studied the problem of representing packed bed reactor dynamics, but in all cases they have ignored the dynamics of the shell-side of the system. The usual assumption is that the coolant temperature around the tubes remains constant for all time, and a single tube is taken as being representative of the reactor. While this may be true under certain conditions, as has been shown in earlier chapters it is not generally true in large industrial units, especially when variations occur in the coolant inlet variables. This chapter develops dynamic models for both co- and counter-currently cooled systems and uses them specifically to investigate the importance of the coolant heat balance during transient operation.

8.2 Co-Current Cooling

8.2.1 Formulation of the Equations

Using the nomenclature and mixing cell arrangement of the steady state model shown in Appendix E, a heat balance over cell i gives:

$$m_c C_{p_c} T'_{c_{(i-1)}} + 4\pi RU \int_{z_1}^{z_2} (T'|_{y=R} - T'_{c_i}) dz = m_c C_{p_c} T'_{c_i} + m_c C_{p_c} \frac{dT'_{c_i}}{d\tau} \quad (8.1)$$

which in dimensionless form becomes:

$$\frac{dT_{c_i}}{d\tau} = T_{c_{(i-1)}} - T_{c_i} + \frac{Nu_w^*}{G_c}\int_{z_1}^{z_2}(T - T_{c_i})\, dz \qquad (8.2)$$

where T is functionally related to $T_{c_{(i)}}$

Thus, for a bundle of N tubes across the diameter there are N equations of the form of equation (8.2) coupled with the dynamic tubeside model of Appendix B. The solution of the co-current dynamic reactor is detailed in Appendix H, equation (8.2), which can be solved by any of the usual initial value problem methods, being evaluated by the Runge-Kutta-Merson routine. The initial value is obtained by setting the derivative terms in equation (8.2) and the tubeside equations to zero and calculating the corresponding steady state values.

In addition to the flow across the tube bundle given above, a transient reactor model must account for the time the coolant spends in moving from one coolant pass to the next. Thus, considering the turnround portion of the coolant circuit to be a perfectly mixed tank, the following expression can be obtained to represent the time delay introduced:

$$\frac{dT_{c_2}}{d\tau} = \frac{1}{\theta_R}(T_{c_2} - T_{c_1}) \qquad (8.3)$$

where T_{c_1} is the coolant temperature leaving a coolant pass and T_{c_2} is the coolant temperature entering the next. θ_R is the residence time of the coolant in the turnround area between passes.

The transient response of a four coolant pass multitubular reactor to a step decrease of 10 K in the inlet coolant temperature is shown in figures 8.1 and 8.2. The data used corresponds to a coolant velocity of 0.25 m/sec together with that tabulated in table 3.1. Since the profiles shown take approximately 450 seconds on a CDC 7600 computer for every 100 seconds of actual reactor response, it is clearly difficult and

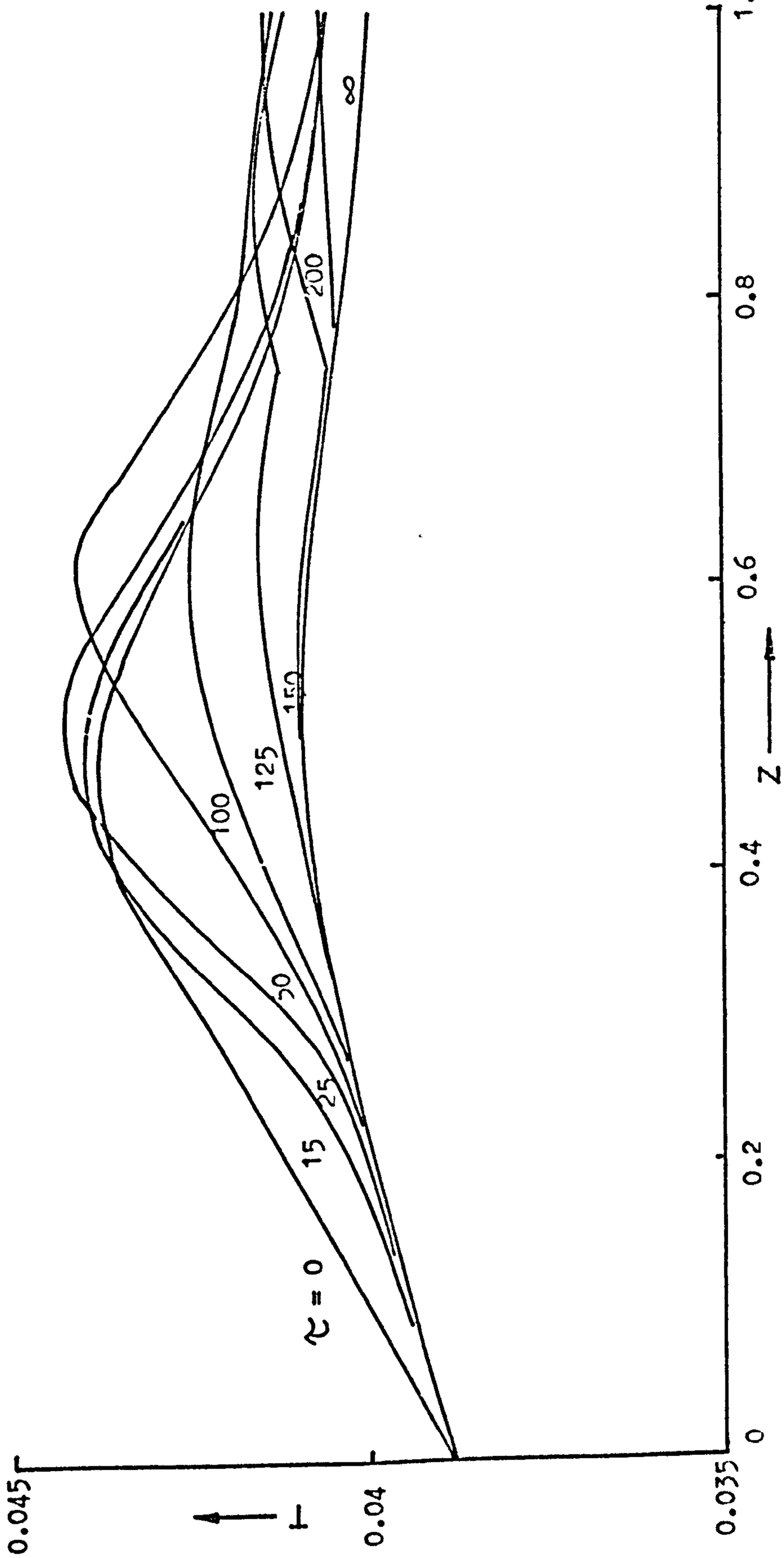

Figure 8.1 Tubeside temperature profiles of tube 1 for a co-current four coolant pass reactor following a step decrease of 10 K in the coolant inlet temperature. No account is taken of the heat capacitance of the reactor fittings. CG = 5.0. (Non-specified data as table 3.1)

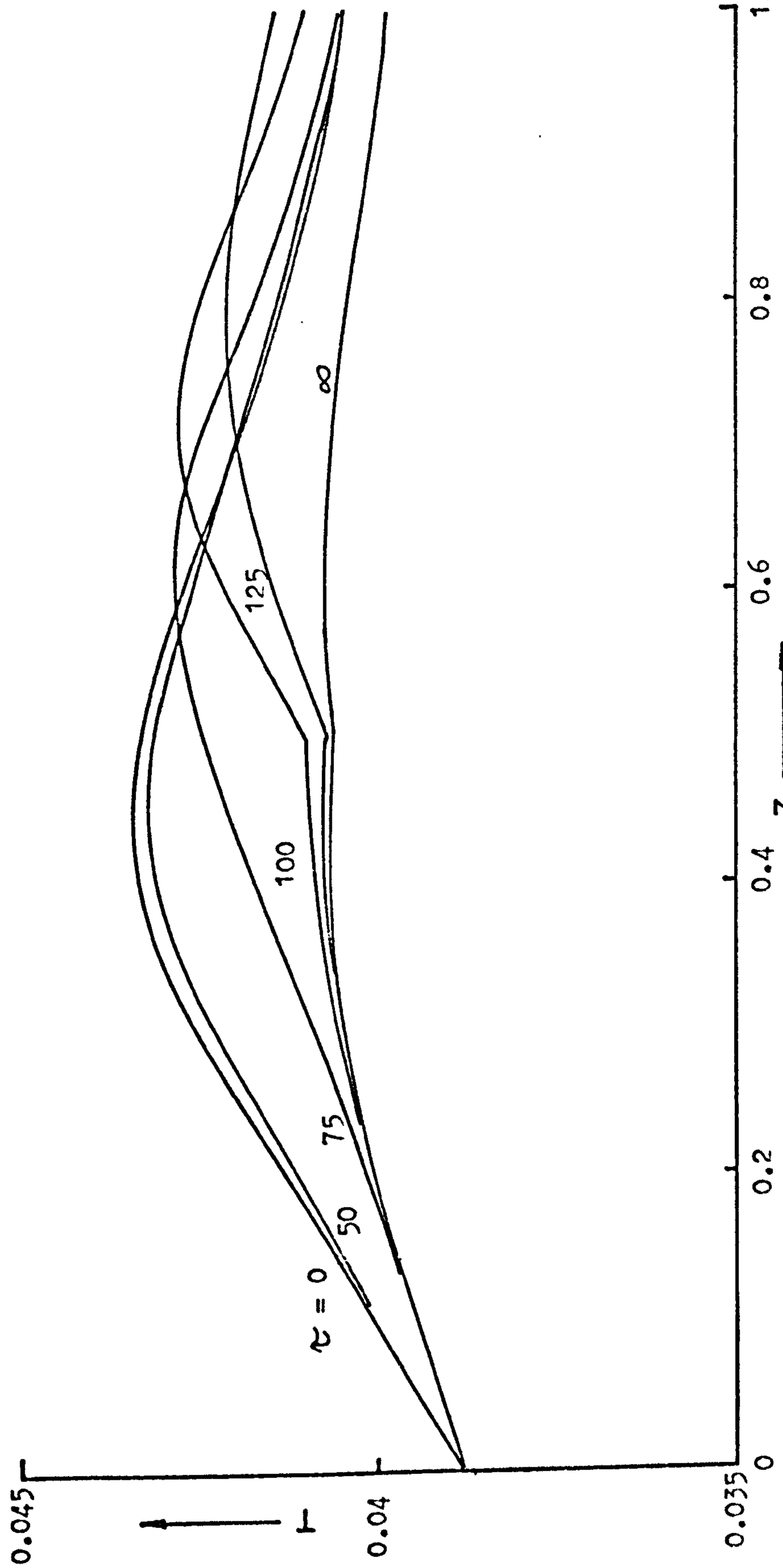

Figure 8.2 Tubeside temperature profiles of tube 50 for the case shown in figure 8.1.

expensive to carry out an extensive survey of operating conditions using the model presented here. It will therefore be instructive to consider ways of reducing the amount of computation necessary to solve the equations before investigating the system performance.

First, the approximation used in the steady state mixing cell model of chapter four can be applied. This assumes that the heat evolved from a tube is approximately constant over a group of tubes. Equation (8.2) then becomes:

$$\frac{dT_{c_i}}{d\tau} = T_{c_{(i-1)}} - T_{c_i} + (N+1)\,\frac{Nu_w^*}{G_c}\int_{z_1}^{z_2}(T - T_{c_i})\,dz \qquad (8.4)$$

where N is an integer denoting the number of mixing cells coupled together. In the steady state, a value of N = 24 can be tolerated at the coolant velocities used here. But, as figure 8.3 shows, for the same perturbation used in figure 8.1, even a value of N = 6 causes the transient response of this approximate model to differ significantly from that predicted by the detailed model. Hence, although the computation time is reduced by a factor of five, the results are not accurate enough to allow this approximation to be used.

A second approach is shown in figure 8.4. Here the working assumption is that the transient term in equation (8.2) is negligible compared to the transient term of the tubeside. The transient behaviour is therefore driven by the tubeside effects, while the coolant goes through a series of pseudo-steady states. Comparison of figure 8.4 and the profiles from the detailed model of figure 8.1 demonstrates that this simplification is not acceptable. The transient term in the coolant equations has a significant effect on the system performance and must be included in the overall heat balance. Indeed this is the basic reason why previous studies are unsatisfactory.

The above results mean that the representation of the coolant heat

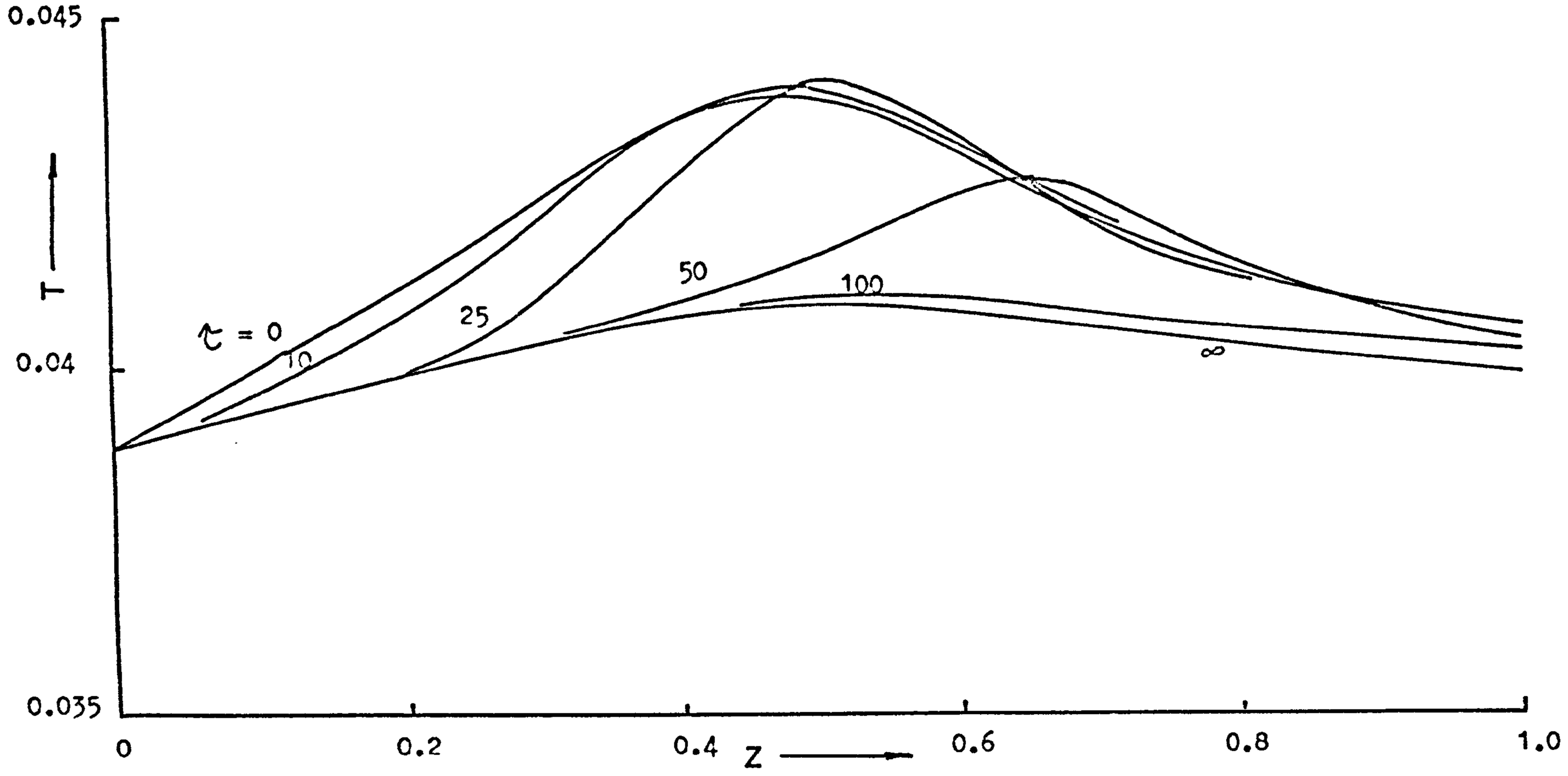

Figure 8.3 Tubeside temperature profiles of tube 1 for a co-current four coolant pass reactor following a step decrease of 10 K in the coolant inlet temperature. The lumping of tubes assumption has been used with N = 6. No account has been taken of the heat capacitance of the reactor fittings. GG = 5.0. (Non-specified data as table 3.1)

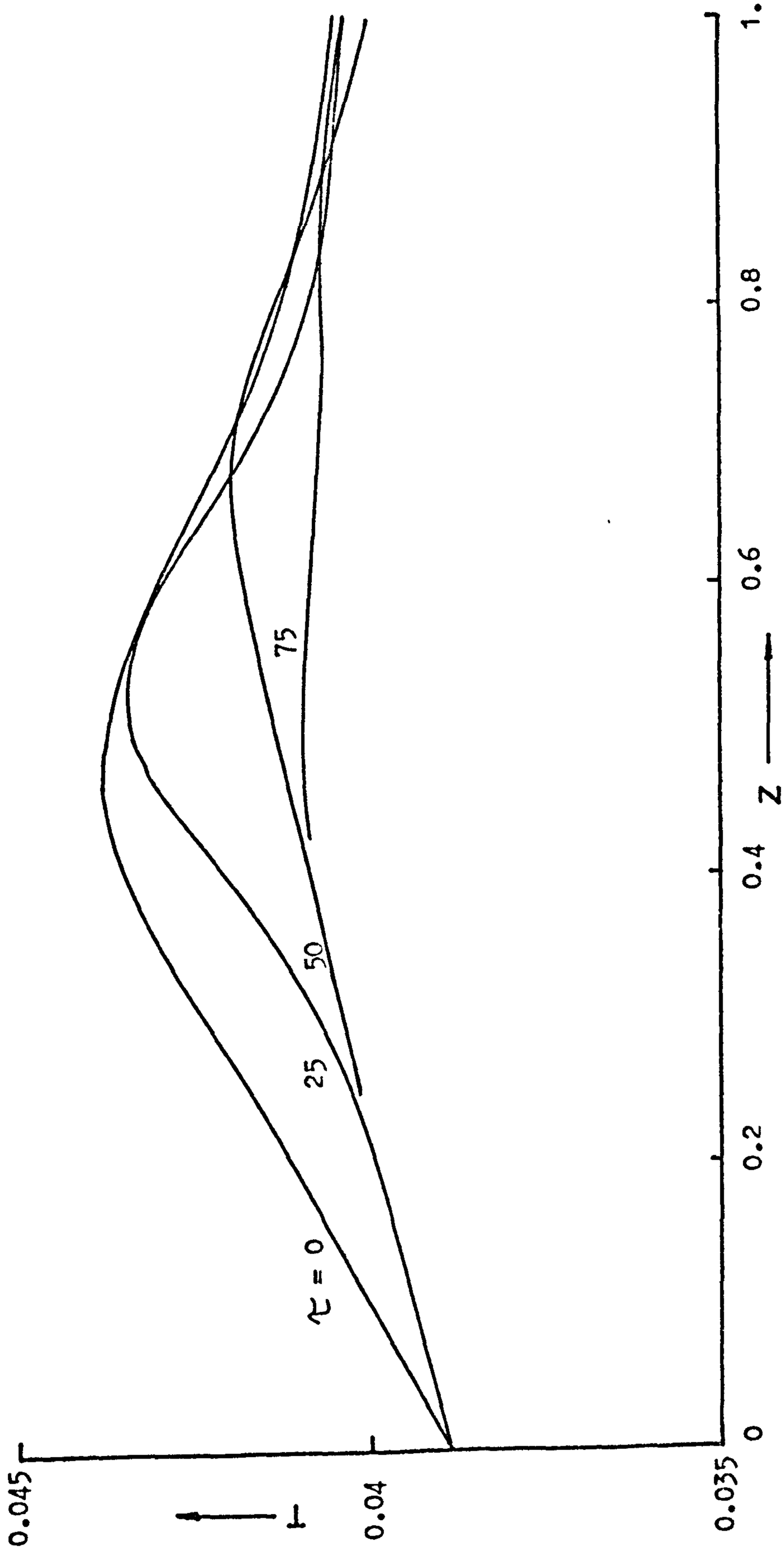

Figure 8.4 Tubeside temperature profiles of tube 1 for a four coolant pass co-current reactor following a step decrease of 10 K in the coolant inlet temperature. No account is taken of either the transient term in the coolant heat balance or the heat capacity of the reactor fittings. GG = 5.0. (Non-specified data as table 3.1)

balance, equation (8.2), cannot be adequately approximated, and so the following study of the transient behaviour of a co-current multitubular reactor will use the detailed mixing cell model. The large computation times necessary must therefore be accepted in order to ensure an adequate representation of the system.

One of the assumptions implicit in the derivation of the coolant heat balance based on equation (8.2) is that the heat capacity of the coolant, together with that of the catalyst pellets, form the only important heat capacitances in the system. This has been shown to be true for single tube reactors[41], where the heat capacity of the tube wall is negligible compared to that of the catalyst packing. However, in the system under consideration here, the fittings in the reactor, the shell, the baffle plates, tie rods etc., constitute a large but ill-defined heat capacity. Consequently, it can only be allowed for approximately, although this is only adequate for identifying the essential characteristics of the system. Bearing this in mind, consider the following approximation.

Let equation (8.2) be rewritten as:

$$\frac{dT_{c_i}}{d\tau} = X * \left\{ T_{c_{(i-1)}} - T_{c_i} + \frac{Nu_w^*}{G_c} \int_{z_1}^{z_2} (T - T_{c_i}) \, dz \right\} \qquad (8.5)$$

where X is a term (between 0 and 1.0), which can be used to slow down the transient response, in the same way as an additional heat capacitance. X = 0 represents a situation where the extra heat capacity is so large that it stops all changes in the values of T_{c_i}, and X = 1.0 results in equation (8.2), which corresponds to no additional heat capacity in the system.

A value of X = 0.5, where the heat capacity of the fittings is of the same order of magnitude as that of the coolant is considered to be a suitable value, and since no other information is available at present, this value will be used throughout the following examples. The effect

of using X = 0.5 can be seen by comparing figure 8.5 with figure 8.1. Both represent the response to step changes in the coolant inlet temperature, the former having X = 0.5 while the latter, which takes no account of the heat capacity of the fittings, has X = 1.0. It can be seen that, as expected, the transient response of the system is slower in figure 8.5. The coolant temperature change has therefore been slowed down because of the capacitance of the reactor body.

8.2.2 The Transient Response of the Reactor

The response of a four coolant pass reactor after a step decrease in coolant inlet temperature is shown in figures 8.5 and 8.6, the former giving the temperature profiles of tube 1 and the latter those of tube 50. The conditions used are those of table 3.1 with a coolant velocity of U_c = 0.25 m/sec, for a coolant temperature change of 10 K. Tube 1 actually experiences an increase in the hotspot temperature during the initial stages of the transient response. Later (see the profile for τ = 300 seconds) two temperature peaks are produced before the final steady state is reached after approximately 400 seconds. The response of tube 50, shows a gradually decreasing profile, with the hotspot moving from coolant pass two to three and then four before the final steady state is reached, again after approximately 400 seconds. An interesting point to note is that the tubeside outlet temperature in all tubes rises above its initial steady state value and then falls to its final value at the end of the transient period. The behaviour of the system following this decrease in the coolant temperature is due to two major effects, namely heat retention by the catalyst packing and the difference in the flowrates of the coolant and the reactants. Both can be explained by considering the configuration of the reactor. The lower temperature coolant entering the system decreases the rate of reaction in tube 1 pass 1, causing the concentration of the reactants leaving this pass to be greater than in the original steady state.

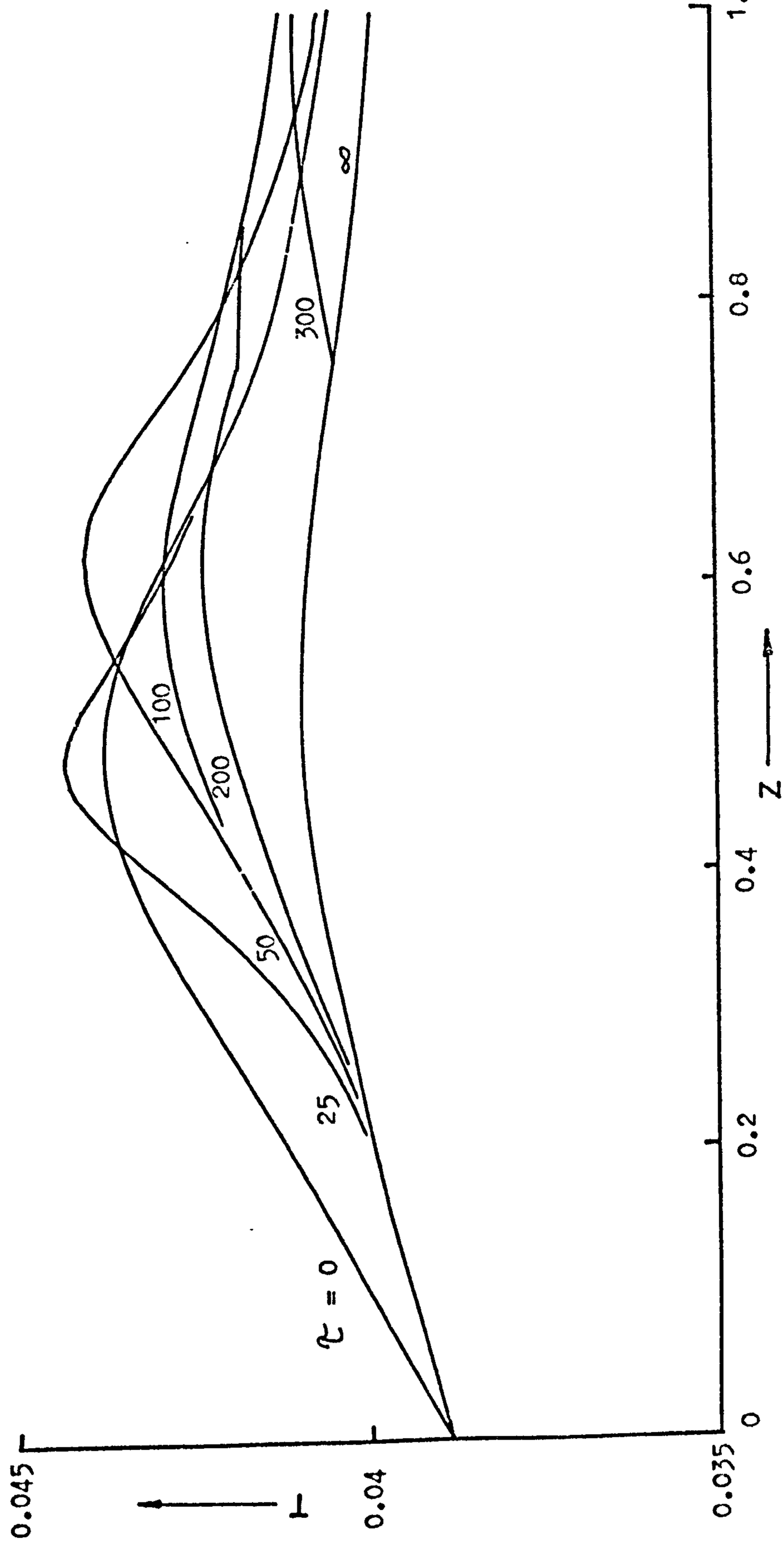

Figure 8.5 Tubeside temperature profiles of tube 1 for a co-current four coolant pass reactor following a step decrease of 10 K in the coolant inlet temperature. GG = 5.0. (Non-specified data as table 3.1)

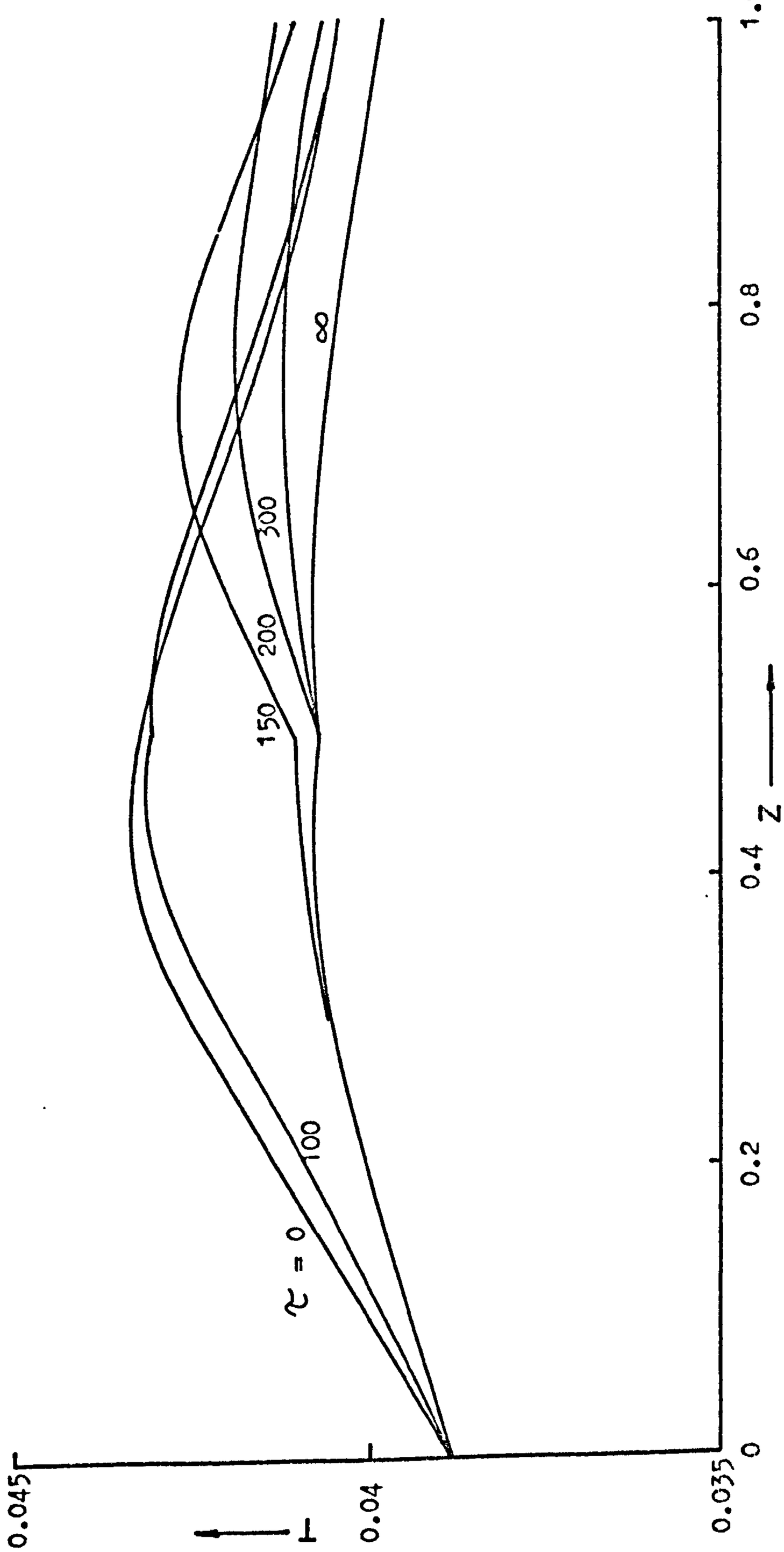

Figure 8.6 Tubeside temperature profiles of tube 50 for the case shown in figure 8.5.

Then, because the flowrate of the reactants is much higher than that of the coolant, the coolant temperature around tube 1 pass 2 is still at the initial value from before the perturbation. Thus, a high concentration of reactants enters a region where the catalyst packing is still hot from the hotspot of the initial steady state, and the coolant environment has not yet decreased in temperature. This results in an increase in the rate of reaction and a consequent increase in the temperature of the tubeside hotspot. Eventually the cooler coolant flows through passes one and two decreasing the reaction rates as it goes, so that the tubeside temperatures gradually fall to their final values. The multiple peak effect is due to similar reasons where a high concentration of reactant is experiencing a region of relatively high catalyst and coolant temperature. Because the tubeside hotspot either increases in temperature or moves towards the reactant outlet during the transient period, the outlet temperatures from the tubes are higher during the transient response, but as the cold coolant decreases the reaction rates throughout the bed, these too finally decrease to the steady state values.

Figures 8.7 and 8.8 show the same perturbation applied to an identical reactor, but with only three coolant passes and the same coolant mass flowrate as the four pass reactor above. The overall behaviour of the systems is very similar, and shows the same general trends, with an increased hotspot temperature during the initial transient response and multiple tubeside temperature peaks. Clearly, the coolant temperature is not a suitable control variable when used by itself, the apparently safe action of decreasing the inlet temperature resulting in temperature increases on the tubeside of the reactor, which can lead to catalyst deactivation, bad selectivity or even tube burnout.

The effect of decreasing the inlet reactant temperature has been

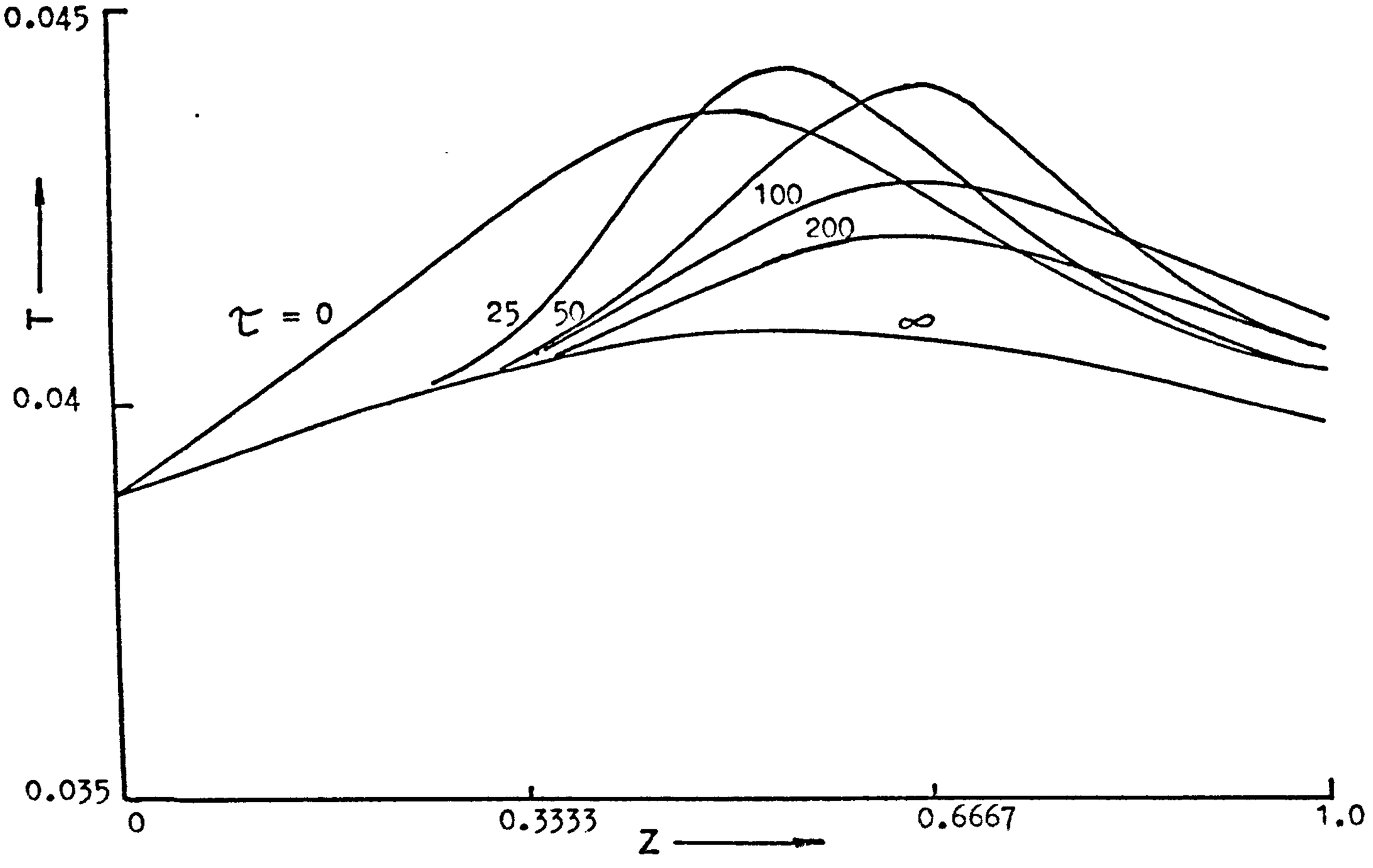

Figure 8.7 Tubeside temperature profiles of tube 1 for a co-current three coolant pass reactor following a step decrease of 10 K in the inlet coolant temperature. GG = 5.0 (Non-specified data as table 3.1)

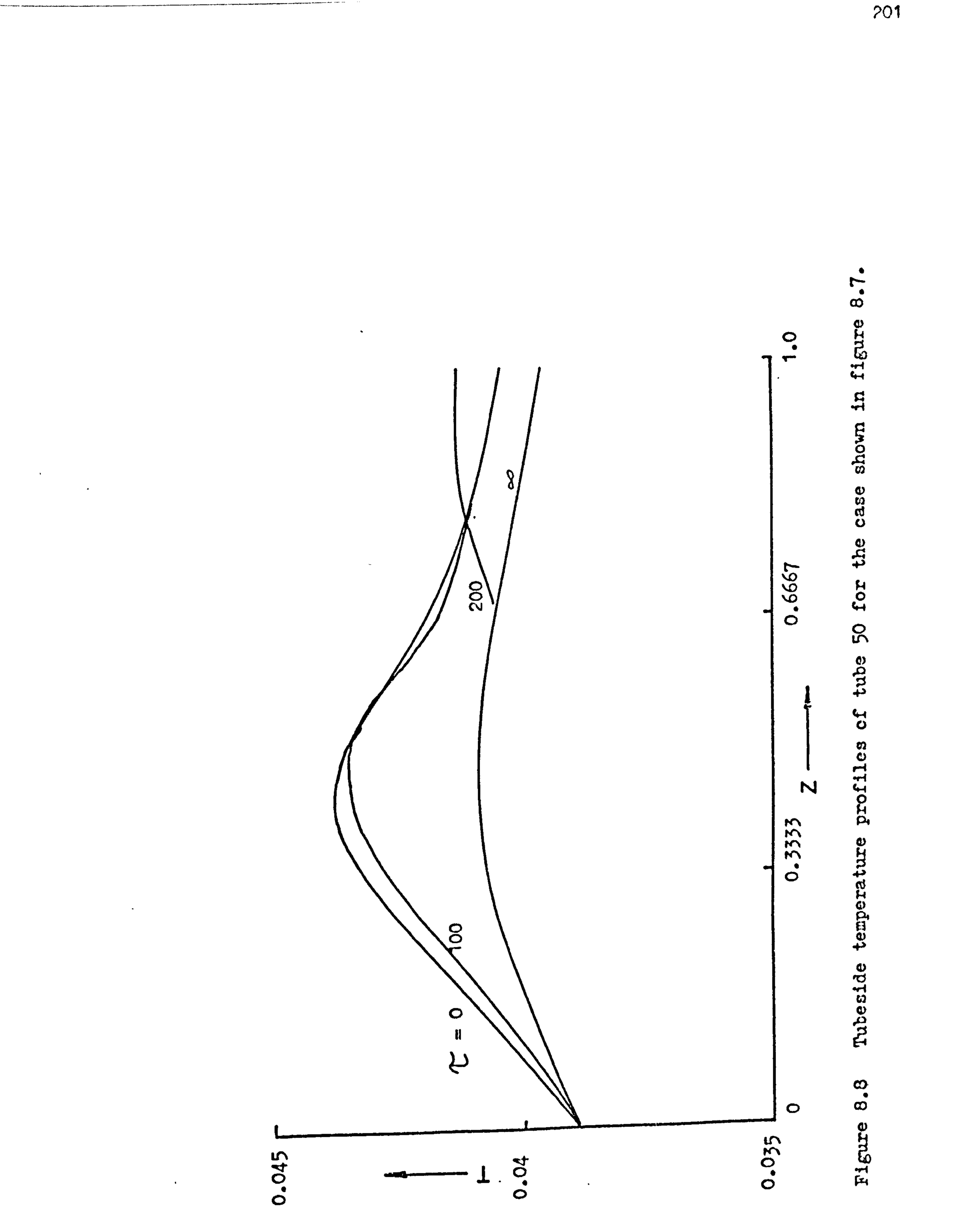

Figure 8.8 Tubeside temperature profiles of tube 50 for the case shown in figure 8.7.

shown[15] to give similar hotspot temperature rises during the transient response of a single tube constant coolant temperature reactor. Figure 8.9 shows the tubeside temperature profiles produced in such a reactor for a 10 K decrease in inlet reactant temperature, the coolant temperature being constant and equal to the initial reactant inlet temperature. A similar reactant temperature decrease in a four coolant pass multitubular reactor, using the data of table 3.1, is shown in figures 8.10, 8.11, 8.12 and 8.13, representing the tubeside temperature profiles for tubes 1 and 50 in a high coolant flowrate (U_c = 0.25 m/sec) and a low coolant flowrate (U_c = 0.1 m/sec) situation respectively. As expected, the latter case is affected more severely than the high flowrate example. This mainly because the low flowrate reactor has higher temperature peaks in the initial steady state.

Such behaviour, which demonstrates the distributed nature of the system, arises from the high heat capacity of the catalyst packing. The low inlet reactant temperature reduces the reaction rate over the initial portion of the bed so that a high concentration of reactants enters the region of the initial steady state hotspot. Here, the catalyst is still at a high temperature and the reaction rate accelerates due to the increased concentration. Thus, the temperature in this region increases. Gradually the cooler reactants decrease the temperature of the packing and the temperature profiles fall to the final steady state values. The transient response lasts approximately 200 to 250 seconds in all the above three cases implying that the effects of the coolant transient term in equation (8.5) are small when dealing with tubeside perturbations.

The final responses to be considered are for step changes in the coolant flowrate. Figures 8.14 and 8.15 show the tubeside temperature profiles for tubes 1 and 50 in a four coolant pass reactor following a 25% decrease in flowrate from GG = 2.0. The profiles gradually change

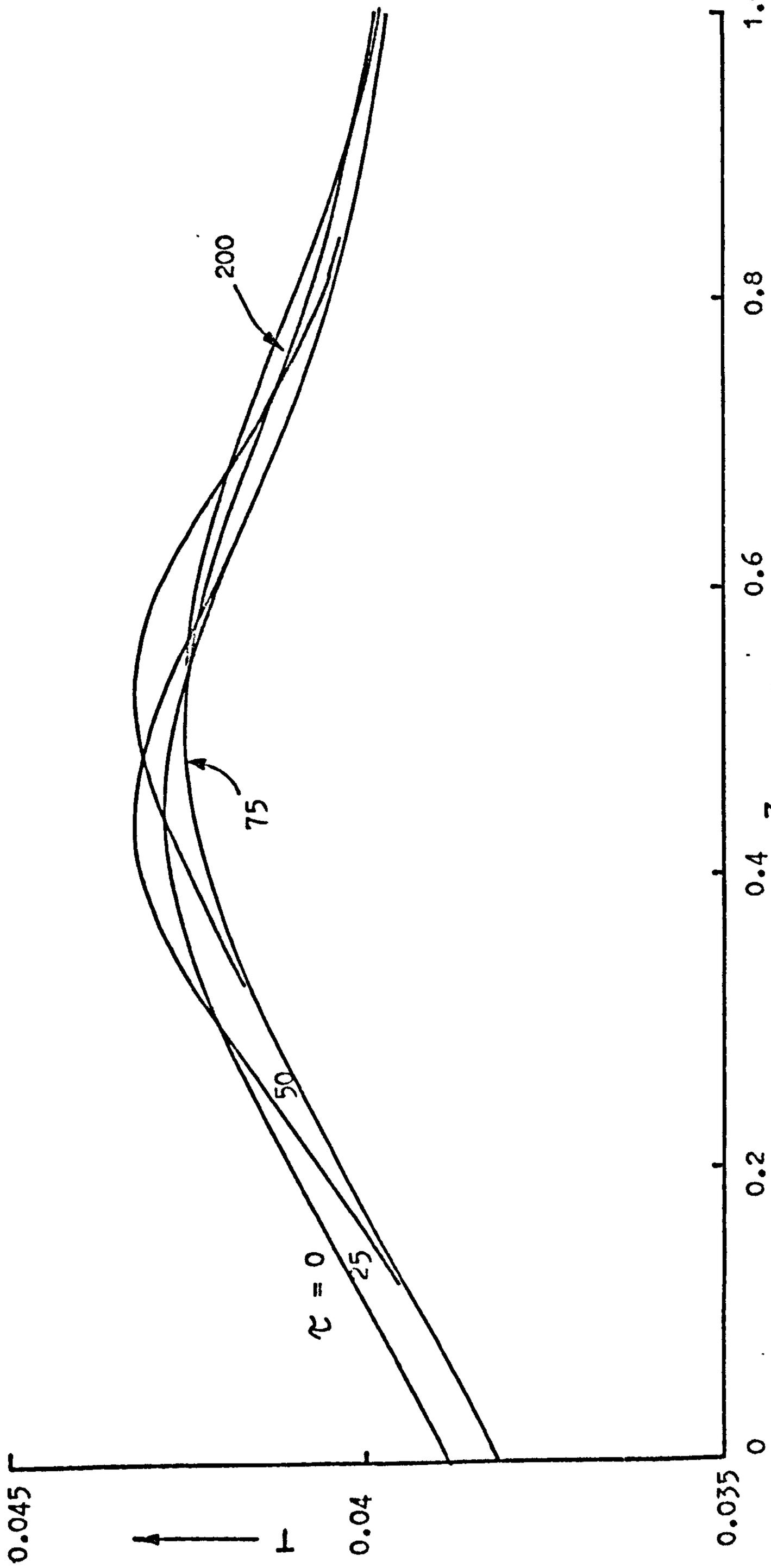

Figure 8.9 The transient response of a single tube, constant coolant temperature reactor following a step decrease of 10 K in the inlet reactant temperature. (Data as table 3.1)

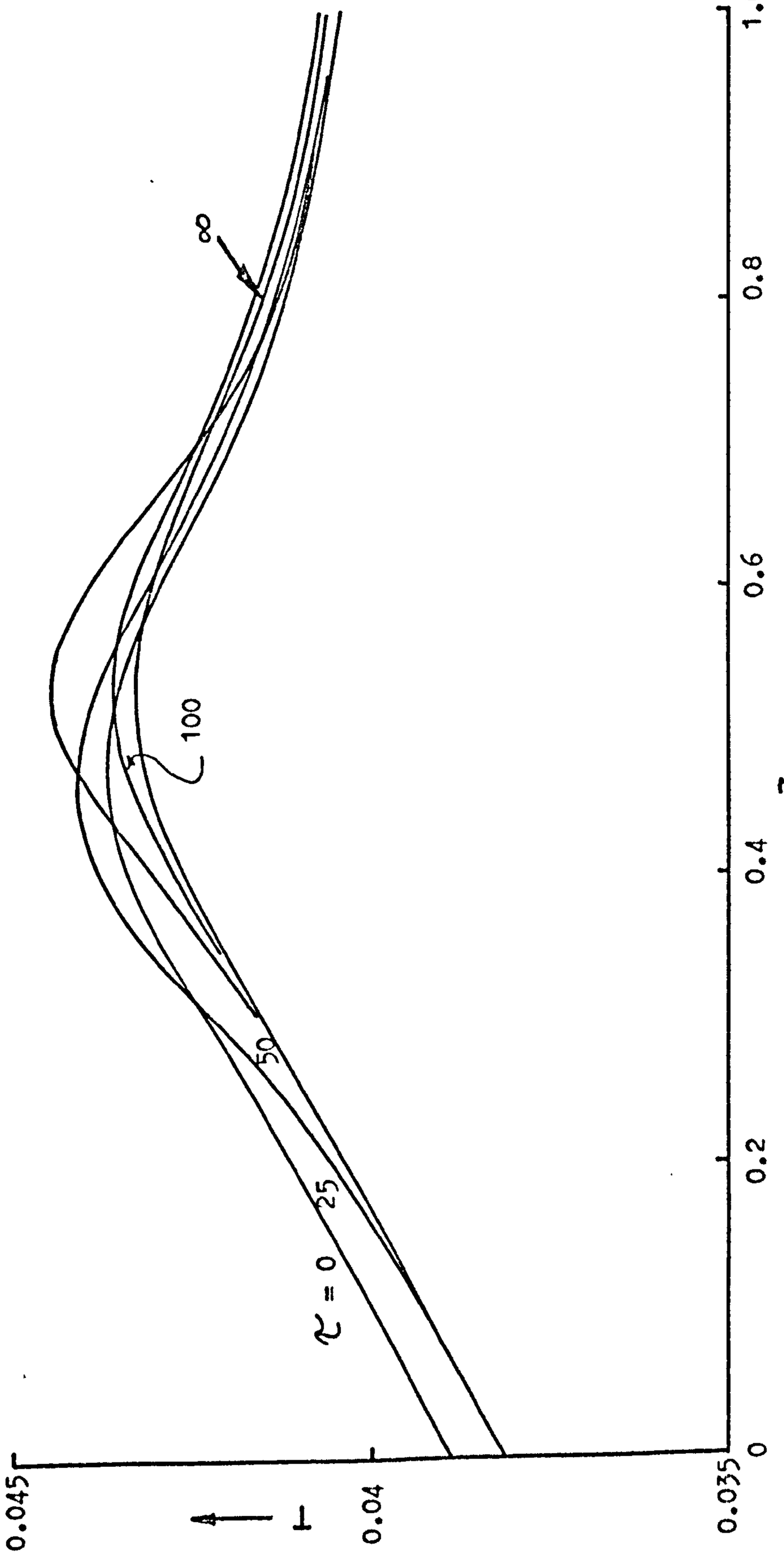

Figure 8.10 Tube side temperature profiles of tube 1 for a four coolant pass co-current reactor following a step decrease of 10 K in the reactant inlet temperature. GG = 5.0. (Non-specified data as table 3.1)

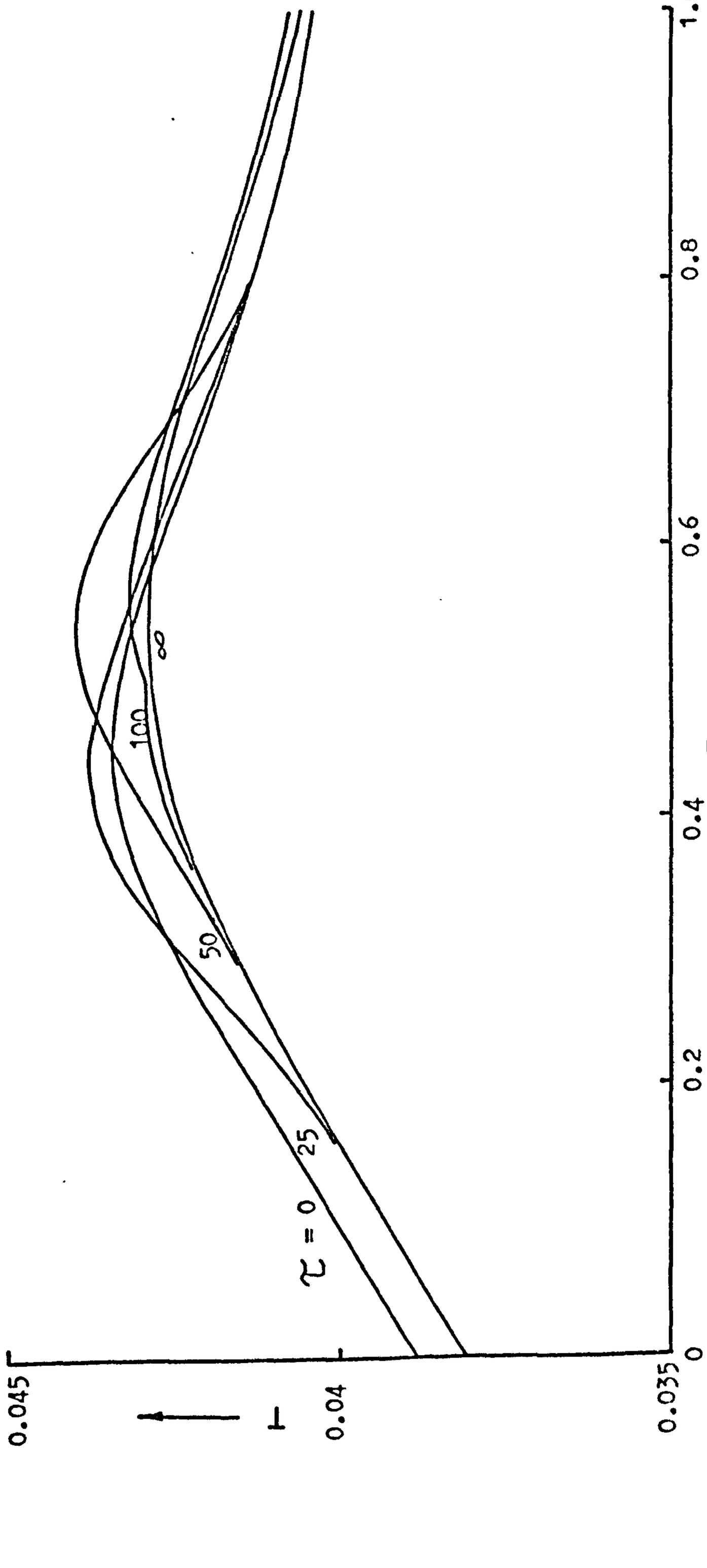

Figure 8.11 Tubeside temperature profiles of tube 50 for the case shown in figure 8.10.

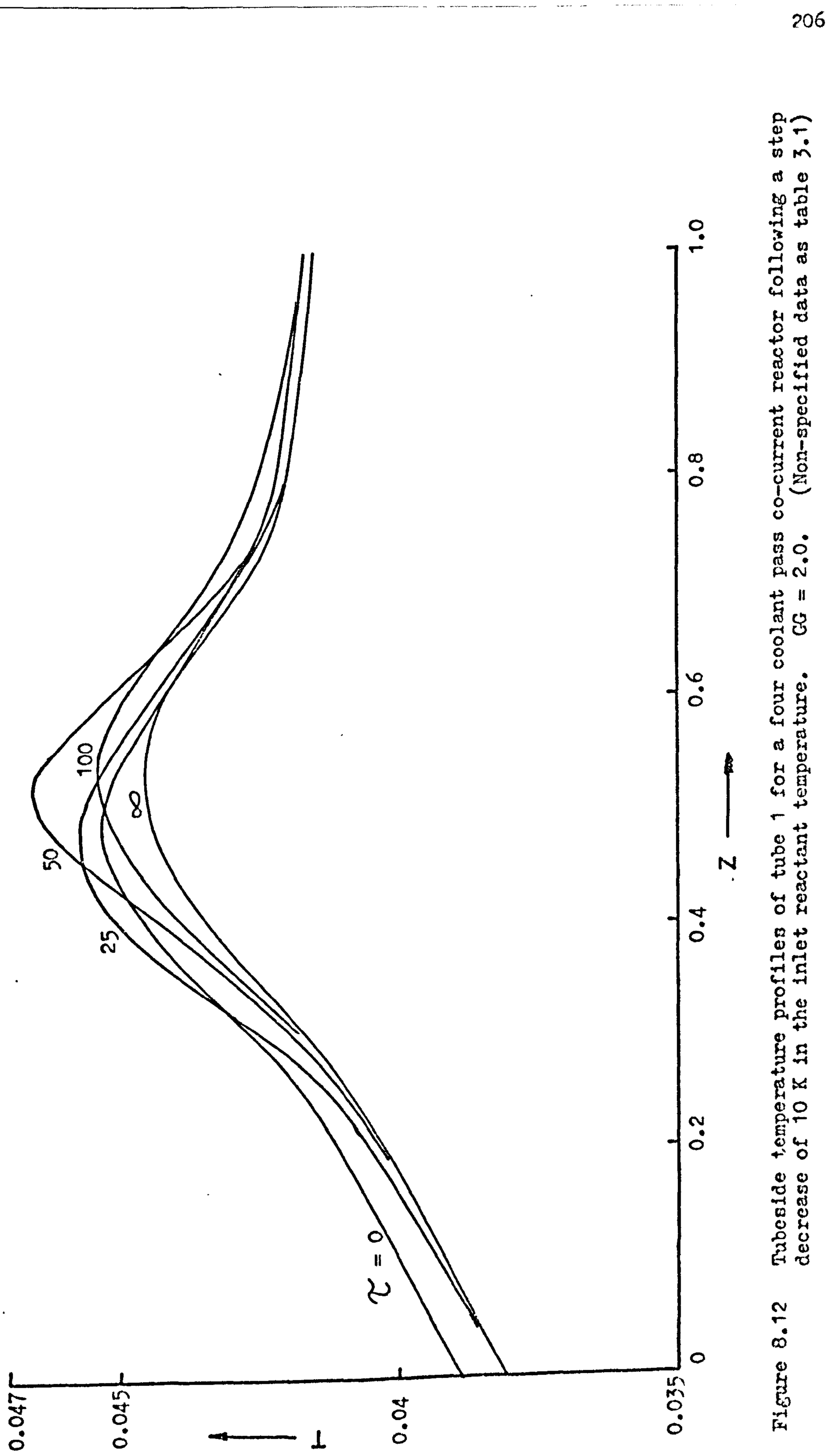

Figure 8.12 Tubeside temperature profiles of tube 1 for a four coolant pass co-current reactor following a step decrease of 10 K in the inlet reactant temperature. GG = 2.0. (Non-specified data as table 3.1)

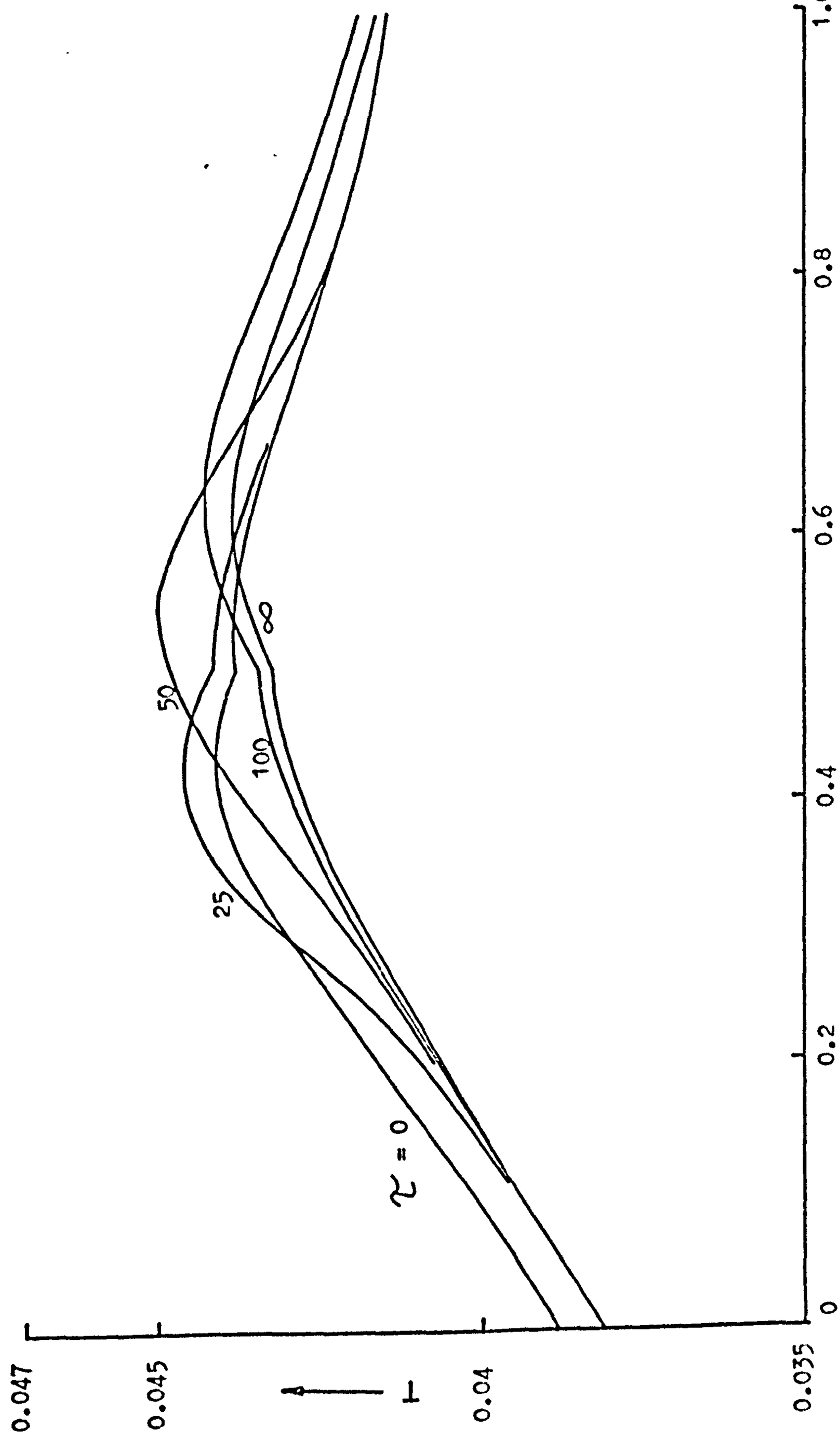

Figure 8.13 Tubeside temperature profiles of tube 50 for the case shown in figure 8.12.

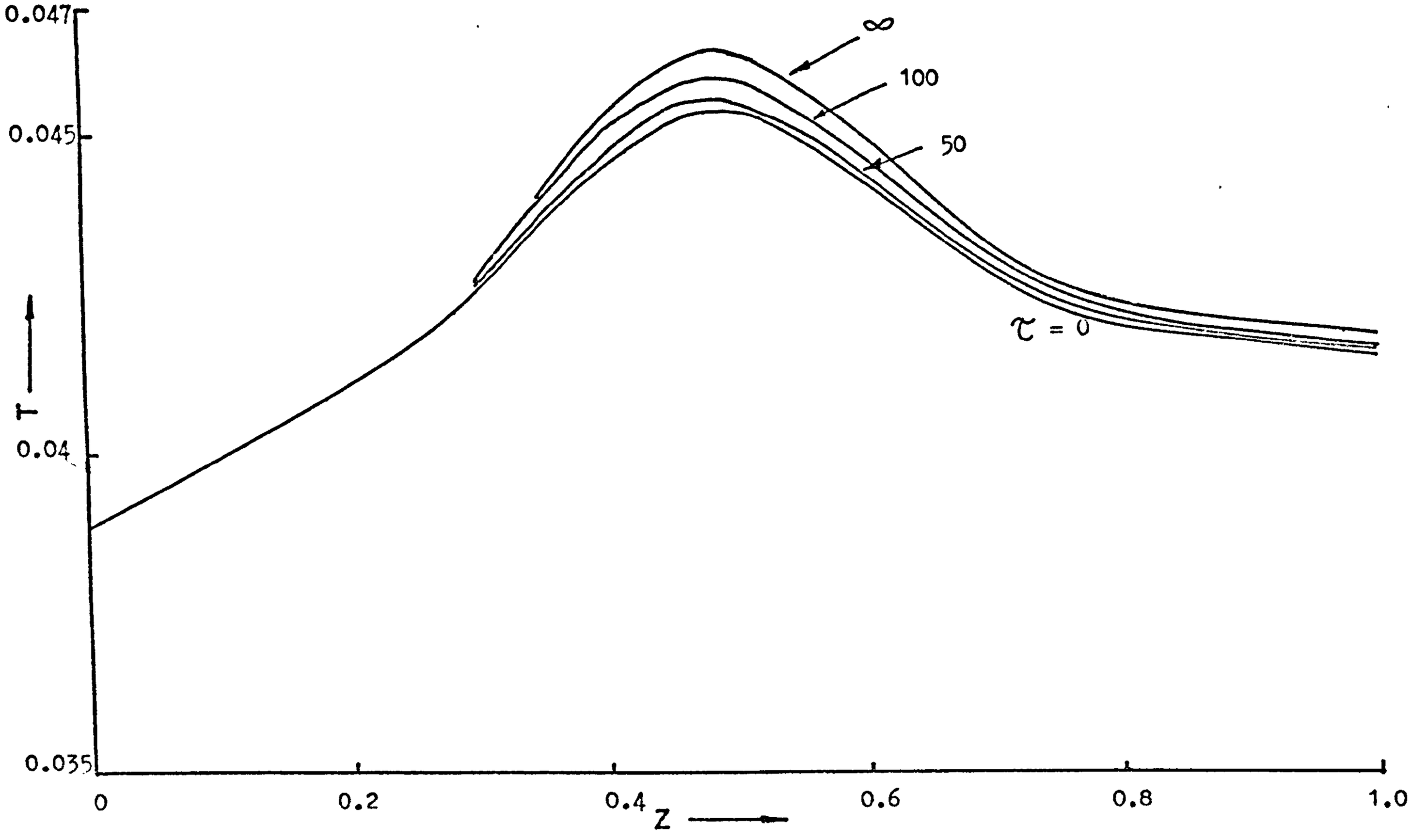

Figure 8.14 Tubeside temperature profiles of tube 1 for a four coolant pass co-current reactor following a step decrease of 25% in the coolant flowrate. Initial value of GG = 2.0. (Non-specified data as table 3.1)

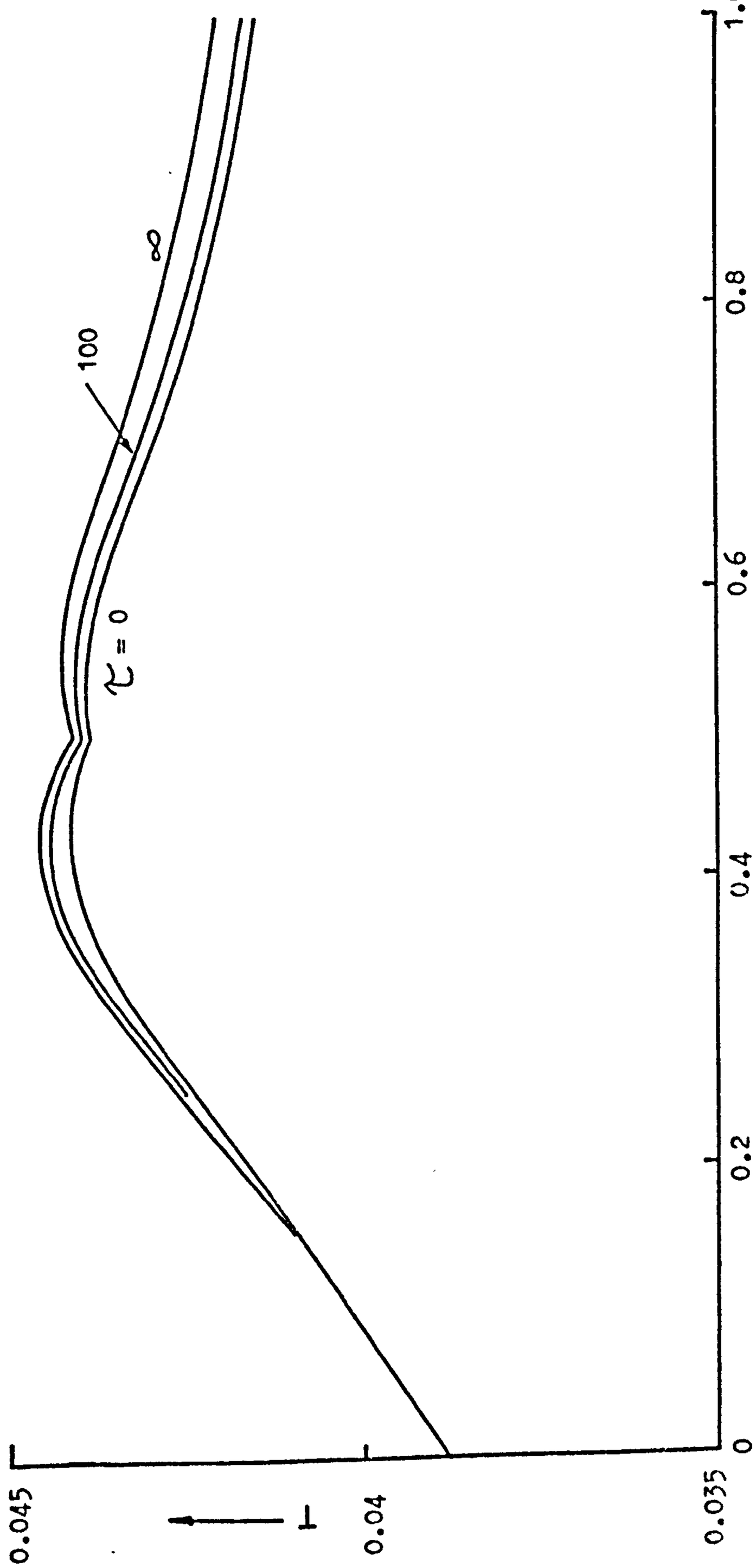

Figure 8.15 Tubeside temperature profiles of tube 50 for the case shown in figure 8.14.

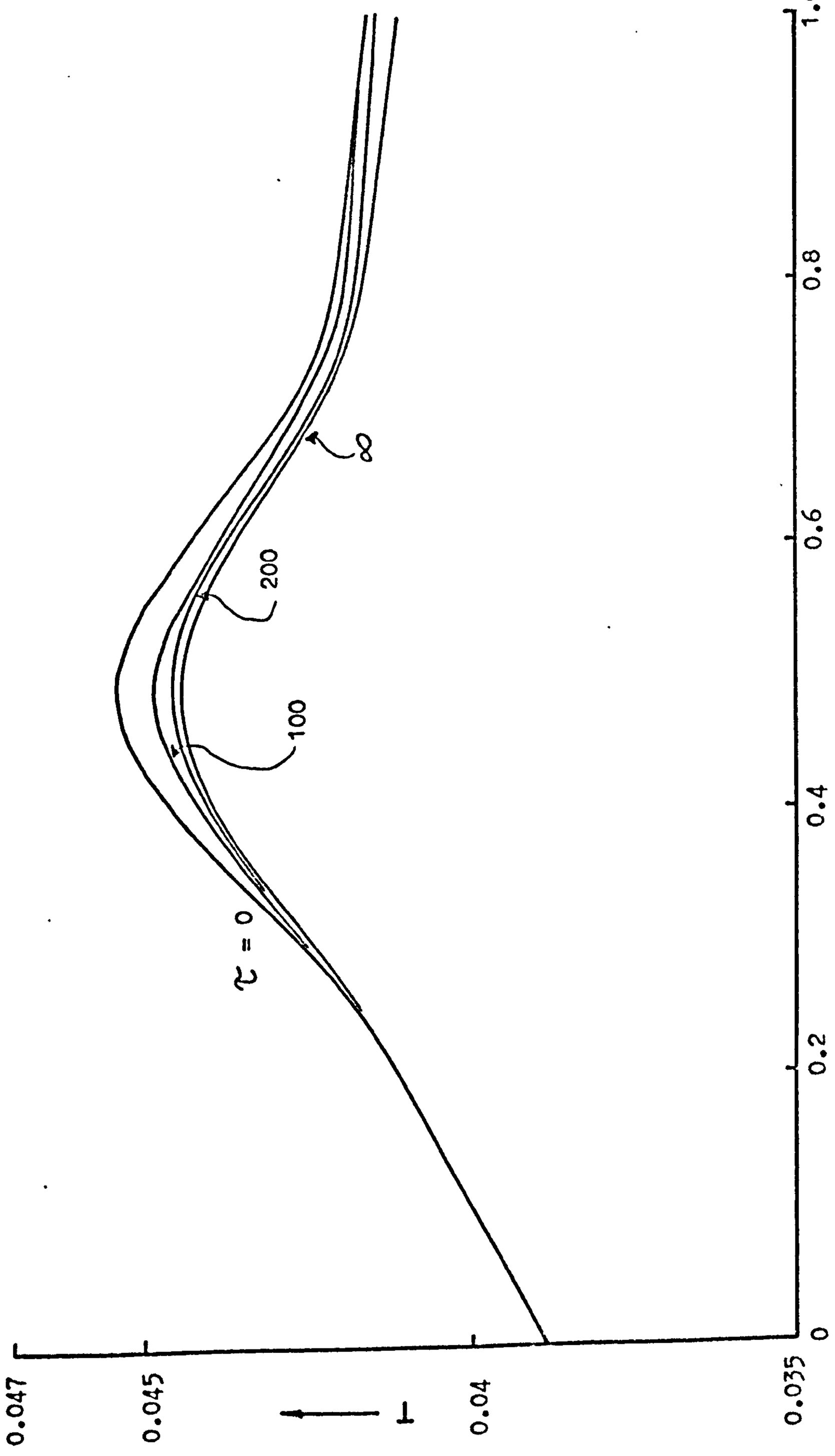

Figure 8.16 Tubeside temperature profiles of tube 1 for a four coolant pass co-current reactor following a step increase of 50% in the coolant flowrate. Initial value of GG = 2.0. (Non-specified data as table 3.1)

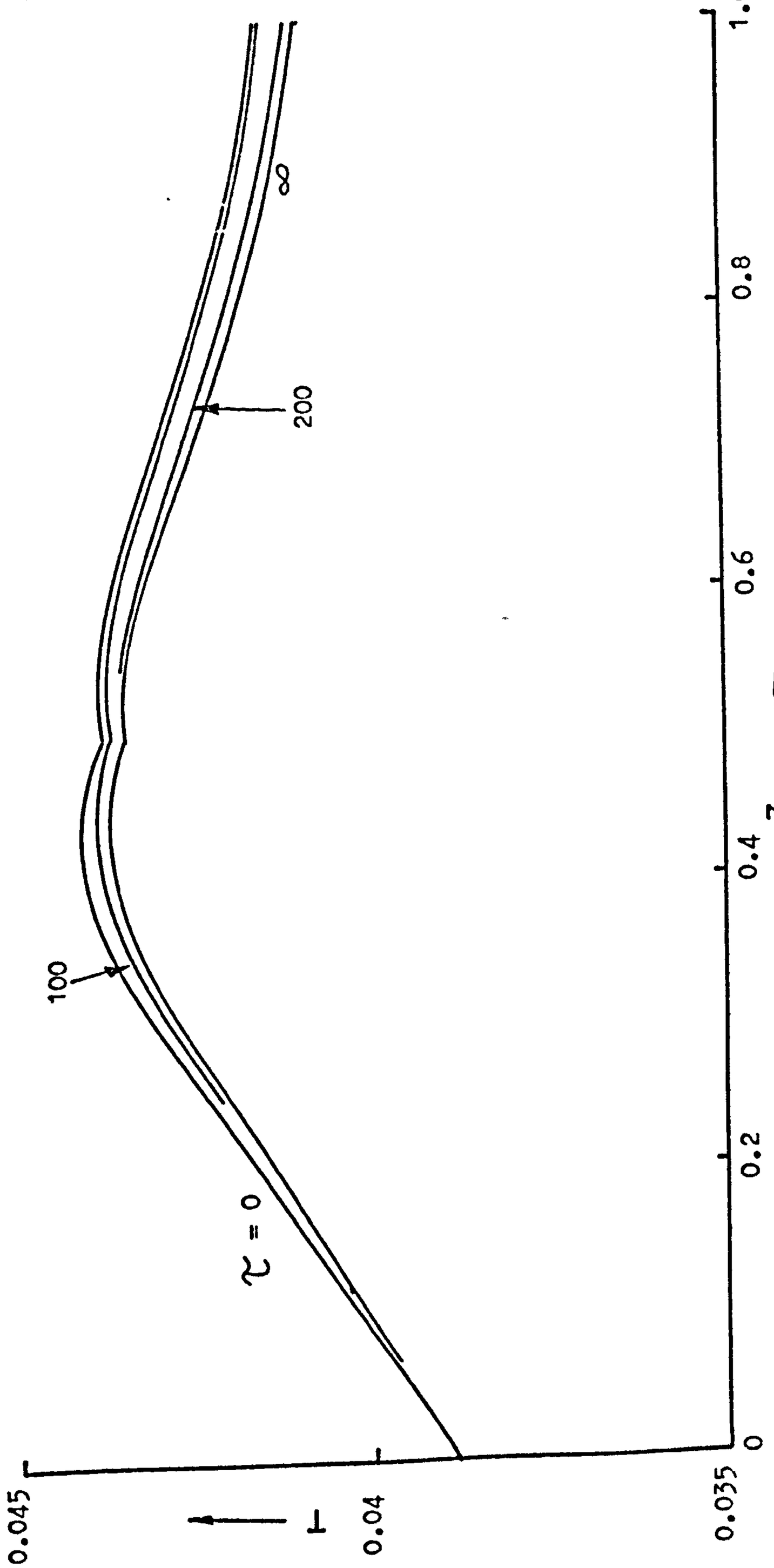

Figure 8.17 Tubeside temperature profiles of tube 50 for the case shown in figure 8.16.

from one steady state to the next and show no real anomolies. A 50% step increase in flowrate, shown in figures 8.16 and 8.17, is also well behaved in the transient response, and as in the coolant flowrate decrease case, attain the final steady state profiles after approximately 300 seconds. The effects of coolant flowrate variations in regions of practical operating conditions are so small that even periodic disturbances, such as a sine wave with an amplitude of 25% and frequency of 0.01 Hz, leaves very little noticeable impression on either the tubeside temperature profiles, concentrations or coolant temperatures. This behaviour is, however, to be expected when the results of chapter seven are considered. For co-current reactors the 'stability' and 'conversion' lines of the $T_{c_{in}}$ vs. GG plots, for example figure 7.7, are only slightly dependant upon the coolant flowrate (the parameter GG) when the flowrate is high enough to give stable operation for the inlet temperatures used here.

8.2.3 The Frequency Response of the Reactor

Although step changes in the inlet variables lead to easily interpreted results, actual disturbances on the plant often occur in a periodic manner. This section considers the simplest periodic distrubance (a sine wave) applied to the inlet coolant temperature. Figures 8.18 and 8.19 give the tubeside and coolant temperatures, plus the outlet fraction of reactant remaining for tube 1 after a sinusoidal disturbance in the coolant inlet temperature of amplitude 10 K and frequency 0.01 Hz. The remaining data is for a four coolant pass reactor with a coolant velocity of U_c = 0.25 m/sec and the information of table 3.1. The plot of tubeside temperatures at various positions versus time shows how the sinusoidal disturbance in the coolant affects the reaction. As the coolant inlet temperature begins to rise, the reaction in tube 1 pass 1 increases, hence the tubeside temperature at z = 0.2 increases. However, because of this increased reaction in the

Figure 8.18 Tubeside temperature variations, at various axial positions in tube 1, during the frequency response to a sinusoidal disturbance, of amplitude 10 K and frequency 0.01 Hz, in the inlet coolant temperature to a four coolant pass reactor. GG = 5.0. (Non-specified data as table 3.1)

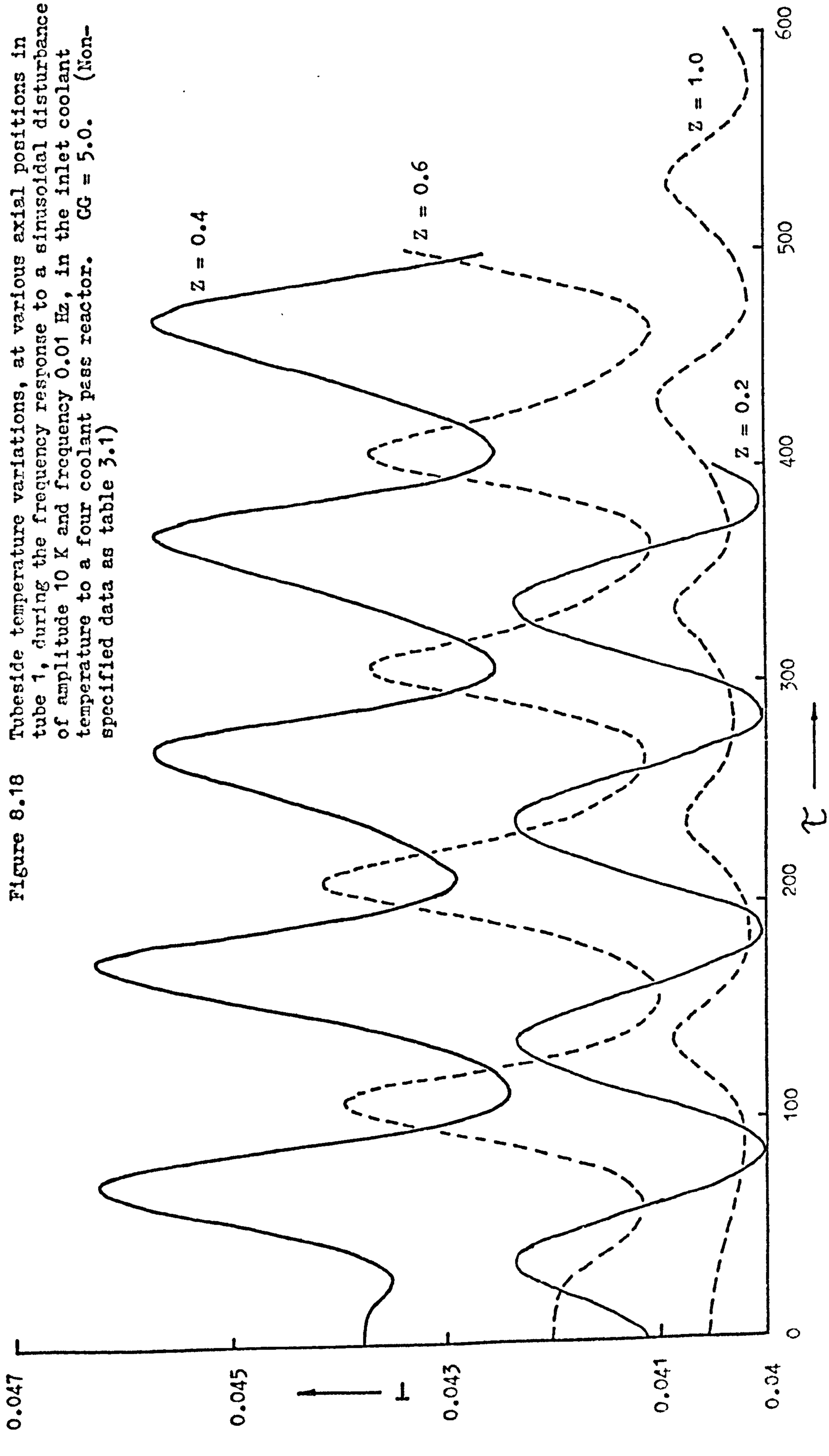

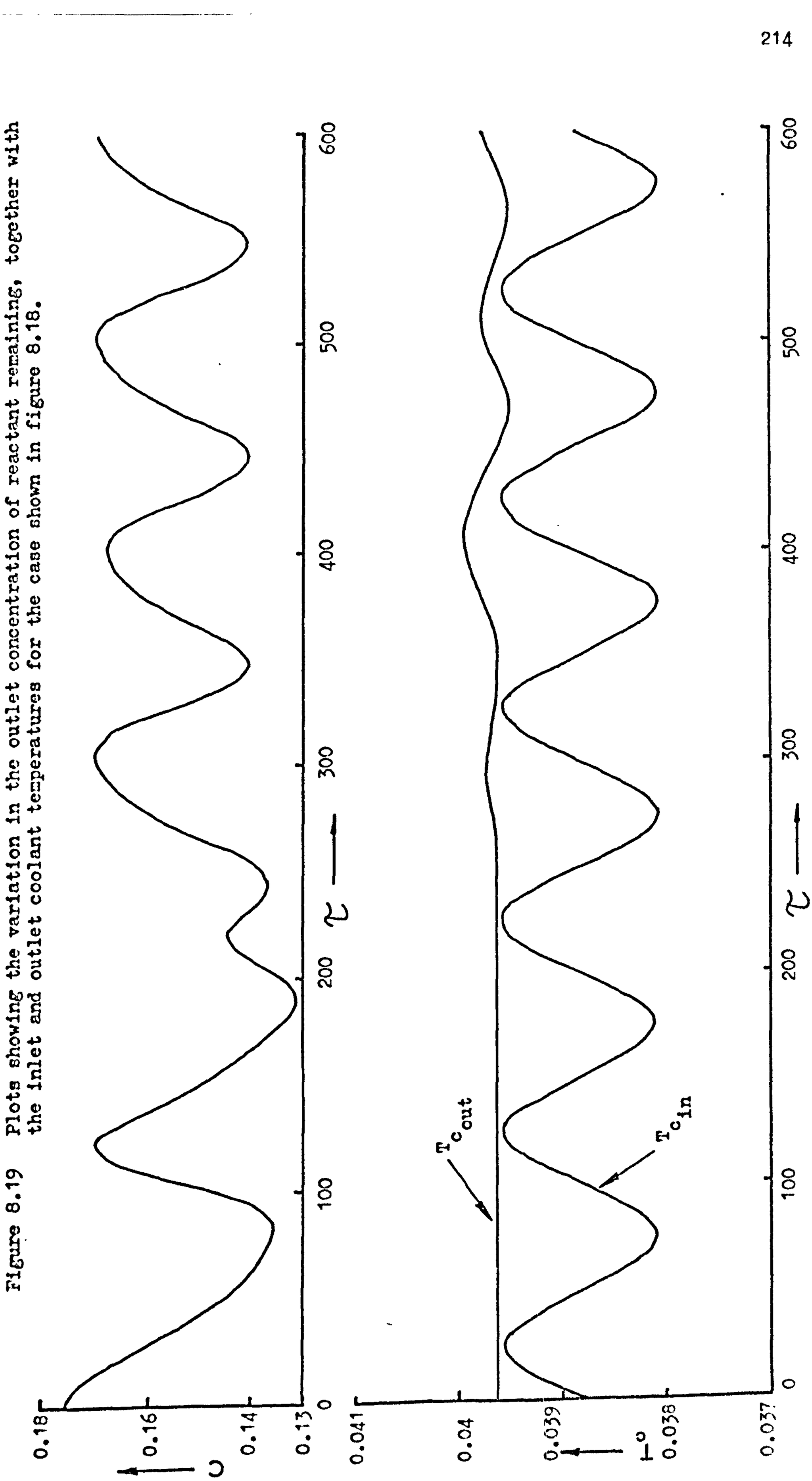

Figure 8.19 Plots showing the variation in the outlet concentration of reactant remaining, together with the inlet and outlet coolant temperatures for the case shown in figure 8.18.

initial part of the bed, less reactant enters subsequent regions and so the reaction, and hence the temperature, decreases. As a result the tubeside temperatures at z = 0.4, z = 0.6 and z = 1.0 begin to fall. After an initial transient period, during which quite high tubeside temperatures are experienced, the system settles down to an oscillatory pseudo-steady state after approximately 500 seconds. An interesting result of the tubeside behaviour is that the fraction of reactant remaining is always less than that of the initial steady state. Hence, for these conditions, better conversions are obtained when the reactor is operated with a sinusoidally varying coolant inlet temperature. The plot of coolant temperature versus time (figure 8.19) gives the inlet perturbation and the outlet temperature. The disturbance takes approximately 250 seconds to make itself noticed in the outlet temperature, and then it appears with a small phase difference and a reduced amplitude. The phase difference between the tubeside temperature and the inlet coolant disturbance varies with the position in the tube. For position z = 0.2, see figure 8.18, the maximum and minimum temperatures occur slightly after those of the inlet coolant temperature. This phase lag is due to the heat capacitances of the catalyst packing and reactor fittings.

Figure 8.20 shows the same plots as above for an identical system disturbed by a sine wave in the coolant inlet temperature of amplitude 10 K and frequency 0.02 Hz. This case is particularly interesting as the disturbance is completely attenuated. The outlet coolant temperature (not shown) is unchanged for a period of over 600 seconds. Overall, the effects on the tubeside are similar to those reported for the lower frequency disturbance, the improved conversion due to the cyclic temperature changes also being present. Unfortunately, the large amount of computation time necessary to follow the frequency response means that it is only feasible to carry out an initial survey.

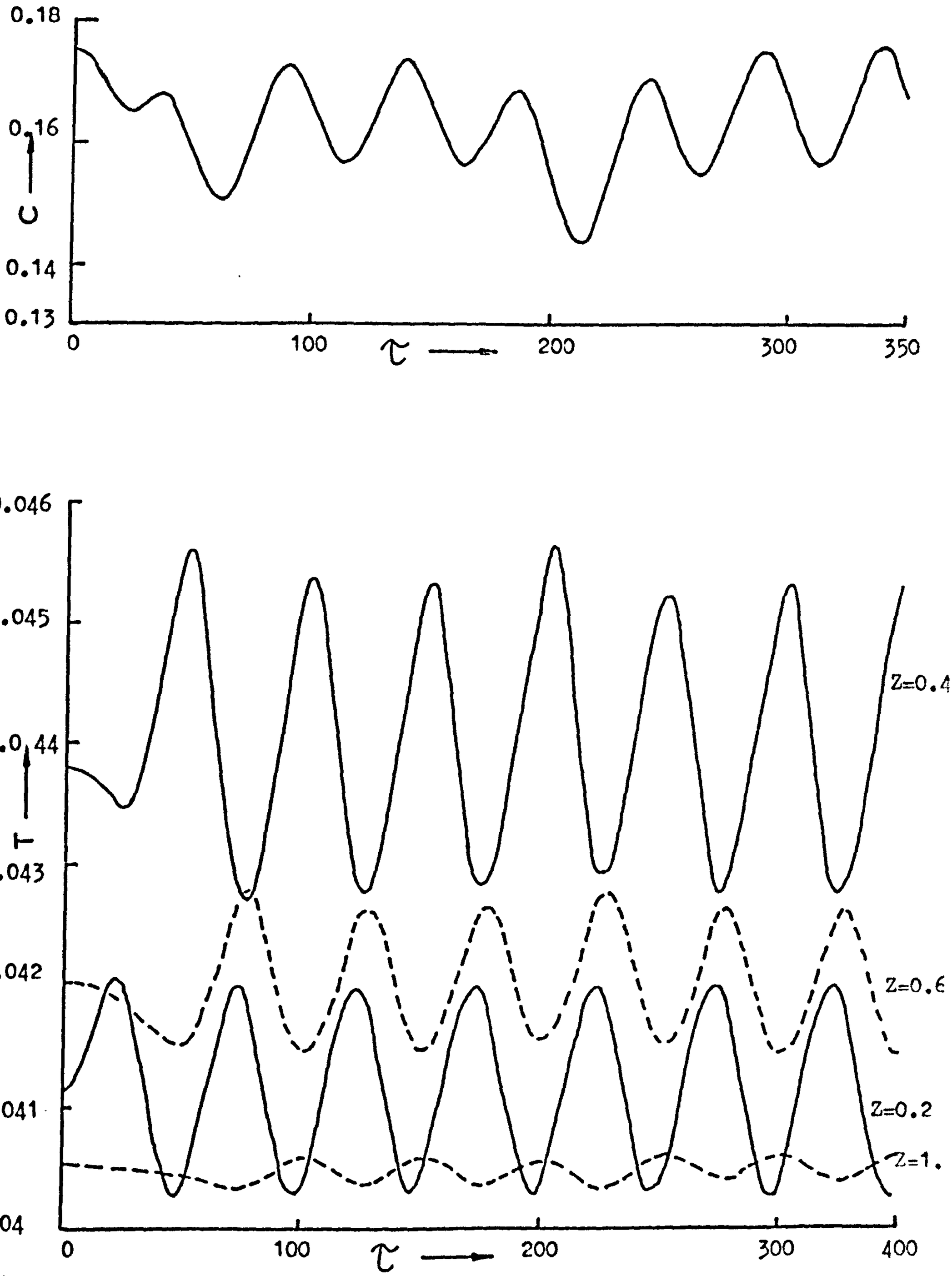

Figure 8.20 Variations in tubeside temperature and outlet concentration of reactant remaining at various axial positions in tube 1 during the frequency response to a sinusoidal disturbance of amplitude 10 K and frequency 0.02 Hz in the inlet coolant temperature to a four coolant pass reactor. GG = 5.0. (Non-specified data as table 3.1)

However, it can be seen that the initial transient response reveals significantly different effects from the final pseudo-steady state and that for simulation studies, especially in relation to control system design, such regions of reactor operation obviously require special study.

8.3 Counter-Current Cooling

8.3.1 Formulation of the Equations

The formulation of a dynamic, counter-currently cooled reactor model is not as straight-forward as that of the co-current model introduced in the last section. This arises from the relative directions of the coolant and reactant flows. Consider solving the reacto_ problem in the same way as the steady state mixing cell model, evaluating the coolant temperatures from the coolant outlet to the inlet by the use of an estimated outlet temperature. Unfortunately, under transient conditions, a perturbation, say in the coolant inlet temperature, would not result immediately in a change in the outlet temperature. Hence, if the model is solved from outlet to inlet, there is great difficulty in accounting for perturbations at the inlet, the same outlet temperature being obtained even though the inlet temperature is changed. Clearly then, a different approach must be adopted. The equations must be solved in the direction of the coolant flow, by a method similar to that used for the counter-current continuum model of chapter six. The heat balance used for the co-current model (equation (8.5)) applies for each coolant pass, and appropriately guessed values of coolant temperature are iterated upon until a final solution is obtained.

Figure 8.21 illustrates the technique for a two coolant pass system. First, the initial steady state of the system is evaluated, as this forms a convenient starting point for the transient calculation. The simplest method of obtaining it is to set the time derivative to zero

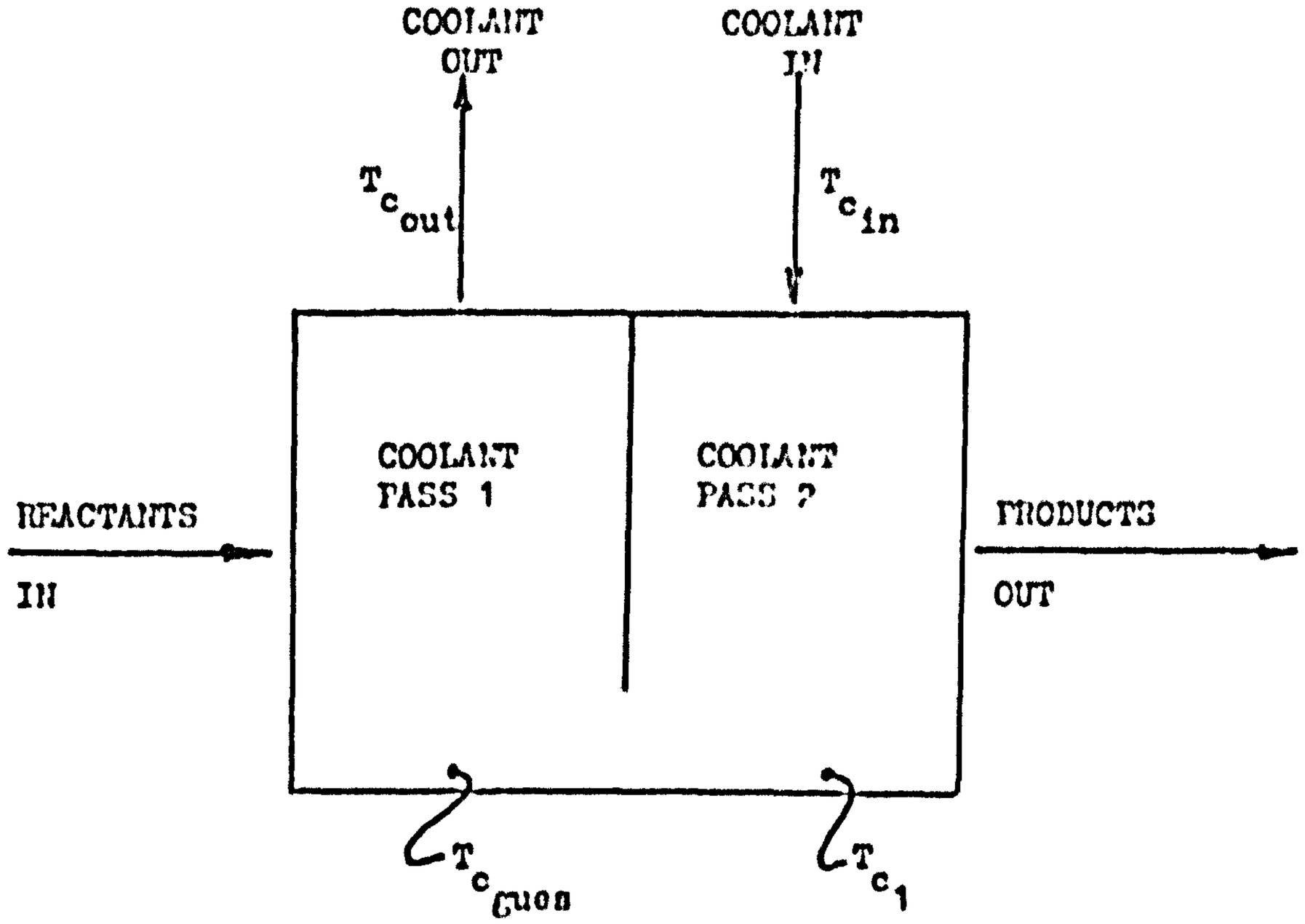

Figure 8.21 Schematic diagram used to demonstrate the method of solution of the counter-current transient reactor model.

in equation (8.5) and use the steady state tubeside equations of Appendix B. The equations are solved assuming the inlet coolant temperature to coolant pass 1, $T_{c_{gues}}$, then, solving the coolant and tubeside equations by marching through the tube bundle, the first approximation to the coolant outlet temperature, $T_{c_{out}}$, can be made. Next, using the known coolant inlet temperature and the stored tubeside conditions entering coolant pass 2, the coolant temperature leaving pass 2, T_{c_1}, can be obtained after evaluating the equations for this pass. If T_{c_1} is equal to $T_{c_{gues}}$ within given limits, the calculation is complete and the profiles are then stored for use in the transient period. If they are not in agreement, a new value of $T_{c_{gues}}$ is assumed and the procedure repeated. The transient period following a disturbance is studied in exactly the same way, except that the transient coolant heat balance, equation (8.5), and the dynamic tubeside model are used instead of the steady state equations. Also, because of the time delay in the coolant circuit caused by the turnround region, the temperature leaving coolant pass 2 must be modified by the use of equation (8.3) before it is compared with the coolant temperature entering pass 1. A detailed description of the solution of the counter-current problem can be found in Appendix I.

Reactors having more than two coolant passes can be represented in a similar manner. For example, a three coolant pass system requires two coolant temperatures to be assumed, these being the inlets to coolant passes one and two. Iteration in this case is nested, the first two coolant passes being converged initially and then by iterating around the last pass the final solution obtained. A four coolant pass reactor requires three assumed temperatures and hence a three nested iterative calculation. Obviously, the computational requirements increase dramatically as more coolant passes are considered.

Because of the need for iteration around the coolant temperature

in the counter-current reactor, computation times are much greater than those for a corresponding co-current simulation. For example, a two coolant pass reactor, counter-currently cooled requires approximately 400 seconds on the CDC 7600 computer for 40 seconds of actual plant time. Since computer time on such a large machine is expensive, a complete survey of operating conditions is obviously impossible, and as a four coolant pass reactor (as used for the co-current simulation) would require larger computation times than a two or three pass, the latter have been adopted in this survey.

The effect of the lumping of tubes approximation, described by equation (8.4), is shown in figures 8.22 and 8.23. These tubeside temperature profiles of tubes 1 and 50 respectively correspond to a 10 K decrease in the coolant inlet temperature for a two coolant pass reactor under the conditions of table 3.1 and with N = 6. The detailed model for exactly the same case is shown in figures 8.24 and 8.25. Clearly, as in the co-current reactor simulations, this approximation is not valid and the detailed cell model must be used in any meaningful study of the system.

8.3.2 The Transient Response of the Reactor

The effect of a step decrease in the inlet coolant temperature has been demonstrated for a two coolant pass reactor in figures 8.24 and 8.25. Unlike the co-current system there is no increased tubeside temperature during the initial transient response, the profiles fall gradually from one steady state to the next. This behaviour, which also applies to a three coolant pass reactor (figure 8.26) is to be expected. The tubeside temperature rises experienced in co-current reactors are the result of decreased reaction rates in the inlet sections of the tubes causing higher reactant concentrations in regions of high coolant and catalyst temperature. In the counter-current case this

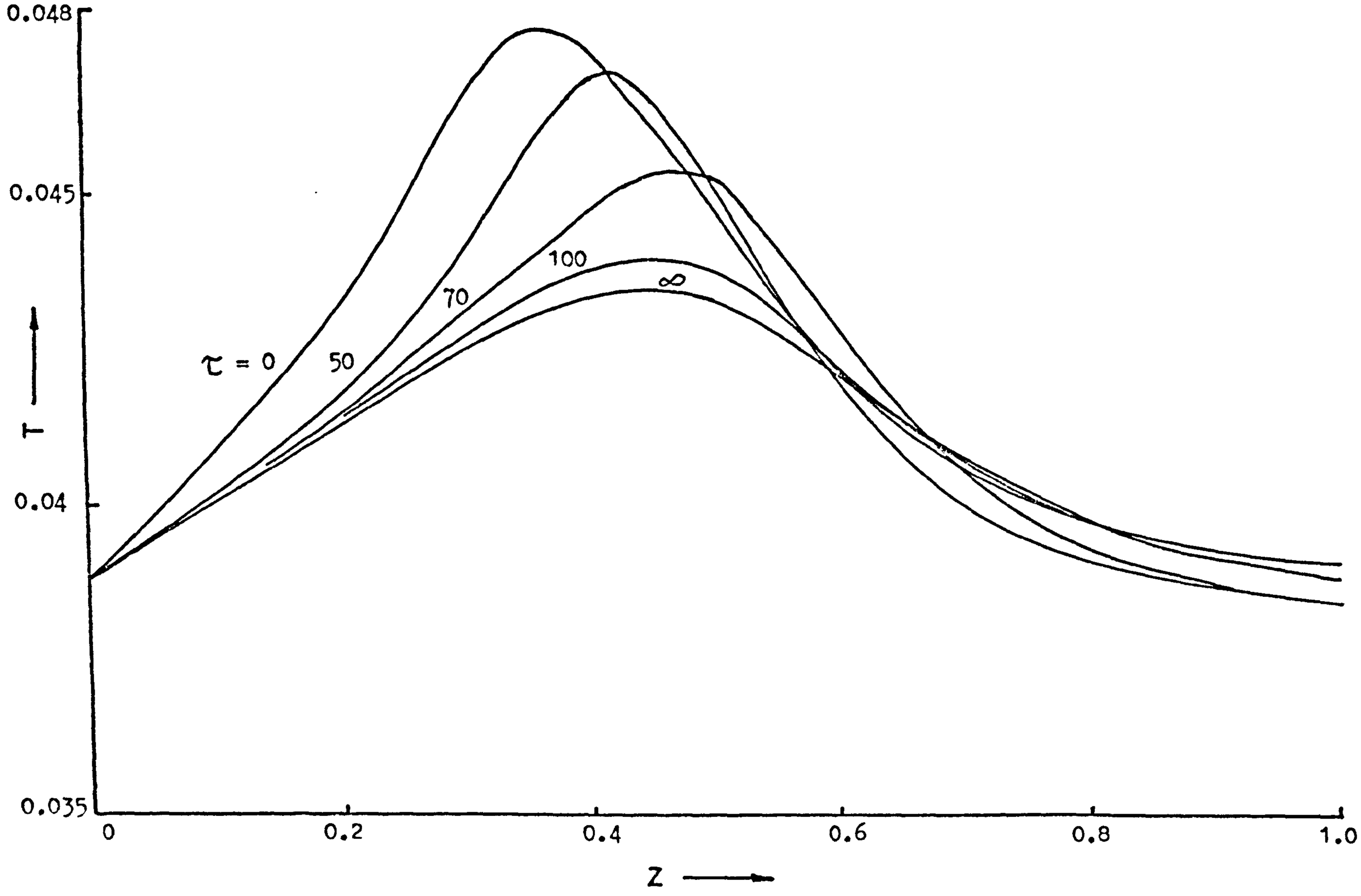

Figure 8.22 Tubeside temperature profiles of tube 1 for a two coolant pass counter-current reactor following a step decrease of 10 K in the coolant inlet temperature. The lumping of tubes assumption has been used with N = 6. GG = 5.0. (Non-specified data as table 3.1)

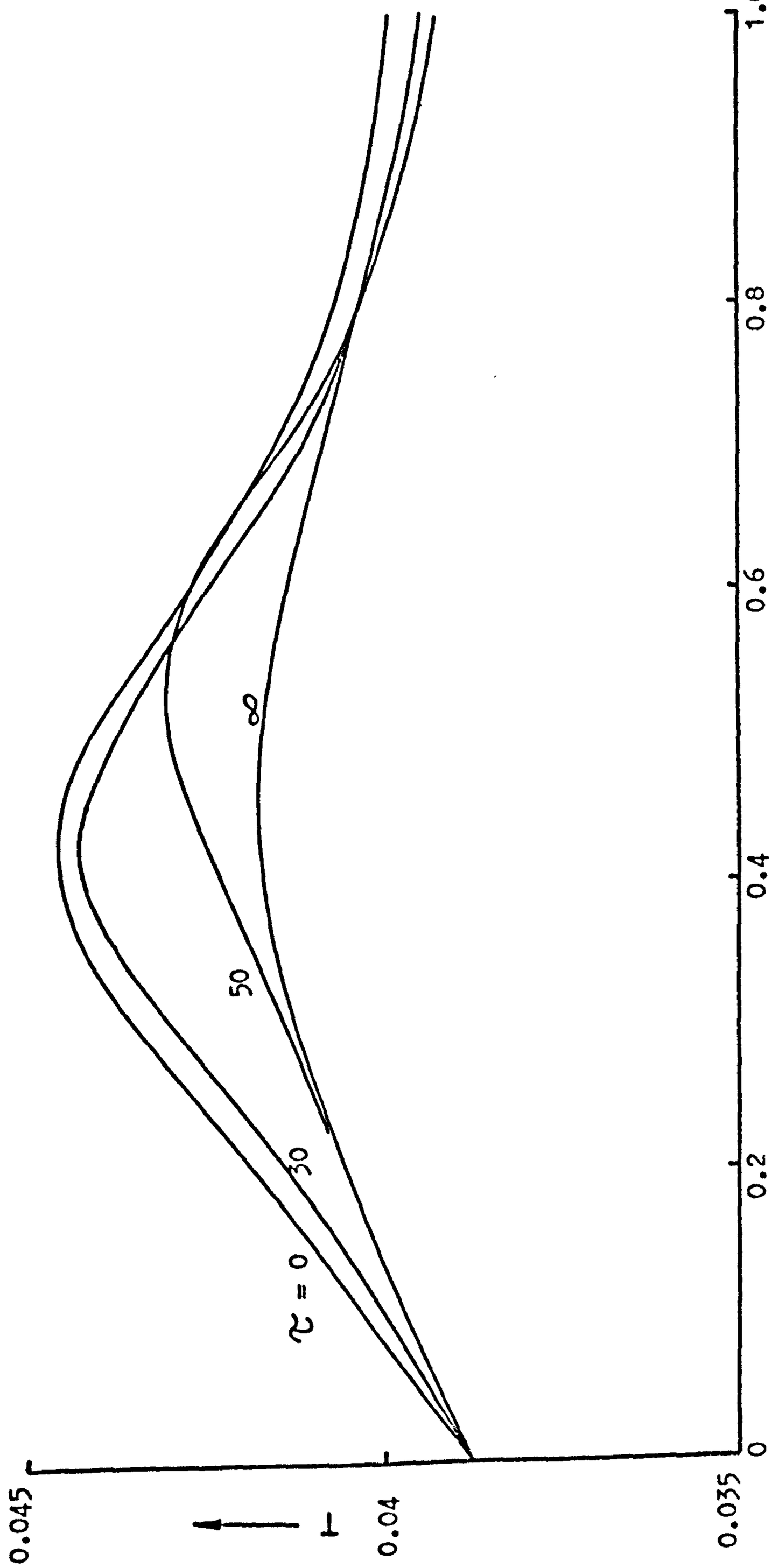

Figure 8.23 Tubeside temperature profiles of tube 50 for the case shown in figure 8.22.

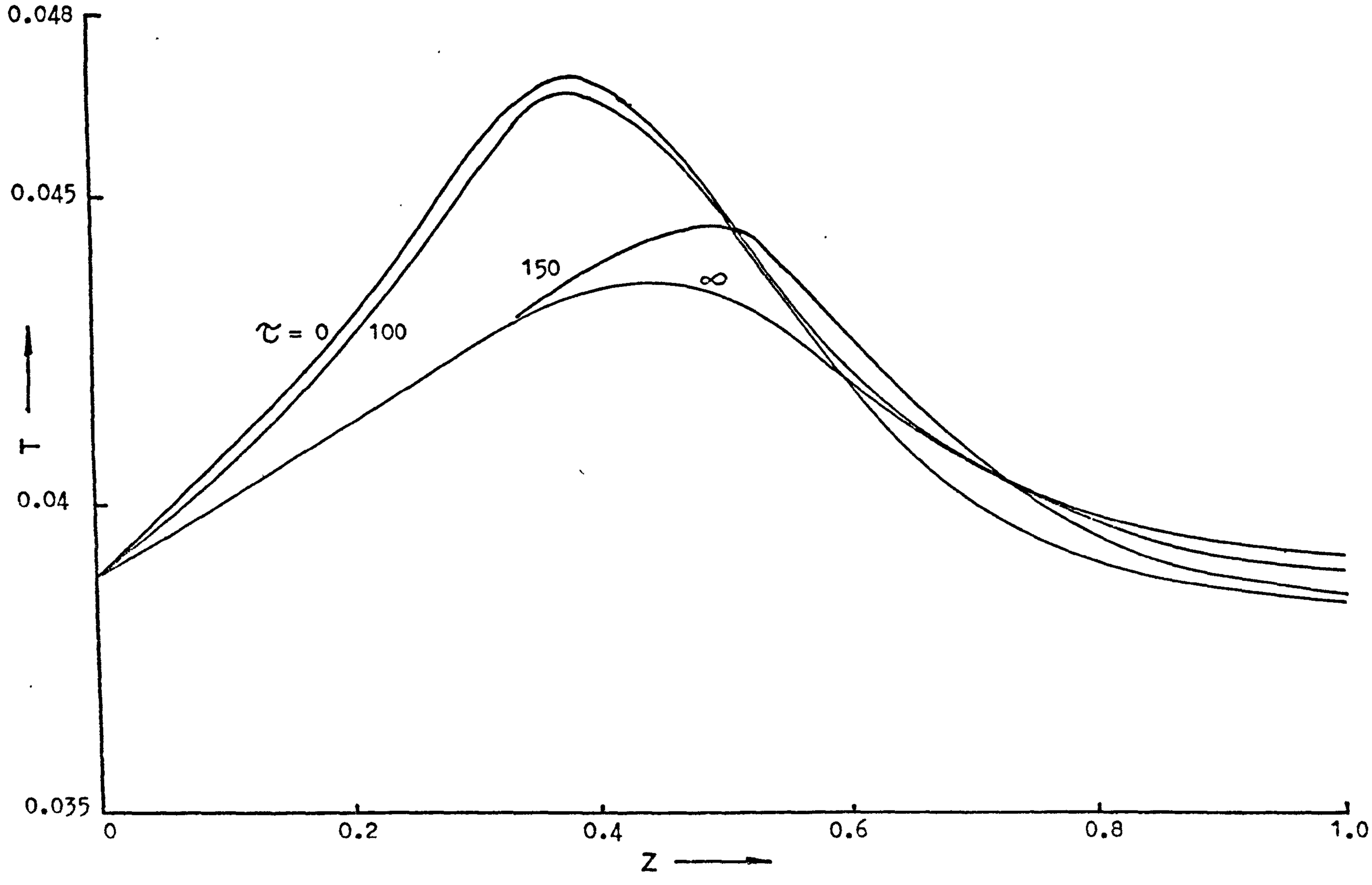

Figure 8.24 Tubeside temperature profiles of tube 1 for a two coolant pass counter-current reactor following a step decrease of 10 K in the coolant inlet temperature. GG = 5.0. (Non-specified data as table 3.1)

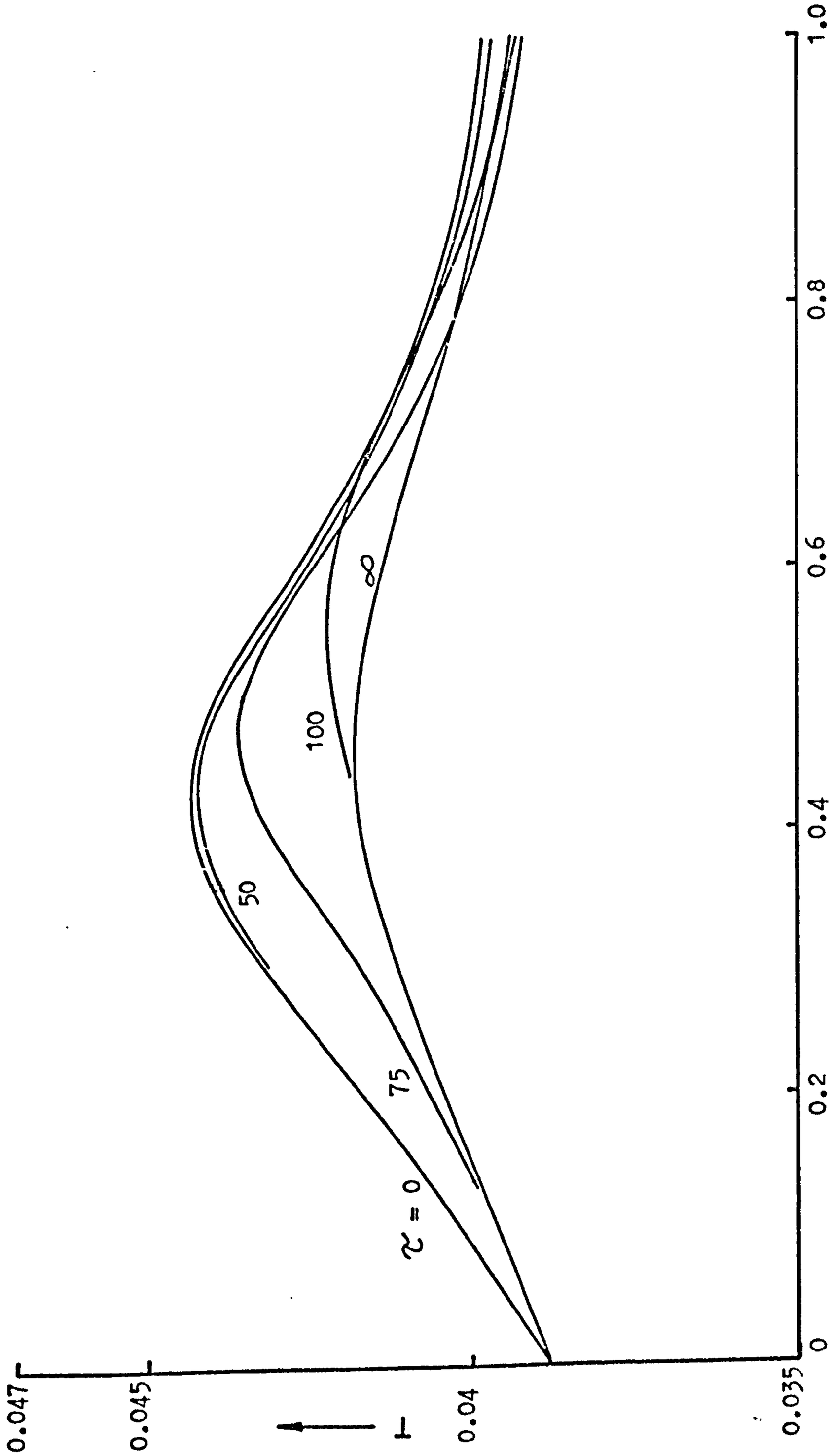

Figure 8.25 Tube beside temperature profiles of tube 50 for the case shown in figure 6.24.

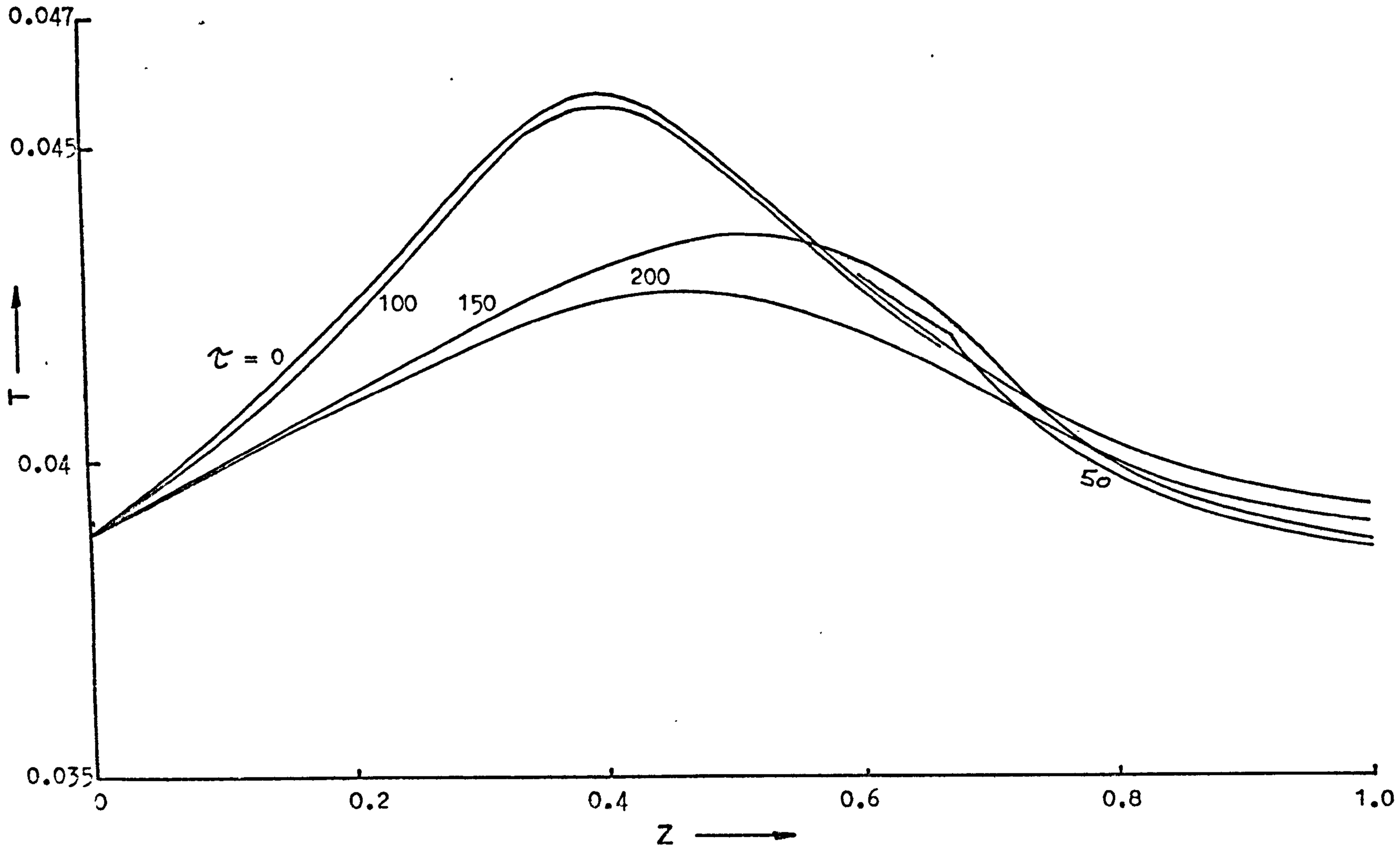

Figure 8.26 Tubeside temperature profiles of tube 1 for a three coolant pass counter-current reactor following a step decrease of 10 K in the coolant inlet temperature. GG = 5.0. (Non-specified data as table 3.1)

cannot occur, the colder coolant does not affect the inlet rate of reaction until after it has decreased the reaction rate (and hence catalyst temperature) further down the tubes. Hence, the counter-currently cooled reactor is not subject to the dangers of co-current systems during coolant temperature changes.

Figures 8.27 and 8.28 show the tubeside temperature profiles for tubes 1 and 50 following a step decrease of 10 K in the inlet reactant temperature to a three coolant pass reactor (data as table 3.1). As in the co-current simulations, this action leads to increased hotspot temperatures during the initial transient response. The tubeside temperature profiles then gradually decrease to their final steady state after approximately 200 seconds.

The final response to be considered is shown in figures 8.29 and 8.30. Here, a step decrease is applied to the mass flowrate of coolant to the system, causing the value of GG to fall from 5.0 to 4.0. Again the transient period results in the gradual increase of the tubeside temperature profiles from the initial to the final steady state. Thus, as in the co-current reactor, variations in the coolant flowrate do not lead to unstable operation unless the steady state profiles are themselves unstable.

8.4 Concluding Remarks

Dynamic models of both the co- and counter-current reactors have been developed using the mixing cell approximation to represent the shell-side heat balance. Attempts to simplify the equations, by the application of the lumping of tubes assumption used in chapter four, were unsatisfactory and the detailed cell model has to be used to ensure that an adequate representation of the system is given. As a result, the very large computation times necessary, especially for the counter-current model, have meant that only a limited survey of the transient

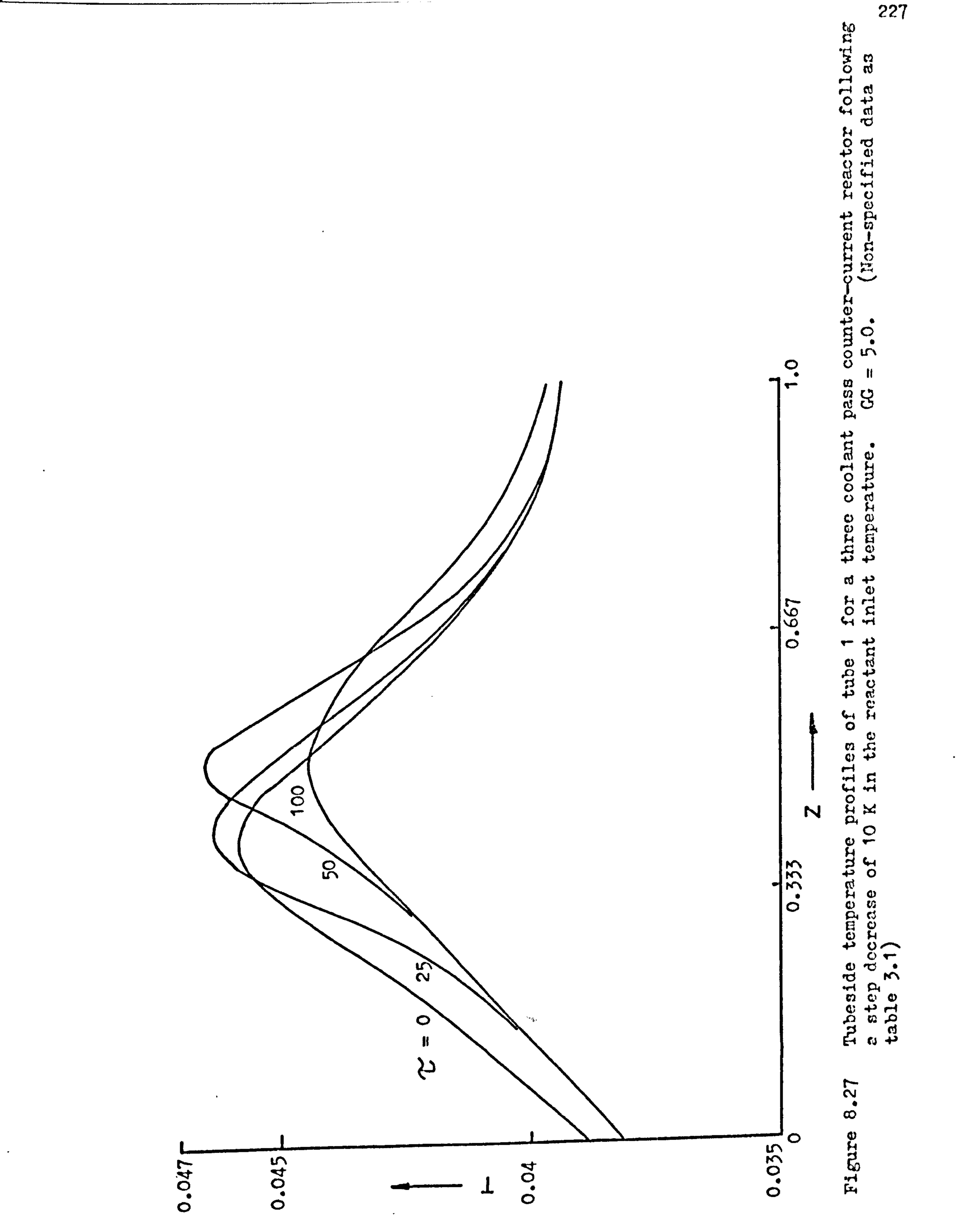

Figure 8.27 Tubeside temperature profiles of tube 1 for a three coolant pass counter-current reactor following a step decrease of 10 K in the reactant inlet temperature. GG = 5.0. (Non-specified data as table 3.1)

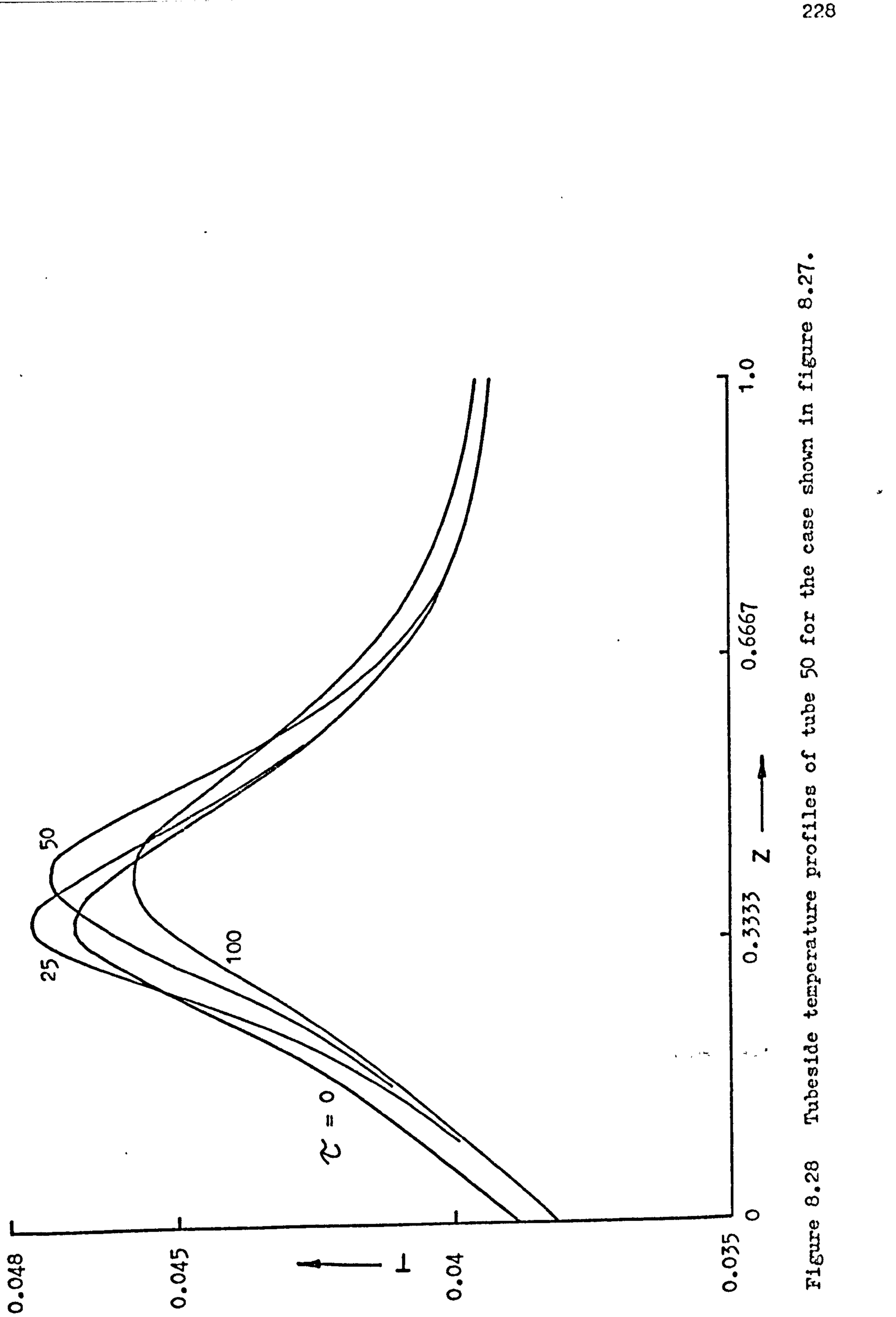

Figure 8.28 Tubeside temperature profiles of tube 50 for the case shown in figure 8.27.

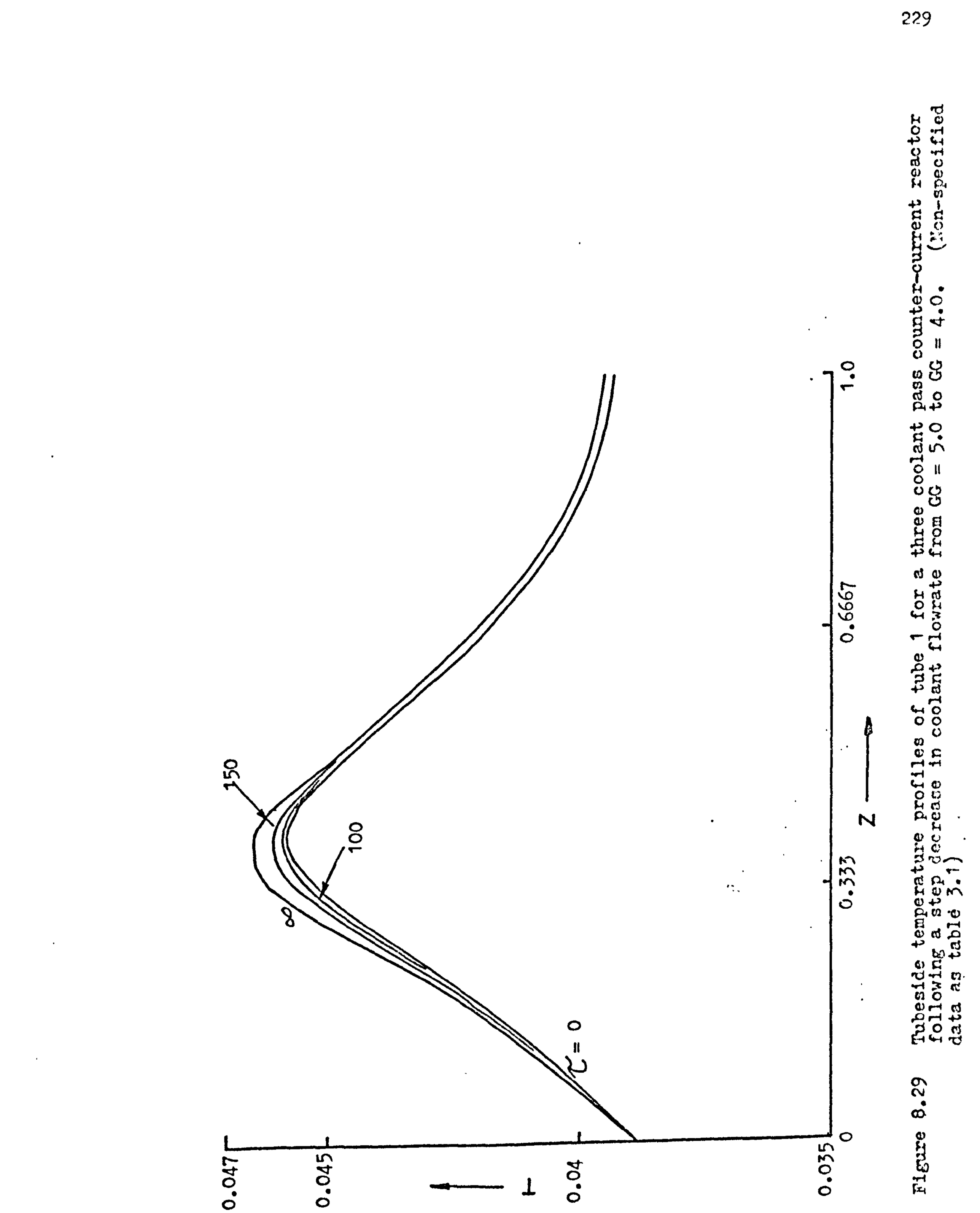

Figure 8.29 Tubeside temperature profiles of tube 1 for a three coolant pass counter-current reactor following a step decrease in coolant flowrate from GG = 5.0 to GG = 4.0. (Non-specified data as table 3.1)

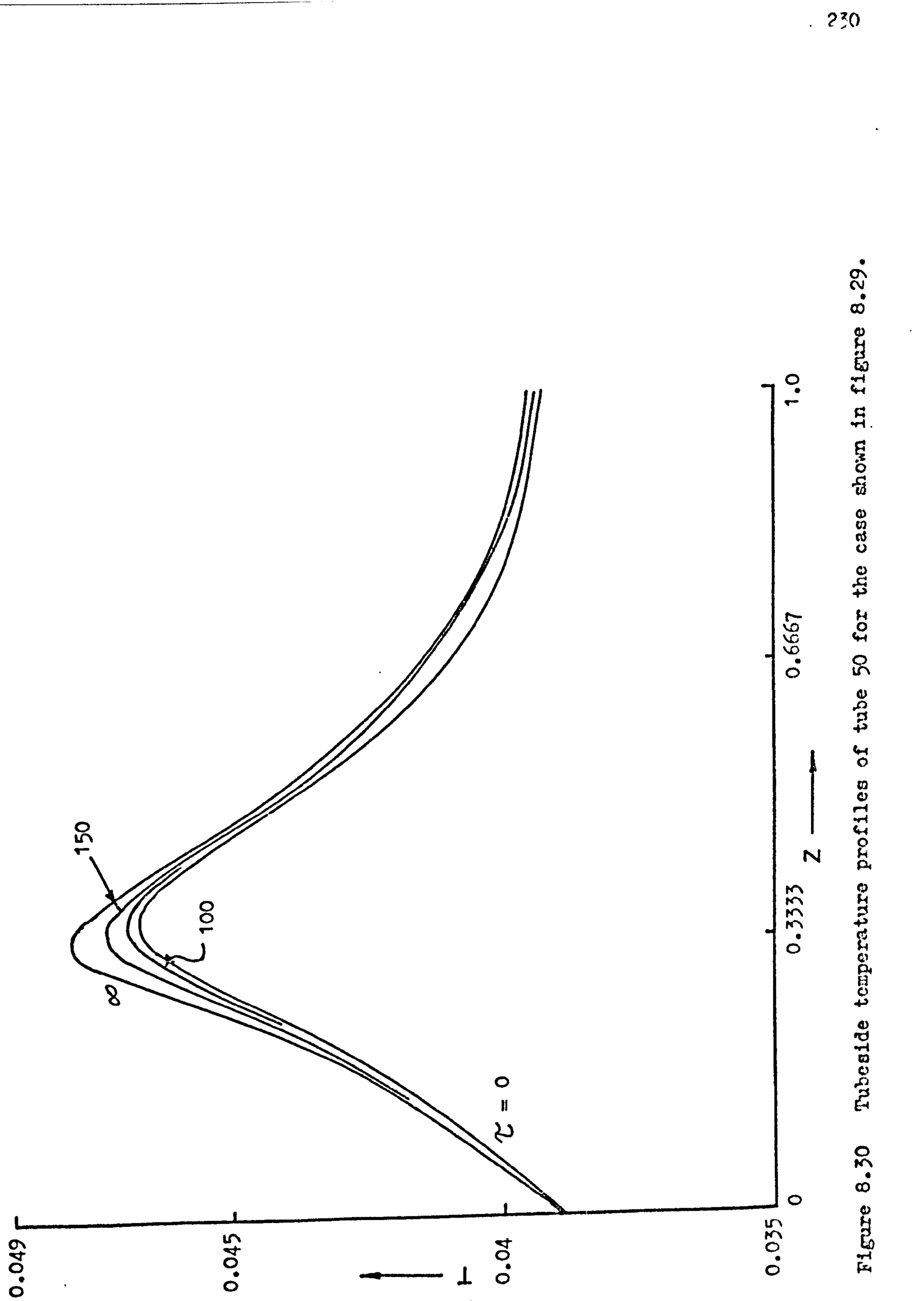

Figure 8.30 Tubeside temperature profiles of tube 50 for the case shown in figure 8.29.

behaviour has been possible.

The transient response of a co-currently cooled reactor following step decreases in either the inlet reactant or coolant temperatures caused increased tubeside temperature peaks during the initial transient period. The counter-current reactor, while behaving similarly for step decreases in reactant temperature, gave only decreasing tubeside temperature profiles for step decreases in inlet coolant temperature. Thus, it would appear that counter-current reactors can give more acceptable behaviour than co-current systems when coolant temperature control is difficult.

The study of the frequency response of the co-current reactor has revealed one aspect of dynamic behaviour which is often ignored. This is the importance of the initial transient response. Although the final pseudo-steady state oscillations of the reactor during, say, a sinusoidal disturbance, may be stable, it is possible that undesirable conditions arise before the final state is reached. For example, large peak temperatures can occur for one or more cycles of the perturbation, and the resulting temperature runaway may cause catalyst deactivation etc. preventing the final pseudo-steady state being achieved.

Clearly, further investigation of the system is necessary. In general the behaviour of a multitubular reactor is controlled by a combination of chemical and thermal effects, the relative magnitudes of which may change considerably with time and position. Hence, the dynamic responses are not easily predicted without extensive simulation. For such studies therefore a reduced model, possibly developed using an effectiveness factor type approximation to represent the tubeside heat generation, is essential. The excessive computation times needed for the detailed cell model excluding all but the most limited surveys.

It would also be desirable to obtain a relationship between the

forcing amplitude and frequency of the oscillation to enable a priori prediction of temperature runaway, both transient and permanent. However, the results described here demonstrate the highly non-linear nature of the reactor and the complexity of the interactions between the important phenomena. It seems likely therefore that this may preclude a general approach to the problem, requiring a more semi-empirical technique.

Consideration of the dynamic behaviour of multitubular reactor models enables an assessment to be made of the emergency procedures necessary in the event of potentially dangerous situations. Then, the safest and most economic method of averting possible catastrophies can be ascertained without relying upon either intuitive reasoning or dangerous experimentation. For instance, intuitively, an effective method of reducing the magnitude of the temperature hotspots in the tubes would be to reduce the coolant temperature, so decreasing the reaction rate. Unfortunately, this action can lead to increased tubeside temperature peaks during the initial transient response, and so, instead of correcting the situation, reducing the peak temperatures, the reverse occurs and the reactor becomes even more unstable. Clearly, it is important to know, not only the final steady state results of an action, but also the dynamic behaviour leading to that result.

CHAPTER 9

Final Comments

9.1 General Findings of the Present Work

Consideration has been given to various aspects of the operational characteristics of multitubular fixed bed catalytic reactors supporting highly exothermic reactions. In particular, the importance of the distribution of the heat of reaction around the system, arising from the flow pattern of the coolant, has been investigated in relation to the performance and stability of the unit.

In order to establish the complexity of the model needed in a representation of the reactor, three different methods of describing it have been examined. A comparison between these alternative representations, which vary in complexity from a single tube constant coolant temperature model to a multitubular approximation accounting for the interactive nature of the heat transfer around the tube bundle, has shown that, in many important characteristics relevant to the design and stability of these systems, the more complex reactor models are highly desirable, even essential. The single tube approximations to the systems commonly employed can give significantly different predictions under conditions where instabilities are developing owing to the failure to account for the interaction between the tubes in the multitubular bundle. Moreover, there are additional problems relating to reactor configuration to be taken into account, for which the single tube models do not make provision. These problems, such as the number of coolant passes to employ, or the best mass flowrate of coolant, are an intrinsic feature of the more complex multitubular model. Too high a coolant flowrate can cause excessive cooling and, therefore, poor reactant conversion, whereas too low a value leads to severe coolant heating and very high tubeside temperatures which can cause poor selectivity or even

temperature runaway. Even at moderate coolant flowrates the nature of the heat dissipation is such that tubes in different parts of the same bundle may exhibit quite different behaviour so that no single tube is representative of the whole. This means that designs and control strategies based only on single tube models could be inappropriate, and so the use of a multitubular model for these purposes is clearly essential.

Recognizing the necessity of including the coolant heat balance and adopting a multitubular model, several different representations of co- or counter-currently cooled multitubular reactor bundles have been considered. On the shell-side, it has been demonstrated that the temperature gradients in the coolant parallel to the tubes could be ignored, so that a mixing cell model is suitable, both in terms of accuracy and computation time. This model, which has the added attraction of the ease with which it can be simplified so as to reduce the computation time still further, has been used to represent all types of reactor configurations throughout this study.

Consideration has also been given to an adequate description of the tubeside behaviour. Although the one dimensional model, with an implicitly assumed parabolic radial temperature profile, is not strictly quantitatively accurate under extreme conditions, it does give very good qualitative agreement with the more complex two dimensional model. As this is primarily a preliminary study of the effects of interactive heat transfer through the coolant in large multitubular bundles, a qualitative picture of the reactor performance is adequate in formulating generalized criteria for the behaviour of such systems. Moreover, because of the uncertainty in the data available for predicting the parameters, a qualitative approach representing a general pattern of behaviour is all that can realistically be expected. Hence, the one dimensional tubeside model has been used throughout this study, although it would be possible to use a more detailed description if required.

A novel feature of this study is that it has been possible to demonstrate how the reactor configuration affects both the stability and performance of multitubular reactors. Counter-currently cooled reactors cannot tolerate large coolant temperature rises because the hot coolant at the exit can cause excessive reaction rates in the inlet stages of the reactor tubes. For this reason high coolant flowrates are necessary with the accompanying high pumping costs. Reactors with co-current cooling on the other hand can give very good performance with high coolant temperature rises. In such systems, the coolant, often ignored in the initial design stages, can be used to distribute the reaction heat around the assembly, inducing further reaction in regions of depleted reactant. Thus, as an example of the economic importance of carrying out surveys on the coolant behaviour, by giving adequate consideration to the effects of the coolant flowrate, increased conversions and decreased pumping costs are possible.

In both modes of coolant flow direction, three or four coolant passes on the shell-side seem, for the data used here, to give the best overall performance for a wide range of operating conditions. Two coolant pass systems tend to have a large distribution of conversions across the tube bundle and hence exhibit undesirable operating conditions unless very high coolant flowrates (giving low coolant temperature rises) are used.

An alternative configuration, the mixed flow reactor, has been explored which tends to produce conditions intermediate to the co- and counter-current reactors. A comparison of the three configurations leads to the conclusion that, for equally sized systems, the co-current reactor is attractive provided large coolant temperature rises can be tolerated in the coolant circuit. If not, then the counter-current system with its small temperature rises and higher pumping costs can be used to produce the same conversion of reactants. The mixed flow

reactor, with its intermediate pumping costs and temperature rises, make it useful when a compromise between the need for low energy costs in the cooling circuit conflicts with the need for low coolant temperature rises.

Maldistribution of reactants to the tubes has been shown to have significant effects not only on the affected tubes, but also on normal tubes because of the interactive nature of the heat transfer between coolant and tubes throughout the bundle. This further indicates the need for multitubular models. Although single tube models can be considered adequate for initial studies under mild operating conditions, problems still arise when the basic assumptions of the models are not met. Hence, in very large multitubular bundles, where maldistribution of feed to the tubes can be a serious problem, the use of the simple models can result in misleading conclusions being reached owing to the complex interaction of the heat transfer in the tube bundle.

In counter-currently cooled reactors the backward movement of heat arising from the coolant flow direction may cause multiple steady states to develop at low coolant flowrates. This undesirable phenomena is more likely to occur in multitubular than single tube systems because of the larger amounts of heat which are generated and the limitations which may be imposed on the coolant flowrate by the pumping costs involved.

A phase plot of inlet coolant temperature versus a parameter GG (based on the coolant flowrate) has been discussed and shown that it can be used to indicate both regions of operability and (for counter-current reactors) regions of multiplicity of the coolant conditions. The charts, which provide a simple and convenient method of investigating the design or control strategies for either co- or counter-current reactors, are dependent on easily obtainable variables, namely the inlet reactant and coolant temperatures and the coolant flowrate (identified as the parameter GG). Thus, the resulting charts, which enable the stability and conversion

of a multitubular reactor to be obtained easily, are suitable for routine use and so have considerable value in the overall assessment of the operational characteristics and the design of control schemes for such systems.

The work has been extended to the evaluation of dynamic models of both co- and counter-current reactors using the mixing cell approximation to represent the shell-side heat balance. The very long computation times necessary, especially for the counter-current reactor model, have meant that only a limited survey of the transient behaviour has been possible. However, the general characteristics of the system have been identified, as have the dangers of relying on a lumped parameter element to represent the reactor. Step decreases in either the inlet reactant or coolant temperatures cause increased tubeside temperature peaks during the initial transient response of a co-currently cooled system. The counter-current reactor, while behaving similarly for step decreases in the reactant temperature, give only falling tubeside temperature profiles for decreases in the inlet coolant temperature. Thus, it would appear that counter-current systems are preferable when coolant temperature control is difficult. The frequency response of co-current reactors during sinusoidal coolant temperature disturbances has demonstrated the importance of considering the initial transient response. Even though the final pseudo-steady state has stable temperature profiles, relatively large unstable temperature peaks giving temperature runaway can develop during the first few cycles of the disturbance. Hence, the final pseudo-steady state may never be reached because of catalyst deactivation due to the high temperatures during the initial transient response.

Variations in the coolant flowrate give rise to safe operating conditions for both co- and counter-current systems, providing that the initial and final steady state temperature profiles of the system are

stable then the profiles during the transient period will also be stable.

The results of the dynamic study of the reactor indicate clearly that a detailed investigation of such systems is necessary. In general, the behaviour of a multitubular reactor is controlled by a combination of chemical and thermal effects, the relative magnitude of which may change considerably with time and position. This results in dynamic responses which are not easily predicted without extensive simulation. The complex interactions which are present emphasise the importance of recognizing the need for adopting a multivariable approach, and clearly, this is essential when considering the structure of a control scheme.

9.2 Assessment of the Present Work

This study has been concerned with developing an understanding of the interaction between the heat removal and generation in large multitubular reactors. An important feature of the work is the alternative approach to the design of large scale units that is presented. Conventional design procedures would tend to place emphasis on methods which consider a single tube to be typical of the entire unit. However, there is a need to examine the overall system, that is the total assembly, to enable a more realistic representation to be obtained. The cases examined here have shown that the specific features of the mechanical design of industrial reactors dictate that not only must the behaviour of the coolant be explicitly accounted for, but also that the interaction between the tubes, arising from the pattern of heat release, must also be taken into consideration.

The important heat transfer mechanism in such reactors is a combination of heat removal from the tubes and heat distribution along the coolant path. Clearly, these two are dependent not only upon each other, but also upon the mechanical arrangement of the reactor. Co-current reactors for instance exhibit a feedforward of heat, the reaction heat

evolved in the first half of the system being carried, via the coolant, to promote reaction in the outlet portions. The feedback of heat in counter-current reactors on the other hand causes higher reaction rates in the inlet stages of the bed. Present design procedures do not give adequate consideration to the layout of the coolant flow path at the process design stage. Indeed, such systems are usually regarded as modified shell and tube heat exchangers and so the designs do not therefore take advantage of the tubeside temperature distribution. The necessity of adopting a multitubular approach has been demonstrated, and its potential for enabling a much better appreciation of the problem highlighted. Moreover, it has pointed to the need for optimization of the reactor configuration.

The mixed flow arrangement, developed in chapter seven, demonstrates that reactor performance can be improved by modifying the shell-side cooling circuit. Although the subject has only been touched upon, there would appear to be a great deal of scope in this type of arrangement for improving the performance of multitubular systems. A particular advantage is that, not only is it simple to apply on an industrial unit, but it has great flexibility in delivering the maximum cooling action to the tubeside hotspots, and it also promotes reaction in regions of depleted reactant. There is very strong evidence that adequate shell-side design can not only reduce the capital cost and improve performance, but also, because the system is potentially more stable (due to the maximum cooling being in the correct region of the reactor), enable much more precise designs and control schemes to be implemented.

9.3 Suggestions for Further Work

This work has been concerned mainly with establishing a qualitative picture of the operational characteristics of multitubular reactors and, as such, has constituted an initial survey of the performance of such

systems. In particular, since for control purposes the centre-line temperature in the reactor tubes is the most critical it must be studied in more detail. It has already been indicated that the computational load of the two dimensional model is too great for routine use. However, Naim[35], has shown that this model can be reduced to a pseudo-one dimensional form, and, although this still requires more computation than the one dimensional model used here, it should be acceptable and could be used for confirming the results of the simpler model.

The problems of the steady state of the multitubular reactor are by no means resolved. A more detailed model must be formulated to include pressure drop effects on the shell-side. This would then enable the study of the variation of coolant velocity across the bundle and also facilitate a more extensive investigation of suitable coolant flowrates. The effects of reactor size, both in terms of the number and the length of the tubes requires study. This is important especially when considering the question of the best mode of operation (co- or counter-current cooling). Applying shell and tube heat exchanger theory, counter-currently cooled systems require less heat transfer area per unit than co-current systems, and so it is possible that counter-current reactors may be capable of the same performance as a co-current system but for a smaller size unit, and hence smaller capital cost. However, the decrease in the size of the counter-current reactor means lower coolant temperature rises and hence lower reaction rates. Thus, for a given production rate the length of tube and the mode of operation constitute an interesting optimization problem.

The results obtained in this present work leave little doubt that the dynamic behaviour of multitubular reactors requires extensive further study. Clearly, there are a whole range of disturbances that could be applied to such a system, but it should be possible to establish some general rules suitable for use in the design of a control scheme.

Attention should be centred on the effects caused by the application of various control actions, such as variation of the reactant flowrate or different types of multivariable approach. Although the work reported here has shown that it is possible to predict the change necessary in any inlet variable when the others are disturbed, if safe operation is to be maintained, no information has been obtained on how these changes should be made. This is particularly important since temperature runaway must be avoided in the transient period as well as in the steady state. The frequency response of multitubular systems also requires further effort, with an attempt to classify the range of frequencies and amplitudes that lead to unstable conditions. This is especially important when considering systems that give stable conditions during the final pseudo-steady state but cause instability during the initial transient response.

Because of the excessive computation times necessary for even limited studies, reduction of the model is essential if it is to be useful for routine design or control use. Such a model, which gives the same general characteristics as the complex model, might be formulated in terms of a lumping approximation. Thus, in an analogous manner to the distribution factor of Turner[42], which modifies the rate terms in a tubular reactor by using assumed, semi-empirical radial temperature and concentration profiles, the lumping factor could represent the effects of the various tubeside conditions for different tubes in the reactor bundle. This would mean that the reactor behaviour can be represented by far fewer tubeside evaluations during simulation.

Finally, experimental work, both on single and multitube reactors will be necessary to confirm the findings of the theoretical investigations. However, at the present stage of the project it is doubtful that much could be gained from studying a laboratory scale tube bundle. Effort should be concentrated on obtaining reliable data from single

tube reactors, as these form the building blocks of the multitubular system. Experimentation on the multitubular reactor can be most profitably done after further detailed theoretical investigations have outlined the best methods of tackling the complex problems in such large systems.

APPENDIX A

The Catalyst Pellet Models

A.1 The Fully Distributed Catalyst Pellet Model

This section introduces a general mathematical model of the catalyst pellet including all the major resistances to heat and mass transport. Catalyst pellets are normally porous so that the maximum number of active sites can be contained in the smallest volume. Hence, the reactants have to diffuse into the pellet, react and then the products diffuse away. This resistance to the transport of heat and mass has the effect of causing conditions within the pellet to differ from those of the fluid and hence influence the rate of reaction. Four significant transport resistances can be readily identified and most models of catalyst particles have been developed to include some or all of them:

1. Mass transfer resistance within the catalyst pellet pores.
2. Mass transfer resistance at the interface of the gas and solid phase.
3. Heat transfer resistance due to the pellet structure.
4. Interphase heat transfer resistance across the pellet to fluid boundary layer.

Unfortunately such a model requires an appreciable amount of computation in its solution, making it of limited use in the design of packed bed reactors. For this reason an approximate representation, the lumped thermal resistance model[12] has been developed and is presented in section A.2. For design purposes a detailed description of the pellet conditions is not really required, a measure of the difference between the actual rate of reaction in the pellet and the rate predicted by the fluid conditions would be perfectly satisfactory.

Such a measure is given by the effectiveness factor, η , which is defined by:

$$\eta = \frac{\text{Actual Reaction Rate at Pellet Conditions}}{\text{Reaction Rate Calculated at Fluid Conditions}}$$

Once known, the effectiveness factor can be used in the global equations of the reactor, and the design carried out assuming a pseudo-homogeneous model based on the fluid conditions.

A.1.1 The Steady State

For a spherical catalyst pellet in which the n^{th} order $A \rightarrow B$ reaction with Arrhenius kinetics occurs, a mass balance on species A gives:

$$\frac{1}{s^2} D_{P_A} \frac{d}{ds}\left\{ s^2 \frac{dC'_{P_A}}{ds} \right\} - A_o \exp\left\{ - \frac{E}{R_g T_p} \right\} C'^{n}_{P_A} = 0 \qquad (A.1)$$

Similarly, a heat balance gives:

$$\frac{1}{s^2} K_p \frac{d}{ds}\left\{ s^2 \frac{dT_p}{ds} \right\} + (-\Delta H) A_o \exp\left\{ - \frac{E}{R_g T_p} \right\} C'^{n}_{P_A} = 0 \qquad (A.2)$$

Equations (A.1) and (A.2) are subject to the boundary conditions

$$\frac{dC'_{P_A}}{ds} = \frac{dT_p}{ds} \quad \text{at } s = 0 \qquad (A.3)$$

$$\left.\begin{aligned} D_{P_A} \frac{dC'_{P_A}}{ds} &= k_{g_A} (C'_{f_A} - C'_{P_A}) \\ K_p \frac{dT_p}{ds} &= h(T' - T_p) \end{aligned}\right\} \text{at } s = b \qquad (A.4)$$

These equations may then be written in dimensionless form as:

$$\frac{d^2 C_{P_A}}{dy^2} - \frac{2}{(1-y)} \frac{dC_{P_A}}{dy} - \theta^2 \exp\left\{ - {}^1/_t \right\} C^n_{P_A} = 0 \qquad (A.5)$$

$$\frac{d^2t}{dy^2} - \frac{2}{(1-y)}\frac{dt}{dy} + B_o\ Nu\ \theta^2\ \exp\left\{-\frac{1}{t}\right\} C_{P_A}^n = 0 \qquad (A.6)$$

with boundary conditions:

$$\frac{dC_{P_A}}{dy} = \frac{dt}{dy} = 0 \qquad \text{at } y = 1 \qquad (A.7)$$

$$\left.\begin{aligned} \frac{dC_{P_A}}{dy} &= \frac{Sh_A'}{2}\left(C_{P_A} - C_A\right) \\ \frac{dt}{dy} &= \frac{Nu'}{2}\left(t - T\right) \end{aligned}\right\} \quad \text{at } y = 0 \qquad (A.8)$$

where: $C_{P_A} = \dfrac{C'_{P_A}}{C_o}$, $C_A = \dfrac{C'_{f_A}}{C_o}$, $t = \dfrac{R_g T_p}{E}$

$$T = \frac{R_g T'}{E},\ y = 1 - \frac{s}{b}$$

$$\theta^2 = \frac{b^2 A_o}{D_{P_A}},\ B_o = \frac{(-\Delta H)\ D_{P_A}\ C_o\ R_g}{2\ b\ h\ E}$$

$$Sh_A' = \frac{2\ b\ k_{g_A}}{D_{P_A}},\ Nu' = \frac{2\ b\ h}{K_p}$$

Equations (A.5) and (A.6) may be solved numerically to give the temperature and concentration profiles within the pellet. The effectiveness factor, η , is given by:

$$\eta = \frac{4\pi\ b^2\ k_{g_A}\ (C'_{f_A} - C'_{P_A}|_{s=b})}{\frac{4}{3}\pi\ b^3\ A_o\ \exp\left\{-\frac{E}{R_g T'}\right\} C_{f_A}'^n}$$

which in dimensionless form becomes:

$$\eta = \frac{1.5\ Sh_A'\left(C_A - C_{P_A}|_{y=0}\right)}{\theta^2\ \exp\left\{-\frac{1}{T}\right\} C_A^n} \qquad (A.9)$$

A.1.2 The Unsteady State

The unsteady state mass balance on the pellet gives:

$$\frac{D_{P_A}}{b^2 e^*}\left[\frac{\partial^2 C_{P_A}}{\partial y^2} - \frac{2}{(1-y)}\frac{\partial C_{P_A}}{\partial y}\right] - \frac{A_o}{e^*}\exp\left\{-\frac{1}{t}\right\} C_{P_A}^n = \frac{\partial C_{P_A}}{\partial \tau} \qquad (A.10)$$

Similarly the unsteady heat balance gives:

$$\frac{K_p}{\rho^* C_p^* b^2}\left[\frac{\partial^2 t}{\partial y^2} - \frac{2}{(1-y)}\frac{\partial t}{\partial y}\right] + \frac{(-\Delta H)\, A_o\, R_g}{\rho^* C_p^* E}\exp\left\{-\frac{1}{t}\right\} C_{P_A}^n = \frac{\partial t}{\partial \tau} \qquad (A.11)$$

with boundary conditions:

$$\left.\begin{aligned} &\frac{\partial C_{P_A}}{\partial y} = \frac{\partial t}{\partial y} = 0 \qquad \text{at } y = 1,\ \tau \geqslant 0 \\ &\frac{\partial C_{P_A}}{\partial y} = \frac{b\, k_{g_A}}{D_{P_A}}\left(C_{P_A} - C_A^{'}\right) \\ &\qquad\qquad \text{at } y = 0,\ \tau \geqslant 0 \\ &\frac{\partial t}{\partial y} = \frac{bh}{K_p}\left(t - T\right) \end{aligned}\right\}$$

$$t = t\big|_{\tau = 0}$$

$$\text{at } \tau = 0,\ 0 \geqslant y \geqslant 1$$

$$C_{P_A} = C_{P_A}\big|_{\tau = 0}$$

Rearranging equations (A.10) and (A.11) and introducing dimensionless groups, they become:

$$\frac{\partial^2 C_{P_A}}{\partial y^2} - \frac{2}{(1-y)}\frac{\partial C_{P_A}}{\partial y} - \theta^2 \exp\left\{-\frac{1}{t}\right\} C_{P_A}^n = K_{cc}\frac{\partial C_{P_A}}{\partial \tau} \qquad (A.12)$$

$$\frac{\partial^2 t}{\partial y^2} - \frac{2}{(1-y)}\frac{\partial t}{\partial y} + B_o\, Nu\, \theta^2 \exp\left\{-\frac{1}{t}\right\} C_{P_A}^n = K_T\frac{\partial t}{\partial \tau} \qquad (A.13)$$

with boundary conditions:

$$\frac{\partial C_{P_A}}{\partial y} = \frac{\partial t}{\partial y} = 0 \qquad \text{at } y = 0, \tau \geqslant 0$$

$$\left.\begin{aligned} \frac{\partial C_{P_A}}{\partial y} &= \frac{Sh_A}{2}\left(C_{P_A} - C_A\right) \\ \frac{\partial t}{\partial y} &= \frac{Nu}{2}\left(t - T\right) \end{aligned}\right\} \quad \text{at } y = 1, \tau \geqslant 0$$

$$t = t_o$$

$$C_{P_A} = C_{P_{A_o}} \qquad \text{at } \tau = 0,\ 0 \geqslant y \geqslant 1$$

where: $K_{cc} = \frac{b^2 e^*}{D_{P_A}}$, $K_T = \frac{\rho^* C_p^* b^2}{K_P}$

Since the thermal capacitance of the system is much greater than the mass capacitance[15], $K_{cc} \ll K_T$, the concentration profiles can be assumed to be at a series of pseudo-steady states and hence equation (A.12) can be replaced by its steady state form, (A.5).

A.2 The Lumped Thermal Resistance Model of the Catalyst Pellet

A.2.1 The Steady State

In this model the resistance to heat transfer within the catalyst pellet is assumed negligible and the pellet is, therefore, isothermal. Thus, the temperature, t, is constant throughout the pellet. The mass balance on the pellet is identical to that used for the fully distributed model. However, since t is not a function of y, equation (A.5) may be solved analytically for first order reactions (n = 1) to give the concentration profile in the pellet. For non-first order reactions a pseudo first order form of the rate expression may be used[41, 71], and the parameter θ is then redefined by:

$$\theta^2 = \frac{b^2 A_o C_{P_A}^{n-1}}{D_{P_A}}$$

Thus equation (A.5) becomes:

$$\frac{d^2C_{P_A}}{dy^2} - \frac{2}{(1-y)} \frac{dC_{P_A}}{dy} - \theta^2 \exp\left\{-1/t\right\} C_{P_A} = 0 \qquad (A.14)$$

with boundary conditions:

$$\frac{dC_{P_A}}{dy} = 0 \qquad \text{at } y = 1$$

$$\frac{dC_{P_A}}{dy} = \frac{Sh_A}{2} (C_{P_A} - C_A) \qquad \text{at } y = 0$$

Analytical solution of equation (A.14) gives:

$$C_{P_A} = \frac{0.5\ Sh_A \sinh (r\ (1 - y))\ C_A}{(r \coth (r) + s)\ (1 - y) \sinh (r)} \qquad (A.15)$$

where: $r = \theta \exp\left\{-1/2t\right\}$, $s = 0.5\ Sh_A - 1$

A heat balance on the isothermal catalyst pellet gives, in dimensionless form:

$$B_o\ Sh_A (C_A - C_{P_A}\Big|_{y=0}) - t + T = 0 \qquad (A.16)$$

$C_{P_A}\Big|_{y=0}$ may be obtained from equation (A.15) as:

$$C_{P_A}\Big|_{y=0} = \frac{0.5\ Sh_A\ C_A}{(r \coth (r) + s)} \qquad (A.17)$$

using (A.17) in equation (A.16) and rearranging gives:

$$t = T + \frac{B\ Sh_A\ (r - g)}{(sg + r)} \qquad (A.18)$$

where $B = B_o\ C_A$ and $g = \tanh\ (r)$

Equation (A.18), therefore, gives the pellet temperature directly and may be solved by any of the normal root-finding techniques e.g. Newton-Raphson.

Using equations (A.17) and (A.18) in the expression for the effectiveness factor, (A.9), enables η to be expressed in terms of t, C_A and T only. Thus:

$$\eta = \frac{1.5\ (t - T)}{B_o\ \theta^2\ \exp\left\{-1/T\right\} C_A} \qquad (A.19)$$

A.2.2 The Unsteady State

As in the fully distributed dynamic model of the catalyst pellet, the concentration profiles may be assumed to be at a series of pseudo-steady states. Therefore the instantaneous concentration profile of species A is given by equation (A.15). An unsteady state heat balance on the isothermal catalyst pellet gives:

$$\frac{2\ K_T}{3\ Nu} \frac{dt}{d\tau} = T - t + B_o\ Sh_A\ (C_A - C_{P_A}\Big|_{y=0}) \qquad (A.20)$$

where $C_{P_A}\Big|_{y=0}$ is given by equation (A.17).

Equation (A.20) may be conveniently solved using the Runge-Kutta-Merson algorithm.

APPENDIX B

The One Dimensional Reactor Model

B.1 The Steady State Model

For the A → B reaction scheme used here, differential heat and mass balances on the reactor give in dimensionless form:

$$\frac{dC_A}{dz} + G_2 \eta \theta^2 \exp\left\{-1/T\right\} C_A^n = 0 \qquad (B.1)$$

$$\frac{dT}{dz} - G_4 (t - T) + \frac{2 Nu_w^*}{G_3} (T - T_c) = 0 \qquad (B.2)$$

with the boundary conditions:

$$T = T\Big|_{z=0}, \; C_A = C_A\Big|_{z=0}$$

where: $G_2 = \dfrac{(1 - e) L D_{P_A}}{b^2 u e}$ $\quad G_3 = \dfrac{R^2 u \rho C_P}{K_f L}$

$$G_4 = \frac{3 (1 - e) h L}{b \rho u e C_P}$$

$$Nu_w^* = \frac{4 Nu_w}{(4 + Nu_w)} \qquad Nu_w = \frac{R U}{K_f e}$$

where the state variables used in equations (B.1) and (B.2) are radial mean values. The modified Nusselt number, Nu_w^*, being introduced to account for the assumed parabolic radial temperature profile[15] in the bed. Thus, the radial temperature profile is given by:

$$T_r = T + 0.25 Nu_w^* (T - T_c) - 0.5 Nu_w^* (T - T_c) r^2 \qquad (B.3)$$

where T is the radial mean temperature obtained from equation (B.2),

and r is the dimensionless radial coordinate in the reactor such that r = 0 at the tube centre.

The modified Nusselt number, Nu_w^*, is defined by:

$$Nu_w^* (T - T_c) = Nu_w \left(T\Big|_{r=1} - T_c\right) \tag{B.4}$$

Using (B.4) and the assumed parabolic profile it may be shown that:

$$Nu_w^* = \frac{4\ Nu_w}{(4 + Nu_w)} \tag{B.5}$$

The pellet temperature, t, and the effectiveness factor, η , are obtained from the catalyst pellet model described in Appendix A.

Equations (B.1) and (B.2) form a coupled initial value problem and can be solved by any appropriate method. The Runge-Kutta-Merson algorithm was used in this study and it was found that for the data used 80 steps were needed in the axial direction to give adequate convergence.

B.2 The Unsteady State Model

The transient fluid field equations for the reactor are in dimensionless form:

$$\frac{\partial C_A}{\partial z} + G_2 \eta\ \theta^2 \exp\left\{-1/T\right\} C_A^{\,n} + G_5 \frac{\partial C_A}{\partial \tau} = 0 \tag{B.6}$$

$$\frac{\partial T}{\partial z} + \frac{2Nu_w^*}{G_3} (T - T_c) - G_4 (t - T) + G_6 \frac{\partial T}{\partial \tau} = 0 \tag{B.7}$$

with the initial conditions:

$$C_A = C_A\Big|_{\tau=0}$$

at z = 0

$$T = T\Big|_{\tau=0}$$

$$C_A = C_A\Big|_{z=0} \qquad \text{at } \tau=0$$

$$T = T\Big|_{z=0}$$

Equations (B.6) and (B.7) are coupled with the dynamic model of the catalyst pellet, equation (A.20). Several workers[15, 35, 41] have shown that the transient response of the reactor predicted by these equations is slow compared with the residence time of the reactants, so that the fluid equations may be solved as if they were at a pseudo-steady state. Thus, in equations (B.6) and (B.7) $G_5 = G_6 = 0$ and the steady state equations (B.1) and (B.2) result. Solution of the system of equations is then similar to the steady state case, the essential difference being that when the bed exit ($z = 1$) is reached the time is updated and the procedure repeated from the bed entrance. Also, at each node of the solution network the dynamic model of the catalyst pellet must be solved to obtain t at the current time. This is accomplished by use of the Runge-Kutta-Merson algorithm, in which case the values of C and T must be supplied over the time interval. Since this is small, it may be assumed that these vary linearly over it.

APPENDIX C

Single Tube, Flowing Coolant Model. (Model B of Chapter 3)

For a single reactor tube with co-currently flowing coolant, a heat balance on the coolant gives:

$$M_c \, C_{P_c} \frac{dT_c'}{dz'} - 2\pi \, RU \left(T'\Big|_{y=R} - T_c'\right) = 0 \qquad (C.1)$$

with the initial condition:

$$T_c' = T_{c_o}' \qquad \text{at } z' = 0$$

$T'\Big|_{y=R}$ is the tubeside temperature at the tube wall.

Making (C.1) dimensionless and expressing the tubeside gas temperature in terms of its radial mean value gives:

$$\frac{dT_c}{dz} - \frac{2Nu_w^*}{G_{cc}} (T - T_c) = 0 \qquad (C.2)$$

with the initial condition: $T_c = T_{c_o}$ at $z = 0$

where $$G_{cc} = \frac{M_c \, C_{Pc}}{\pi L \, K_f \, e}$$

Equation (C.2) is coupled with the tubeside equations given in Appendix B, through T and T_c, and must, therefore be solved simultaneously with them. The Runge-Kutta-Merson algorithm used previously being suitable for this purpose.

APPENDIX D

The Continuum Coolant Heat Balance

The heat balance for a coolant flowing over a bank of tubes can be described by the following equation:

$$-\nabla\cdot(u_c \dot{\rho}_c C_{P_c} \epsilon_c T_c) - \nabla\cdot(-K_c' e_c \nabla T_c) + UA\,(T\Big|_{y=R} - T_c) = 0 \qquad (D.1)$$

Applying the assumption that in a large bundle the row of tubes across the bundle diameter is representative, equation (D.1) reduces to:

$$K_c' e_c \frac{\partial^2 T_c'}{\partial z'^2} - u_c \rho_c C_{P_c} \epsilon_c \frac{\partial T_c'}{\partial x'} + UA'\,(T\Big|_{y=R} - T_c') = 0 \qquad (D.2)$$

with boundary conditions:

$$T_c' = T_{c_o} \qquad \text{at } x' = 0,\ 0 \leqslant z' \leqslant L_B$$

$$\left.\begin{aligned} \frac{\partial T_c'}{\partial z'} = 0 \qquad \text{at } z' &= 0 \\ z' &= L_B \end{aligned}\right\} 0 \leqslant x' \leqslant L_c$$

where x' is the co-ordinate in the direction of coolant flow and z' perpendicular to the coolant flow.

Rearrangement of equation (D.2) in dimensionless form gives:

$$\frac{\partial^2 T_c}{\partial z_c^2} - A_1 \frac{\partial T_c}{\partial x} + A_2 Nu_w^* (T - T_c) = 0 \qquad (D.3)$$

with boundary conditions:

$$\dot{T}_c = T_{c_o} \qquad \text{at } x = 0,\ 0 \leqslant z_c \leqslant 1$$

$$\left.\begin{aligned} \frac{\partial T_c}{\partial z_c} = 0 \qquad \text{at } z_c &= 0 \\ z_c &= 1 \end{aligned}\right\} 0 \leqslant x \leqslant 1 \qquad (D.4)$$

where: $z_c = \frac{z'}{L_B}$, $x = \frac{x'}{L_c}$

$$A_1 = \frac{u_c \rho_c C_{P_c} \epsilon_c L_B^2}{K_c' L_c e_c} \quad , \quad A_2 = \frac{A' K_f e L_B^2}{K_c' e_c R}$$

Equation (D.3) coupled with the boundary conditions (D.4) can be solved by finite difference.

Writing equation (D.3) in a general form we get:

$$\frac{\partial^2 f}{\partial z^2} + K \frac{\partial f}{\partial x} + R' f + R'' = 0 \qquad (D.5)$$

with boundary conditions:

$f = f_o$ at $x = 0$, $0 \leqslant z \leqslant 1$

$\frac{\partial f}{\partial z} = 0$ at $z = 0$, $z = 1$ $\Big\}$ $0 \leqslant x \leqslant 1$

In finite difference form, the terms in equation (D.5) become:

$$\frac{\partial^2 f}{\partial z^2} = \frac{1}{h^2} \left(Q \left(f_{i+1} - 2f_i + f_{i-1}\right) + (1 - Q) \left(x f_{i+1} - 2 x f_i + x f_{i-1}\right)\right)$$

$$K \frac{\partial f}{\partial x} = \frac{K}{k} \left(f_i - x f_i\right)$$

$$R' f = Q R_i' f_i + (1 - Q) \times R_i' \times f_i$$

$$R'' = Q R_i'' + (1 - Q) \times R_i''$$

where:

the prefix 'x' indicates the value of the variable at the previous axial (z) position.

h is the step length in the axial direction

k is the step length across the tube bundle (in the x-direction)

Q is a constant, $0 < Q \leqslant 1$, such that when $Q = 0.5$ the equations are of the Crank-Nicolson form.

Replacing the terms in equation (D.5) by the expressions given above, and rearranging, gives:

$$m_i \, f_{i+1} + p_i \, f_i + n_i \, f_{i-1} = a_i \qquad \text{(D.6)}$$

where: $m_i = \frac{Q}{h^2}$

$$p_i = -\frac{2Q}{h^2} + \frac{K}{k} + QR_i'$$

$$n_i = \frac{Q}{h^2}$$

$$a_i = -x\, f_{i+1}\left\{\frac{(1-Q)}{h^2}\right\} - x\, f_i\left\{-2\,\frac{(1-Q)}{h^2} - \frac{K}{k} + (1-Q)\,x\,R_i'\right\}$$

$$- x\, f_{i-1}\left\{\frac{(1-Q)}{h^2}\right\} - QR_i'' - (1-Q)\,x\,R_i''$$

These expressions hold for $1 \leqslant i \leqslant (N-1)$ where 0 and N are the numbers of the finite difference nodes at each baffle plate (i.e. at $z = 0$ and $z = 1$).

Applying the boundary conditions at $z = 0$ and $z = 1$ enables the elimination of the terms at the hypothetical nodes $(N+1)$ and $(N-1)$. This leads to the following expression at the zero'th node:

$$m_o \, f_{+1} + p_o \, f_o = a_o \qquad \text{(D.7)}$$

where: $m_o = \frac{2Q}{h^2}$

$$p_o = - \frac{2Q}{h^2} + \frac{K}{k} + QR_o'$$

$$a_o = - xf_o\left\{ - \frac{2(1 - Q)}{h^2} - \frac{K}{k} + (1 - Q) \times R_o' \right\}$$

$$- xf_{+1}\left\{ \frac{2(1 - Q)}{h^2} \right\} - QR_o'' - (1 - Q) \times R_o''$$

And at the Nth node:

$$p_N f_N + n_N f_{N-1} = a_N \qquad \text{(D.8)}$$

where: $$p_N = - \frac{2Q}{h^2} + \frac{K}{k} + QR_N'$$

$$n_N = \frac{2Q}{h^2}$$

$$a_N = - x f_{N-1}\left\{ \frac{2(1 - Q)}{h^2} \right\}$$

$$- x f_N\left\{ - \frac{2(1 - Q)}{h^2} - \frac{K}{k} + (1 - Q) \times R_N' \right\}$$

$$- Q R_N'' - (1 - Q) R_N''$$

Equations (D.6), (D.7) and (D.8) represent a system of simultaneous algebraic equations of the form:

$$\underline{A}\ \underline{f} = \underline{a}$$

where the coefficient matrix $\underline{A}$, is given by:

$$\underline{A} = \begin{bmatrix} p_o & m_o & & & \\ n_i & p_i & m_i & & \\ & & & & \\ & & n_N & p_N & \end{bmatrix}$$

This tridiagonal matrix, $\underline{A}$, can be solved using the computationally efficient algorithm of Thomas[72].

The above heat balance refers to flow of coolant over a bank of tubes, without any reference to the direction of flow of the coolant relative to the direction of flow of the tubeside gases.

The following solution method refers to the case of a reactor with co-current flowing coolant, for counter-current cooling see chapter 4.

The solution of the finite difference equations for a co-current, crossflow reactor may be accomplished by marching across the bundle from the coolant inlet to the coolant outlet in each coolant pass as follows:

1. Assume a coolant temperature profile perpendicular to the direction of coolant flow at the first (i.e. inlet) or next position along the direction of flow.

2. Using this temperature profile solve the tubeside model for the length of tube in the pass under consideration.

3. Using the tubeside temperature profile from step (2) solve the coolant finite difference equations in the direction perpendicular to coolant flow to obtain a new coolant temperature profile in this direction.

4. Check whether the coolant temperature profile calculated at step (3) agrees with the one assumed at step (1). If not, using the profile from step (3) repeat the calculation from step (2). If convergence is obtained and $x < 1$ (i.e. the outlet from the coolant pass is not reached) go on to the next position in the direction of coolant flow and repeat from step (1). If $x = 1$ (i.e. the outlet from the coolant pass is reached), go on to the next coolant pass and repeat from step (1).

At the end of each pass, where the flow direction is reversed for the next pass, it is assumed that complete coolant mixing occurs so that it enters each pass at a uniform temperature.

APPENDIX E

The Co-Current Mixing Cell Model

The assumptions for the mixing cell model are basically the same as those for the continuum model and have already been detailed in section 4.1. Figure E.1 shows the layout of the mixing cells in a typical reactor cross-section, the coolant, being perfectly mixed in each cell flows from cell i to cell i + 1 until the end of each coolant pass. From the point of view of heat generation there are effectively two tubes in each cell.

A heat balance over cell i gives:

$$m_c\, C_{P_c}\, T'_{c(i-1)} + 4\pi RU \int_{z_1'}^{z_2'} \left(T'\big|_{y=R} - T'_{c(i)} \right) dz' = m_c\, C_{P_c}\, T'_{ci} \qquad (E.1)$$

where: $m_c = u_c\, \rho_c\, L_B\, L_T$

z_1' and z_2' are the limits of the length of the baffle section

$T'\big|_{y=R}$ is the tubeside wall temperature, a function of $T_{c(i)}$

In dimensionless form, equation (E.1) becomes:

$$T_{c(i)} = T_{c(i-1)} + \frac{Nu_w}{G_c} \int_{z_1}^{z_2} \left(T\big|_{r=1} - T_{c(i)} \right) dz \qquad (E.2)$$

where: $G_c = \dfrac{m_c\, C_{P_c}}{4\pi\, K_f\, e\, L_B}$

Although the above equation uses the tubeside wall temperature, use of the effective wall Nusselt number, Nu_w^*, enables equation E.2 to be expressed in terms of the radial mean tubeside temperature, hence it may be written:

$$T_{c(i)} = T_{c(i-1)} + \frac{Nu_w^*}{G_c} \int_{z_1}^{z_2} (T - T_{c(i)})\, dz \qquad (E.3)$$

The method of solution of the model is as follows:

1. Assume a value of T_c at the first or next cell.

2. Solve the tubeside equation for the length of the cell using this value of T_c.

3. Using the tubeside temperature profile from step (2) evaluate the integral term in equation (E.3).

4. Solve equation (E.3) using the value obtained from step (3) to give a new value of T_c.

5. Compare the value of T_c from step (4) with that assumed in step (1). If the two values are converged to within a given accuracy, move on to the next cell and repeat from (1). If the values are not converged use the value of T_c from step (4) and repeat from step (2).

This procedure is repeated in each coolant pass until the exit cell is reached, the solution is then complete.

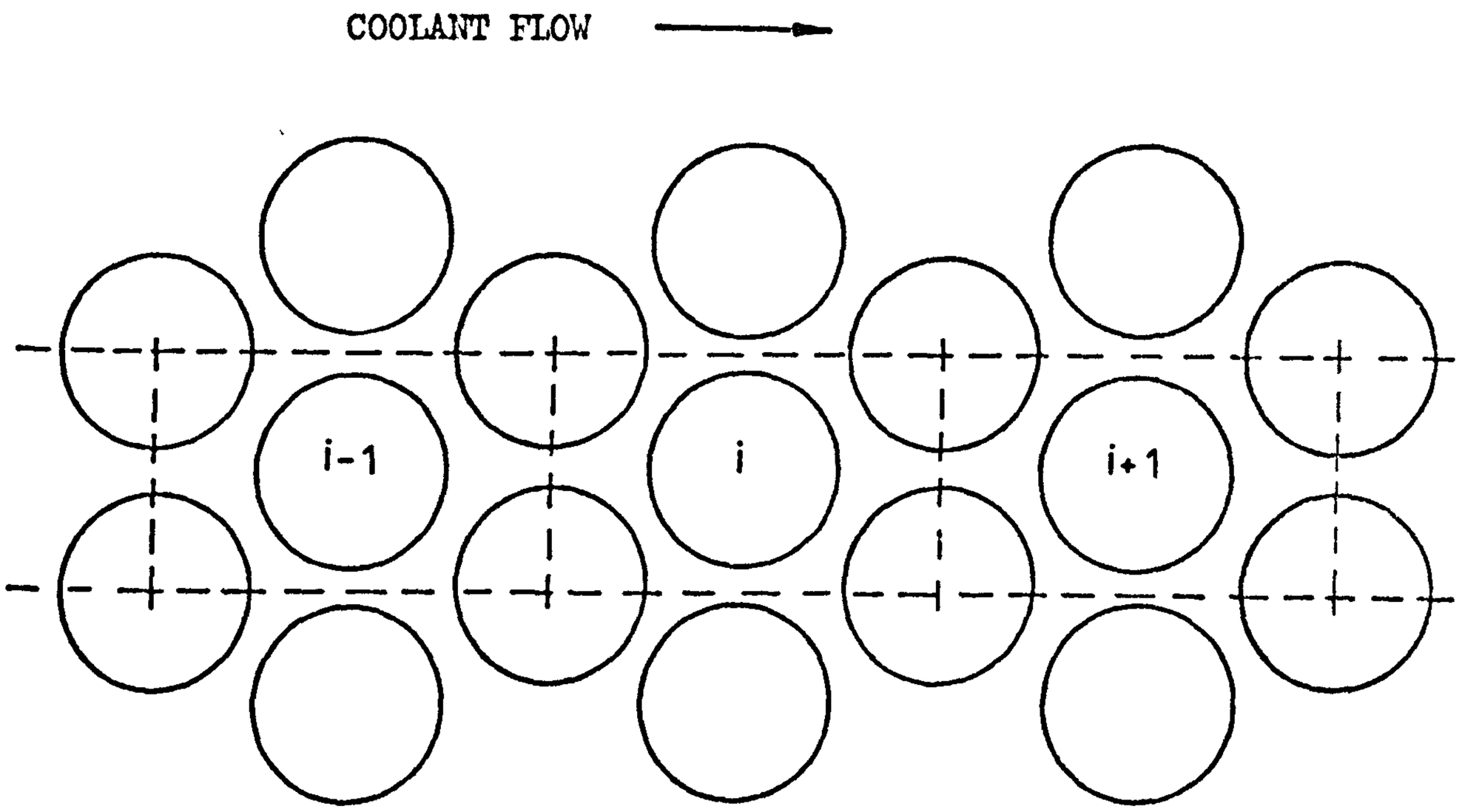

Figure E.1 Schematic diagram of the tube bundle, showing the arrangement of the mixing cells in the co-current cross-flow model.

APPENDIX F

The Counter-Current Mixing Cell Model

The only difference between this reactor configuration and the co-current is the direction of flow of the coolant relative to the flow of the tubeside gases. This, together with the tube labelling system is shown schematically in figure F.1.

Using the same nomenclature as in Appendix E, a heat balance on cell i gives:

$$T_{c(i)} = T_{c(i-1)} - \frac{Nu_w^*}{G_c} \int_{z_1}^{z_2} (T - T_{c(i)})\, dz \qquad (F.1)$$

where T, the radial mean tubeside temperature is a function of $T_{c(i)}$.

The method of solution is as follows:

1. Assume a value for T_c at the cell at the coolant exit from the bundle.

2. Solve the tubeside equations using this value.

3. Compute the value of T_c in the next cell in the direction opposite to coolant flow.

4. Check whether the last cell in the bundle (i.e. at the coolant entrance) has been reached. If not, repeat from step (2) using the value of T_c from step (3). If the last cell has been reached go on to step (5).

5. Compare the computed value of the coolant inlet temperature from step (3) with the actual value. If the values are the same, to a given accuracy, the the solution is complete. If not, repeat from step (1).

The method of repeated subsstitution appears to be adequate to obtain convergence of the coolant inlet temperature within three or four iterations. However, under severe conditions, such as in the region of multiple solutions, a more sophisticated approximation procedure (e.g. a quadratic convergence routine) is recommended.

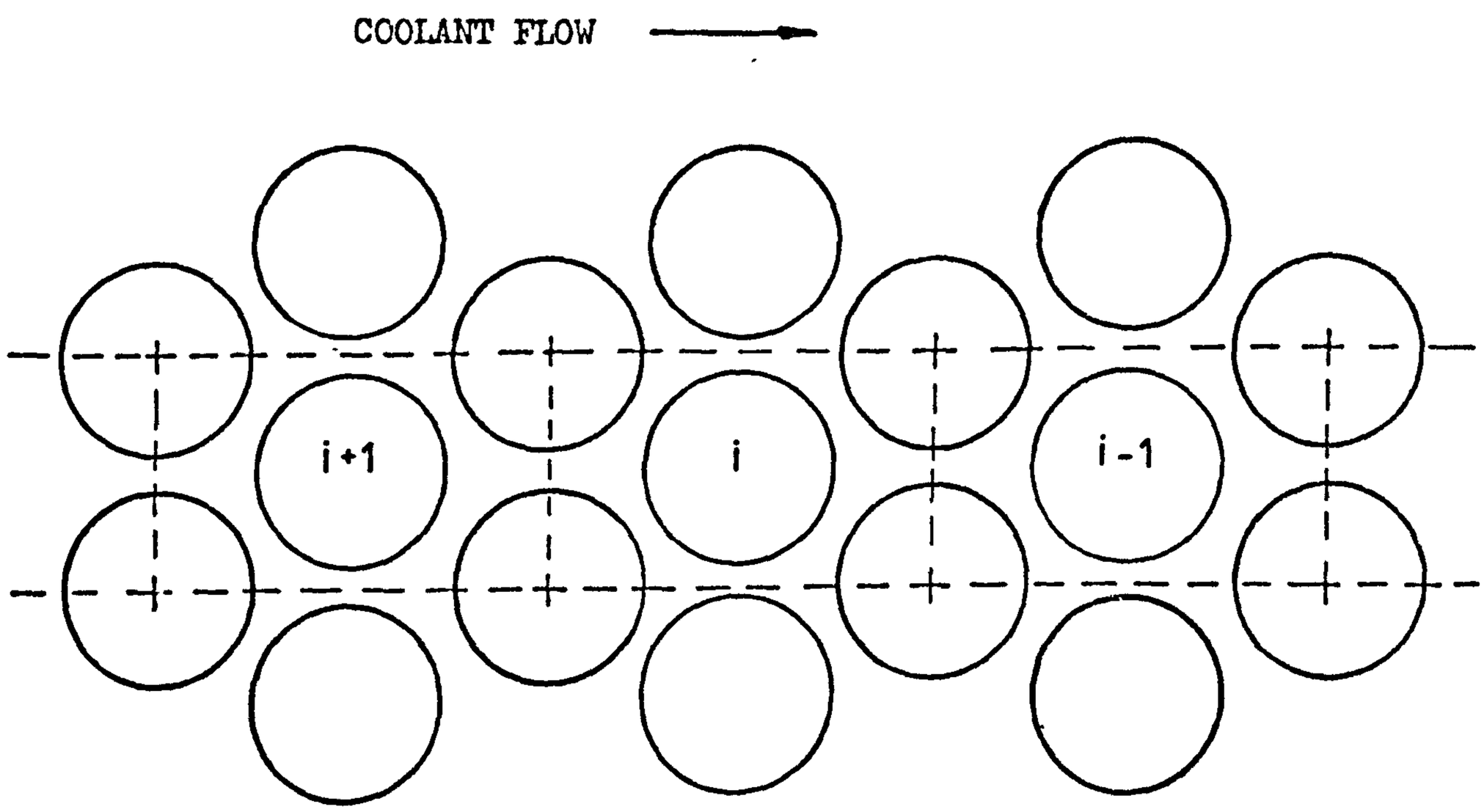

Figure F.1 Schematic diagram of the tube bundle, showing the arrangement of the mixing cells in the counter-current cross-flow model.

APPENDIX G

The Two Dimensional Tubeside Reactor Model

For a fixed bed catalytic reactor the differential heat and mass balance equations, using the nomenclature of Appendix B, can be written in dimensionless form as:

$$\frac{1}{r}\frac{\partial}{\partial r}\left\{r\frac{\partial C_A}{\partial r}\right\} - G_1\frac{\partial C_A}{\partial z} - G_1\, G_2\, \eta\, \phi^2\, C_A = 0 \qquad (G.1)$$

$$\frac{1}{r}\frac{\partial}{\partial r}\left\{r\frac{\partial T}{\partial r}\right\} - G_3\frac{\partial T}{\partial z} + G_3\, G_4\, (t - T) = 0 \qquad (G.2)$$

with the initial conditions:

$$\left.\begin{aligned} C_A &= C_{A_o} \\ T &= T_o \end{aligned}\right\} \quad @\ z = 0,\ 0 \leqslant r \leqslant 1$$

and the boundary conditions:

$$\frac{\partial C_A}{\partial r} = \frac{\partial T}{\partial r} = 0 \qquad r = 0 \text{ and } z \geqslant 0$$

$$\left.\begin{aligned} \frac{\partial C_A}{\partial r} &= 0 \qquad (G.3) \\ \frac{\partial T}{\partial r} &= Nu_w\,(T_c - T) \qquad (G.4) \end{aligned}\right\} \quad @\ r = 1,\ z \geqslant 0$$

where: $G_1 = \dfrac{R^2 u}{L\, D_{f_A}}$, $\phi^2 = \theta^2 \exp\left\{-\dfrac{1}{T}\right\}$

Equations (G.1) and (G.2) are coupled with the catalyst pellet model given in Appendix A through the variables η and t.

The solution of equations of the form of (G.1) and (G.2) has been accomplished by Naim[35] using the method of orthogonal collocation.

Basically this entails substitution of the radial operators in the above equations and the elimination of the boundary conditions. This is simply achieved by the following substitutions:

$$\frac{1}{r}\frac{\partial}{\partial r}\left\{r\frac{\partial Y}{\partial r}\right\}\Big|_{r_J} = \sum_{i=1}^{n+1} B_{J,i} \cdot Y(r_i)$$

$$\text{and } \frac{dY}{dr}\Big|_J = \sum_{i=1}^{n+1} A_{J,i} \cdot Y(r_i)$$

where Y is the state variable being considered and $A_{J,i}$ and $B_{J,i}$ are the collocation coefficients for the first and second order differential operators. N being the number of interior zeros of the orthogonal polynomial used.

Performing the above substitutions on equations (G.1) and (G.2) we obtain:

$$\frac{dC_A}{dz}\Big|_J = \frac{1}{G_1}\sum_{i=1}^{N} Q_{J,i}\, C_{A_i} - G_2 \eta_J \phi^2 C_{A_J} \qquad (G.5)$$

$$\frac{dT}{dz}\Big|_J = \frac{1}{G_3}\sum_{i=1}^{N} W_{J,i} \cdot T_i + \frac{1}{G_3} \cdot V_J + G_4 (t_J - T_J) \qquad (G.6)$$

for J = 1, 2, ..., N

with the initial conditions:

$$\left.\begin{aligned} C_A(z) &= C_{A_J}(0) \\ T(z) &= T_J(0) \end{aligned}\right\} \text{ at } z = 0,\ 0 \leqslant r \leqslant 1$$

where: $\sum_{i=1}^{N} W_{J,i} = \sum_{i=1}^{N} \left\{B_{J,i} - \frac{B_{J,N+1} \cdot A_{N+1,i}}{Nu_w + A_{N+1,\,N+1}}\right\}$

$$\sum_{i=1}^{N} Q_{J,i} = \sum_{i=1}^{N} \left\{ B_{J,i} - \frac{B_{J,N+1} \cdot A_{N+1,i}}{A_{N+1,\ N+1}} \right\}$$

and $$V_J = \frac{B_{J,N+1} \cdot Nu_w \cdot T_c}{Nu_w + A_{N+1,\ N+1}}$$

Equations (G.5) and (G.6), coupled with the catalyst pellet equation can now be solved by any of the standard initial value methods. The Runge-Kutta-Merson routine being used in this study because of the possibility of severe temperature gradients in the axial direction. The values of the $A_{J,i}$ and $B_{J,i}$ matrices are dependant upon the type of polynomial used to represent the radial temperature gradient. Values obtained from the squared roots of Legendre polynomials, recommended by Naim[35], gave excellent results, and the matrices for several values of N are given in table G.1.

Solution of equations (G.5) and (G.6) gives the values of the state variables at the roots of the polynomials, the values at the tube wall and centre-line have to be calculated separately. Thus, the tubeside temperature at the wall, T_{N+1}, is obtained by substituting into the boundary condition equation, (G.4), giving:

$$T_{N+1} = \frac{\left(Nu_w\ T_c - \sum_{i=1}^{N} A_{i,N+1}\ T_i \right)}{(Nu_w + A_{N+1,\ N+1})}$$

Similarly, the concentration at the tube wall is obtained by substitution into equation (G.3), giving:

$$C_{A_{N+1}} = \frac{-\sum_{i=1}^{N} A_{N+1,i} \cdot C_{A_i}}{A_{N+1,\ N+1}}$$

The centre-line values are best obtained by the method outlined by Finlayson[73] involving a matrix inversion.

Hence, the centre-line temperature, T_{CL}, is given by:

$$T_{CL} = \sum_{i=1}^{N+1} QQ^{-1}_{1.i}\ T_i$$

and, the centre-line concentration, $C_{A_{CL}}$, by:

$$C_{A_{CL}} = \sum_{i=1}^{N+1} QQ^{-1}_{1,i}\ C_{A_i}$$

where, the QQ matrix, needed to calculate the A and B matrices, is defined by:

$$[QQ] = \begin{bmatrix} 1 & x_1^2 & \cdot & \cdot & \cdot & x_1^{2N} \\ \cdot & \cdot & \cdot & \cdot & \cdot & \cdot \\ \cdot & \cdot & \cdot & \cdot & \cdot & \cdot \\ \cdot & \cdot & \cdot & \cdot & \cdot & \cdot \\ 1 & x_{N+1}^2 & \cdot & \cdot & \cdot & x_{N+1}^{2N} \end{bmatrix}$$

The collocation points x_1, x_2, ..., x_N that appear here are the roots of the polynomial used and x_{N+1} is unity.

T A B L E G.1

Collocation Constants for Cylindrical Symmetry

Using the Squares of Legendre Zeros

N+1	i	x_i^2	A_{i1}	A_{i2}	A_{i3}	A_{i4}
3	1	0.2113248	-1.1744576	1.8501968	-0.6757392	
3	2	0.7886751	-1.080966	-1.4409269	2.5218930	
3	3	1.0	1.3706100	-8.7552254	7.3846153	
4	1	0.1227016	-1.4691708	1.8026562	-0.5965425	0.2630571
4	2	0.5000	-2.220537	1.0196078	2.0104531	-0.8095238
4	3	0.8872983	1.1175509	-3.0575581	-2.7493166	4.6893238
4	4	1.0	-1.7580995	4.3921570	-16.729295	14.095238
5	1	0.06943184	-1.9476331	2.2136892	-0.35694403	0.1752583
5	2	0.3300094	-3.8216261	2.7872708	1.3354975	-0.57105127
5	3	0.6699905	2.6435722	-5.7293136	1.3146075	3.059090
5	4	0.9305681	-1.9885867	3.7532664	-4.6866995	-4.8025616
5	5	1.0	3.3237324	-6.1591694	6.8508831	-26.819184

(continued from previous column)

N+1	i	A_{i5}	B_{i1}	B_{i2}	B_{i3}	B_{i4}	B_{i5}
3	1		-10.467457	15.873371	-5.4059136		
3	2		6.2804747	-26.455619	20.175144		
3	3		17.245355	-54.168432	36.923076		
4	1		-24.952452	30.117647	-9.1805593	4.0153650	
4	2		5.3048488	-17.882353	19.625123	-7.0466191	
4	3		-8.7466123	30.117647	-84.403290	63.032254	
4	4		-45.954990	109.17647	-190.45957	127.23809	
5	1	-0.08437034	-54.231907	61.049615	-9.1147009	4.4222004	-2.125071
5	2	0.26990897	4.0022945	-20.626417	20.723789	-7.6398847	3.5402183
5	3	-1.2879563	-1.1121886	12.996080	-35.221296	36.831517	-13.494115
5	4	7.7245804	23.422373	-46.438045	76.771487	-210.66803	156.91221
5	5	22.803738	144.87523	-265.57488	276.42928	-476.47729	320.74765

APPENDIX H

The Solution of the Co-Currently Cooled Transient Reactor Model

The coolant heating as it flows through the tube bundle is governed by equation (8.5), which can be solved by any of the usual initial value methods. The technique used on the tubeside equations (Runge-Kutta-Merson) has been found to be suitable because it is both robust and simple to program.

Equation (8.3), representing the time the coolant spends in moving from one coolant pass to the next, can be approximated by a backward difference formula giving:

$$T'_{c2} = T_{c2} + \frac{\Delta\tau}{\theta_R}(T_{c1} - T_{c2}) \qquad (H.1)$$

where T'_{c2} is the inlet coolant temperature to the next coolant pass at the next time step and $\Delta\tau$ is the time interval used.

The method of solution of the co-current reactor model is as follows:

1. Calculate the initial steady state using the model of Appendix E.

2. Begin a transient perturbation.

3. Guess a value of $T_{c(i)}$ at the first or next cell at time $\tau = \tau$.

4. Evaluate the tubeside conditions at $\tau = \tau$ using the value of $T_{c(i)}$ from step (3) and the dynamic tubeside model of Appendix B.

5. Using equation (8.5), calculate a new value of $T_{c(i)}$ at time $\tau = \tau$.

6. Compare the value of $T_{c(i)}$ from step (4) with that assumed at step (3). If the two values are in agreement to a given accuracy and the exit of the coolant pass is not reached, move on to the next cell and repeat from (3). If the values do not agree, use the

value from step (5) and repeat from step (4).

7. If the exit of the coolant pass is reached, but not the exit of the reactor, then use equation (H.1) to calculate the coolant inlet temperature to the next pass at time $\tau = \tau$ and continue from step (4) as for the previous coolant pass.

8. When the exit of the reactor is reached the calculations are repeated from step (3) for $\tau = \tau + \Delta\tau$.

Evaluation of equation (8.5) by the Runge-Kutta-Merson routine requires values of the integral term to be supplied over the time interval. This is achieved by assuming a linear variation in this term, and for the cases considered here, time intervals of one second give satisfactory performance of the reactor model.

APPENDIX I

The Solution of the Counter-Currently Cooled Transient Reactor Model

The solution of the two-coolant pass, counter-current, dynamic reactor model is accomplished as follows, with reference to figure 8.21:

1. Evaluate the initial steady state:

   (i) Assume the inlet coolant temperature to coolant pass 1, $T_{c_{gues}}$.

   (ii) Using the transient heat balance, equation (8.5), with the time derivative set to zero, and the steady state tubeside equation of Appendix B, the first approximation to the outlet coolant temperature is obtained by marching across the tube bundle as done in the co-current steady state model of Appendix E.

   (iii) A similar technique, starting with the known coolant inlet temperature and marching across the bundle in pass 2, gives the outlet coolant temperature from pass 2, T_{c_1}.

   (iv) If $T_{c_{gues}}$ equals T_{c_1} within error bounds, the calculation is complete. If not. assume a new value of $T_{c_{gues}}$ and repeat from (ii).

   (v) Store the relevant state variables etc. for use in the transient period.

2. Begin the perturbation.

3. Assume a coolant inlet temperature to coolant pass 1, $T_{c_{gues}}$, at time $\tau = \tau$.

4. Using equation (8.5) and the transient tubeside model of Appendix B, march across the tube bundle in the direction of the coolant and

calculate the first approximation to the coolant outlet temperature in the same way as the co-current solution was obtained for each pass in Appendix H.

5. Starting with the known inlet coolant temperature at $\tau = \tau$, march across the bundle in coolant pass 2, as in (4) above, using the stored outlet tubeside values from coolant pass 1 in the tubeside equations. and calculate the outlet coolant temperature from this pass, T_{c_1}.

6. Apply equation (H.1) to the value of T_{c_1} and obtain the value of the coolant inlet temperature, T'_{c_1}, entering coolant pass 1 from coolant pass 2 under the assumed conditions at time $\tau = \tau$.

7. Compare the value of T'_{c_1} with the initial guess $T_{c_{gues}}$. If these are equal within given bounds, the calculation at time $\tau = \tau$ is complete. If not, a new value of $T_{c_{gues}}$ is assumed and the procedure repeated from step (4).

8. Store the relevant state variables needed for the next time step, set $\tau = \tau + \Delta\tau$ and then repeat from step (3).

The method of repeated substitution gives three or four iterations on the assumed coolant temperature under the conditions used in this study. Should more severe operating conditions be explored, a more sophisticated technique would be necessary to obtain a solution without an excessive number of iterations.

NOMENCLATURE

a_i — Matrix element in the finite difference formulation of the differential equations.

A' — Surface area of the reactor tubes per unit volume of the tube bundle.

$A_{i,J}$ — Matrix representing the first order radial differential operator for cylindrical geometry.

A_1, A_2 — Parameters defined and used in the continuum model of the multitubular bundle.

A_o — Arrhenius pre-exponential factor.

b — Pellet radius.

B_o — Dimensionless exothermicity factor = $\dfrac{(-\Delta H)\ D_{P_A}\ C_o\ R_g}{2\ b\ h\ e}$

B — Thermal load factor = $B_o * C_A$

$B_{i,J}$ — Matrix representing the radial Laplacian operator for cylindrical geometry.

C_A — Dimensionless concentration of reactants in the fluid = $\dfrac{C'_{f_A}}{C_o}$

C_{A_o} — Value of C_A at the reactor inlet.

C_{P_A} — Dimensionless concentration of reactants within the catalyst pellet = $\dfrac{C'_{P_A}}{C_o}$

C'_{f_A} — Reactant concentration within the fluid.

C'_{P_A} — Reactant concentration within the catalyst pellet.

C_o — Reference concentration of reactant A.

C_P, C^*_P, C_{P_c} — Specific heats of the fluid, catalyst pellet and coolant respectively.

D — Distribution factor, introduced in chapter 2.

D_{f_A} — Effective interstitial radial diffusivity in the fluid.

D_{P_A} — Effective radial diffusivity within the catalyst pellet.

e, e^* — Porosity of the fixed bed and catalyst pellet, respectively.

e_c — Voidage of the tube bundle in the direction perpendicular to coolant flow.

E	Activation energy of the reaction.
f	Dependent variable in the general form of the differential equations.
$F_{(i)}$	Function defined in chapter 4.
g	tanh (r)
GG	Parameter, proportional to coolant flowrate, used in chapters 6 and 7.
G_1 to G_6	Parameters used in the tubeside reactor models and defined in Appendix B.
G_{cc}	Parameter used in the single tube flowing cooling model and defined in Appendix C.
G_c	Parameter used in the cell model of the multitubular bundle and defined in Appendix E.
h	Effective pellet to fluid surface heat transfer coefficient.
i	Number of the cell in the cell model of the multitubular bundle.
k_{g_A}	Fluid to pellet mass transfer coefficient.
K_c	Effective interstitial thermal conductivity of the coolant in the direction perpendicular to coolant flow.
K_{cc}	'Capacitance' of the catalyst pellet to absorb mass = $\frac{b^2 e^*}{D_{P_A}}$
K_f	Effective interstitial radial thermal conductivity of the fluid.
K_p	Effective thermal conductivity of the catalyst pellet.
K_T	'Capacitance' of the catalyst pellet to absorb heat = $\frac{b^2 \rho^* C_p^*}{K_p}$
L_B	Distance between baffle plates.
L_C	Diameter of the tube bundle.
L_T	Minimum distance between adjacent tubes.
L	Reactor tube length.
m_c	Mass flowrate of the coolant across the tube bundle in each coolant pass.
m_i	Element of the tridiagonal matrix in the finite difference formation of the differential equations.

M_c	Mass flowrate of coolant along the outside of the single tube, flowing coolant model.
n_i	Element of the tridiagonal matrix in the finite difference formulation of the differential equations.
n	Order of the reaction.
N_T	Number of tubes across the diameter of the tube bundle.
Nu	Modified Nusselt number for heat transfer between the pellet and the fluid = $\frac{2\ b\ h}{K_p}$
Nu_w	Nusselt number for heat transfer between the fluid and the coolant = $\frac{R\ U}{K_f\ e}$
Nu_w^*	Effective overall Nusselt number for heat transfer between the fluid and the coolant based on the radial mean fluid temperature. Used in the one dimensional model of the reactor tube.
p_i	Element of the tridiagonal matrix in the finite difference formulation of the differential equations.
P_D	Pitch circle diameter in multitubular reactor.
Q	Heat evolved or removed.
Q	Weighting constant in the finite difference representation of the differential equations such that $0 < Q \leqslant 1$.
r	Dimensionless radial position in the reactor tube = y/R.
r	$\theta \exp(-1/2t)$.
R	Inside radius of the reactor tube.
R', R''	Non-linear terms used in the general forms of the differential equations.
R_g	The gas constant.
R_2	Outside radius of the reactor tube.
s	$\frac{Sh_A}{2} - 1$.
s	Distance from the centre of the catalyst pellet.
Sh_A	Modified Sherwood number = $\frac{2\ b\ k_{g_A}}{D_{P_A}}$
t	Dimensionless pellet temperature = $\frac{R_g\ T_P}{E}$
T	Dimensionless fluid temperature = $\frac{R_g\ T'}{E}$

T'	Temperature of the fluid.
T_o, T'_o	Values of T and T' respectively at the reactor inlet.
T_c	Dimensionless coolant temperature = $\frac{R_g T'_c}{E}$
T'_c	Temperature of the coolant.
$T_{c_{in}}$, $T'_{c_{in}}$	Values of T_c and T'_c respectively at the coolant inlet.
$T_{c_{out}}$, $T'_{c_{out}}$	Values of T_c and T'_c respectively at the coolant outlet.
$T_{c(i)}$	Value of T_c in the cell i in the mixing cell model of the multitubular reactor.
T_{CL}	Dimensionless axial fluid temperature.
T_p	Temperature of the catalyst pellet.
u	Interstitial fluid velocity.
u_c	Interstitial coolant velocity.
U	Fluid to coolant overall heat transfer coefficient.
x	Dimensionless co-cordinate across the tube bundle in the direction of coolant flow = $\frac{x'}{L_c}$
x'	Distance across the tube bundle in the direction of coolant flow.
y	Distance from the reactor tube axis.
y	Dimensionless pellet co-ordinate = 1 - $\frac{s}{b}$ (Appendix A).
z	Dimensionless axial co-ordinate along the reactor tube = $\frac{z'}{L}$.
z'	Axial distance along the reactor tube.
z''	Axial distance along the reactor tubes in each coolant pass.
z_c	Dimensionless co-ordinate along the reactor tubes in each coolant pass measured between the baffle plates = $\frac{z''}{L_B}$.
z'_1, z'_2	Values of z' at the baffle plates in each coolant pass in the multitubular reactor.
z_1, z_2	Values of z at the baffle plates in each coolant pass = $\frac{z'_1}{L}$, $\frac{z'_2}{L}$.

Greek Symbols

ϵ_c — Voidage of the tube bundle in the direction of coolant flow.

$(-\Delta H)$ — Heat of reaction.

η — Effectiveness factor.

θ — Reaction-diffusion modulus = $b\sqrt{\frac{A_o}{D_{P_A}}}$.

θ_R — Residense time of coolant in the portion of the reactor between coolant passes.

ρ, ρ^*, ρ_c — Densities of the fluid, catalyst pellet and coolant respectively.

τ — Time (seconds).

ϕ — Thiele modulus evaluated at fluid conditions $= \theta \exp\left\{-\frac{1}{2T}\right\}$.

BIBLIOGRAPHY

1. AMUNDSON, N.R.; Ind. and Engng. Chem. 48, 26, (1956)

2. THOMAS, J.M. and THOMAS, W.J.; "Introduction to Principles of Heterogeneous Catalysis", Academic Press, London (1967)

3. SATTERFIELD, C.N., "Mass Transfer in Heterogeneous Catalysis", MIT Press (1970)

4. ARIS, R., "Introduction to the Analysis of Chemical Reactors", Prentice-Hall Inc., New Jersey, (1965)

5. PETERSEN, E.E., "Chemical Reaction Analysis", Prentice-Hall Inc., New Jersey, (1965)

6. DENBIGH, K. and TURNER, J., "Chemical Reactor Theory", Cambridge University Press, London, (1971)

7. PERLMUTTER, D.D., "Stability of Chemical Reactors", Prentice-Hall Inc., New Jersey, (1972)

8. FROMENT, G.F., "Symposium on Reactor Engineering", University of Leeds, England (1971)

9. FROMENT, G.F., "Second International/Fifth European Symposium on Chemical Reaction Engineering", Amsterdam (1972)

10. HLAVACEK, V., Ind. Eng. Chem., 62, 8,(1970)

11. RAY, W.H., "Second International/Fifth European Symposium on Chemical Reaction Engineering", Amsterdam (1972)

12. CRESSWELL, D.L., Ph.D. Dissertation, University of Leeds (1969)

13. PETERSEN, E.E., Chem. Eng. Sci., 17, 987, (1962)

14. PETERSEN, E.E., ibid., 20, 587, (1965)

15. THORNTON, J.M., Ph.D. Dissertation, University of Leeds, (1970)

16. PATERSON, W.R. and CRESSWELL, D.L., Chem. Eng. Sci., 26, 605, (1971)

17. HLAVACEK, V. and KUBICEK, M., Chem. Eng. Sci., 25, 1537, (1970)

18. HLAVACEK, V. and KUBICEK, M., ibid, 25, 1761, (1970)

19. CUNNINGHAM, R.A. et al, A.I.Ch.E. JL, 11, 636 (1965)

20. MILLER, F.W. and DEANS, H.A., ibid, 13, 45 (1967)

21. IRVING, J.P. and BUTT, J.B., Chem. Eng. Sci., 22, 1859 (1967)

22. RAMASWAMI, D., Ph.D. Dissertation, University of Wisconsin (1961)

23. HUGHES, R. and KOH, H.P., Chem. Eng. JL, 1, 186 (1970)

24. FEICK, J. and QUON, D., Can. JL Chem. Eng., 48, 205, (1970)

25. VON ROSENBERG, D.V. et al, Brit. Chem. Eng., 7, 186, (1962)

26. FROMENT, G.F., Chem. Eng. Sci., 17, 849, (1962)

27. BEEK, J., Adv. in Chem. Eng., 3, 203, (1962)

28. HANSEN, K.W., LIVBJERG, H. and VILLADSEN, J., Fifth European/ Second International Symposium on Chem. Reaction Engineering, Amsterdam, (1972)

29. CARBERRY, J.J. and WENDAL, M.M., A.I.Ch.E. JL, 9, 129, (1963)

30. KARENTH, N.G. and HUGHES, R., Paper at "Symposium on Heterogeneous Reactors", University of Salford (1972)

31. DEANS, H.A. and LAPIDUS, L., A.I.Ch.E. JL, 6, 656, (1960)

32. McGUIRE, M.L. and LAPIDUS, L., ibid, 11, 85, (1965)

33. CRIDER, J.E. and FOSS, A.S., ibid, 14, 77, (1968)

34. FEICK, J., Ph.D. Dissertation, University of Alberta, (1968)

35. NAIM, H.M., Ph.D. Dissertation, University of Leeds, (1974)

36. VILLADSEN, J.V., "Selected Approximation Methods for Chemical Engineering Problems"

37. FERGUSON, N.B. and FINLAYSON, B.A., Chem. Eng. JL, 1, 327 (1970)

38. McGREAVY, C. and CRESSWELL, D.L., "4th European Symposium on Chemical Reaction Engineering", Brussels, (1968)

39. FEICK, J. and QUON, D., Can. JL. Chem. Eng., 48, 205, (1970)

40. HANSEN, K.W., Chem. Eng. Sci., 26, 1555, (1971)

41. ADDERLEY, C.I., Ph.D. Dissertation, University of Leeds (1973)

42. TURNER, K., Ph.D. Dissertation, University of Leeds (1970)

43. BISCHOFF, K.B., Chem. Eng. Sci., 23, 251, (1968)

44. COPELOWITZ, I. and ARIS, R., ibid, 25, 285, (1970)

45. HLAVACEK, V. and KUBICEK, M. ibid, 25, 1527, (1970)

46. BRUSSET, H., et al, ibid, 27, 1475 (1972)

47. SHADMAN-YAZDI, F. and PETERSEN, E.E., ibid, 27, 227 (1972)

48. CALDERBANK, P.H. et al, Fourth European Symposium on Chemical Reaction Engineering, Brussels (1968)

49. STEWART, W.E. and SØRENSEN, J.P., Fifth European/Second International Symposium on Chemical Reaction Engineering, Amsterdam (1972)

50. JONES, D.A., Ph.D. Dissertation, University of Leeds (1971)

51. ERVIN, M.A. and LUSS, D., A.I.Ch.E. JL, 16, 979, (1970)

52. VALSTAR, J.M., "A Study of the Fixed Bed Reactor with Application to the Synthesis of Vinyl Acetate", Delftsche Vitgevers Maatschappij, N.V. Delft (1969)

53. STANEK, V. and SZEKELY, J., Canadian JL, Chem. Eng., 51, 22, (1973)

54. HOIBERG, J.A., LYCHE, B.C. and FOSS, A.S., A.I.Ch.E. JL, 17, 1434 (1971)

55. PARIS, J.R. and STEVENS, W.F., Fourth European Symposium on Chemical Reaction Engineering, Brussels (1968)

56. VAN HEERDEN, C., Ind. Eng. Chem., 45, 1242 (1953)

57. LUSS, D. and MEDELLIN, P., Fifth European/Second International Symposium on Chemical Reaction Engineering, Amsterdam (1972)

58. BANCHERO, J.T. and SMITH, T.G., A.I.Ch.E./A.S.M.E. Heat Transfer Conference, Denver, Colorado (1972)

59. WANKA, O. and GÜTLHUBER, F., paper at "Symposium on Heterogeneous Reactors", University of Salford, England (1972)

60. CARDOSO, M.A.A. and LUSS, D., Chem. Eng. Sci., 24, 1699, (1969)

61. HATFIELD, B. and ARIS, R., ibid, 24, 1913 (1969)

62. HATFIELD, B. and ARIS, R., ibid, 24, 1220 (1969)

63. KAO, Y.K. and BANKOFF, S.G., ibid, 26, 189 (1971)

64. McGOWAN, C. and PERLMUTTER, D.D., A.I.Ch.E. JL, 17, 831, (1971)

65. MATSUYAMA, H., Chem. Eng. JL, Japan, 5, 427, (1972)

66. FULTON, J.W. and CROSSER, O.K., A.I.Ch.E. JL, 11, 513, (1965)

67. McGREAVY, C. and DUNBOBBIN, B.R., 6th European/4th International Symposium on Chemical Reaction Engineering, Heidelberg (1976)

68. McGREAVY, C. and ADDERLEY, C.I., Chem. Eng. Sci., 28, 577 (1973)

69. FRICKE, L.H., MORRIS, H.J., OTTO, R.E. and WILLIAMS, T.J., C.E.P. Symposium Series, 56, No. 31, 80 (1960)

70. CHECHETKIN, A.V., 'High Temperature Heat Carriers', Pergamon Press, (1963)

71. RAWLINGS, N., Ph.D. Dissertation, University of Leeds (1975)

72. LAPIDUS, L., 'Digital Computation for Chemical Engineers', McGraw-Hill (1962)

73. FINLAYSON, B.A., Chem. Eng. Sci., 26, 1086, (1971)

74. DROTT, D.W., Ph.D. Dissertation, University of Minnesota (1972)

75. ARIS, R., "The Mathematical Theory of Diffusion and Reaction in Permeable Catalysts", Vol. I "The Theory of the Steady State" Vol. II "Questions of Uniqueness, Stability, and Transient Behaviour", Clarendon Press, Oxford, (1975)

76. THIELE, E.W., Ind. Eng. Chem., 31, 916, (1939)

77. ZELDOWITSCH, J.B., Acta Physicochim U.S.S.R., 10, 583, (1939)